

UNCLASSIFIED

AD NUMBER

AD848086

LIMITATION CHANGES

TO:

Approved for public release; distribution is unlimited.

FROM:

Distribution authorized to U.S. Gov't. agencies and their contractors; Critical Technology; AUG 1968. Other requests shall be referred to Air Force Armament Laboratory, Attn: ATTI, Eglin AFB, FL 32542. This document contains export-controlled technical data.

AUTHORITY

AFATL ltr, 20 Feb 1976

THIS PAGE IS UNCLASSIFIED

THIS REPORT HAS BEEN DELIMITED
AND CLEARED FOR PUBLIC RELEASE
UNDER DOD DIRECTIVE 5200.20 AND
NO RESTRICTIONS ARE IMPOSED UPON
ITS USE AND DISCLOSURE.

DISTRIBUTION STATEMENT A

APPROVED FOR PUBLIC RELEASE;
DISTRIBUTION UNLIMITED.

AD848086

AFATL-TR-68-91

Exploratory Development of Illuminating Flares

Joseph T. Hamrick
John D. Stanitz
Perry L. Blackshear, Jr., et al

Aerospace Research Corporation

Technical Report AFATL-TR-68-91

AUGUST 1968

This document is subject to special export controls and each transmittal to foreign governments or foreign nationals may be made only with prior approval of the Air Force Armament Laboratory (ATTI), Eglin Air Force Base, Florida 32542.

AIR FORCE ARMAMENT LABORATORY

AIR FORCE SYSTEMS COMMAND

EGLIN AIR FORCE BASE, FLORIDA

BEST AVAILABLE COPY

EXPLORATORY DEVELOPMENT OF ILLUMINATING FLARES

Joseph T. Hamrick
John D. Stanitz
Perry L. Blackshear, Jr., et al

This document is subject to special export controls and each transmittal to foreign governments or foreign nationals may be made only with prior approval of the Air Force Armament Laboratory (ATTI), Eglin Air Force Base, Florida 32542.

FOREWORD

This report was prepared by Aerospace Research Corporation, Roanoke, Virginia, on Air Force Contract F08635-67-C-0161 in cooperation with Ordnance Research Incorporated, Fort Walton Beach, Florida; the University of Minnesota, Minneapolis, Minnesota; Thiokol Chemical Corporation, Denville, New Jersey; Hollins College, Hollins, Virginia; and John D. Stanitz, Research Consultant in Fluid Mechanics, Cleveland, Ohio. The work was administered under the direction of the Illumination Branch, Targets and Missiles Division, Air Force Armament Laboratory, Eglin Air Force Base, Florida. Mr. Larry W. Moran was project scientist for the Armament Laboratory. The studies presented began in July 1967 and were completed in July 1968. Mr. Joseph T. Hamrick of Aerospace Research Corporation was program manager.

Report sections, their authors and contributing personnel are as follows:

Section II - MATHEMATICAL FLOW MODEL AND FLOW COMPUTATIONS by John D. Stanitz

The mathematical flow model was programmed for computer by Edward J. Davis, Reaction Motors Division, Thiokol Chemical Corporation, and field plots for the five numerical examples were prepared by Anne Hopkins, Hollins College, with the help of undergraduate students at Hollins College.

Section III - THERMOCHEMICAL CALCULATIONS AND CORRELATION WITH EXPERIMENTAL RESULTS by J. T. Hamrick, L. C. Rose, Aerospace Research Corporation, and Edward J. Davis.

Section IV - FLAME CHARACTERISTICS AND SPECTRAL ANALYSIS by Perry L. Blackshear, Jr., Kanury A. Murty, Kenneth Barnes, and Frank D. Dorman, University of Minnesota.

Undergraduate research assistants, Dennis Springer and John Kiland, helped in conducting measurements during and after burning the flare. Emil Pfender and Joachim Heberlein, with the help of Gary Knowles and Ron Haglind, conducted and interpreted the spectroscopic surveys. Frederick Ahlgren assisted in the optical depth determination.

Section V - LUMINOUS INTENSITY DISTRIBUTION by Hal R. Waite and Donald R. Stewart, Ordnance Research Incorporated


SECTION VI - DISCUSSION OF RESULTS by Joseph T. Hamrick and
Ralph G. Steinhardt, Jr., Hollins College

Ralph G. Steinhardt, Jr., served as special consultant on all phases of the program.

The Aerospace Research Corporation report number designation is ET-402.

Information in this report is embargoed under the Department of State International Traffic In Arms Regulations. This report may be released to foreign governments by departments or agencies of the U. S. Government subject to approval of the Air Force Armament Laboratory (ATTI), Eglin AFB, Florida 32542, or higher authority within the Department of the Air Force. Private individuals or firms require a Department of State export license.

This technical report has been reviewed and is approved.



A. J. Cupper, Lt. Colonel, USAF
Chief, Targets and Missiles Division

ABSTRACT

A mathematical flow model has been developed for plane two-dimensional illuminating flares dropping through the atmosphere and simulating face down burning. Numerical results are given in field plots showing streamlines, velocity potential lines, constant velocity lines, and constant time lines for two-dimensional, incompressible flow. Thermochemical calculations based on shifting equilibrium were made for combustion in the flare plume over a range of various mixture ratios. The results are provided in the form of curves and tables showing reaction products, equilibrium temperature, and other thermodynamic data. Temperatures in plumes of one inch diameter flares were measured by thermocouple. A theoretical evaluation of optical density in the plume and experiments to evaluate optical density were performed. The results are provided in tables, photographs of plumes, and traces obtained by spectrograph. Relative luminous intensity distribution in the plumes of downward burning flares was determined and the results are shown in terms of relative intensity contours, plots of relative intensity versus plume area, and plots of percent total intensity versus percent of plume area. An analysis of overall results was made utilizing information from the literature as well as that obtained in the program.

This document is subject to special export controls and each transmittal to foreign governments or foreign nationals may be made only with prior approval of the Air Force Armament Laboratory (ATTI), Eglin AFB, Florida 32542.

TABLE OF CONTENTS

	<u>Page</u>
I. INTRODUCTION.....	1
II. MATHEMATICAL FLOW MODEL AND FLOW COMPUTATIONS.....	2
ANALYSIS.....	3
Preliminary Considerations.....	3
Swarz-Christoffel Transformation.....	13
Synthesis of Flow in Transformed t-plane.....	17
Flow Field in Physical z-plane.....	22
NUMERICAL PROCEDURE.....	28
NUMERICAL RESULTS AND DISCUSSION.....	29
SUMMARY.....	44
LIST OF REFERENCES.....	46
III. THERMOCHEMICAL CALCULATIONS AND CORRELATION WITH EXPERIMENTAL RESULTS.....	47
THERMOCHEMICAL CALCULATIONS.....	47
EXPERIMENTAL RESULTS.....	52
ANALYSIS OF RESULTS.....	60
SUMMARY.....	64
LIST OF REFERENCES.....	67
IV. FLAME CHARACTERISTICS AND SPECTRAL ANALYSIS.....	68
THEORETICAL CONSIDERATIONS.....	69
EXPERIMENTAL APPROACH.....	75
Test Apparatus.....	75
EXPERIMENTAL RESULTS.....	81
Spectroscopic Studies.....	81
DISCUSSION.....	89
Plume Spectra.....	89
CONCLUDING REMARKS.....	96
SUMMARY.....	96
LIST OF REFERENCES.....	98
V. LUMINOUS INTENSITY DISTRIBUTION.....	99
INSTRUMENTATION.....	100
EXPERIMENTAL PROCEDURE.....	101
DATA REDUCTION.....	104
EXPERIMENTAL RESULTS.....	105
SUMMARY.....	113
VI. DISCUSSION OF RESULTS.....	115
1. Temperature Measurements and Correlation with Luminous Intensity.....	115
2. Analysis of Particle Behavior in the Plume.....	116
3. Effects of Magnesium Particle Size.....	116
4. Effect of Velocities of Particles Within the Plume.....	117
5. Effect of Surrounding Gaseous Medium.....	118
6. Effects of Flare Diameter Variation.....	118
7. Binder Formulations.....	120
8. Casing Effects.....	122
LIST OF REFERENCES.....	123

TABLE OF CONTENTS (Cont)

	<u>Page</u>
VII. SUMMARY OF RESULTS.....	124
VIII. AREAS FOR FURTHER EXPLORATORY DEVELOPMENT.....	126
APPENDIXES	
I. LIST OF ABBREVIATIONS AND SYMBOLS FOR SECTION II.....	127
II. SOLUTION OF INTEGRAL EQUATION (6e).....	130
III. COMPUTER PROGRAM FOR TWO-DIMENSIONAL-FLARE-PLUME FLOW MODEL.....	131
IV. LIST OF ABBREVIATIONS AND SYMBOLS FOR SECTION III.....	140
V. THERMOCHEMICAL COMPUTATIONS FOR MAGNESIUM-LAMINAC- SODIUM NITRATE FLARE COMPOSITIONS.....	141
VI. THERMOCHEMICAL COMPUTATIONS FOR MAGNESIUM-GLYCIDYL METHACRYLATE-SODIUM PERCHLORATE FLARE COMPOSITIONS and COMPUTATIONS FOR ONE MAGNESIUM-GLYCIDYL METHACRYLATE- SODIUM NITRATE FLARE COMPOSITION.....	167
VII. THERMOCHEMICAL CALCULATIONS FOR MAGNESIUM, VITON A, TETRAFLUOROETHYLENE, AND SODIUM NITRATE.....	173
VIII. THERMOCHEMICAL COMPUTATIONS FOR SILICON, VITON A, TETRAFLUOROETHYLENE, AND SODIUM NITRATE.....	180
IX. THERMOCHEMICAL CALCULATIONS FOR FLARES AND FLARE COMPONENTS BURNING IN AIR.....	186
X. LIST OF ABBREVIATIONS AND SYMBOLS FOR SECTION IV.....	191

LIST OF FIGURES

<u>Figure</u>	<u>Page</u>
1 Comparison of cylindrical flare geometry, for axisymmetric, two-dimensional flow field, with rectangular parallelepiped flare geometry, for plane, two-dimensional flow field.....	4
2 xy-coordinates in the physical z-plane, together with vector directions for drop rate v_B^*	6
3 Relative velocity triangle in the physical z-plane.....	8
4 Schwarz-Christoffel transformation from exterior of flare in z-plane to upper-half of t-plane.....	9
5 "Approach flow", due to drop rate of flare, in (a) transformed t-plane, and (b) physical z-plane.....	10
6 "Source flow", due to burning rate of flare, in (a) transformed t-plane, and (b) physical z-plane.....	11
7 Combined flows, from figures 5 and 6, in (a) transformed t-plane, and (b) physical z-plane.....	12
8 General form of Schwarz-Christoffel transformation, showing deflection angles $\alpha, \beta, \gamma, \dots$ at vertices in z-plane, and corresponding locations a, b, c, \dots of vertices in t-plane.....	14
9 Simple, closed polygon corresponding to rectangular profile of flare in physical z-plane.....	15
10 Continuous distribution of source strength m_t along burning face of flare.....	15
11 Location y_0 of stagnation point between plume and surrounding air..	27
12 Streamlines ($\psi = \text{constant}$) and velocity potential lines ($\phi = \text{constant}$) in X-Y plane for two dimensional flare with dimensionless drop rate given by $K = 0$. Also shown are lines of constant gas velocity Q (local velocity divided by constant velocity v_B^* normal to burning flare surface) and lines of constant time ratio, τ	33
13 Streamlines ($\psi = \text{constant}$) and velocity potential lines ($\phi = \text{constant}$) in X-Y plane for two dimensional flare with dimensionless drop rate given by $K = 0.1$. Also shown are lines of constant gas velocity Q (local velocity divided by constant velocity v_B^* normal to burning flare surface) and lines of constant time ratio, τ	35

LIST OF FIGURES (Cont)

<u>Figure</u>	<u>Page</u>
14 Streamlines ($\psi = \text{constant}$) and velocity potential ($\phi = \text{constant}$) in X-Y plane for two dimensional flare with dimensionless drop rate given by $K = 0.3$. Also shown are lines of constant gas velocity Q (local velocity divided by constant velocity v_B^* normal to burning flare surface) and lines of constant time ratio, τ	37
15 Streamlines ($\psi = \text{constant}$) and velocity potential lines ($\phi = \text{constant}$) in X-Y plane for two dimensional flare with dimensionless drop rate given by $K = 0.5$. Also shown are lines of constant gas velocity Q (local velocity divided by constant velocity v_B^* normal to burning flare surface) and lines of constant time ratio, τ	39
16 Streamlines ($\psi = \text{constant}$) and velocity potential lines ($\phi = \text{constant}$) in X-Y plane for two dimensional flare with dimensionless drop rate given by $K = 0.7$. Also shown are lines of constant gas velocity Q (local velocity divided by constant velocity v_B^* normal to burning flare surface).....	41
17 Induced flow of air due to jet-mixing between plume and surrounding air (stationary flare, $K = 0$).....	43
18 Computer results for flares burning in an inert atmosphere. Flare composition - 5% Laminac, magnesium as shown and remainder sodium nitrate.....	49
19 Computer results for flares burning in an inert atmosphere. Flare composition - 15% glycidyl methacrylate, magnesium as shown, and remainder sodium perchlorate. Encircled points show result of replacing sodium perchlorate with sodium nitrate.....	51
20 Computer results for flares burning in an inert atmosphere. Flare composition - 11% Viton, 11% Teflon, magnesium as shown and remainder sodium nitrate.....	53
21 Computer results for flares burning in an inert atmosphere. Flare composition number one - 11% Viton, 40% Na NO_3 , silicon as shown, and remainder Teflon. Flare composition number two - 11% Viton, 30% Na NO_3 , silicon as shown and remainder Teflon.....	54
22 Temperatures in the flare plume as measured by chromel-alumel thermocouple with .062 in. dia. inconel sheath. Points represent average for minimum of 3 tests. Burning occurred in an inert atmosphere.....	56

LIST OF FIGURES (Cont)

<u>Figure</u>		<u>Page</u>
23	Temperatures along flare plume centerline. Points represent average for minimum of 3 tests in an inert atmosphere.....	57
24	Temperatures along flare plume centerline. Points represent average for minimum of 3 tests except at 3.75 inches for which there was only one test. All tests were made in an inert atmosphere.....	58
25	Typical temperature - time trace for chromel-alumel thermocouple 3 3/4 inches above a 60 percent magnesium - 5 percent Laminac - 35 percent sodium nitrate flare.....	59
26	Luminous efficiency versus percent magnesium for various diameter cylindrical flares. Data from RDTR No. 105 Vol. I, Page 26. Composition 5% Laminac, magnesium as shown and remainder sodium nitrate. Magnesium particle size 30/50 mesh.....	61
27	Luminous efficiency and burn rate versus particle size for 46.5 magnesium/52.5 sodium nitrate/1.0 percent vinyl alcohol acetate resin flare system. Flare diameter 1.33 inches with .05 inch thick paper case. (Data from Reference 9).....	65
28	Curves from reference 2.....	70
29	Schematic of optical apparatus.....	76
30	Photographs of spectroscopic setup.....	77
31	Photographs of X-ray apparatus.....	79
32	Apparatus to study orientation effects on plume shape.....	80
33	Wavelength dependence of flare intensity, .75 inches above burning surface.....	82
34	Wavelength dependence of the flare intensity, 6 inches above burning surface.....	82
35	Self-absorption of the Na D-Doublet, 6 inches above the burning surface.....	82
36	X-ray photograph of flare burning in helium chamber. (X-ray power 15 KV, 20 Ma with 3 second exposure on Polaroid film type 51).....	86

LIST OF FIGURES (Concluded)

<u>Figure</u>	<u>Page</u>
37 Flare plume.....	86
38 Flare with burning surface facing sideways; distance between flare and lens 20 inches; Polaroid film type 55; exposure 1/200 second, f32 with 1.5 neutral density filter; reference mesh size 1 inch; flare wrapped with four layers of masking tape.....	88
39 Burning flare showing particle ejection from the plume. Burning surface facing up; bright part of the plume is masked; Polaroid film type 55; exposure 1/200 second; f22; no neutral density filters; reference mesh size 1 inch.....	88
40 Particle micrographs.....	90
41 Distribution of MgO deposit on the support surface after several runs.....	91
42 A segment of the spectrum near D-line.....	92
43 Typical scanner radiometer display.....	102
44 Typical EG&G radiometer display.....	102
45 Flare test stand and physical arrangement.....	103
46 Relative luminous intensity of AeReCo 800 type flares burning in air and nitrogen. Last two digits indicate percent magnesium. Nitrogen velocity was approximately 6 feet per second upward.....	107
47 Plots of relative luminous intensity versus plume area as determined from results shown in figure 4. Note abscissa scale difference for AeReCo 868-2 flare. Relative luminous intensity contour points are shown.....	109
48 Plots of percent of total luminous intensity versus percent of plume area as determined from figure 5. Relative luminous intensity contour points are shown.....	111
49 Plume of a cast flare 4.75 inches in diameter. Flare and photograph provided by Ordnance Research Incorporated. Scale 7/16 inch = 1 foot zero inches.....	121

SECTION I

INTRODUCTION

A large amount of work has been accomplished on illuminating flares, especially with regard to particle sizes, casings, diameter, luminosity measurements, spectral data, and combinations of materials. Most of the work was empirical in nature and although many experimenters have gained an intuitive knowledge of the art of flare design, there is very little information regarding the mechanism by which maximum illumination can be achieved. It was believed at the outset of this program that achievement of a good understanding of the light producing mechanism would require the recruitment of several disciplines including specialists in fluid mechanics, thermodynamics, combustion, illumination, and spectroscopy. A team consisting of the members listed in the foreword was assembled and the results achieved in the program to date tend to support the original premise.

In order that the reader may clearly understand the work and viewpoints of the separate investigators, the reports as written by each have been assembled as SECTIONS II through V. They are followed by a summary of results in which an attempt is made to correlate all of the results. These sections contain, in order, (SECTION II) a flow model with figures showing streamline distributions and related curves for a simulated flare burning downward and falling in air; (SECTION III) results of thermochemical calculations and thermocouple measurements in flare plumes; (SECTION IV) results of optical density computations, spectral measurements, and photographs of flare plumes; and (SECTION V) luminous intensity distributions in the form of relative luminous intensity contours, graphs showing relative intensity versus plume area, and graphs showing percent intensity versus percent plume area. Each of the sections provide a discussion of results and summary within the section. A list of symbols for each section (except SECTION V) is contained in the appendixes and is identified with the section to which it applies. Lists of references for each section are contained in the section and the numbers in the text for each reference apply only to the references at the end of that section. Figures and tables referred to in a section apply only to the figures and tables in that section. The discussion of results contained in SECTION VI draws not only from the results reported in SECTIONS II through V, but also, results reported in references, where required to implement an analysis. From the discussion of results it is easy to draw conclusions as to what areas lack adequate experimental results to arrive at conclusions, but it is not easy to determine what priority should be given to each in further exploration. The results are summarized in SECTION VII and areas that require further exploratory development are listed in SECTION VIII. The order in which they are listed is not an indication of preference as to priority.

SECTION II

MATHEMATICAL FLOW MODEL AND FLOW COMPUTATIONS

INTRODUCTION

The total problem of understanding the performance of illuminating flares involves the complex interaction of a large number of disciplines, including chemistry, thermodynamics, radiation, heat conduction and fluid mechanics. To understand how these disciplines interact in an illuminating flare, it is necessary to have a mathematical model that acts as the structure, or skeleton, on which new knowledge can be placed in proper relationship to older knowledge, and on which the interaction among disciplines can be viewed in proper perspective.

The development of the above model is itself a complex undertaking; thus, the purpose of Part I of this report is to make only an initial, or preliminary, effort in this direction--but one that will be of some immediate use. Part I presents a mathematical model for plane, two-dimensional, incompressible, potential flow in the plume (and surrounding air) of illuminating flares dropping through the atmosphere. The analysis is followed by numerical examples that show the effect of drop rate on the flow pattern; and, finally, recommendations are given for future work on the mathematical model.

ANALYSIS

In this part of the report, assumptions are presented and equations are developed for the two-dimensional flow field within and around the plumes of illuminating flares dropping through the atmosphere.

Preliminary Considerations

An ideal model. Consider the following idealized model of an illuminating flare moving through the atmosphere with a constant drop rate v_D^* (see footnote) toward the earth's surface. The flare is a circular cylinder, of finite length, with flat ends that are normal to the axis. The axis is parallel to v_D^* and therefore perpendicular to the earth's surface. The end of the flare that faces the earth is burning, and emits a luminous plume of hot gas. This plume is surrounded by the relatively cold air of the atmosphere, which streams past the plume as a result of the drop rate v_D^* . The hot gas of the plume radiates energy to the surrounding environment, and, in addition, mixes with the colder air of the atmosphere that surrounds it. For this ideal model, flow conditions are steady and axi-symmetric. Thus, the velocity components and the gaseous composition, density and temperature are functions of only two coordinates: (1) distance measured along the axis, and (2) distance measured normal to the axis. The flow is two-dimensional, compressible and viscous.

The above ideal model, when properly executed, should give a reasonably satisfactory picture of the flow field in and around the plume of a homogenous, illuminating flare operating under ideal, steady-state conditions. In this report, an initial step is taken toward the long-range goal represented by the above model.

Assumptions. For the mathematical model of this report, which model is preliminary, it is assumed that the essential features of the two-dimensional flow field are similar for axi-symmetric and for plane two-dimensional flow. Thus, it is assumed that the two-dimensional flow is planar. Such plane, two-dimensional flows would occur for solid flare bodies with the same profile in the flow plane (see figure 1) as the axi-symmetric flare, but with an infinite extent normal to the plane, as shown in figure 1(b).

Symbols are defined in Appendix I. Velocities and linear quantities marked by an asterisk are dimensional; otherwise, non-dimensional.

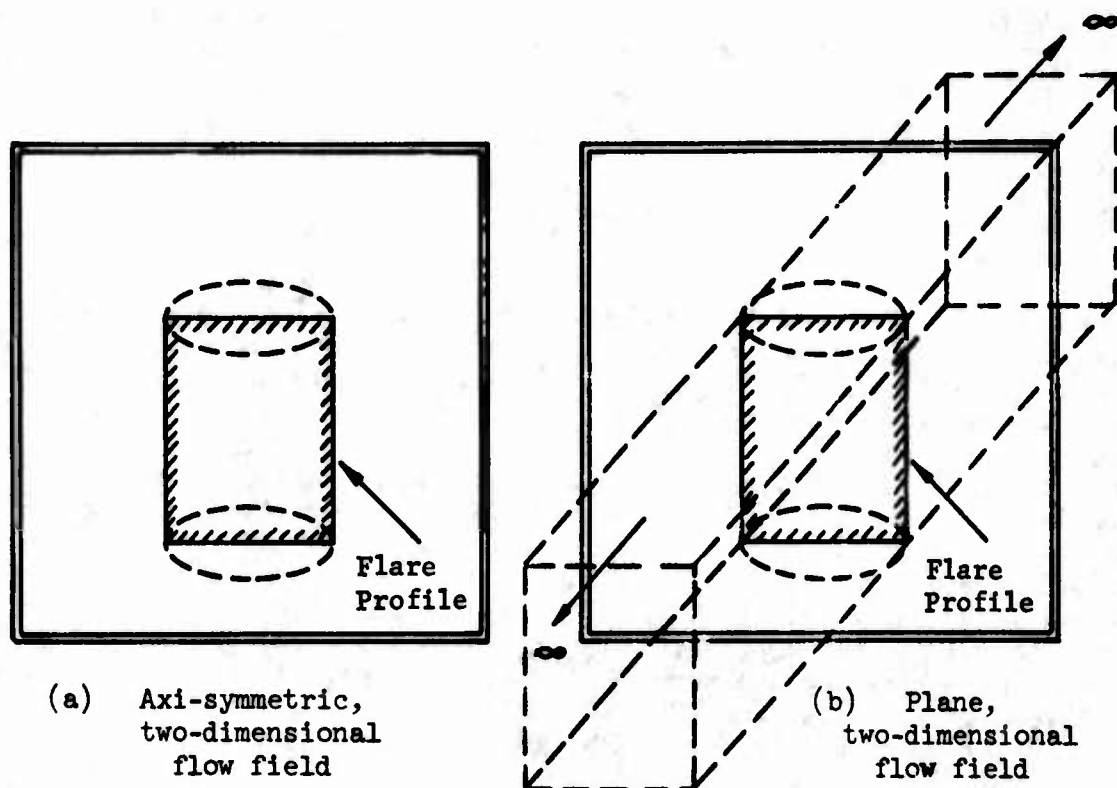


Figure 1. - Comparison of cylindrical flare geometry, for axi-symmetric, two-dimensional flow field, with rectangular parallelopiped flare geometry, for plane, two-dimensional flow field.

As in the ideal model of the preceding section, the burning surface of the flare is assumed to be flat, and in particular, no boundary wall is formed by the inhibitor downstream from the burning face.

Additional assumptions of this analysis are:

(1) The burning rates v_B^* of flares are sufficiently low that resulting Mach numbers are small and aerodynamic compressibility effects can be neglected. [Based on usual burning rates, the velocity components normal to the burning surface are low. However, it will be shown later in this report that at the edge of the burning surface, very high velocities are possible. Errors associated with this "edge" effect are ignored in this preliminary analysis.]

(2) The drop rates v_D^* of flares are sufficiently low that resulting Mach numbers are small and aerodynamic compressibility effects can be neglected.

(3) The temperatures of the flares and of the surrounding medium are constant and equal (isothermal flares). Thus, the analysis does not include the effects of radiation and mixing on the dynamics of the flow pattern. And, more importantly, the analysis assumes that the temperatures, and therefore the densities, of the plume and of the surrounding air in the atmosphere are the same. [Of course, the much higher density of the surrounding air has, in fact, a dominant influence on the shape of the plume. This influence will be accounted for in this analysis by introduction of an "effective" drop rate for the flare. Also, note that in the absence of drop rate, buoyancy forces can be expected to play an important role affecting plume configuration.]

(4) The flow is irrotational. This flow condition results if the fluid is iso-energetic (see assumption number 3) and if forces acting on the fluid are conservative (i.e., if viscous and mixing forces, for example, are negligible).

From the above assumptions, the flow is plane, two-dimensional, incompressible and irrotational. The flow is therefore given by the complex potential $w = \phi + i\psi$ as an analytic function of the complex variable $z = x + iy$. Thus,

$$w = \phi + i\psi = w(z) = w(x + iy) \quad (1)$$

where ψ is the stream function (constant along streamlines), ϕ is the velocity potential (constant along lines normal to the streamlines), and where x and y are the abscissa and ordinate, respectively, in the z -plane.

Coordinates in the physical z -plane. The two-dimensional flow field within and around the plume of the flare lies in the physical z -plane. The x - y coordinate system of the z -plane is attached to the burning face of the flare, as shown in figure 2. In this analysis, linear distance is dimensionless (unless marked by an asterisk), being expressed in units of the half-width, or radius r^* , of the burning face. Thus, the burning surface of the flare lies on the x -axis between ± 1.0 . The centerline of the flare lies on the y -axis, and the sides of the flare extend indefinitely far downward, in the negative y -direction, starting from the ± 1.0 positions on the x -axis (see figure 2). Because the flow field is symmetrical about the y -axis, the analysis and numerical results are limited to positive values of x .

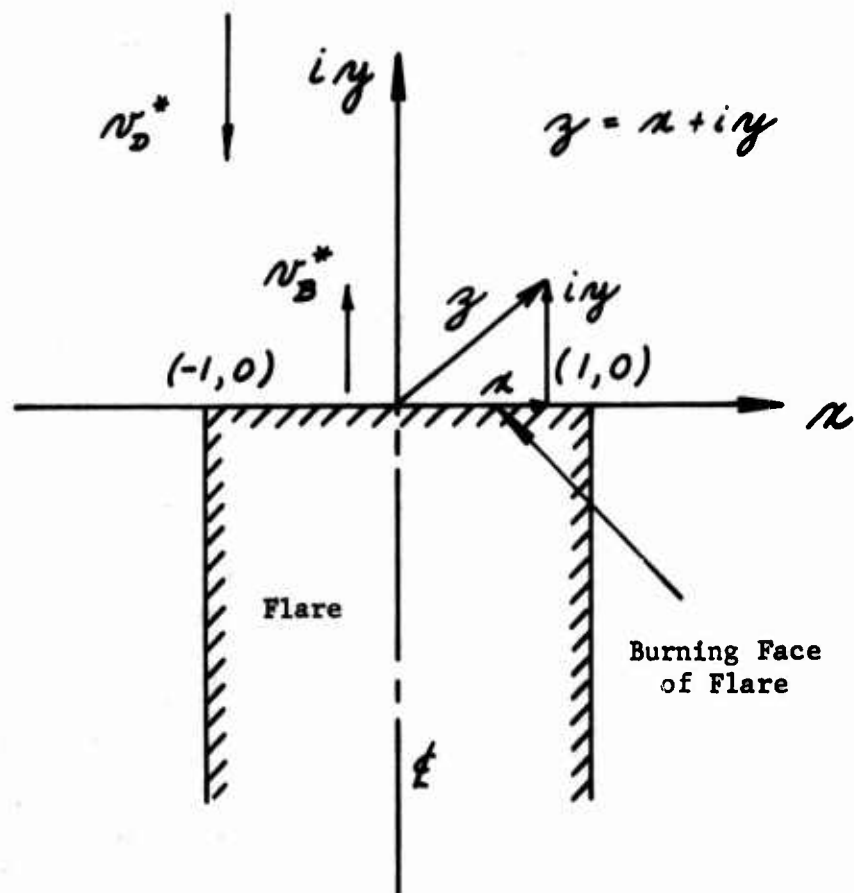


Figure 2. - xy -coordinates in the physical z -plane, together with vector directions for drop rate v_D^* and burning rate v_B^* .

Velocity components. Because the coordinate system is attached to the flare, which itself moves through the atmosphere with a constant drop rate v_D^* , velocities in the z -plane are measured relative to the flare. Thus, for the flare orientation given in figure 2, the velocity component v_B^* of the plume gases normal to the burning surface is in the positive y -direction, and the relative velocity of the atmosphere, due to the drop rate v_D^* , is in the negative y -direction (see figure 2).

At any given point in the flow field, the (relative) velocity q has components u and v in the x and y directions, respectively, (see figure 3). Thus,

$$q = \sqrt{u^2 + v^2} \quad (2a)$$

and

$$\alpha = \tan^{-1}\left(\frac{v}{u}\right) \quad (2b)$$

where α is the flow direction measured counterclockwise from the x -axis.

In this analysis, velocities are dimensionless (unless marked by an asterisk), being expressed in units of the (constant) velocity component v_B^* normal to the burning surface. Thus, along the burning surface, v (but not q) is constant and equal to 1.0.

Outline of the method. Because $w = \phi + i\psi$ is an analytic function of $z = x + iy$, the governing equations are linear. Thus, it is possible to synthesize the flow of gases within the plume (due to burning rate v_B^*) and the flow of air outside the plume (due to drop rate v_D^*) by the proper superposition of flow elements. To do this synthesis, however, it is first necessary to simplify the flow boundaries by transforming the flow field exterior to the flare in the z -plane to the upper half of the $t = \xi + i\eta$ plane (figure 4). Thus, the rectangular shape of the flare in the physical z -plane transforms into a straight line (the ξ -axis) in the transformed t -plane. This transformation is obtained from the Schwarz-Christoffel Theorem. The transformation is made so that the edges of the burning surface at ± 1.0 on the x -axis in the z -plane transform into the points ± 1.0 on the ξ -axis in the t -plane.

Now, in the t -plane, the flow field associated with the drop rate v_D^* of the flare is given by an "approach flow" (figure 5a) that impinges on the ξ -axis from large positive values of η . This flow field in the t -plane transforms (Schwarz-Christoffel transformation) into the z -plane as shown in figure 5b.

Likewise, in the t -plane, the flow field associated with the burning rate v_B^* at the flare surface is given by a distribution of point sources (figure 6a) along the ξ -axis between ± 1.0 . This flow field in the t -plane transforms (Schwarz-Christoffel transformation) into the z -plane as shown in figure 6b.

Finally, again in the t -plane, the two flows from figures 5a and 6a are combined by linear superposition to give the combined flow (figure 7a) due to the drop rate v_D^* and the burning rate v_B^* . This combined flow field in the t -plane transforms (Schwarz-Christoffel) into the z -plane as shown in figure 7b.

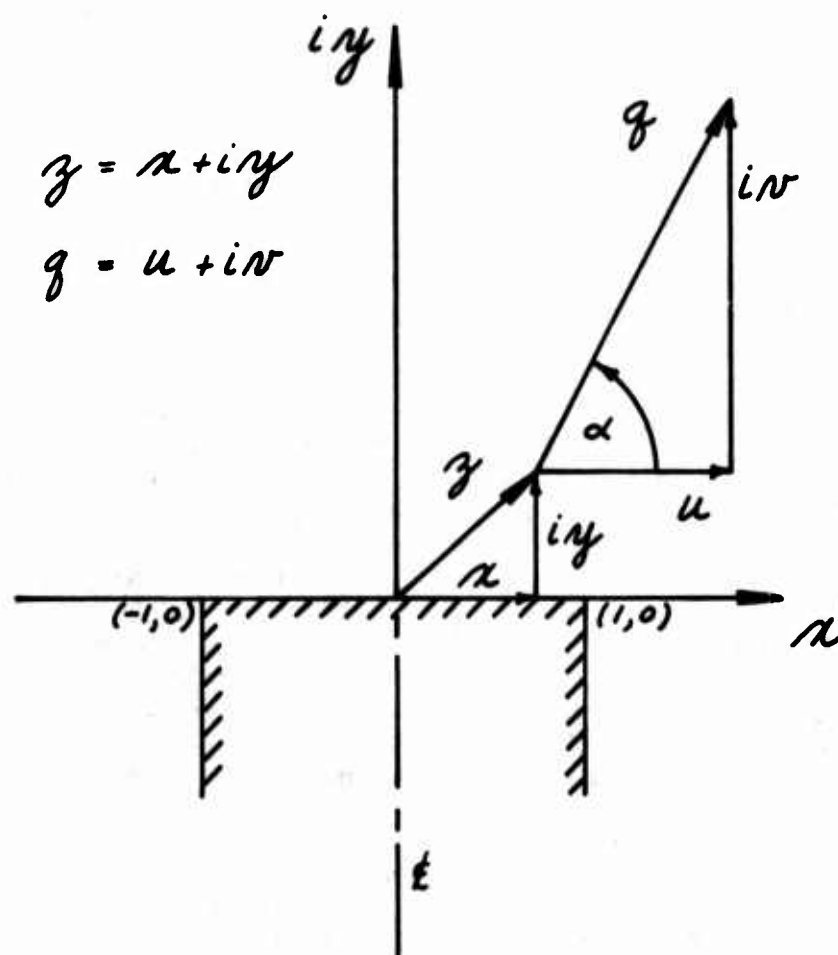


Figure 3. - Relative velocity triangle in the physical z -plane.

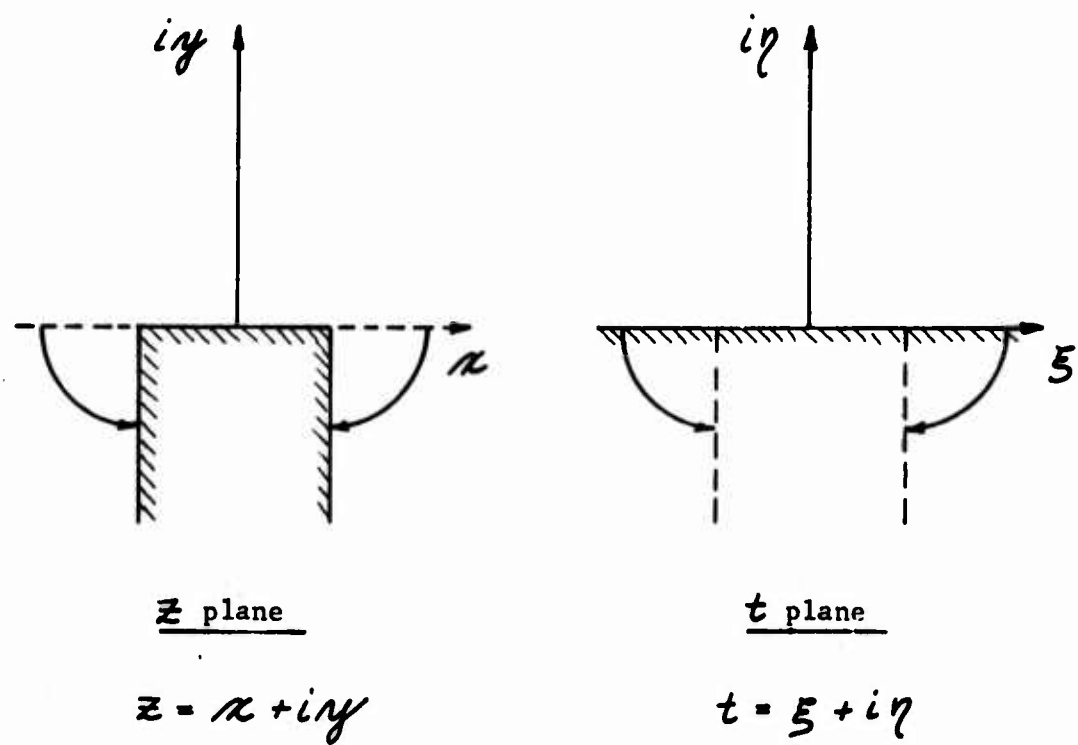
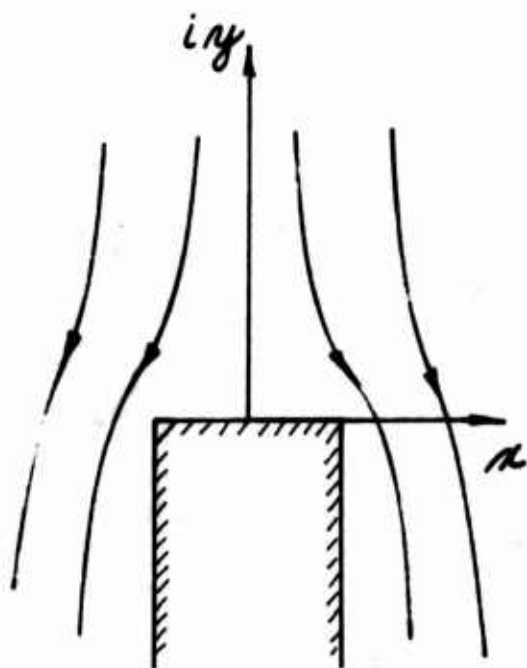


Figure 4. - Schwarz-Christoffel transformation from exterior of flare in z -plane to upper-half of t -plane.

(b) z - plane



(a) t - plane

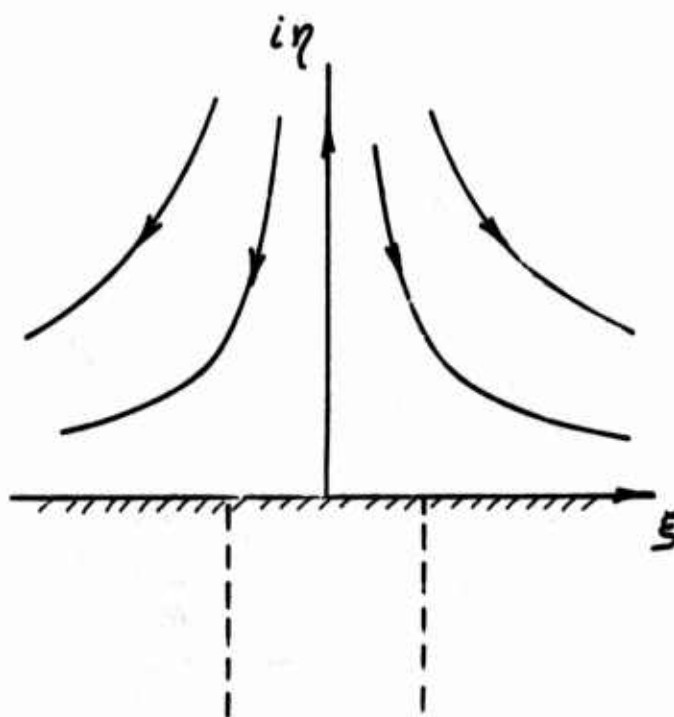


Figure 5. - "Approach flow", due to drop rate of flare, in (a) transformed t -plane, and (b) physical z -plane.

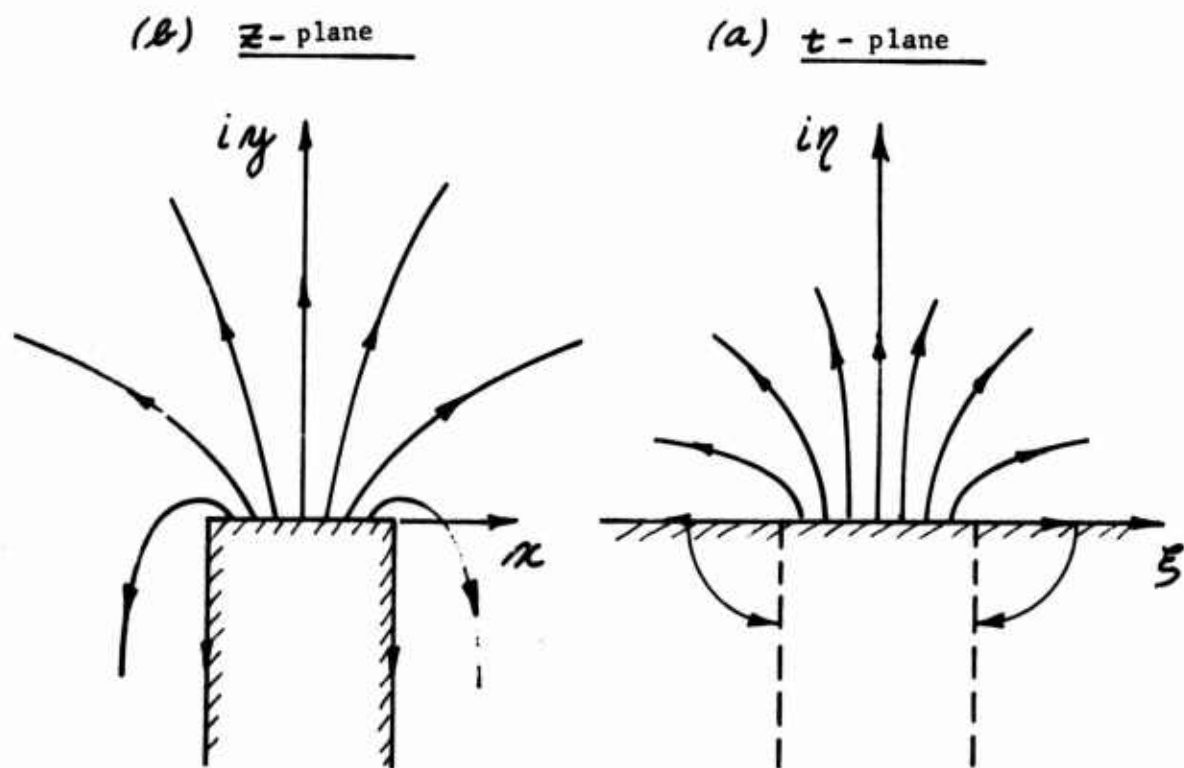


Figure 6. - "Source flow", due to burning rate of flare, in (a) transformed t-plane, and (b) physical z-plane.

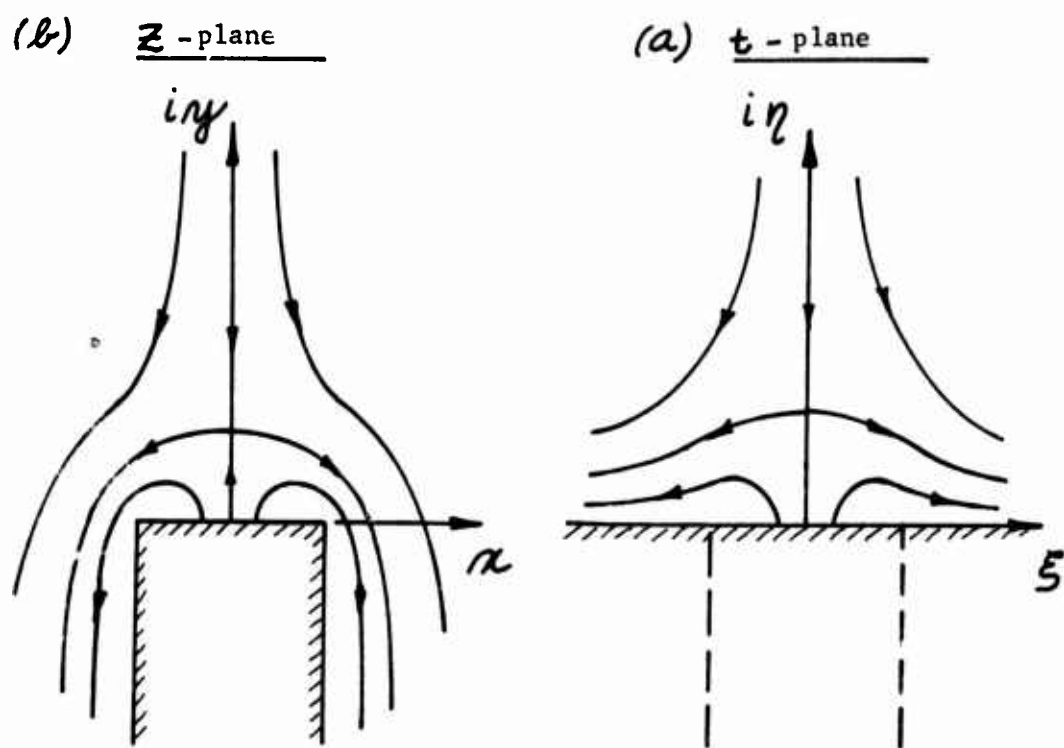


Figure 7. - Combined flows, from figures 5 and 6, in (a) transformed t-plane, and (b) physical z-plane.

From the above synthesis in the t -plane and the subsequent transformation onto the z -plane, the distributions of streamlines (constant ψ) and velocity potential lines (constant ϕ) are known in the physical flow field (z -plane). From these distributions of ϕ and ψ , the velocity components, flow direction and other related parameters of the flow field can be determined.

The remainder of this analysis develops the equations for plane, two-dimensional flow within and around the plumes of illuminating flares, dropping through the atmosphere, according to the methods outlined above.

Schwarz-Christoffel Transformation

General theorem. The Schwarz-Christoffel transformation maps the inside of an arbitrary, simple, closed polygon in the z -plane onto the upper half of the t -plane (see figure 8 of this report, and reference 1, pages 156-163). The transformation is given by

$$z = A \int \frac{dt}{(a-t)^{\alpha/\pi} (b-t)^{\beta/\pi} (c-t)^{\gamma/\pi} \dots} + B \quad (3a)$$

where a, b, c, \dots are locations in ascending order on the real ξ -axis of the t -plane corresponding to the vertices of the polygon in the z -plane, where $\alpha, \beta, \gamma, \dots$ are deflection angles (positive or negative) at the corresponding vertices in the z -plane (see figure 8), and where A and B are complex constants that determine the size, angular orientation and location of the polygon in the z -plane. It is observed that when the vertex of a polygon is located at infinity on the ξ -axis in the t -plane, the term involving that vertex becomes unity in equation (3a).

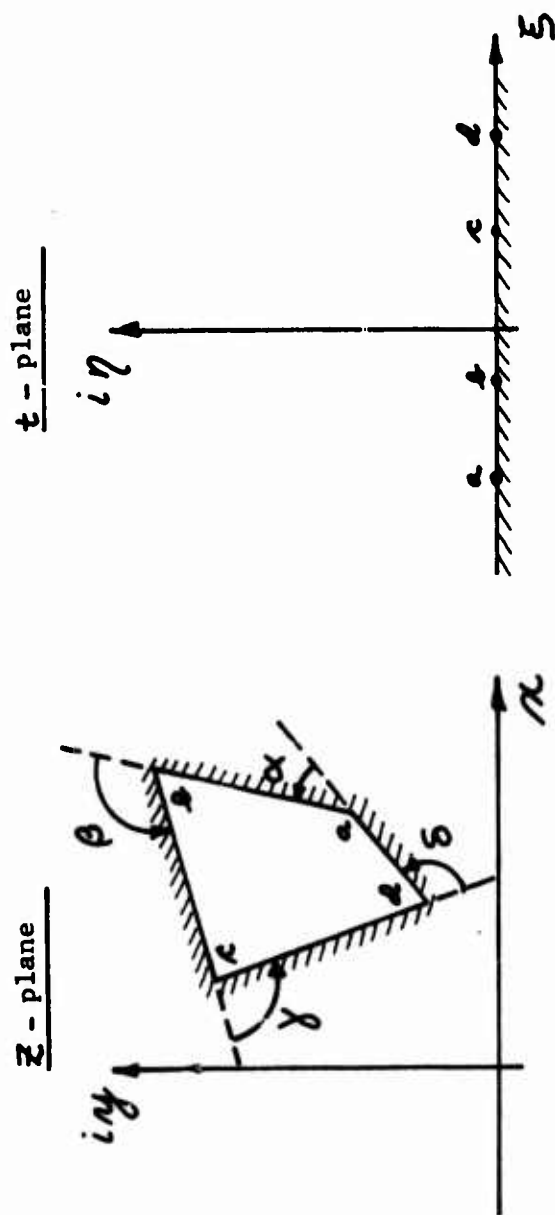
Schwarz-Christoffel transformation for rectangular flare. The polygon corresponding to the rectangular profile of a flare in the z -plane is shown in figure 9. The interior of the polygon corresponds to the flow field exterior to the body of the flare. It is noted that six of the eight vertices are located at infinity (the other two being located at ± 1.0 on the x -axis). If these six vertices are located at infinity on the ξ -axis of the t -plane, then all but two terms in the integrand of equation (3a) become unity. Thus,

$$z = A \int \frac{dt}{(a-t)^{\alpha/\pi} (b-t)^{\beta/\pi}} + B \quad (3b)$$

If the two vertices at ± 1.0 on the x -axis are located at ± 1.0 , respectively, on the ξ -axis of the t -plane, then

$$\left. \begin{array}{l} a = -1.0 \\ b = +1.0 \end{array} \right\} \quad (3c)$$

Furthermore, from figures (8) and (9),



$$\frac{dz}{dt} = A(a-t)^{-\alpha/\pi}(b-t)^{-\beta/\pi}(c-t)^{-\gamma/\pi} \dots$$

Figure 8. - General form of Schwarz-Christoffel transformation, showing deflection angles $\alpha, \beta, \gamma, \dots$ at vertices in z-plane, and corresponding locations a, b, c, \dots of vertices in t-plane.

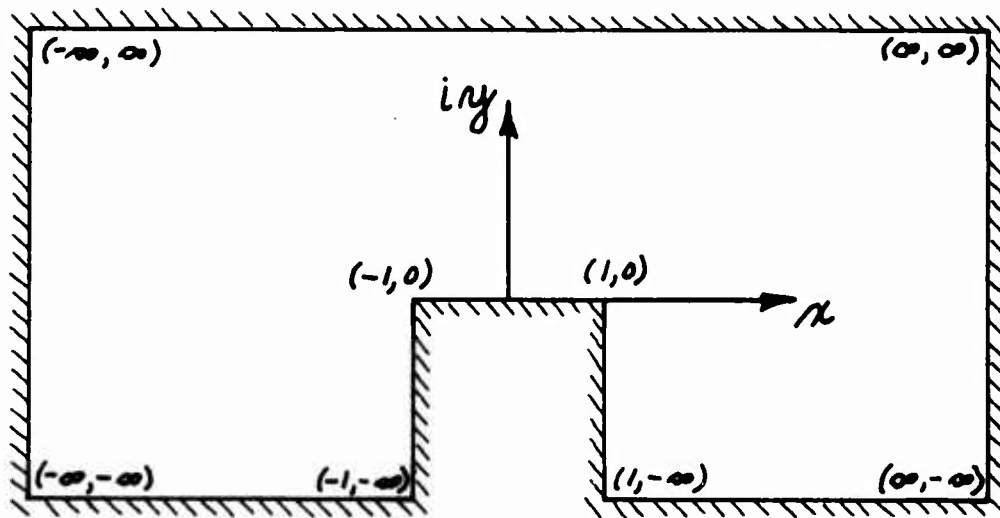


Figure 9. - Simple, closed polygon corresponding to rectangular profile of flare in physical z-plane.

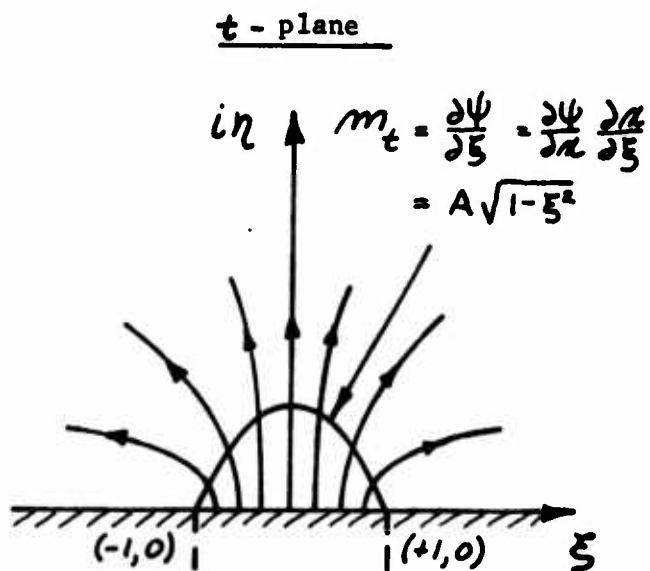


Figure 10. - Continuous distribution of source strength m_t along burning face of flare.

$$\left. \begin{aligned} \alpha &= -\pi/2 \\ \beta &= -\pi/2 \end{aligned} \right\} \quad (3d)$$

where the negative signs indicate clockwise deflection angles. Thus, equation (3b) becomes

$$z = A \int \sqrt{-(1+t)(1-t)} \, dt + B$$

which integrates to give

$$z = i \left(\frac{A}{2} \right) \left[t \sqrt{1-t^2} + \sin^{-1} t \right] + B \quad (3e)$$

The constants A and B equal $-(4i/\pi)$ and 0, respectively, if the vertices at ± 1.0 on the x-axis are located at ± 1.0 on the ξ -axis in the t-plane, and if the origin on the z-plane maps into the origin on the t-plane. Thus,

$$z = \frac{2}{\pi} \left[t \sqrt{1-t^2} + \sin^{-1} t \right] \quad (3f)$$

Equation (3f) is the Schwarz-Christoffel transformation that maps the exterior of a rectangular flare in the z-plane on the upper-half of the t-plane. This transformation relates the location of any point (ξ, η) in the t-plane to the location of a corresponding point (x, y) in the z-plane, and vice versa.

Equations relating x and y to ξ and η . In equation (3f),

$$\text{and} \quad \left. \begin{aligned} z &= x + i y \\ t &= \xi + i \eta \end{aligned} \right\} \quad (4)$$

Substituting equations (4) into equation (3f), and equating the real terms, and also the imaginary terms, on opposite sides of the equation, gives

$$x = \left(\frac{2}{\pi} \right) \left\{ \left[\xi \cos \frac{\theta}{2} - \eta \sin \frac{\theta}{2} \right] \sqrt{R} + \tan^{-1} \left[\frac{\xi + \sqrt{R} \sin \frac{\theta}{2}}{-\eta + \sqrt{R} \cos \frac{\theta}{2}} \right] \right\} \quad (5a)$$

and

$$y = \left(\frac{2}{\pi} \right) \left\{ \left[\eta \cos \frac{\theta}{2} + \xi \sin \frac{\theta}{2} \right] \sqrt{R} - \frac{1}{2} \ln \left[(-\eta + \sqrt{R} \cos \frac{\theta}{2})^2 + (\xi + \sqrt{R} \sin \frac{\theta}{2})^2 \right] \right\} \quad (5b)$$

where

$$R = \sqrt{(1-\xi^2 + \eta^2)^2 + (2\xi\eta)^2} \quad (5c)$$

and

$$\theta = \tan^{-1} \left(\frac{-2\xi\eta}{1-\xi^2 + \eta^2} \right) \quad (5d)$$

In equation (5a),

$$0 \leq \tan^{-1} \left[\frac{\xi + \sqrt{R} \sin \frac{\theta}{2}}{-\eta + \sqrt{R} \cos \frac{\theta}{2}} \right] \leq \pi \quad (5e)$$

Also, in equation (5d),

$$\left. \begin{array}{l} \text{(a)} \quad -\pi \leq \theta \leq 0 \\ \text{(b)} \quad \text{If } \eta \text{ equals zero, then} \\ \quad \theta = 0 \quad \text{when } \xi < 1 \\ \quad \theta = -\pi \quad \text{when } \xi > 1 \\ \text{(c)} \quad \text{If } \xi \text{ equals zero, then} \\ \quad \theta = 0 \end{array} \right\} \quad (5f)$$

Equations (5a) and (5b) relate x and y in the z -plane to the corresponding point (ξ, η) in the t -plane.

Synthesis of Flow in Transformed t -plane

The flow field in the t -plane is synthesized by combining the complex potential ($w = \phi + i\psi$) for an "approach flow" (figure 5a), which is associated with the drop rate v_D^* , with the complex potential for a source distribution (figure 6a), which is associated with the burning rate v_B^* .

Complex potential w_1 for point-source distribution along ξ -axis. The efflux of gas from the burning surface of flares is simulated in the t -plane by a distribution of point sources along the ξ -axis between ± 1.0 . The complex potential w_1 associated with this distribution of point sources is given by

$$w_1 = \phi_1 + i\psi_1 = \int_{-1}^{+1} m_t(\xi) \ln(t-\xi) d\xi \quad (6a)$$

where the source strength $m_t(\xi)$ is a function of ξ over the range ± 1.0 (see figure 10).

The local source strength $m_t(\xi)$ determines the local gradient of ψ along the burning surface. Thus,

$$m_t(\xi) = (\text{constant}) \frac{\partial \psi}{\partial \xi}$$

But,

$$\frac{\partial \psi}{\partial \xi} = \frac{\partial \psi}{\partial x} \frac{dx}{d\xi}$$

so that

$$m_t(\xi) = (\text{constant}) \frac{\partial \psi}{\partial x} \frac{dx}{d\xi} \quad (6b)$$

Now, in the physical z -plane, because of the uniform generation of gases across the burning face of the flare, the distribution of point sources along the burning face is constant. Thus,

$$m_z(x) = (\text{constant}) \frac{\partial \psi}{\partial x} = \text{constant} \quad (6c)$$

Also, from equation (5a), with η equal to zero,

$$\frac{dx}{d\xi} = \left(\frac{4}{\pi}\right) \sqrt{1-\xi^2} \quad (6d)$$

Thus, from equations (6b), (6c) and (6d),

$$m_t(\xi) = (\text{constant}) \sqrt{1-\xi^2}$$

and equation (6a) becomes

$$w_1 = A_1 \int_{-1}^{+1} \sqrt{1-\xi^2} \ln(t-\xi) d\xi \quad (6e)$$

where A_1 is a (real) constant to be determined.

Equation (6e) integrates (Appendix II) to give

$$w_1 = \frac{A_1}{2} \left[t^2 - t \sqrt{t^2-1} + \ln(t + \sqrt{t^2-1}) \right] + (B_\phi + i B_\psi) \quad (6f)$$

where $(B_\phi + i B_\psi)$ is a complex constant of integration, to be determined later. Equation (6f) gives the complex potential w_1 for the point-source distribution (along the ξ -axis) associated with the burning rate v_B^* of the flare.

Equations for ϕ_1 and ψ_1 in t -plane. In equation (6f),

$$\left. \begin{aligned} w_1 &= \phi_1 + i \psi_1 \\ \text{and} \quad t &= \xi + i \eta \end{aligned} \right\} \quad (6g)$$

Substituting equations (6g) into equation (6f) and equating real terms on opposite sides of the resulting equation gives

$$\phi_1 = \frac{A_1}{2} \left[(\xi - \eta^2) - \sqrt{R} \left(\xi \cos \frac{\beta}{2} - \eta \sin \frac{\beta}{2} \right) + \ln \sqrt{(\xi + \sqrt{R} \cos \frac{\beta}{2})^2 + (\eta + \sqrt{R} \sin \frac{\beta}{2})^2} \right] + B_\phi \quad (6h)$$

and, likewise, equating imaginary terms gives

$$\psi_1 = \frac{A_1}{2} \left[2\xi\eta - \sqrt{R} \left(\eta \cos \frac{\beta}{2} + \xi \sin \frac{\beta}{2} \right) + \tan^{-1} \left(\frac{\eta + \sqrt{R} \sin \frac{\beta}{2}}{\xi + \sqrt{R} \cos \frac{\beta}{2}} \right) \right] + B_\psi \quad (6i)$$

where R is given by equation (5c) and where

$$\beta = \tan^{-1} \left(\frac{2\xi\eta}{\xi^2 - \eta^2 - 1} \right) \quad (6j)$$

To determine the constants A_1 , B_ϕ and B_ψ , first note that

$$\frac{\partial \psi_1}{\partial x} = -v_1$$

Thus, in the z-plane, along the burning face of the flare on the x-axis ($0 \leq x \leq 1.0$), where, by definition, v_1 is equal to 1.0,

$$\Delta \psi_1 = - \int_0^{1.0} dx = -1.0$$

Therefore, if ψ_1 is arbitrarily set equal to 1.0 at the origin ($x = 0$), then ψ_1 is equal to 0 at the edge ($x = 1.0$). These same values of ψ_1 must exist at the corresponding points (0 and 1.0) along the ξ -axis in the t-plane. Thus, to establish A_1 , B_ϕ and B_ψ , let

$$\left. \begin{aligned} \psi_1 &= 1.0 \quad \text{when } \xi = 0 \text{ and } \eta = 0 \\ \psi_1 &= 0 \quad \text{when } \xi = 1.0 \text{ and } \eta = 0 \\ \phi_1 &= 0 \quad \text{when } \xi = 0 \text{ and } \eta = 0 \end{aligned} \right\} \quad (6k)$$

In (6k), ϕ_1 has been arbitrarily assigned the value zero when $\xi = 0$ and $\eta = 0$.

From equations (6h), (6i) and the conditions given by (6k)

$$\left. \begin{aligned} A_1 &= 4/\pi \\ B_\phi &= 0 \\ B_\psi &= 0 \end{aligned} \right\} \quad (6l)$$

Equations (6h), (6i) and (6l) determine ϕ_1 and ψ_1 as functions of ξ and η in the t-plane.

Complex potential w_2 for "approach flow". The drop rate of flares is simulated in the t-plane by an "approach flow" (figure 5a) that impinges on the ξ -axis from large (infinite) positive values of η . The complex potential w_2 associated with this approach flow is given by

$$w_2 = \phi_2 + i \psi_2 = \frac{A_2}{2} t^2 \quad (7a)$$

where A_2 is a constant, to be determined later.

Equations for ϕ_2 and ψ_2 in t-plane. In equation (7a),

$$\left. \begin{aligned} w_2 &= \phi_2 + i \psi_2 \\ \text{and} \\ t &= \xi + i \eta \end{aligned} \right\} \quad (7b)$$

Substituting equations (7b) into equation (7a) and equating real terms on opposite sides of the resulting equation gives

$$\phi_2 = \frac{A_2}{2} (\xi^2 - \eta^2) \quad (7c)$$

and, likewise, equating imaginary terms gives

$$\psi_2 = \frac{A_2}{2} (2\xi\eta) \quad (7d)$$

To determine A_2 , note that at large (infinite) values of y in the z -plane the (dimensionless) velocity v_2 is given by

$$v_2 = \frac{-v_D^{**}}{v_B^*} = -K \quad (7e)$$

where v_D^{**} is the "effective" drop rate of the flare (to be defined and evaluated later). But,

$$v_2 = \frac{\partial \phi_2}{\partial y} = \frac{\partial \phi_2}{\partial \eta} \frac{d\eta}{dy} \quad (7f)$$

where, from equation (7c),

$$\frac{\partial \phi_2}{\partial \eta} = -A_2 \eta \quad (7g)$$

and, from equation (5b), for large (infinite) values of η and small (zero) values of ξ ,

$$\frac{dy}{d\eta} = \left(\frac{4}{\pi} \right) \eta \quad (7h)$$

so that, from equations (7e), (7f), (7g) and (7h),

$$A_2 = \left(\frac{4}{\pi} \right) K \quad (7i)$$

Equations (7c), (7d) and (7i) determine ϕ_2 and ψ_2 as functions of ξ and η in the t -plane.

Combined complex potential w . Because w_1 and w_2 are analytic, they can be combined linearly to obtain the complex potential w for the combined flow field associated with the drop rate of a two-dimensional flare and with its burning rate. Thus,

$$w = w_1 + w_2$$

or

$$w = \phi + i\psi = (\phi_1 + \phi_2) + i(\psi_1 + \psi_2) \quad (8)$$

Equation (8) is the complex potential for the combined flows.

Final equations for ϕ and ψ in t -plane. From equation (8)

$$\begin{aligned} \phi &= \phi_1 + \phi_2 \\ \psi &= \psi_1 + \psi_2 \end{aligned} \quad (9a)$$

so that, from equations (6b), (6k), (7c), (7i) and (9a),

$$\begin{aligned} \phi &= \left(\frac{2}{\pi}\right) \left[(\xi^2 - \eta^2) - \sqrt{R} \left(\xi \cos \frac{\beta}{2} - \eta \sin \frac{\beta}{2} \right) + \ln \sqrt{(\xi + \sqrt{R} \cos \frac{\beta}{2})^2 + (\eta + \sqrt{R} \sin \frac{\beta}{2})^2} \right] \\ &\quad + K \left(\frac{2}{\pi}\right) (\xi^2 - \eta^2) \end{aligned} \quad (9b)$$

where

$$\begin{aligned} \beta &= \tan^{-1} \left(\frac{2\xi\eta}{\xi^2 - \eta^2 - 1} \right) \\ (a) \quad 0 &\leq \beta \leq \pi \\ (b) \quad \text{If } \eta &= 0, \text{ then } \beta = \pi, \text{ when } \xi < 1.0 \\ &\quad \text{If } \eta = 0, \text{ then } \beta = 0, \text{ when } \xi > 1.0 \\ &\quad \text{If } \xi = 0, \text{ then } \beta = \pi \end{aligned} \quad (9c)$$

and, from equations (6i), (6k), (7d), (7i) and (9a)

$$\begin{aligned} \psi &= \left(\frac{2}{\pi}\right) \left[2\xi\eta - \sqrt{R} \left(\eta \cos \frac{\beta}{2} + \xi \sin \frac{\beta}{2} \right) + \tan^{-1} \left(\frac{\eta + \sqrt{R} \sin \frac{\beta}{2}}{\xi + \sqrt{R} \cos \frac{\beta}{2}} \right) \right] \\ &\quad + K \left(\frac{2}{\pi}\right) (2\xi\eta) \end{aligned} \quad (9d)$$

where

$$0 \leq \tan^{-1} \left(\frac{\eta + \sqrt{R} \sin \frac{\beta}{2}}{\xi + \sqrt{R} \cos \frac{\beta}{2}} \right) \leq \frac{\pi}{2} \quad (9e)$$

Equations (9b) and (9d), together with the conditions specified by (9c) and (9e), determine ϕ and ψ , respectively, for the combined flow as functions of ξ and η in the t -plane.

Flow Field in Physical z-plane

Distribution of ϕ and ψ in z-plane. The distributions of ϕ and ψ as functions of ξ and η in the t-plane are known from equations (9b) and (9d), respectively. Also, the distributions of x and y as functions of ξ and η are known from equations (5a) and (5b), respectively. Therefore, from equations (5a), (5b) and (9b), the distribution of ϕ is known as a function of x and y in the physical z-plane; and likewise, from equations (5a), (5b) and (9d), the distribution of ψ is known as a function of x and y .

Distribution of u and v in z-plane. To determine the distributions of u and v in the z-plane, note that

$$\begin{aligned}\frac{\partial \phi}{\partial \xi} &= \frac{\partial \phi}{\partial x} \frac{\partial x}{\partial \xi} + \frac{\partial \phi}{\partial y} \frac{\partial y}{\partial \xi} \\ &= u \frac{\partial x}{\partial \xi} + v \frac{\partial y}{\partial \xi}\end{aligned}\tag{10a}$$

and

$$\begin{aligned}\frac{\partial \phi}{\partial \eta} &= \frac{\partial \phi}{\partial x} \frac{\partial x}{\partial \eta} + \frac{\partial \phi}{\partial y} \frac{\partial y}{\partial \eta} \\ &= u \frac{\partial x}{\partial \eta} + v \frac{\partial y}{\partial \eta}\end{aligned}\tag{10b}$$

Equations (10a) and (10b) can be solved for u and v . Thus,

$$u = \frac{\left(\frac{\partial \phi}{\partial \xi}\right)\left(\frac{\partial y}{\partial \eta}\right) - \left(\frac{\partial \phi}{\partial \eta}\right)\left(\frac{\partial y}{\partial \xi}\right)}{\left(\frac{\partial x}{\partial \xi}\right)\left(\frac{\partial y}{\partial \eta}\right) - \left(\frac{\partial x}{\partial \eta}\right)\left(\frac{\partial y}{\partial \xi}\right)}\tag{10c}$$

and

$$v = \frac{\left(\frac{\partial \phi}{\partial \xi}\right)\left(\frac{\partial x}{\partial \eta}\right) - \left(\frac{\partial \phi}{\partial \eta}\right)\left(\frac{\partial x}{\partial \xi}\right)}{\left(\frac{\partial y}{\partial \xi}\right)\left(\frac{\partial x}{\partial \eta}\right) - \left(\frac{\partial y}{\partial \eta}\right)\left(\frac{\partial x}{\partial \xi}\right)}\tag{10d}$$

The various terms on the right hand sides of equations (10c) and (10d) are obtained from equations (5a), (5b) and (9b). Thus, from equation (5a),

$$\frac{\partial x}{\partial \eta} = \left(\frac{2}{\pi}\right) \left[-(GG) - \frac{\sqrt{R}}{2} (I)(E) + \frac{(H)(C)}{2\sqrt{R}} \right]\tag{10e}$$

and

$$\frac{\partial x}{\partial \xi} = \left(\frac{2}{\pi}\right) \left[G - \frac{\sqrt{R}}{2} (I)(D) + \frac{(H)(B)}{2\sqrt{R}} \right]\tag{10f}$$

where

$$\begin{aligned}
 A &= (1 - \xi^2 + \eta^2)^2 + (2\xi\eta)^2 \\
 B &= \frac{\partial R}{\partial \xi} = \frac{1}{\sqrt{A}} \left[2\xi(\xi^2 - 1) + 2\xi\eta^2 \right] \\
 C &= \frac{\partial R}{\partial \eta} = \frac{1}{\sqrt{A}} \left[2\eta(1 + \eta^2) + 2\xi^2\eta \right] \\
 D &= \frac{\partial \theta}{\partial \xi} = \frac{1}{A} \left[-2\eta(1 + \xi^2 + \eta^2) \right] \\
 E &= \frac{\partial \theta}{\partial \eta} = \frac{1}{A} \left[-2\xi(1 - \xi^2 - \eta^2) \right] \\
 F &= (-\eta + \sqrt{R} \cos \frac{\theta}{2})^2 + (\xi + \sqrt{R} \sin \frac{\theta}{2})^2 \\
 G &= \sqrt{R} \cos \frac{\theta}{2} + \frac{1}{F} (-\eta + \sqrt{R} \cos \frac{\theta}{2}) \\
 GG &= \sqrt{R} \sin \frac{\theta}{2} - \frac{1}{F} (\xi + \sqrt{R} \sin \frac{\theta}{2}) \\
 H &= (\xi \cos \frac{\theta}{2} - \eta \sin \frac{\theta}{2}) - \frac{1}{F} (\xi \cos \frac{\theta}{2} + \eta \sin \frac{\theta}{2}) \\
 I &= (\eta \cos \frac{\theta}{2} + \xi \sin \frac{\theta}{2}) - \frac{1}{F} (-\eta \cos \frac{\theta}{2} + \xi \sin \frac{\theta}{2} + \sqrt{R})
 \end{aligned} \tag{10g}$$

Next, from equation (5b),

$$\frac{\partial y}{\partial \eta} = \left(\frac{2}{\pi} \right) \left[G + \frac{\sqrt{R}}{2} (H)(E) + \frac{(I)(C)}{2\sqrt{R}} \right] \tag{10h}$$

and

$$\frac{\partial y}{\partial \xi} = \left(\frac{2}{\pi} \right) \left[(GG) + \frac{\sqrt{R}}{2} (H)(D) + \frac{(I)(B)}{2\sqrt{R}} \right] \tag{10i}$$

Then, from equation (9b),

$$\frac{\partial \phi}{\partial \xi} = \left(\frac{4}{\pi} \right) \left[(1 + K) \xi - \sqrt{R} \cos \frac{\theta}{2} \right] \tag{10j}$$

and

$$\frac{\partial \phi}{\partial \eta} = \left(\frac{4}{\pi} \right) \left[-(1 + K)\eta + \sqrt{R} \sin \frac{\theta}{2} \right] \tag{10k}$$

Thus, the velocity components u and v in the z -plane are given as functions of ξ and η by equations (10c) and (10d), respectively, together with the auxiliary equations (10e), (10f), (10g), (10h), (10i), (10j) and (10k). Finally, because x and y are known functions of ξ and η from equations (5a) and (5b), the velocity components u and v in the z -plane are known functions of x and y .

Distribution of q and α in z -plane. From the preceding section, the distributions of u and v in the z -plane are known. Thus, from figure 3,

$$q = \sqrt{u^2 + v^2} \quad (11a)$$

and

$$\alpha = \tan^{-1}\left(\frac{v}{u}\right) \quad (11b)$$

Equations (11a) and (11b) determine the distributions of q and α in the z -plane.

Drop rate parameter K . The drop rate parameter K is defined in equation (7e) as the ratio of "effective" drop rate v_D^{**} to actual burning velocity v_B^* . Thus,

$$K = \frac{v_D^{**}}{v_B^*} \quad (7e)$$

First, consider the "effective" drop rate v_D^{**} . So far, in this analysis, the density of the plume and the density of the surrounding air have been treated as equal. In fact, they are not, and, as pointed out in the section on assumptions, the higher momentum of the drop rate due to the higher density of the air must have an important influence on the shape and extent of the plume. To correct for this influence, an "effective" drop rate v_D^{**} is defined so that the momentum of the "effective" drop rate based on plume density is equal to the momentum of the actual drop rate based on air density. Thus,

$$v_D^{**} \rho_{\text{gas}} = v_D^* \rho_{\text{air}} \quad (12a)$$

where ρ_{gas} and ρ_{air} are the actual densities of the plume gas and atmospheric air, respectively, and where v_D^* is the actual drop rate of the flare. Thus, from (12a)

$$v_D^{**} = v_D^* \left(\frac{\rho_{\text{air}}}{\rho_{\text{gas}}} \right) \quad (12b)$$

Thus, the effective drop rate v_D^{**} of the flare is equal to its actual drop rate multiplied by the ratio of air density to plume density. (Note that the effective drop rate is higher than the actual drop rate, because air density is higher than plume density.)

Next, consider the burning v_B^* . This velocity is defined as the (constant) velocity component of the plume gas normal to the burning face of the flare. From continuity considerations,

$$v_B^* \rho_{\text{gas}} = v_{\text{FL}}^* \rho_{\text{FL}} \quad (12c)$$

where v_{FL}^* and ρ_{FL} are the actual burning rate and density of the solid flare material, respectively. From equations (7e), (12b) and (12c),

$$K = \frac{v_D^{**}}{v_B^*} = \left(\frac{v_D^*}{v_{FL}^*} \right) \left(\frac{\rho_{air}}{\rho_{FL}} \right) \quad (12d)$$

Thus, from equation (12d), the drop rate parameter K , which is the only input variable for numerical calculations (other than the selection of grid points in the flow field), is equal to the ratio of actual drop rate to actual burning rate (of solid flare material) multiplied by the ratio of air density to density of solid flare material. This drop rate parameter corrects (approximately) for the influence of high-density air on the shape of the lower-density plume.

Pressure distribution in z-plane. The pressure distribution in the z-plane is obtained from the velocity distribution as follows. In the flow field of the surrounding air,

$$(p_t)_{air} = p_a + \frac{\rho_{gas}}{2g} (v_D^{**})^2 \quad (13a)$$

where p_t is total pressure and p_a is atmospheric static pressure. The density ρ_{gas} is used in equation (13a), because the "effective" drop rate v_D^{**} is used.

In the flow field of the gas plume,

$$(p_t)_{plume} = p + \frac{\rho_{gas}}{2g} (q v_B^*)^2 \quad (13b)$$

where $(q v_B^*)$ is the local (dimensional) velocity.

The total pressures in (13a) and (13b) are equal, so that subtracting (13a) from (13b) and rearranging gives

$$P = \frac{p - p_a}{\frac{\rho_{gas}}{2g} (v_B^*)^2} = K^2 - q^2 \quad (13c)$$

Equation (13c) gives the (dimensionless) static pressure parameter P in terms of the drop rate parameter K and the local (dimensionless) velocity q . For negative values of P , the local static pressure is less than atmospheric.

Stagnation point location. For flares falling through the atmosphere ($K > 0$), the maximum penetration of the plume upstream from the burning face occurs on the y-axis, as shown in figure 7(a). This point can be determined analytically by noting that it is a stagnation point. Furthermore, this stagnation point on the y-axis in the z-plane is likewise a stagnation point on the η -axis in the t-plane (see figure 7(a)). Now, from equation (10j), the velocity $\partial\phi/\partial\xi$ in the t-plane is everywhere zero along the η -axis (where ξ equals zero). Thus, the stagnation point occurs on the η -axis at that value of η (equals η_0) for which the velocity $\partial\phi/\partial\eta$ is zero. From equation (10k), with ξ equal to zero,

$$\frac{\partial \phi}{\partial \eta} = 0 = \left(\frac{4}{\pi} \right) \left[- (1 + K) \eta_0 + \sqrt{1 + \eta_0^2} \right]$$

or

$$\eta_0 = \frac{1}{\sqrt{2K + K^2}} \quad (14a)$$

Equation (14a) gives η_0 as a function of the drop rate parameter K . The corresponding value of y_0 is obtained from equation (5b) with ξ equal to zero and with η given by equation (14a). Thus,

$$y_0 = \left(\frac{2}{\pi} \right) \left[\frac{1 + K}{2K + K^2} + \frac{1}{2} \ln \left(\frac{2}{K} + 1 \right) \right] \quad (14b)$$

Equation (14b) gives the location y_0 of the stagnation point on the y -axis as a function of the drop rate parameter K . Tabulated values of y_0 as a function of K are given in the table below, and the relationship is plotted in figure 11, where it is noted that y_0 goes to infinity as the drop rate (*i.e.*, K) goes to zero.

K	y_0
0	∞
0.1	4.3038
0.2	2.4995
0.3	1.8478
0.4	1.4987
0.5	1.2762
0.6	1.1197
0.7	1.0023
0.8	0.9103
0.9	0.8359
1.0	0.7741
1.2	0.6769
1.4	0.6034
1.6	0.5455
1.8	0.4985
2.0	0.4594

Dimensionless time parameter τ . A parameter of some interest, particularly when considering the variation in fluid particle temperature with time due to radiation, is the dimensionless time parameter τ . The value of this parameter at any point in the flow field (of the plume) determines the time that the fluid particle at that point has existed since leaving the burning face of the flare. The parameter is determined by integrating time as the fluid particle moves along its streamline. Thus,

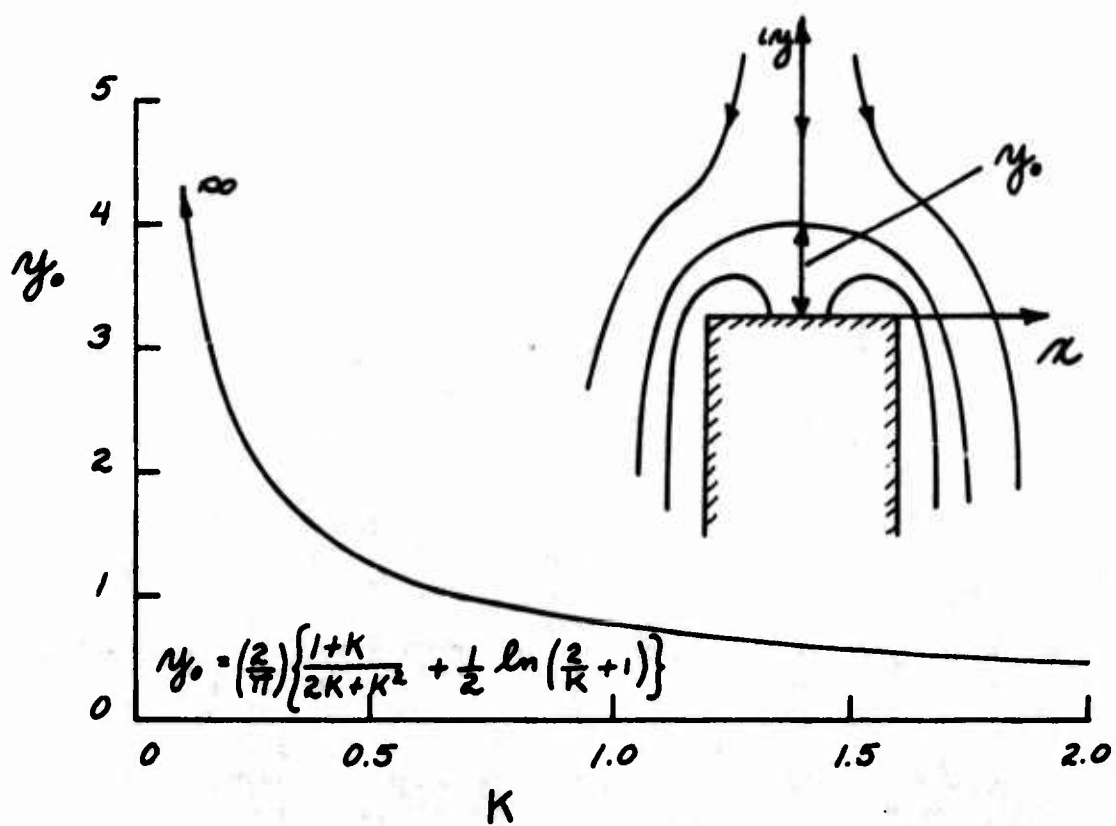


Figure 11. - Location y_0 of stagnation point between plume and surrounding air.

$$t = \int_0^t dt \quad (15a)$$

But,

$$q^* = \frac{ds^*}{dt}$$

or, in dimensionless form,

$$q = \left(\frac{r^*}{v_B^*} \right) \frac{ds}{dt} \quad (15b)$$

so that, from equations (15a) and (15b),

$$\tau = \frac{t v_B^*}{r^*} = \int_0^s \frac{ds}{q} \quad (15c)$$

Equation (15c) gives the dimensionless time parameter τ . This parameter is evaluated by numerical integration after the streamlines and velocity distribution have been plotted in the physical z -plane.

NUMERICAL PROCEDURE

In this part of the report, the numerical procedure, including inputs, outputs and the computer program are presented and discussed briefly.

Outline of procedure. The object of the numerical calculations is to determine, in the physical z -plane, the flow net (streamlines and velocity potential lines) and the distribution of various fluid properties (velocity components, flow direction and static pressure) for a plane, two-dimensional flare dropping through the atmosphere. The solutions are obtained in the transformed t -plane at points (ξ, η) of an arbitrarily-selected grid. At each of these grid points, the corresponding point (x, y) in the z -plane is determined, together with the stream function ψ , velocity potential ϕ and all other fluid properties in the physical z -plane.

Inputs. Once the grid points have been selected in the t -plane, the only required input is the drop rate parameter K , which relates the "effective" drop rate of the flare to the burning rate (see equation 12d).

Numerical procedure. At selected grid points (ξ, η) in the transformed t -plane, the following quantities are computed for the physical z -plane:

<u>Quantity</u>	<u>Equation</u>
R	(5c)
θ	(5d) and (5f)
x	(5a) and (5e)
y	(5b)
ϕ	(9b) and (9c)
ψ	(9d) and (9e)
u	(10c) } together with (10e), (10f),
v	(10d) } (10g), (10h), (10i), (10j), and (10k)
q	(11a)
α	(11b)
and P	(13c)

This numerical procedure has been programed for computer calculation. A brief description of the program, together with the program listing and instructions for preparation of input cards, is given in Appendix III.

Outputs. Outputs, in the order listed on the computer print-out, are:

ξ , η , x , y , ϕ , ψ , u , v , q , α , and P .

NUMERICAL RESULTS AND DISCUSSION

Five numerical examples are presented and analyzed. In addition, the so-called "edge-effect" is discussed, and recommendations for future work are made.

Typical value for K. Before presenting the numerical examples, a typical value for the drop rate parameter K is determined. From equation (12d),

$$K = \left(\frac{v_D^*}{v_{FL}^*} \right) \left(\frac{\rho_{air}}{\rho_{FL}} \right) \quad (12d)$$

In equation (12d), let

v_D^* = actual drop rate of flare = 12 ft/sec

v_{FL}^* = burning rate of solid flare material = 9 ins/min = 0.0125 ft/sec

ρ_{air} = weight density of air = 0.0765 lb/ft³

ρ_{FL} = weight density of solid flare material = 180 lb/ft³

so that
$$K = \left(\frac{12}{0.0125} \right) \left(\frac{0.0765}{180} \right) = 0.408$$

Thus, a typical value for K is 0.4. (Of course, K is zero for a stationary flare)

Numerical examples. Numerical results are presented for five values of K : 0, 0.1, 0.3, 0.5 and 0.7. These results are presented in figures 12 through 16, which show the two-dimensional flow field (x - y coordinates) surrounding the flare in the physical z -plane. (The computer output tables for the five examples are listed in Appendix III.) Because the flow is symmetrical about the centerline of the flare, which lies along the y -axis, the flow field presented in the figures is limited to positive values of x . In each of these figures, the orthogonal network of streamlines (constant ψ) and velocity potential lines (constant ϕ) is shown together with lines of constant velocity Q (equals q) and lines of constant time parameter τ .

In this analysis, for all values of K , the streamfunction ψ is zero along the side of the flare ($x = 1, y \leq 0$), and is unity for the straight, centerline streamline, which starts at the center ($x = 0$) of the burning face and rises along the positive y -axis. If the flare has a drop rate ($K > 0$), then along this centerline streamline, the plume gas rising ($v > 0$) from the burning face of the flare meets the air descending ($v < 0$, due to the drop rate) from the atmosphere. At the resulting stagnation point (y_0 , see equation (14b) and figure 11), the streamline ($\psi = 1.0$) branches left and right, and forms the boundary between the plume and the surrounding air. Thus, for $K > 0$, the streamline $\psi = 1.0$ determines the shape of the plume. (In this analysis, for $K = 0$, the plume occupies the entire flow area.) A comparison of figures 13 through 16 shows the effect of drop rate on the size and shape of the plume. It is noted that as drop rate (K) increases, the size of the plume decreases.

For all values of K , the v component of the velocity q (equals Q in figures 12 through 16) is, from continuity, constant along the burning face of the flare ($0 \leq x \leq 1$ and $y = 0$), and is, by definition, equal to 1.0. At the center of the flare (origin; $x = 0$ and $y = 0$), the u component of velocity is, from symmetry, zero, so that the velocity q is unity. As x increases from the center (origin), the u component increases, and the velocity q increases to infinity at the edge ($x = 1, y = 0$). This increase to infinite velocity at the edge is, however, a highly localized effect. For example, the velocity at $x = 0.9626$ (i.e., within 3.74 percent of a flare radius r^* from the edge) is (only) 3.65 for $K = 0.7$ and is less for lower values of K . This "edge-effect" results (theoretically) in an infinite negative pressure P at the edge, which pressure supplies the necessary force to turn the flow around the sharp corner at the edge. In fact, for real fluids, this force cannot exist, and separated flow of some type occurs at the edge to prevent the infinite velocity.

Elsewhere in the flow field, the velocity is zero at the stagnation point (figures 13 through 16), and the stagnation point is encircled by lines of constant q . Also, far downstream from the burning face of the flare, the velocity in the plume approaches the value of the drop rate parameter K . A comparison of figures 12 through 16 shows the effect of drop rate on the velocity distribution. It is noted that as drop rate (K) increases, the velocities within the plume increase. It should also be noted that, because K is based on an "effective" drop rate (equation 12d), the velocities in the air outside of the plume are fictitious. These fictitious velocities are corrected (approximately) when multiplied by $\rho_{\text{gas}}/\rho_{\text{air}}$ (see equation 12b).

Lines of constant time parameter τ in figures 12 through 16 indicate the time (in dimensionless form) that a fluid particle at any point (x,y) in the plume has existed since leaving the burning face of the flare. Presumably, for a particle radiating energy, the longer this time the cooler the particle. (Note that τ -lines exist within the plume only.) A comparison of the τ -lines in figures 12 through 15 shows that, as the drop rate K increases, a line of constant τ (1.4, for example) encompasses areas of moderately different shape, but of nearly equal areas. Thus, it is concluded that drop rate K may not have a pronounced effect on intensity of illumination.

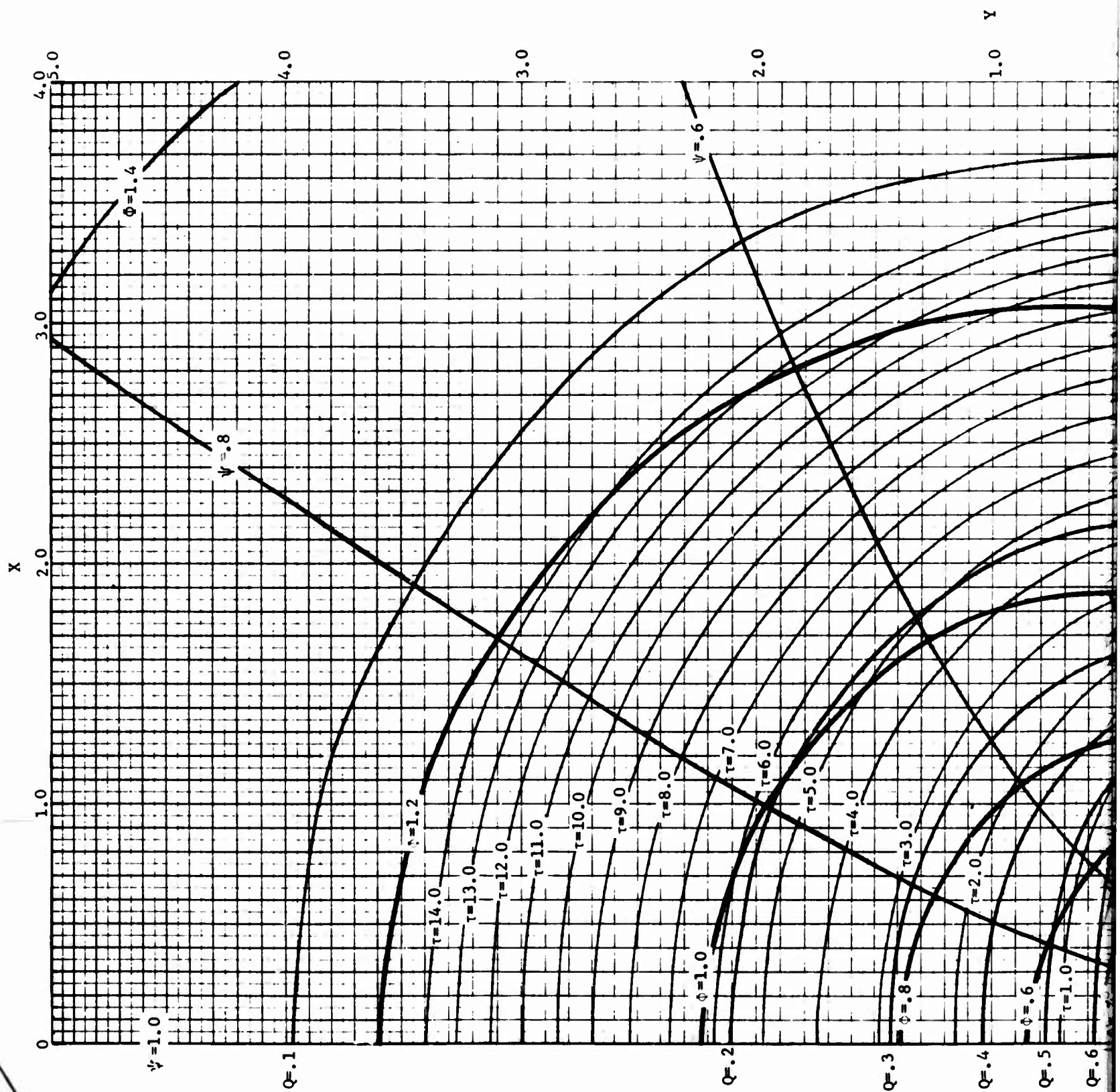
It is noted from equation (15c) that, for a given value τ at a given point in the flow field, the larger the flare radius r^* and the lower the burning rate v_B^* the longer the time t that the fluid particle has existed in the plume. Therefore, if longer time means lower particle temperature, it can be concluded that the luminosity per unit area of burning surface is higher for smaller burning areas, i.e., for smaller r^* . Thus, for a given weight of flare material, one large flare may be less efficient than a multiplicity of smaller flares with the same total burning area. Likewise, it is concluded that the luminosity per unit area of burning surface is higher for higher burning rates v_B^* .

"Edge-effect". For the analysis of this report, an infinite velocity results from flow around the sharp corners at the two edges ($x = \pm 1, y = 0$) of the flare. For real fluids, infinite velocities, with infinite negative pressures (equation 13c), cannot exist. Thus, for real fluids, this "edge-effect" is eliminated by some type of separation that prevents flow around the sharp corner. For a stationary flare ($K = 0$), the separated flow region may be atmospheric air, the flow of which is induced by jet-mixing of the plume (figure 17). For a moving flare ($K > 0$), the separated flow may be a bubble of the plume gas itself. In either case, the separated flow at each edge is given by a two-dimensional vortex conforming to the boundaries of the solid flare and its plume.

For a stationary flare ($K = 0$), the size of the vortex will be large and its center (a singularity) will be located far from the edge of the burning surface. As K increases, however, the size of the vortex will decrease, and its center will move progressively closer to the edge. (One criterion, of course, for the size and location of the vortex is the elimination of infinite velocity at the edge.) It is recommended that the (preliminary) mathematical model of this report be modified to include the above vortices.

Recommendations. There is much fruitful work yet to be done on a mathematical model for illuminating flares. First emphasis for future work should be placed on resolution of the "edge-effect," as outlined in the previous section. Additional problems to be considered include:

- (1) Effects of radiation and heat conduction within the flare.
- (2) Effects of mixing between the plume and the surrounding air or other gases.
- (3) Effects of axial symmetry (as opposed to the plane, two-dimensional treatment of the present report).
- (4) Effect of two fluids (two densities; one for the plume and one for the surrounding air).



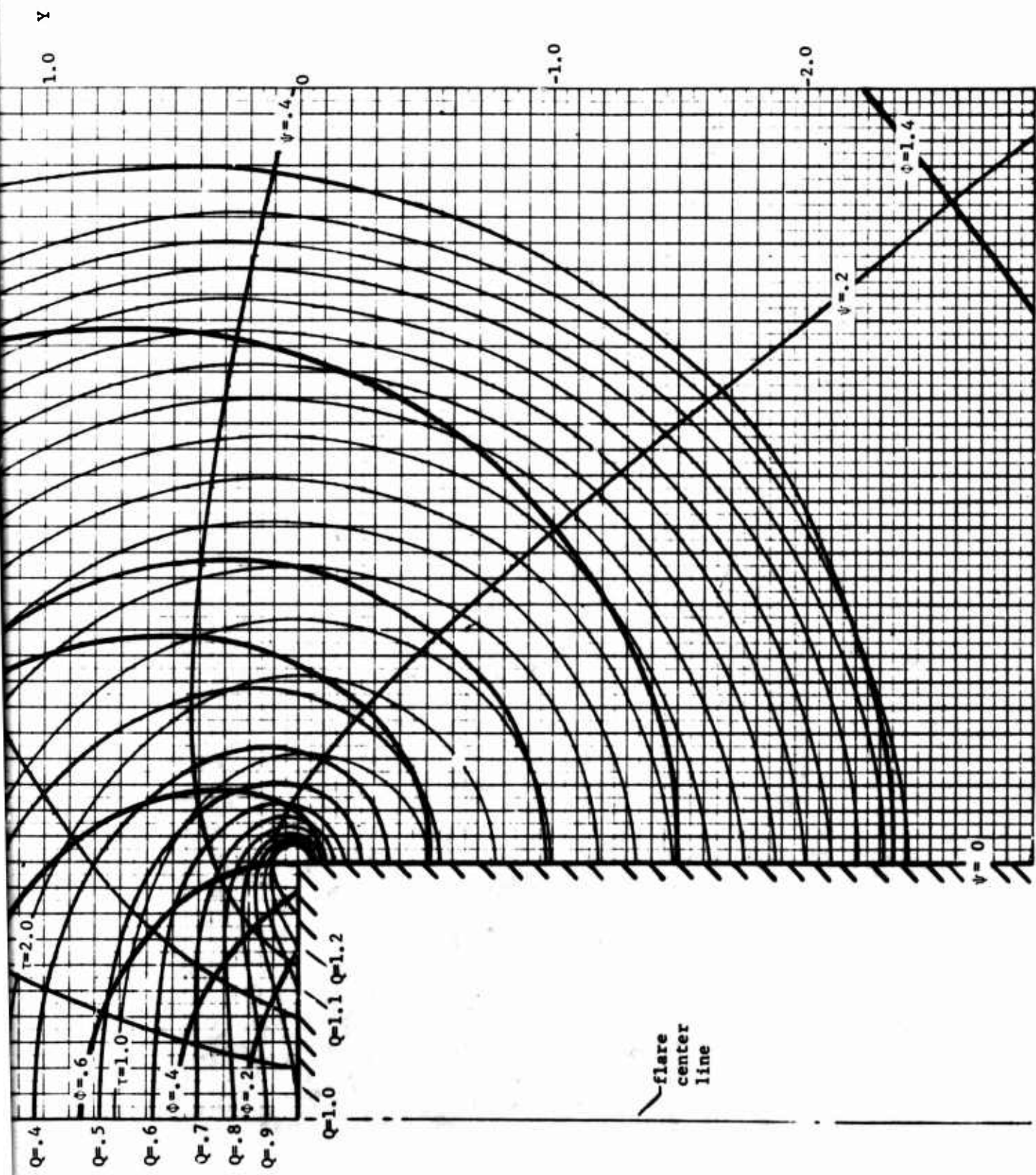
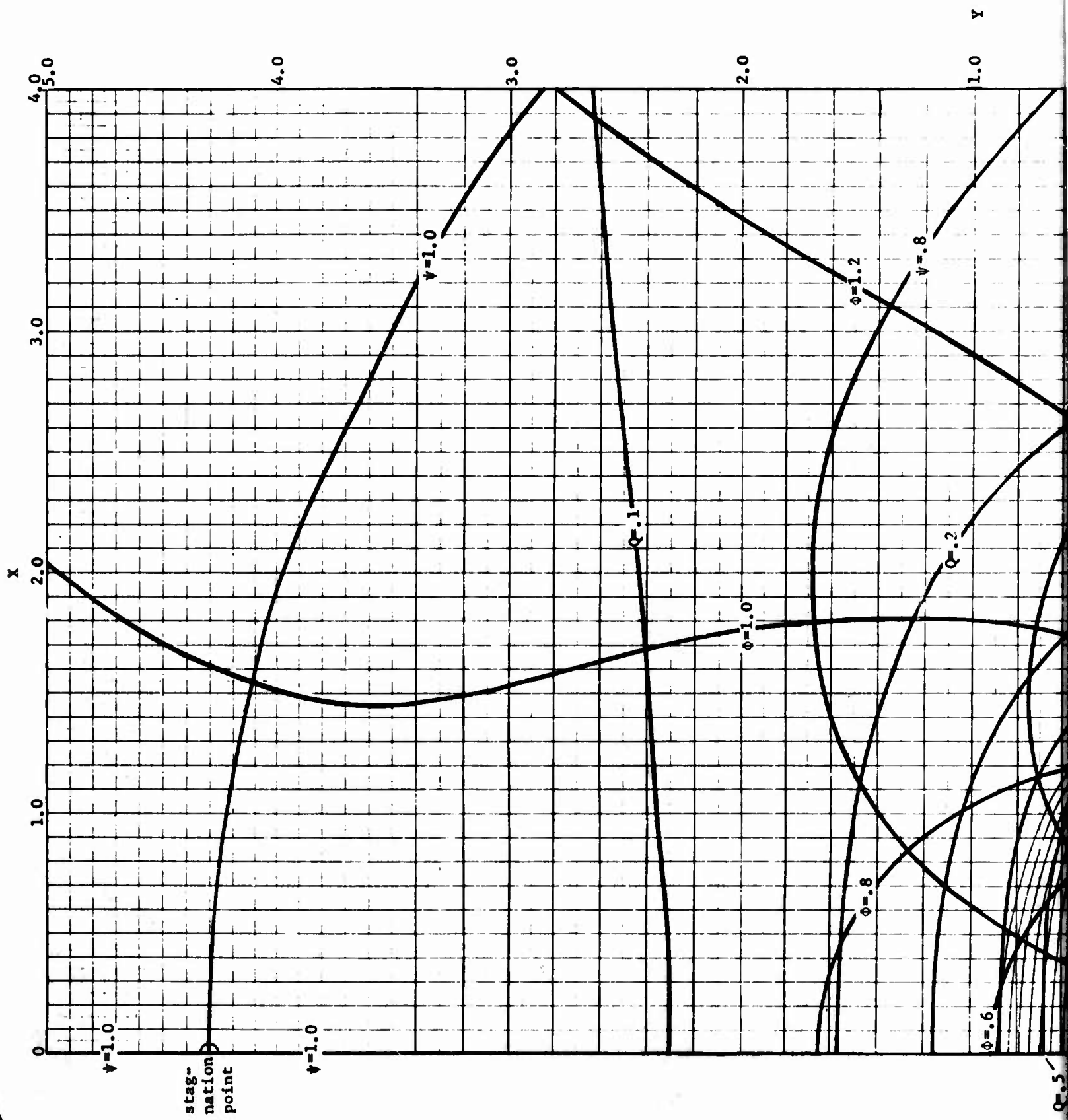
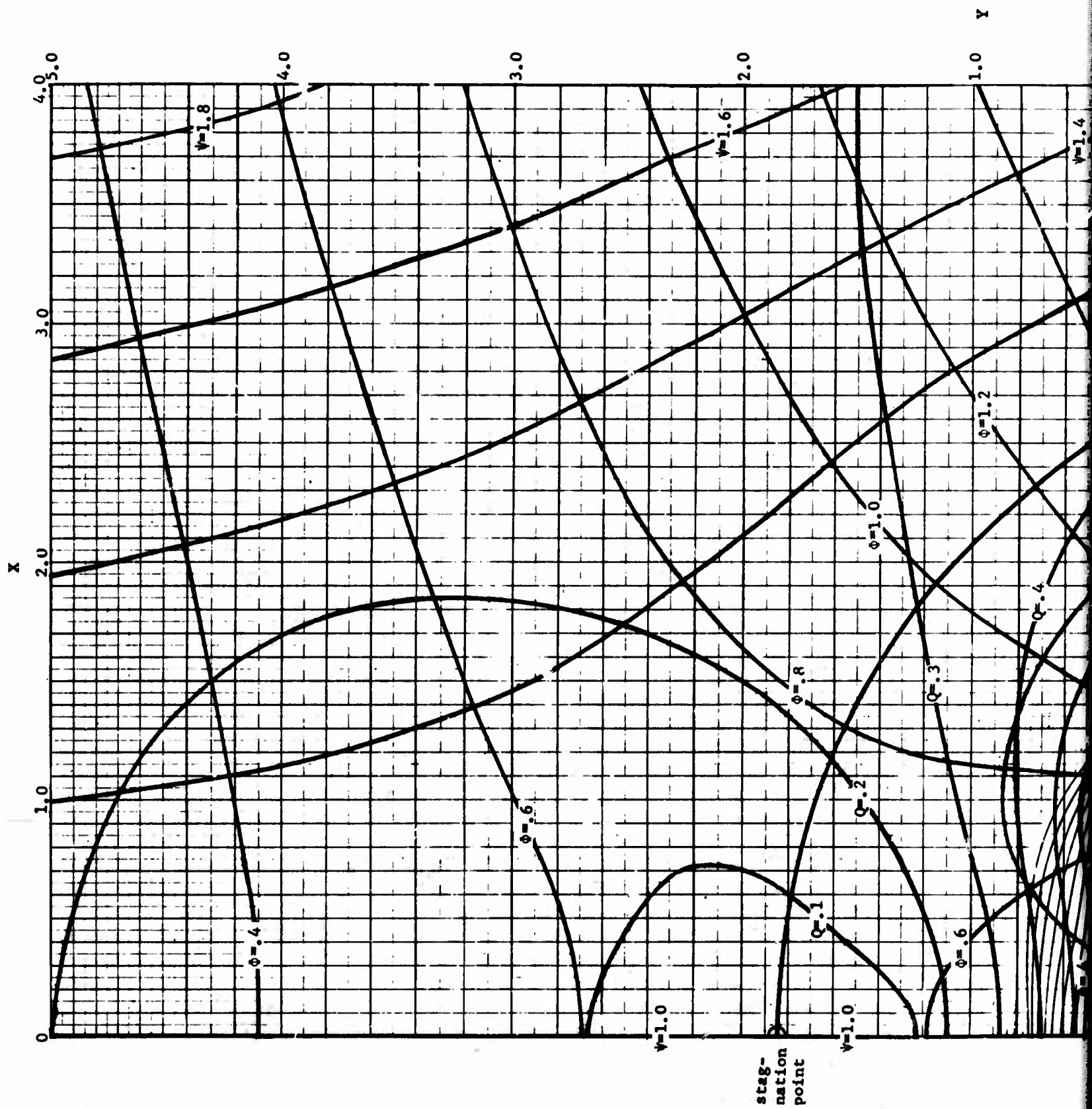


Figure 12 - Streamlines ($\psi = \text{constant}$) and velocity potential lines ($\phi = \text{constant}$) in X-Y plane for two dimensional flare with dimensionless drop rate given by $K = 0$. Also shown are lines of constant gas velocity Q (local velocity divided by constant velocity v_B normal to burning flare surface) and lines of constant time ratio, τ .

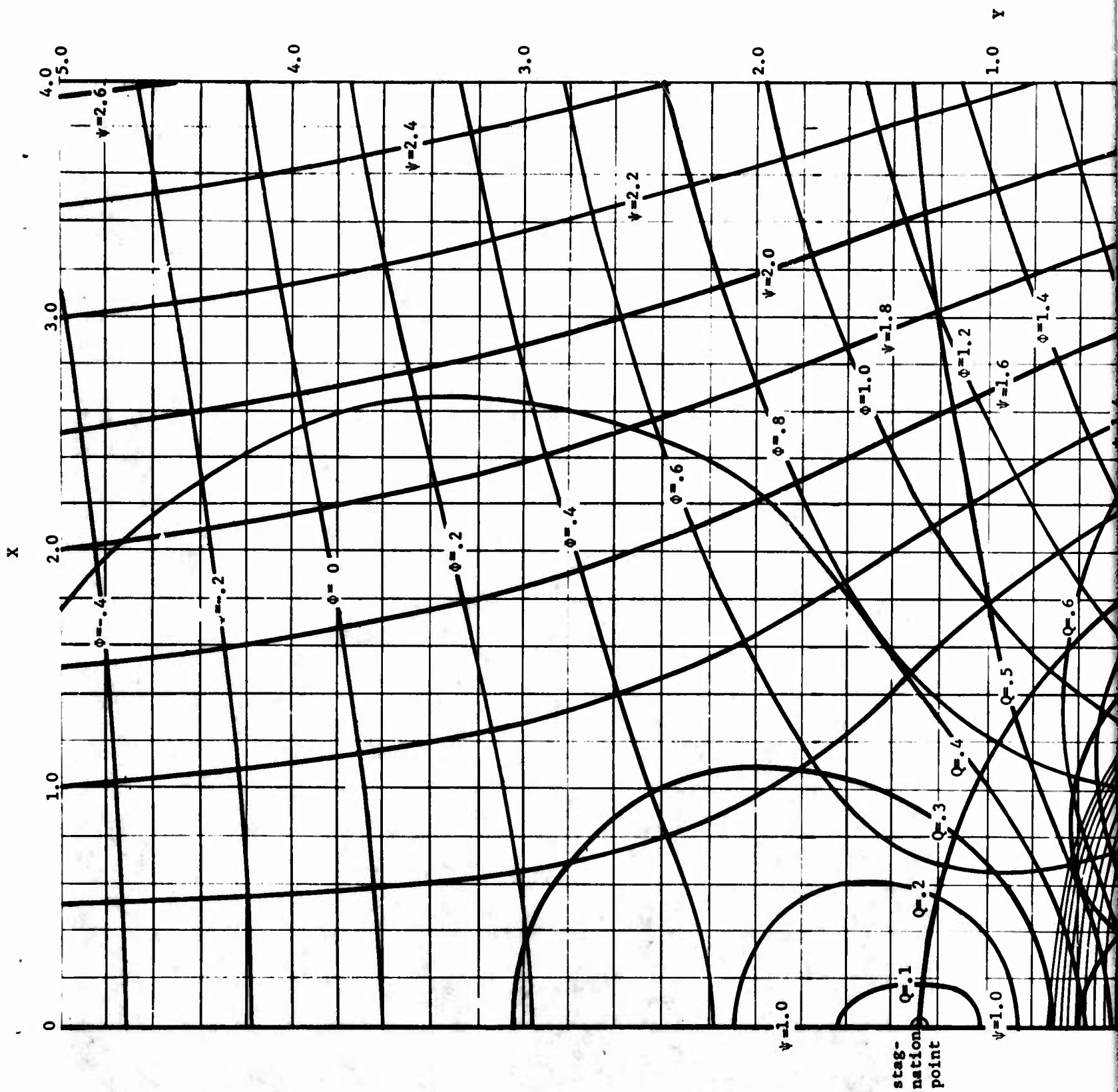
B



A



2



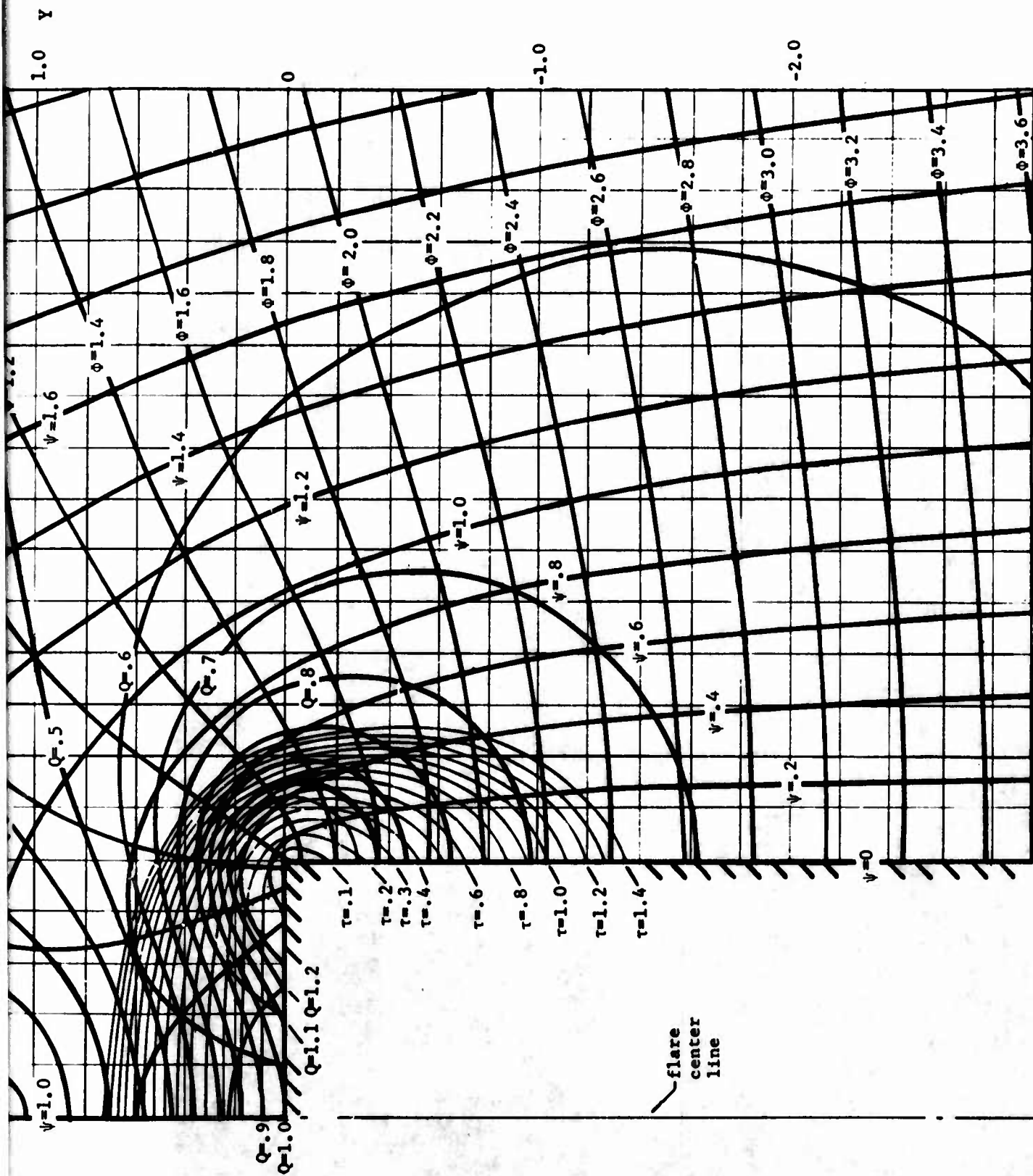
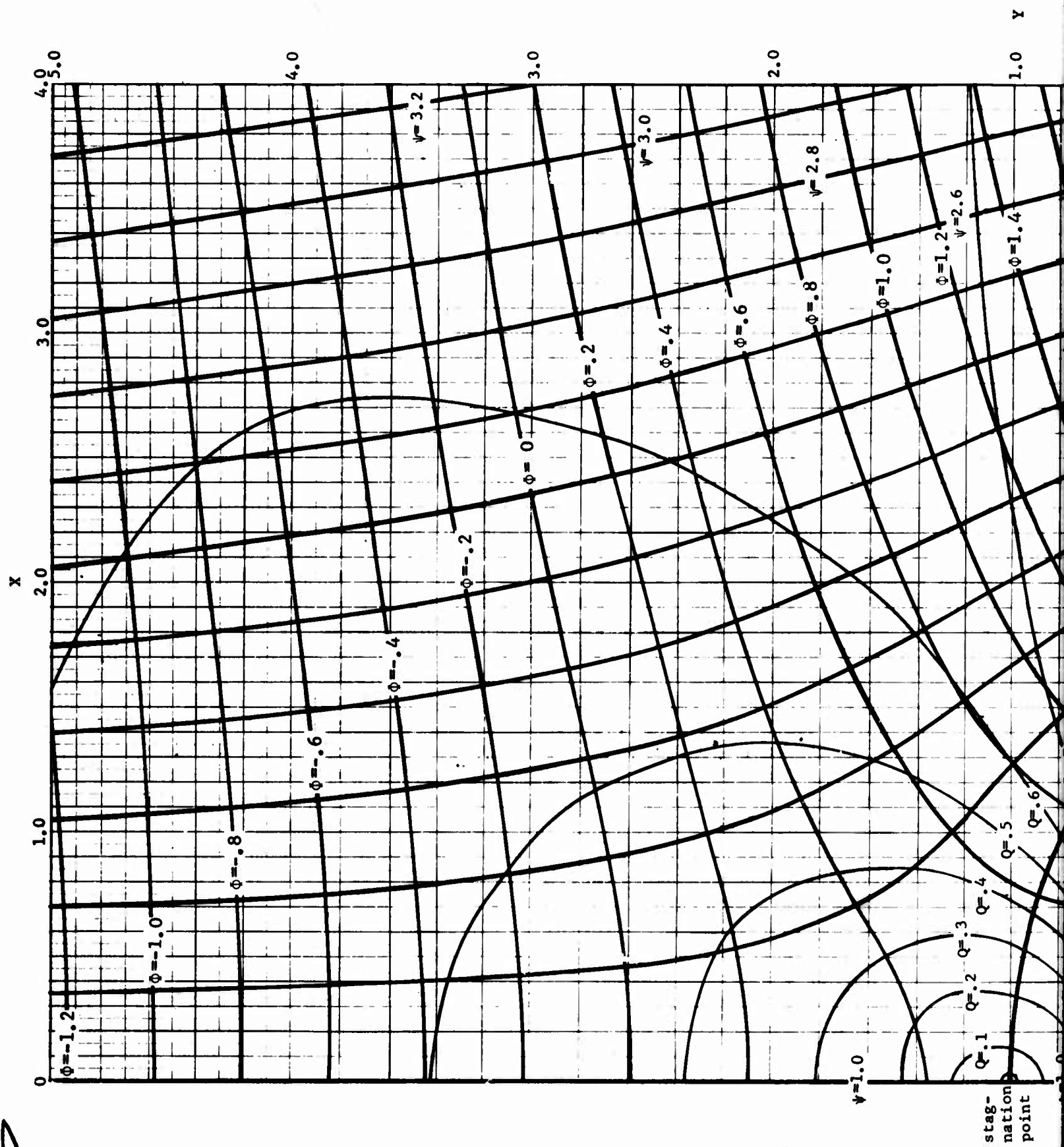


Figure 15 - Streamlines ($\psi = \text{constant}$) and velocity potential lines ($\phi = \text{constant}$) in X-Y plane for two dimensional flare with dimensionless drop rate given by $K = 0.5$. Also shown are lines of constant gas velocity Q (local velocity divided by constant velocity v_B normal to burning flare surface) and lines of constant time ratio, τ .

2



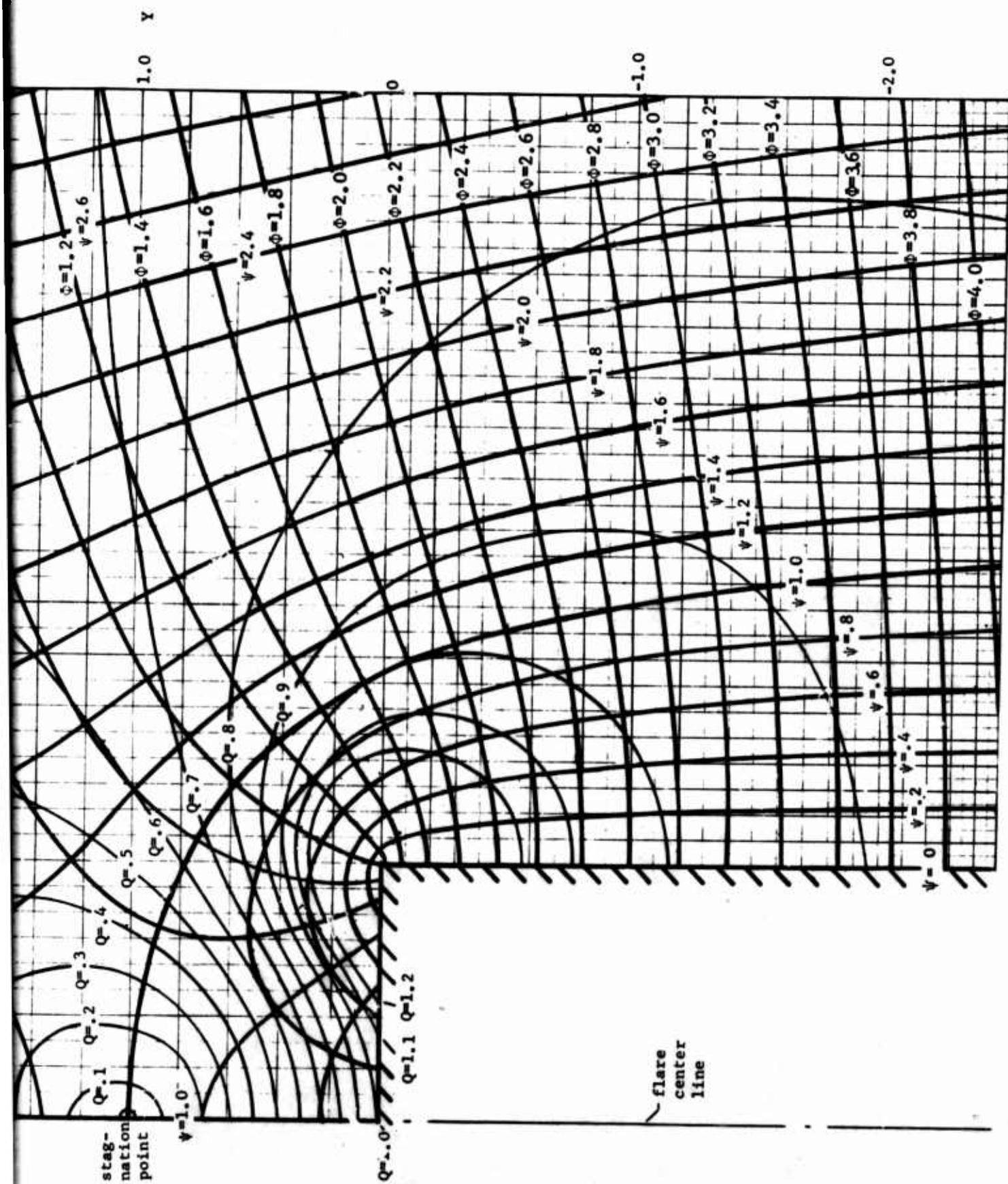


Figure 16 - Streamlines ($\psi = \text{constant}$) and velocity potential lines ($\phi = \text{constant}$) in X-Y plane for two dimensional flame with dimensionless drop rate given by $K = 0.7$. Also shown are lines of constant gas velocity Q (local velocity divided by constant velocity v_B normal to burning flare surface).

B

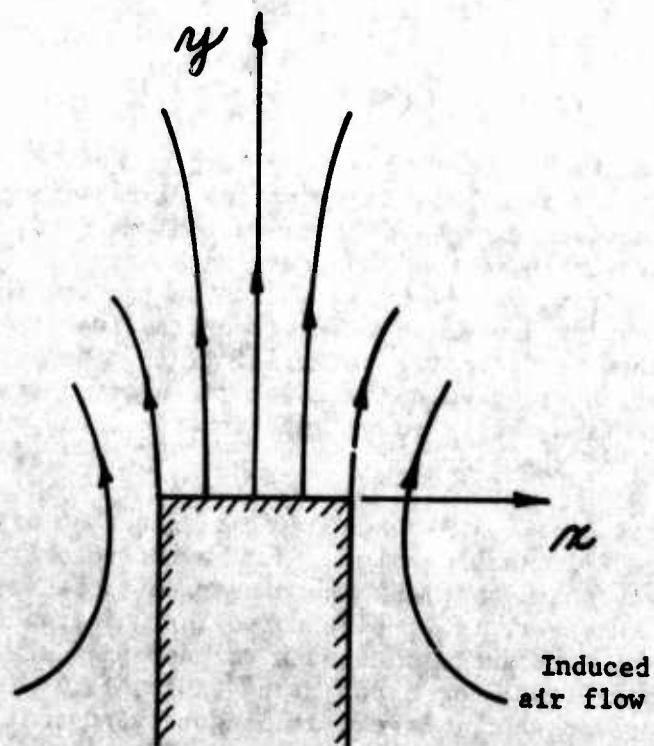


Figure 17. - Induced flow of air due to jet-mixing between plume and surrounding air (stationary flare, $K = 0$).

- (5) Effect of compressibility (variable density due to temperature and pressure variations).
- (6) Effects of buoyancy and cross-wind on plume configuration.
- (7) Effect of burning surface shape on plume configuration.

All of the above effects can be factored into the ultimate mathematical model for illuminating flares.

SUMMARY

A mathematical model, based on incompressible, potential flow, is developed for plane, two-dimensional illuminating flares dropping through the atmosphere. With the equations expressed in dimensionless form, the results depend on a single input variable; the drop rate parameter K . Five numerical examples are presented for five values of K , including the stationary case ($K = 0$). The numerical results are given by plots of the two-dimensional, orthogonal network of streamlines and velocity potential lines. Superimposed on these flow fields are lines of constant velocity q and lines of constant time parameter τ , where τ measures the time that a local fluid particle has existed since leaving the burning face of the flare.

Comparison of the plots shows the effect of drop rate K on the size and shape of the illuminating plume, and on the velocity distribution within the plume. It is noted that, as the drop rate increases, the size of the plume decreases. However, it is also noted that, as the drop rate K increases, a given line of constant τ continues to encompass areas of nearly equal magnitude. Thus, assuming that, for a radiating fluid, light intensity is approximately constant for constant τ lines, it is concluded that drop rate K may not have an important effect on illuminating intensity.

Other points of interest are as follows:

(1) For the mathematical model developed in this report, the (dimensionless) velocity along the burning face of the flare increases from 1.0 at the center to infinity at the edge. (This increase to very high velocities near the edge is, however, a highly localized "edge-effect".) The very high (infinite) velocity associated with the "edge-effect" cannot exist in real fluids, and it is concluded that separated flow occurs (at the edge) to eliminate it. A vortex model is proposed to account for this separation.

(2) It is concluded that the luminosity per unit area of burning surface is higher for smaller burning areas, i.e., for smaller flares. Thus, for a given weight of flare material, one large flare may be less efficient than a multiplicity of smaller flares with the same total burning area.

(3) Also, it is concluded that the luminosity per unit area of burning surface is higher for higher burning rates.

Finally, there is much fruitful work yet to be done on the mathematical model for illuminating flares. First emphasis should be placed on the high velocity problem associated with the "edge-effect". After completion of this effort, seven additional areas are recommended for future work.

LIST OF REFERENCES - SECTION II

1. Streeter, Victor L.: Fluid Dynamics. McGraw-Hill, New York, 1948.

SECTION III

THERMOCHEMICAL CALCULATIONS AND CORRELATION WITH EXPERIMENTAL RESULTS

INTRODUCTION

The ability to predict flare plume temperatures by use of a computer or to show what temperature should be realized for a given formulation can be of significant value in analysis of flare performance, interpretation of results, and subsequent development. As a first step in attempting to accomplish this, thermochemical calculations were made on a digital computer by means of an automatic computation method which for given formulations and pressures gave the mole fractions of combustion products and equilibrium temperatures. Then an attempt was made to determine the degree of correlation that could be established between the theoretical and experimental. Computations were made for a number of flare formulations and temperatures were experimentally measured for magnesium-Laminac*- sodium nitrate flares of varying magnesium ratios. The objective was to see if correlation between computed and experimental values for formulations composed of varying amounts of one set of chemical components could be achieved in order to establish a confidence factor for the computational procedure. Temperature measurements were made with chromel-alumel thermocouples where temperatures were below approximately 2300°F and tungsten-5% rhenium/tungsten-26% rhenium thermocouples were used for temperatures above 2300°F. The results of the thermochemical computations are given in the form of curves for discussion purposes and complete results are provided in tables in the appendixes for more detailed study. The results of the temperature measurements are given in plots of temperature versus distance from the flare surface. Analysis of results and recommendations for further study are included.

THERMOCHEMICAL CALCULATIONS

The thermochemical calculations were made on a digital computer using a modified version of the program outlined in reference 1. That program, which was developed for rocket propellants, is completely general. It must be assumed, however, that for flares burning in the atmosphere the chamber walls are, in effect, composed of surrounding inert gases. The following input data are required by the main calculating program for the solution of equilibrium compositions and temperature following an adiabatic combustion process:

- (1) The reaction products to be considered
- (2) Gram atoms of elements in 1 gram of fuel and 1 gram of oxidant
- (3) Enthalpies of fuel and oxidant per gram of fuel and oxidant
- (4) Oxidant to fuel weight ratio O/F (or percent fuel or equivalence ratio r). For computational convenience, all constituents may be treated as fuel.
- (5) Thermodynamic data for products considered
- (6) Chamber pressure
- (7) Initial estimate of temperature, composition, and number of formula weights.

*Laminac 4116 - a polyester-styrene copolymer, a product of American Cyanamid Company

(One difficulty encountered in the use of the program was acquisition of input data for flares containing barium and strontium. Attempts were made to compute temperatures for formulations reported in reference 2 but data on barium and strontium products had not been developed, primarily because they are not normally used in rocket fuels. These are the only two elements for which this difficulty was encountered.)

The program written in reference 1 is for an IBM 650 computer with 2000 words of drum storage and 60 words of high speed core storage. It is limited to 30 reaction products. The modified program uses an IBM 360 model 50 computer and can accommodate 90 reaction products.

A typical result from the computer is shown in appendix V. The symbols used are explained in the list of abbreviations and symbols, appendix IV. The table is self-explanatory except possibly the designations of chamber, throat, and exit which apply principally to rocket motors. As was noted, the program was initially set up for rocket fuels and although not all of the items shown are required for this application, they were not deleted from the program in the event that they may be useful in the future.

Computations were made for a range of ingredient ratios for formulations including a number of binder systems and the results of the computations are included in the appendixes for evaluation of the parameters. The results were plotted as shown in figures 18, 19, 20, and 21. These are discussed from standpoint of theoretical performance in the following subsections.

Magnesium-Laminac-sodium nitrate - Pressed formulations containing magnesium, Laminac, and sodium nitrate are widely used. Calculations were made primarily for flares of this formulation containing 5% Laminac. However, the Mark-24 flare contains 4.5% Laminac and separate calculations were made for that formulation. A plot of plume temperature and principal gaseous and solid components are plotted against weight percent magnesium in figure 18. There are several observations that can be made. The first is that for 68% Mg the maximum plume temperature is low enough to be measured with chromel-alumel thermocouples. The second is that for 58% magnesium which most closely approximates the Mark-24 flare formulation, the theoretical temperature is less than 4000°F which is substantially below the temperatures for formulations having 30 to 50 percent magnesium. Computations for the Mark-24 formulation (58 percent magnesium, 4.5 percent Laminac, and 37.5 percent sodium nitrate) are included in appendix V. The maximum theoretical temperature for the Mark-24 formulation is 4256°F at sea level.

A third observation is that the maximum sodium gas content is obtained with approximately 30 percent magnesium and at a temperature of 4962°F. This temperature of 4962°F is 700°F higher than the theoretical for the Mark-24 flare and the mole percent of sodium gas is 50 percent greater. If sodium is a major source of illumination this could be significant. The mole percent of magnesium gas drops almost to zero from 36 mole percent in going from 58 percent to 30 percent magnesium and the magnesium oxide rises from 32 mole percent to 38 mole percent.

Computations were also made at 0.39 psi (approximately 81,000 feet altitude) to evaluate altitude effects. The results of these computations are given in appendix V and effects on equilibrium temperatures are shown in figure 18. The sensitivity of temperature to pressure below 60 percent

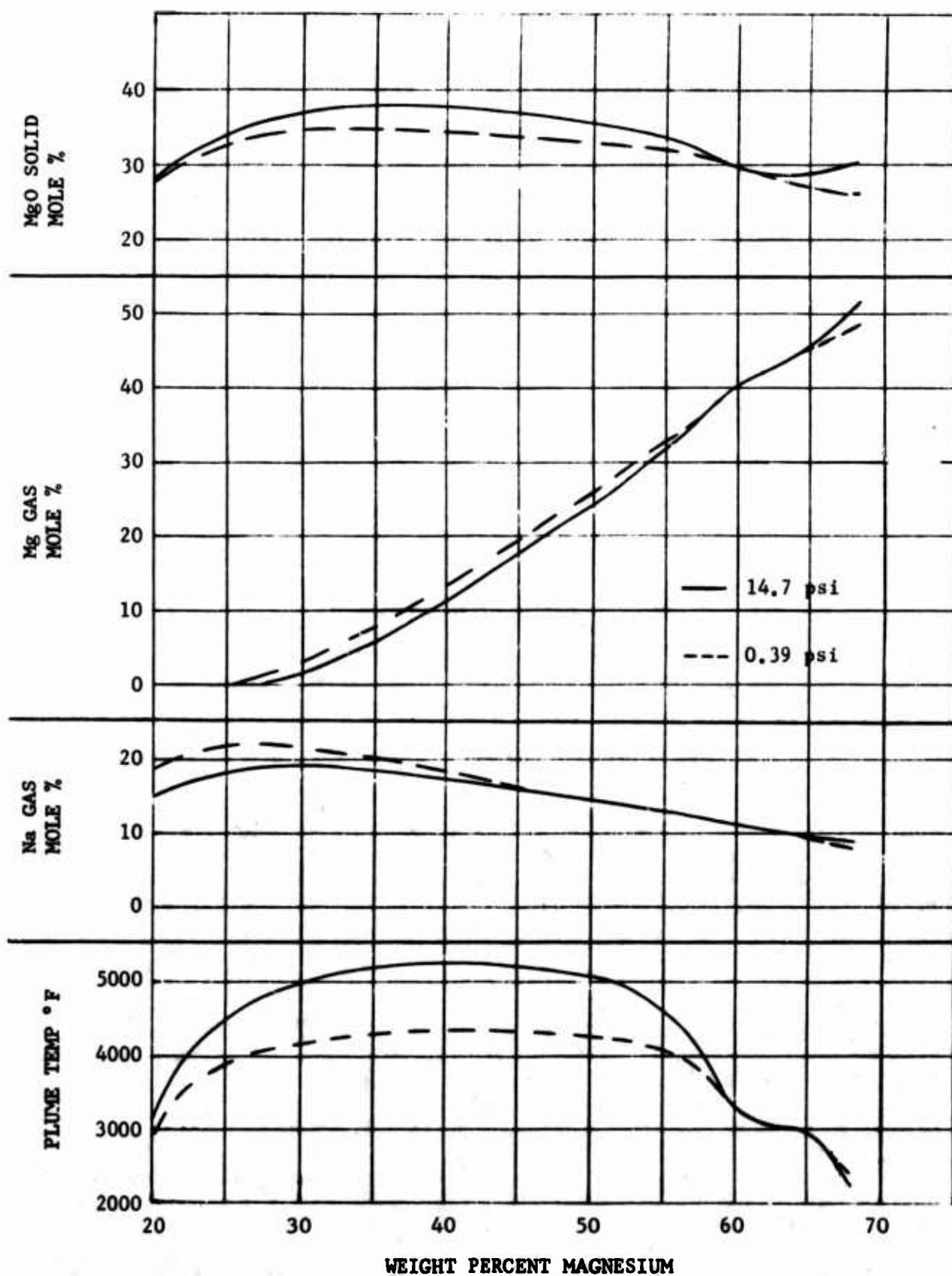


Figure 18- Computer results: for flares burning in an inert atmosphere. Flare composition - 5% Laminac, magnesium as shown and remainder sodium nitrate.

magnesium is apparent. Further examination of figure 18 indicates that with a decrease in pressure and for magnesium content below 60 percent there is an increase in gaseous magnesium and a decrease in magnesium oxide. The heat lost in vaporization of magnesium and the smaller amount of heat generated by the lesser amount of magnesium being oxidized probably accounts for the lower temperature. Between 60 and 65 percent magnesium content there is little change and above 65 percent the decrease in magnesium vapor apparently offsets the decreased magnesium oxide resulting in a smaller change in temperature. Further consideration of pressure effects will be given in the analysis of results section.

Magnesium-glycidyl methacrylate-sodium perchlorate - Cast formulations using magnesium, glycidyl methacrylate, and sodium perchlorate have been investigated, and the experimental results are contained in references 3 and 4. Thermochemical computations were made for varying percentages of magnesium and sodium perchlorate while holding the glycidyl methacrylate content at 15 percent. The numerical results are shown in appendix VI and a plot of plume temperature and principal gaseous and solid components versus weight percent magnesium is shown in figure 19. It can be seen from the results shown in figure 19 that the gaseous sodium in the plume is only approximately half that in the magnesium-Laminac-sodium nitrate flare plumes. An unknown factor regarding the glycidyl-methacrylate formulations is the illumination that may be expected from the sodium chloride gas in the plume. For example, with 15 percent glycidyl methacrylate, 42.5 percent magnesium, and 42.5 percent sodium perchlorate the mole percent of sodium chloride is 5.9. This mole percent, together with the sodium gas mole percent of 3.85, provides a total sodium content that would be more in line with that provided by the flares containing sodium nitrate but, as previously stated, adequate information is not available to make an assessment. As with the Laminac-bound flares the equilibrium temperature remains high as the weight percent of magnesium is decreased. The mole percent of sodium remains approximately constant below 40 weight percent magnesium.

Computations of performance at altitude were not made for this formulation or any of the remaining formulations. One computation was made for sodium nitrate as a replacement for sodium perchlorate and the results of the computations are shown in figure 19 as single points. The computations are included in appendix VI. It can be observed in figure 19 that the temperature for the sodium nitrate composition is 700°F lower than for the sodium perchlorate flare but that the mole percent of sodium gas is more than three times as great.

Viton A-Teflon-magnesium-sodium nitrate - Tetrafluoroethylene (TFE) binder systems apparently have not been widely used in flare manufacturing. However, they were evaluated and reported in reference 2. One possible advantage of TFE binders is that the binder is an oxidizer and can play a role in flare formulation that is not possible for the fuel binders. A combination of TFE (Teflon) and Viton A, which is a hydrogenated TFE type compound, has been successfully used in pressed formulations with magnesium and barium nitrate for gas generation in supersonic aircraft engine fire extinguishers, reference 5.

Thermochemical computations were made for formulations ranging from 34 to 54 percent magnesium with 11 percent Teflon, 11 percent Viton A, and the remainder sodium nitrate. The results of the computations are shown in

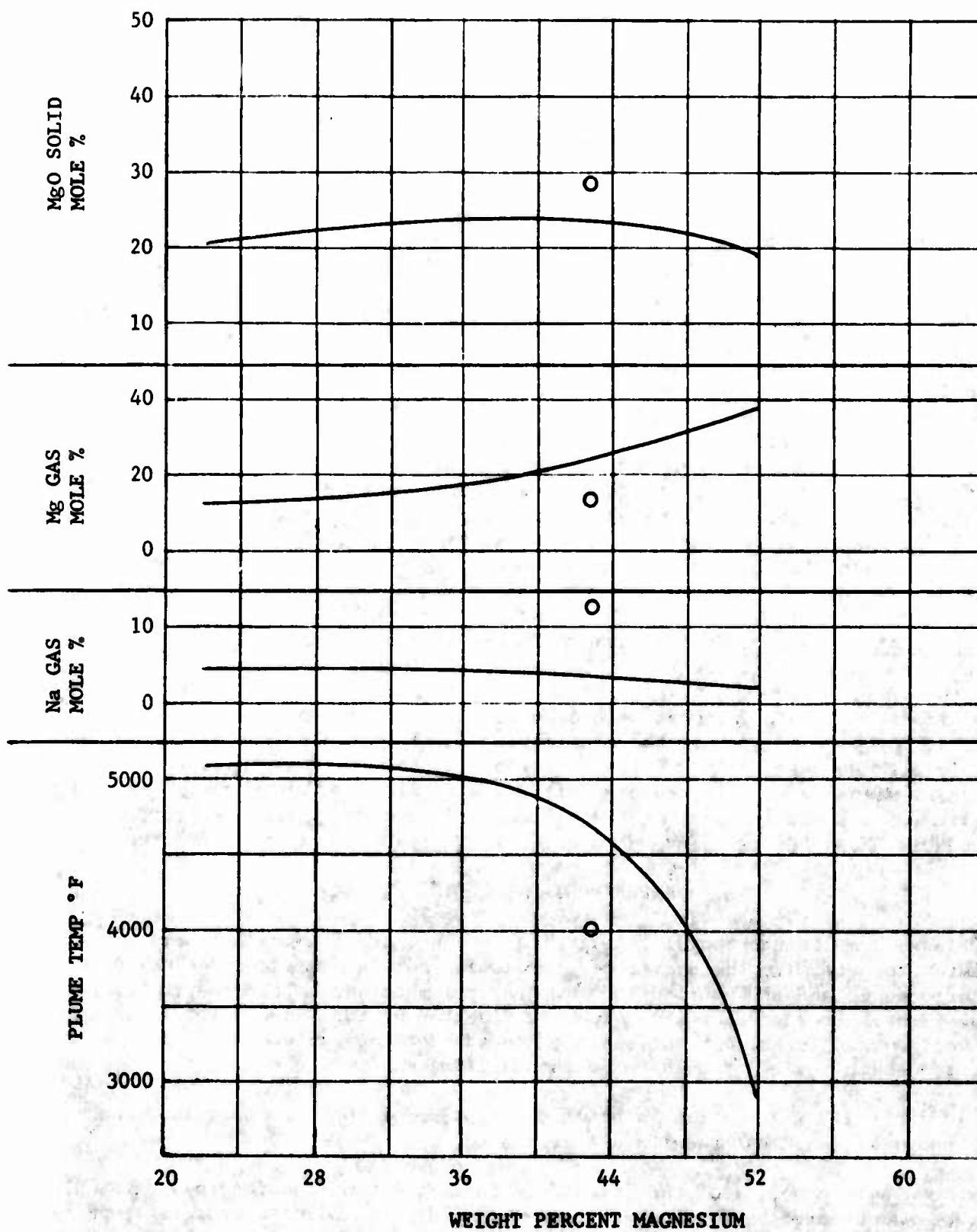


Figure 19 - Computer results for flares burning in an inert atmosphere. Flare composition - 15% glycidyl methacrylate, magnesium as shown, and remainder sodium perchlorate. Encircled points show result of replacing sodium perchlorate with sodium nitrate.

appendix VII and plots of temperature and principle components of the gases in the plume versus weight percent of magnesium are shown in figure 20. It can be seen from figure 20 that the 5000°F temperature level is reached only when the weight percent of magnesium is reduced below 38 percent. The sodium gas content remains approximately constant below 48 percent magnesium and is twice that for the glycidyl methacrylate flares. As with flares containing perchlorates which result in a combination of sodium and chlorine, the sodium in these formulations is combined with fluorine and it is not known what effect this may have on the luminous efficiency. Flares using TFE binders with magnesium were not prepared or tested in this program.

Silicon-tetrafluoroethylene-sodium nitrate - In an attempt to assess the feasibility of flares containing no magnesium and a minimum of solid products in the exhaust, thermochemical computations were made for flares containing silicon, a TFE binder, and sodium nitrate. The formulation consisted of various percentages of silicon, Teflon, Viton A, and sodium nitrate. The results of the computations are shown in appendix VIII and figure 21. The plume temperature and quantity of sodium in the exhaust gas are plotted versus the percentage of silicon in figure 21. It can be readily seen that the plume temperatures are much below those for the flares containing magnesium, with the temperature approaching 4000°F for percentages of silicon below 13. One consideration for choosing this formulation was to attempt an evaluation of sodium as a light source in the absence of magnesium. Formulations prepared with silicon showed poor burning characteristics at atmospheric pressure and therefore further evaluation was not made. The results have been included herein because of the possibility that with burning under pressure, the smoke from silicon flares may be less obscuring than magnesium smoke and, therefore, further evaluation may be desirable.

Burning in air - The computations shown in appendixes V through VIII were made with the assumption that burning would take place in an inert atmosphere. In order to arrive at some indication of what might occur with burning in air, computations were made for complete combustion of the Mark-24 flare in air. It should not be assumed that the equilibrium conditions that would be required to achieve these results do exist. Nevertheless, these results plus results of burning magnesium in air, burning of sodium in air, and burning a 68 percent magnesium, 5 percent Laminac, and 27 percent sodium nitrate flare are presented in appendix IX. They may serve as a guide in analysis of experimental results.

EXPERIMENTAL RESULTS

Flare formulations containing varying percentages of magnesium were evaluated to determine the degree of correlation between temperatures measured by thermocouple and the equilibrium temperatures obtained in the thermochemical calculations. Pressed flares one inch in diameter by two and one-fourth inches long were burned in the upright position in an inert atmosphere at ambient pressures which varied from 28 to 30 inches of mercury.

In the following sections a brief description of the thermocouples, the test apparatus, and test results are presented.

Thermocouples - A survey of the literature indicated that considerable difficulty had been encountered by investigators in using thermocouples to measure temperatures in flare plumes. Furthermore, other temperature measuring methods such as optical pyrometers had not been completely successful. Personnel at the Naval

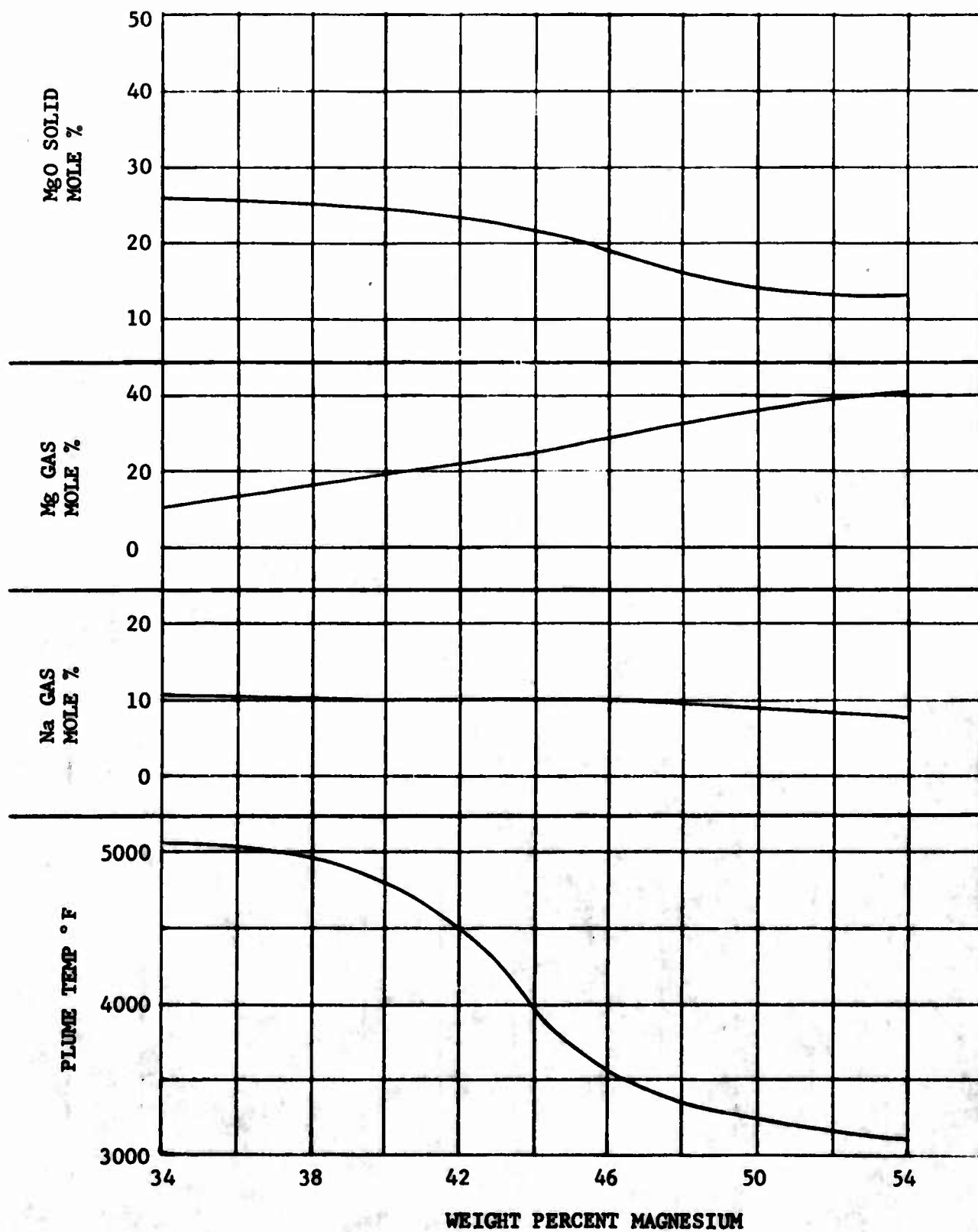


Figure 20 - Computer results for flares burning in an inert atmosphere. Flare composition - 11% Viton, 11% Teflon, magnesium as shown and remainder sodium nitrate.

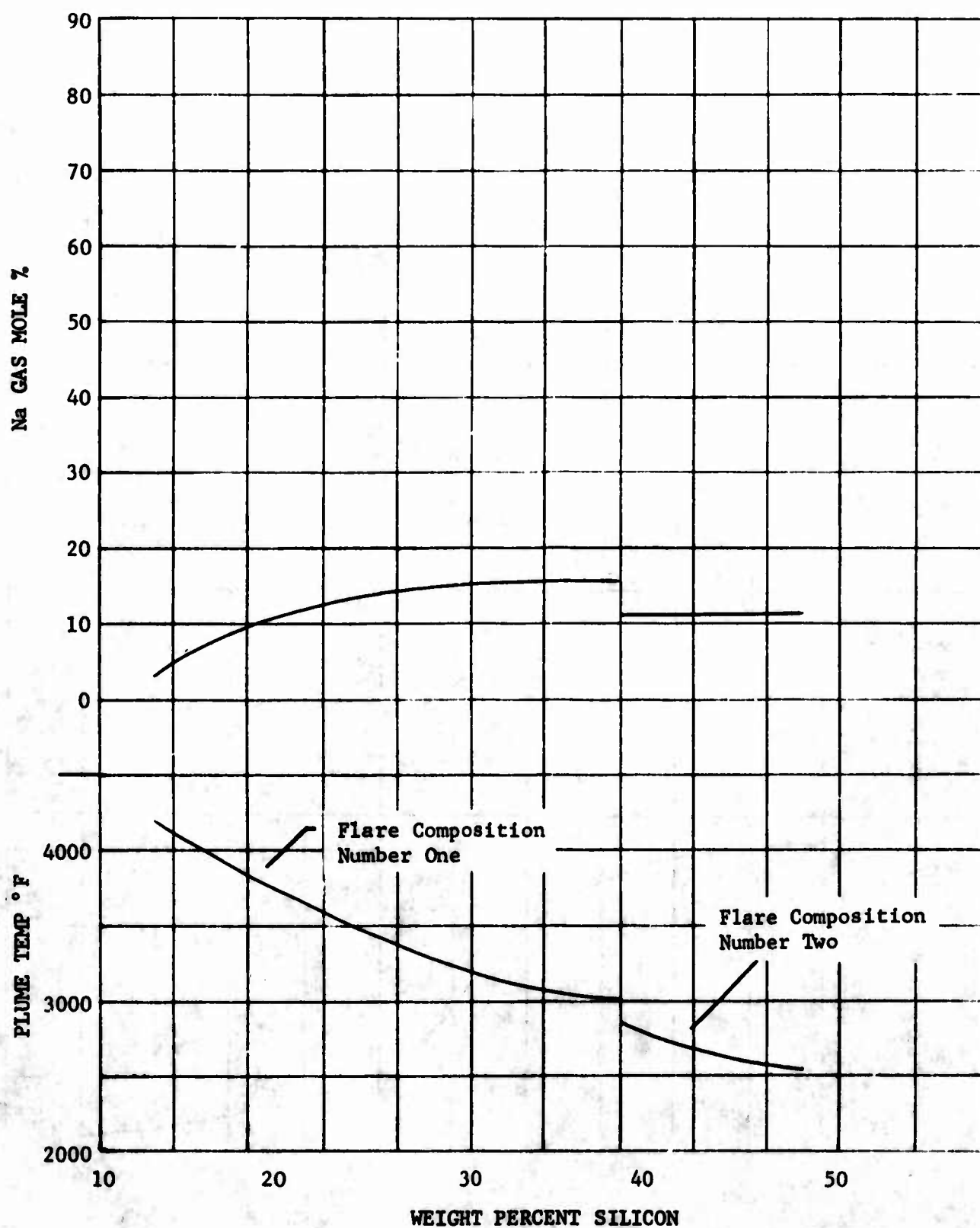


Figure 21 - Computer results for flares burning in an inert atmosphere. Flare composition number one - 11% Viton, 40% NaNO_3 , silicon as shown, and remainder Teflon. Flare composition number two - 11% Viton, 30% NaNO_3 , silicon as shown and remainder Teflon.

Ammunition Depot at Crane, Indiana have devised a method of measuring temperature which has been found to be accurate, but which requires expert judgment on the part of the user.

On the basis of the results of the computations, especially those shown in figure 18, it was decided that at least for those formulations having low temperatures such as the 68 percent magnesium, 5 percent Laminac, and 27 percent sodium nitrate for which maximum plume temperature was 2300°F, chromel-alumel thermocouples would suffice. Further, it was determined that for at least a part of the temperature range, tungsten 5%-rhenium/tungsten 26% rhenium thermocouples with tantalum sheaths would suffice. For temperatures exceeding 3500°F, tungsten rhenium thermocouples with titanium diboride coatings were fabricated. The chromel-alumel thermocouples employed a one-sixteenth inch outside diameter inconel sheath. The Tantalum sheaths were also one-sixteenth inch in diameter. The tantalum diboride coating was a minimum of 0.005 inches thick.

Experimental Setup - In order to provide an inert atmosphere the one-inch diameter flares were placed in the center of a six and three-eighths inch inside diameter vertical stainless steel tube, thirty-six inches high. The tube was purged with either argon or nitrogen prior to igniting the flare with an acetylene torch. Whether nitrogen or argon was used appeared to make no difference. Burning in air destroyed the thermocouple. In the initial test with 60 percent magnesium flares, it was not considered necessary to have a constant position of the thermocouples with respect to the plume. However, as the amount of the magnesium was decreased, the high temperature zone for the flare moved closer to the flare face, and it was necessary to devise a mechanism to elevate the flare as it burned, keeping the burning face a constant distance from the thermocouple. A satisfactory device was fabricated and was used with all flares except those containing 68 percent magnesium. Two temperature recorders were used and several flares were burned in order to get complete coverage.

Temperature Measurements - Temperature measurements were made for 5 percent Laminac flares containing 55, 60 and 68 percent magnesium with the remainder sodium nitrate. The results are plotted in figures 22, 23, and 24. A typical recorded temperature is shown in figure 25. The approximate thirty-second burn time for the flare was found adequate to provide leveling off of recorded temperature. It can be seen in figure 22 that the temperatures at two and three inches are very close to the computed equilibrium temperature with a rapid drop off between three and four inches above the flare. Because the high temperature zone occurred two inches from the flare with 68 percent magnesium, it was assumed that a similar situation would exist with other flares. This was not the case. For the 60 percent flare the high temperature zone moved away from the thermocouple so rapidly that equilibrium temperature was not reached. Therefore, as previously mentioned it was necessary to devise a cam mechanism driven by a low speed motor which would keep the flare face at a fixed position with respect to the thermocouple. This was arranged and the temperature measurements shown in figure 23 were made. It can be seen that the average maximum equilibrium temperature is approximately 100°F below the computed equilibrium temperature. The four measured values at one-half inch from the face of the flare were 3295°F, 2940°F, 3400°F, and 3110°F. At 0.75 inches the temperatures were 2975°F, 3130°F, 3275°F, and 3135°F. If it is kept in mind that each of these temperatures represents a different flare, it can be seen that fair agreement with the theoretical was obtained. For temperatures close to 2000°F and below, chromel-alumel thermocouples were used as shown in figure 23.

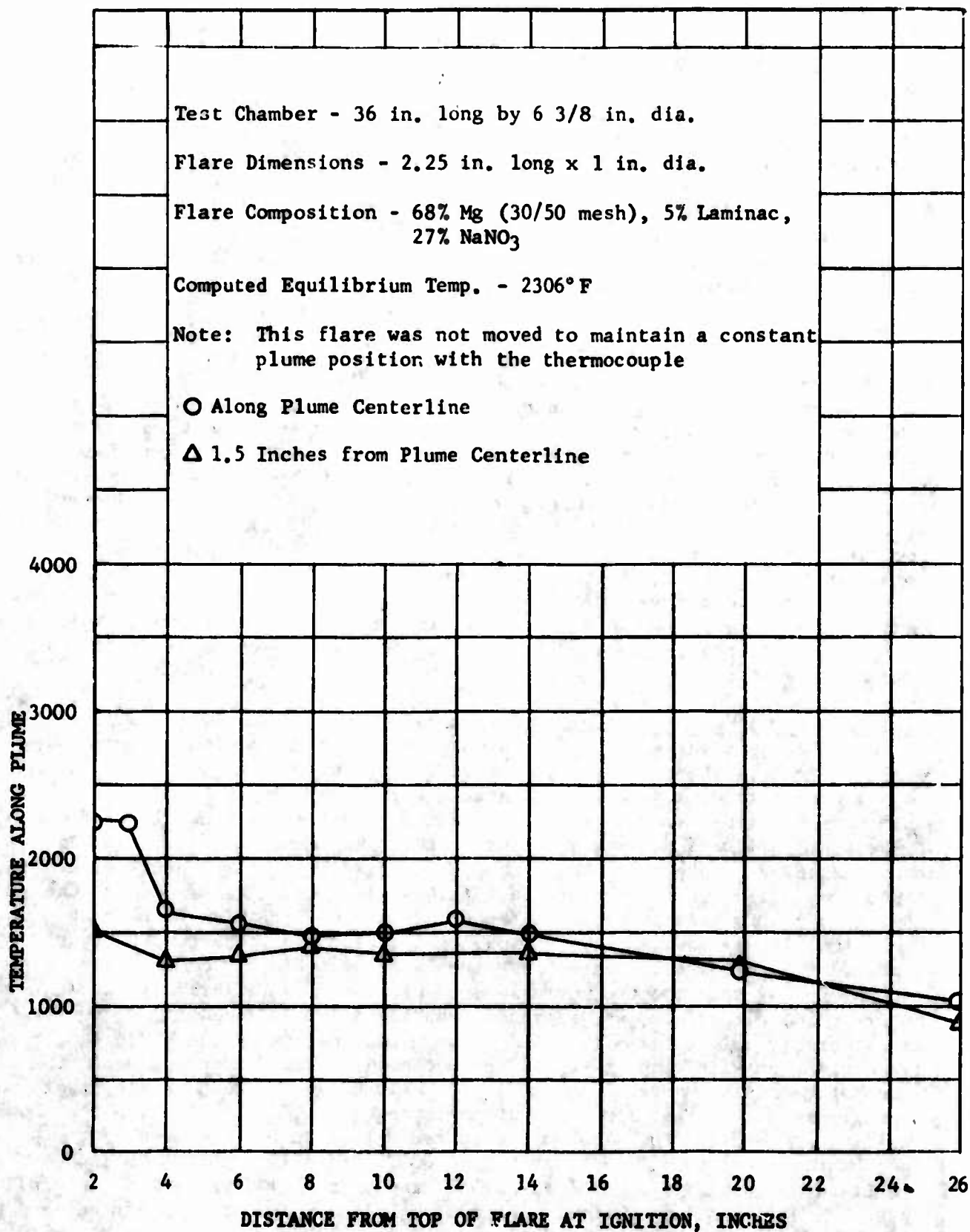


Figure 22 - Temperatures in the flare plume as measured by chromel-alumel thermocouple with .062 in. dia. inconel sheath. Points represent average for minimum of 3 tests. Burning occurred in an inert atmosphere.

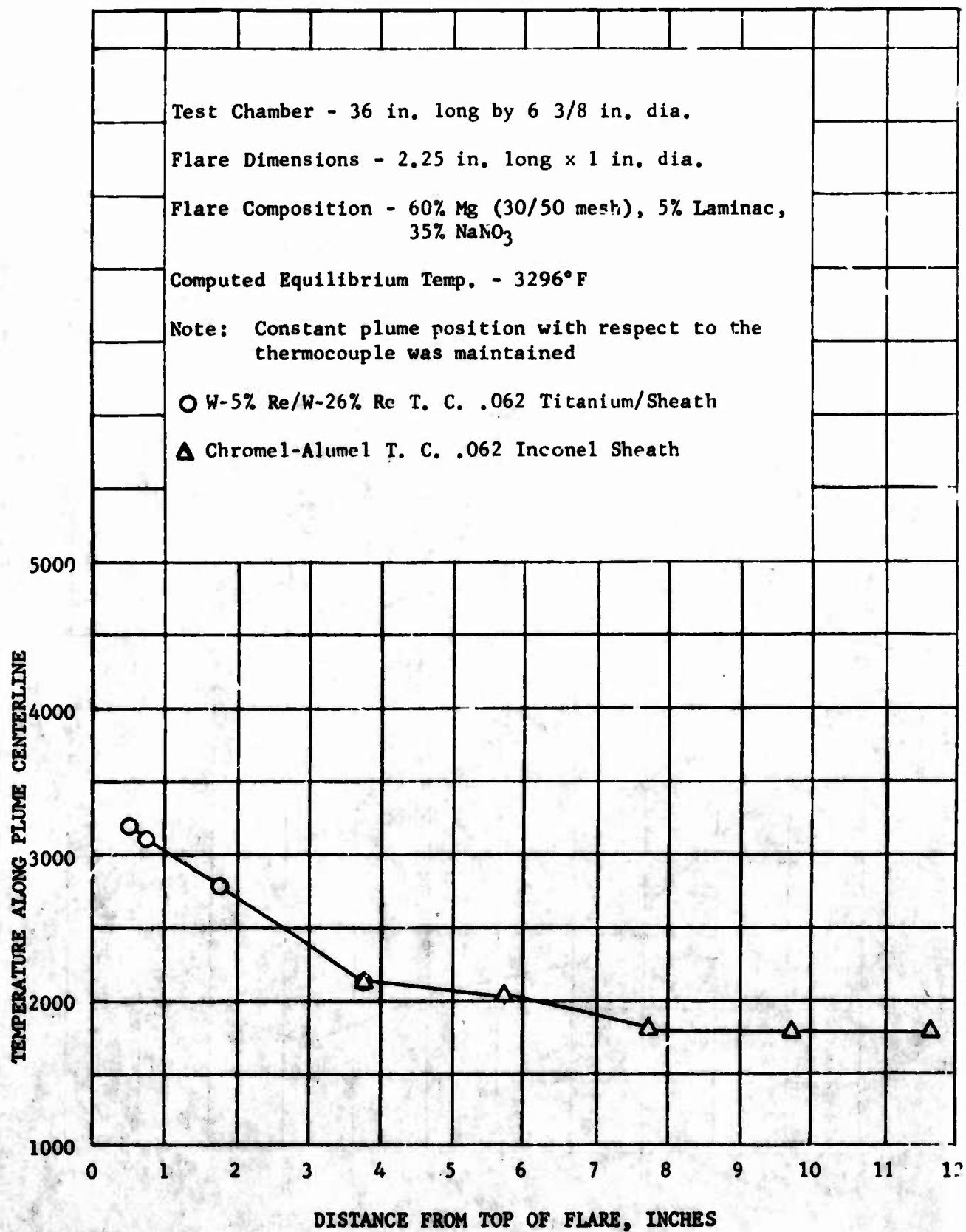


Figure 23 - Temperatures along flare plume centerline. Points represent average for minimum of 3 tests in an inert atmosphere.

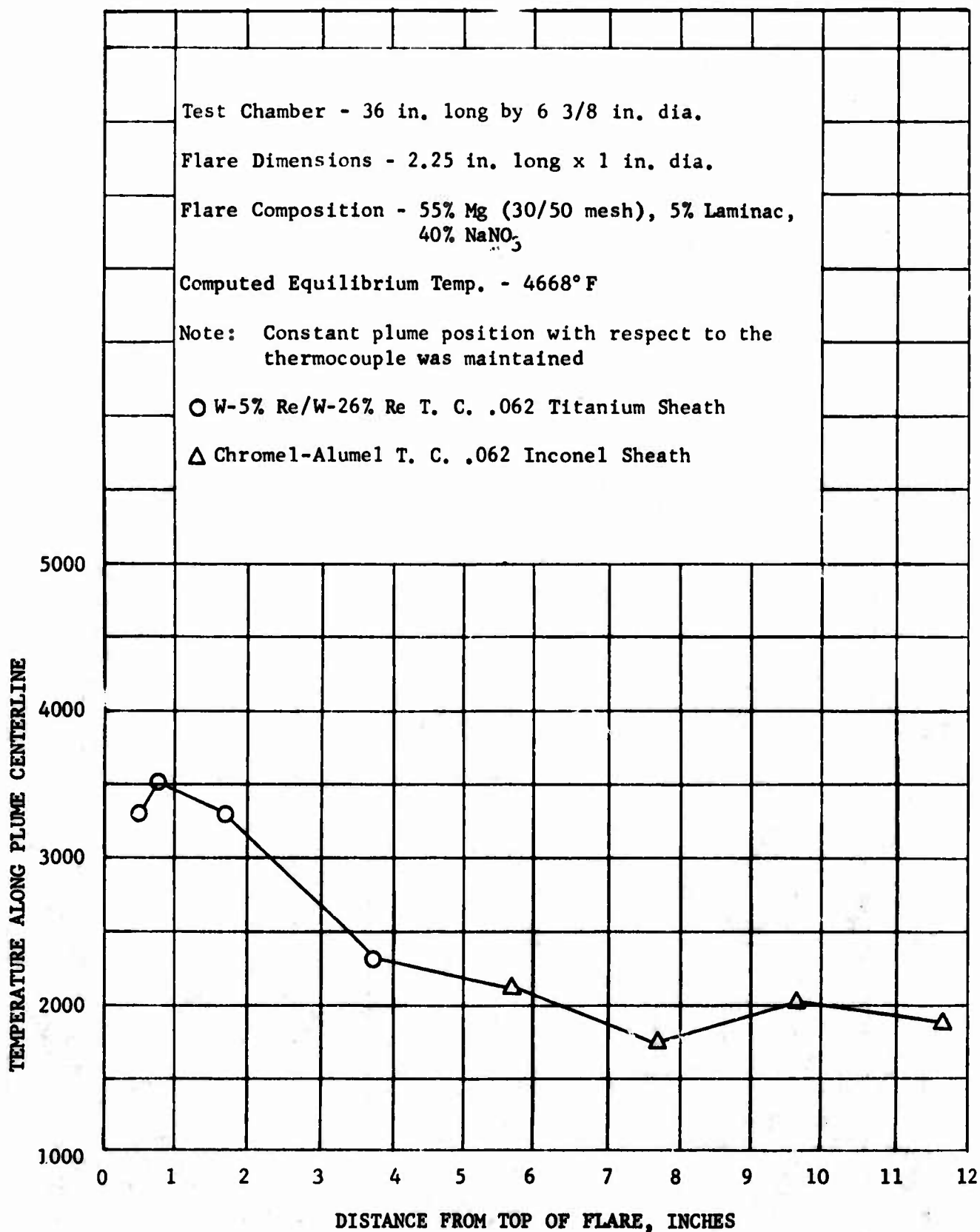


Figure 24 - Temperatures along flare plume centerline. Points represent average for minimum of 3 tests except at 3.75 inches for which there was only one test. All tests were made in an inert atmosphere.

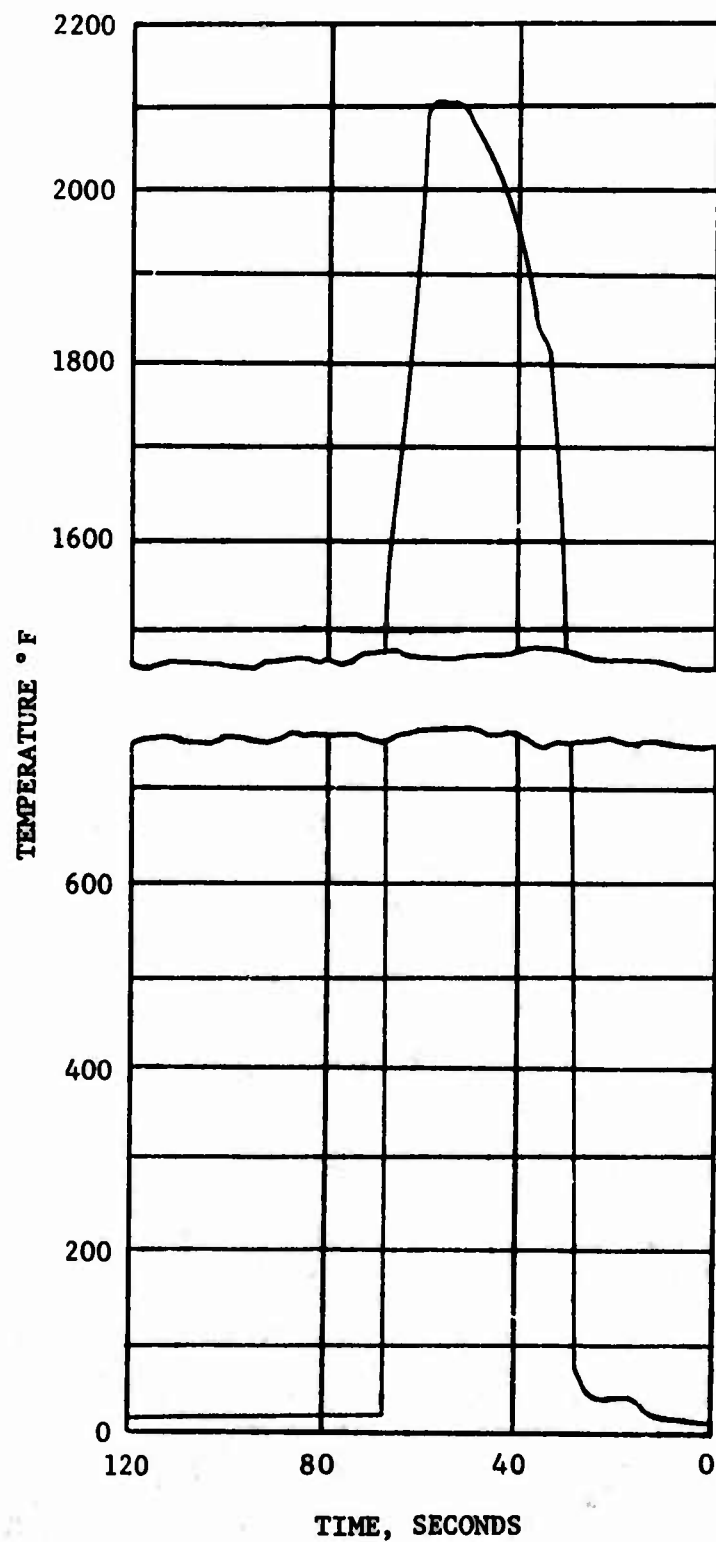


Figure 25- Typical temperature - time trace for chromel-alumel thermocouple 3 3/4 inches above a 60 percent magnesium - 5 percent Laminac - 35 percent sodium nitrate flare.

For the flare composition containing 55 percent magnesium, the computed equilibrium temperature was not reached. Temperature measurements at the center of the plume are shown in figure 24. It can be seen that the maximum average temperature for the 55 percent magnesium flare is more than 1100°F lower than the computed equilibrium temperature.

ANALYSIS OF RESULTS

The primary concern in this part of the program was to determine the degree of correlation that could be obtained between the theoretical temperatures and that obtained experimentally with thermocouples or other means. It was determined that agreement between the measured and theoretical could be achieved with flares containing 60 to 68 percent magnesium, 5 percent Laminac, and the remainder sodium nitrate. Furthermore, it was found that with certain formulations the maximum plume temperatures were low enough to permit the use of chromel-alumel thermocouples which have a long use history. These were also used to cross-check the tungsten/rhenium type thermocouples. Thus it can be stated with a high degree of confidence that thermocouple measurements in flares are reliable and meaningful. However, due to the low response time of a shielded thermocouple it would measure the mean and would not reflect short excursions to higher (or lower) temperatures such as might be expected with random burning of magnesium particles.

Upon reviewing the results of the thermochemical calculations and the temperature measurements a further review of the literature was made to determine if there were experimental results available which might provide additional information.

Plume Temperature - Reference is made to figure 18 which shows the results of the thermochemical calculations for flares containing 20 to 68 percent magnesium. Because of the large difference between theoretical and experimental temperatures for the 55 percent magnesium formulation the tests were repeated to verify the results and a search of the literature was made to determine whether or not such a result had previously been encountered. What appears to be a parallel result was obtained in the work reported in reference 4. The objective of one of the tests conducted in that program was to determine the effect of flare diameter on luminous efficiency with varying formulations including one set in which the percent of magnesium was varied. It was found that with both 1.76 inch and 2.66 inch diameter flares there was a drop in luminous efficiency for a magnesium content below approximately 62 percent. This result was replotted from data in figure 9 of reference 4 and is included herein as figure 26. It was stated in reference 4 that there was doubt concerning the test results shown for the small diameter 55 percent magnesium flares. It is believed that in light of the results obtained with the 55 percent magnesium flares in this program, that the results shown in reference 4 are valid. The primary problem that must be solved is the reason for the low temperature and low luminous efficiency with the 55 percent magnesium flare in the smaller diameters. As can be seen by figure 26, for the 4.25 inch diameter flares the luminous efficiency is highest with 55 percent magnesium. A further evaluation of this result may be made by considering the results of reference 6. In that reference the Mark-24 formulation (58 percent magnesium) produced an experimental temperature of 2736°K which compares favorably with the theoretical temperature of 2620°K. It would appear, therefore, that combustion with the 4.25 inch diameter flare is more efficient than with the

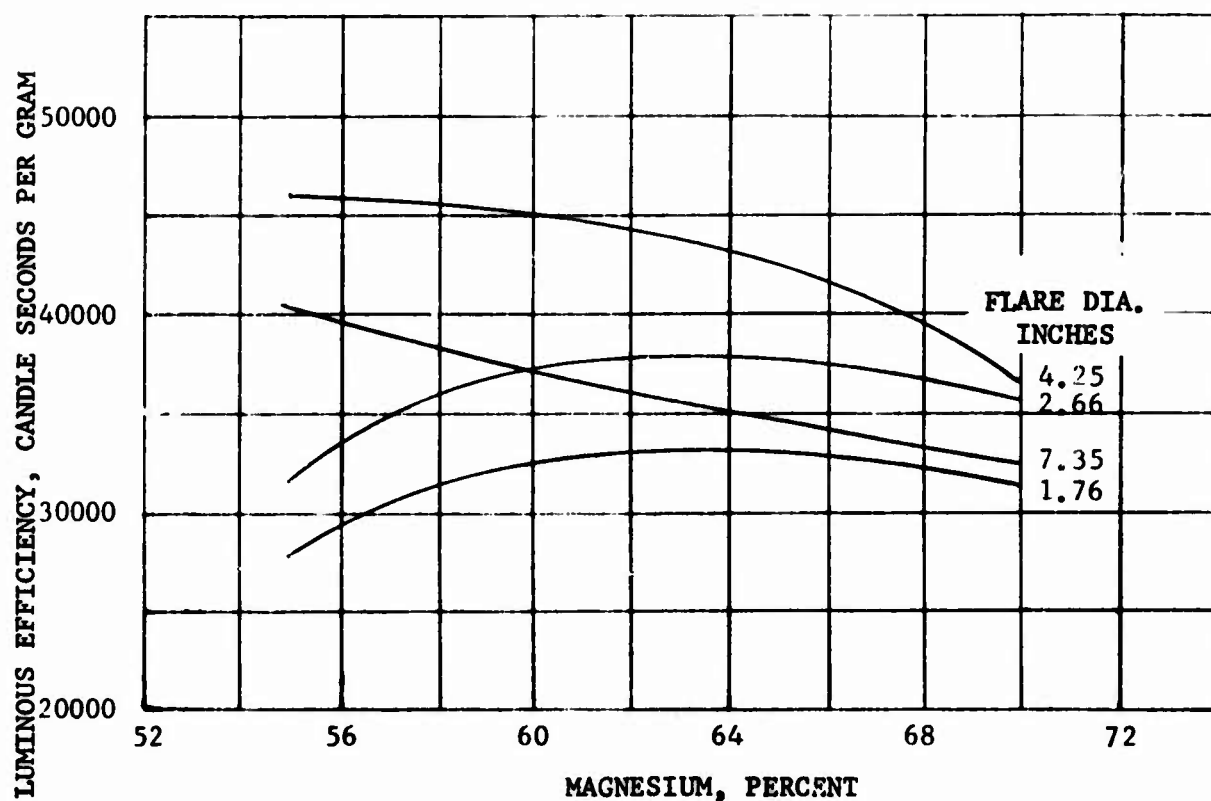


Figure 26 - Luminous efficiency versus percent magnesium for various diameter cylindrical flares. Data from RDTR No. 105 Vol. I, Page 26. Composition 5% Laminac, magnesium as shown and remainder sodium nitrate. Magnesium particle size 30/50 mesh.

smaller diameter flares. It may be argued that there is a difference in the structure of the flare plume which results in either a higher measurement of luminous efficiency or a smaller degree of radiation of heat from the plume in the 4.25 inch diameter size. However, referring to figure 18, there is approximately a 10 percent increase in magnesium oxide in the plume in dropping from 64 percent magnesium to 55 percent magnesium, a factor which should result in optically thicker layers within the plume and therefore a smaller amount of radiation from it.

Further indication of effects of reducing the magnesium content may be seen in the results shown for the cast flares on page 6 of reference 3. The graph therein shows a rise in average candleseconds per gram from 12000 at 73 percent magnesium to 29000 at 48 percent magnesium. As the magnesium content is decreased below 48 percent, the light output decreases to 10000 candleseconds per gram at 22 percent magnesium. It can be seen from figure 19 herein that the theoretical temperature is highest between 22 and 40 percent magnesium. Thus, there is agreement between the fall off in theoretical temperature and luminous efficiency above 48 percent magnesium but not below 48 percent. Also, below 48 percent magnesium both the sodium and sodium chloride vapor content increases. A clue to this behavior may be provided in considering the effect of altitude and pressure.

Altitude Effects - Evaluations of altitude effects upon luminous efficiency are contained in both reference 2 and reference 7. The results of reference 7 which pertain to magnesium-sodium nitrate flares are most closely related to the results shown in figure 18. It should be noted, however, that the flares of reference 7 did not use a binder. They were 0.625 inches in diameter by approximately 4.0 inches long and were encased in waxed kraft paper tubes. Some of the results taken from reference 7 are as follows:

TABLE I - DATA FROM REFERENCE 7

Mixture Ratio	Efficiency-Candle- seconds per Gram		Burn Rate- in/min	
	80000 ft.	Sea Level	80000 ft.	Sea Level
60-40 Mg*- NaNO ₃	230	13,700	17.1	60.4
70-30 Mg - NaNO ₃	310	19,400	20.1	56.2
80-20 Mg - NaNO ₃	590	30,600	16.4	48.3
90-10 Mg - NaNO ₃	-	7,400	-	19.1

*Mg - 200/325 mesh, no binder

The lower luminous efficiency at 80000 feet reflects the result shown in figure 18. However, the very low efficiency at altitude cannot be accounted for by the difference in plume temperature shown on figure 18. This indicates that there are other factors, such as radiation of energy from the plume, which become more significant at altitude and affect efficiency, but which are not taken into account in the thermochemical calculations. Similar decreases in efficiency with decreasing pressure were reported in reference 2. Perhaps the effects of pressure on combustion should be considered at this point.

Pressure Effects - The burn rate sensitivity to changes in pressure for solid propellants is well known. At least two examples of magnesium fueled Aerospace Research Corporation gas generator propellants are available. The first of these uses 13.5 percent magnesium and was previously mentioned herein as an example of a propellant using a tetrafluoroethylene binder, reference 5. This propellant will not ignite at sea level temperature and pressure but will ignite and burn efficiently at 600 psi. Although the solids content in the combustion products is 30 percent, in over 100 tests plugging of the gas generator exhaust nozzle has not occurred. The second propellant uses 25 percent magnesium, 20 percent binder and the remainder ammonium perchlorate. Efficient combustion is achieved at 300 psi. Solids in the combustion products have presented no problem. Inasmuch as the propellants were developed for these specific chamber pressures, there were no evaluations made at lower pressures. Also, the illumination efficiencies of gases issuing from an exhaust nozzle were not evaluated.

Particle Size Effects - The effect of atomized magnesium particle size on burn rate and luminous efficiency has been given a preliminary evaluation by personnel at Picatinny Arsenal and is reported in references 8 and 9. As reported in reference 9, with decreasing particle size there is a decrease in luminous efficiency and an increase in burning rate. For reference, the luminous efficiency

and burn rate data for three 46.5/52.5/1 magnesium/sodium nitrate/vinyl alcohol acetate resin flare systems containing 200/325, 50/100, and 30/50 mesh magnesium powder as reported in reference 9 is given in the following table:

TABLE II - DATA FROM REFERENCE 9

	Mean Efficiency for Group of Five Candles, Kilocandle sec/gm		Mean Burn Rate for Group of Five Candles, Inches/Min.	
Case Internal Diameter (in.):	0.62	1.33	0.62	1.33
200/325 system (22 ± 8 microns)				
Thin wall*	13.8	12.6	33.3	30.2
Medium wall	13.0	12.8	33.7	28.7
Thick wall	11.5	12.1	33.5	28.6
50/100 system (200 ± 25 microns)				
Thin wall	22.1	18.7	12.4	12.3
Medium wall	21.0	19.4	12.3	12.3
Thick wall	18.9	19.4	12.5	12.1
30/50 system (350 ± 50 microns)				
Thin wall	22.6	29.1	5.9	6.9
Medium wall	21.7	28.3	5.9	6.4
Thick wall	16.9	30.9	5.6	6.4

*Paper Case Wall Thicknesses 0.03, 0.05, 0.08 inches for 0.62 in. diameter and 0.03, 0.04, and 0.10 inches for 1.33 in. diameter.

Note that the binder content of this system is only one percent which may account for this 46.5 percent, 30/50 mesh, magnesium flare approaching the luminous efficiency of the 55 percent, 30/50 mesh, flare of 1.76 inches diameter as reported in reference 4. Note that there is a significant case effect for the 0.62 inch diameter flares but not for the 1.33 inch diameter flares. The increase in luminous efficiency with increase in diameter for 30/50 mesh magnesium flares agrees with the results reported in reference 4. The 200/325 and 50/100 systems show little change in luminous efficiency as the diameter is increased. Data have not been found in the literature for flares using larger particle sizes than 30/50 mesh.

General Remarks - There appears to be a relation between the luminous efficiency and the volume of gas generated in the plume whether due to low plume pressure, high burn rate, or composition of combustion products. For example, the burn rate decreases with increasing altitude, but due to the low pressure, the specific volume of the combustion products is significantly larger than at sea level. Whether or not this is the main cause has not been determined, but there is a large drop in luminous efficiency. With a decrease in magnesium particle size there is a large increase in burn rate and thus an increase in the volume of the combustion products flowing per unit time. Again, this has not been established as the main cause, but there is an accompanying large drop in luminous

efficiency. With decreasing magnesium content in a flare there is an accompanying increase in gases other than magnesium. As shown in figure 26, for small diameter flares, the luminous efficiency decreases as the magnesium content is decreased. For large diameter flares there is an increase in luminous efficiency with decrease in magnesium. This suggests that the plume size and residence time in the plume of the combustion products are factors in performance. These are dependent upon flare composition, combustion pressure, flare diameter, volatility of the combustion products, and composition of the combustion products.

For example, for small flares it may be desirable to use magnesium particle sizes below 30/50 mesh. Plots of burning rate and luminous efficiency versus particle size from reference 9 are shown in figure 27 with extrapolations to include a 450 micron (20/50 mesh) particle size. If, by the use of 20/50 mesh magnesium, the flare burn rate could be cut to 3.5 inches per minute as is indicated by the extrapolations, a one-inch diameter 30/50 mesh magnesium flare could be increased to 1.36 inches, thereby increasing the plume size and presumably the luminous efficiency. This, of course, would allow the length to be reduced by one half for the same burn time. The increased diameter would also reduce the effect of the case on performance and the performance at altitude should be improved.

Another change which might improve efficiency would be incorporation of a material such as sodium peroxide, if possible, as a replacement for sodium nitrate. This would decrease the specific volume of the combustion products by eliminating the nitrogen gas.

SUMMARY

Thermochemical calculations were made for a number of flare formulations and temperatures were measured in magnesium-Laminac-sodium nitrate flare plumes. An attempt was made to correlate the results of the thermochemical calculations with measured temperatures as well as other experimental data in the literature. The principal conclusions are as follows:

1. Thermochemical calculations provide a rapid means of determining maximum equilibrium temperature and exhaust products in the plume of an illuminating flare.
2. The flare temperatures determined by the thermochemical calculations agree with the maximum temperatures measured by thermocouple in the plumes of one-inch diameter magnesium-Laminac-sodium nitrate flares containing 60 percent magnesium or greater.
3. The maximum temperature points for the 55 and 60 percent magnesium flares was much closer to the flare surface than for the 68 percent magnesium flare.
4. The flame temperatures determined by the thermochemical calculations agree with the maximum temperatures determined by gray body emission for Mark-24 Mod 2 flares as reported in RDTR 44, NAD, Crane, Indiana.
5. For magnesium-Laminac-sodium nitrate flares the thermochemical calculations predict lower flame temperatures at 81000 feet than at

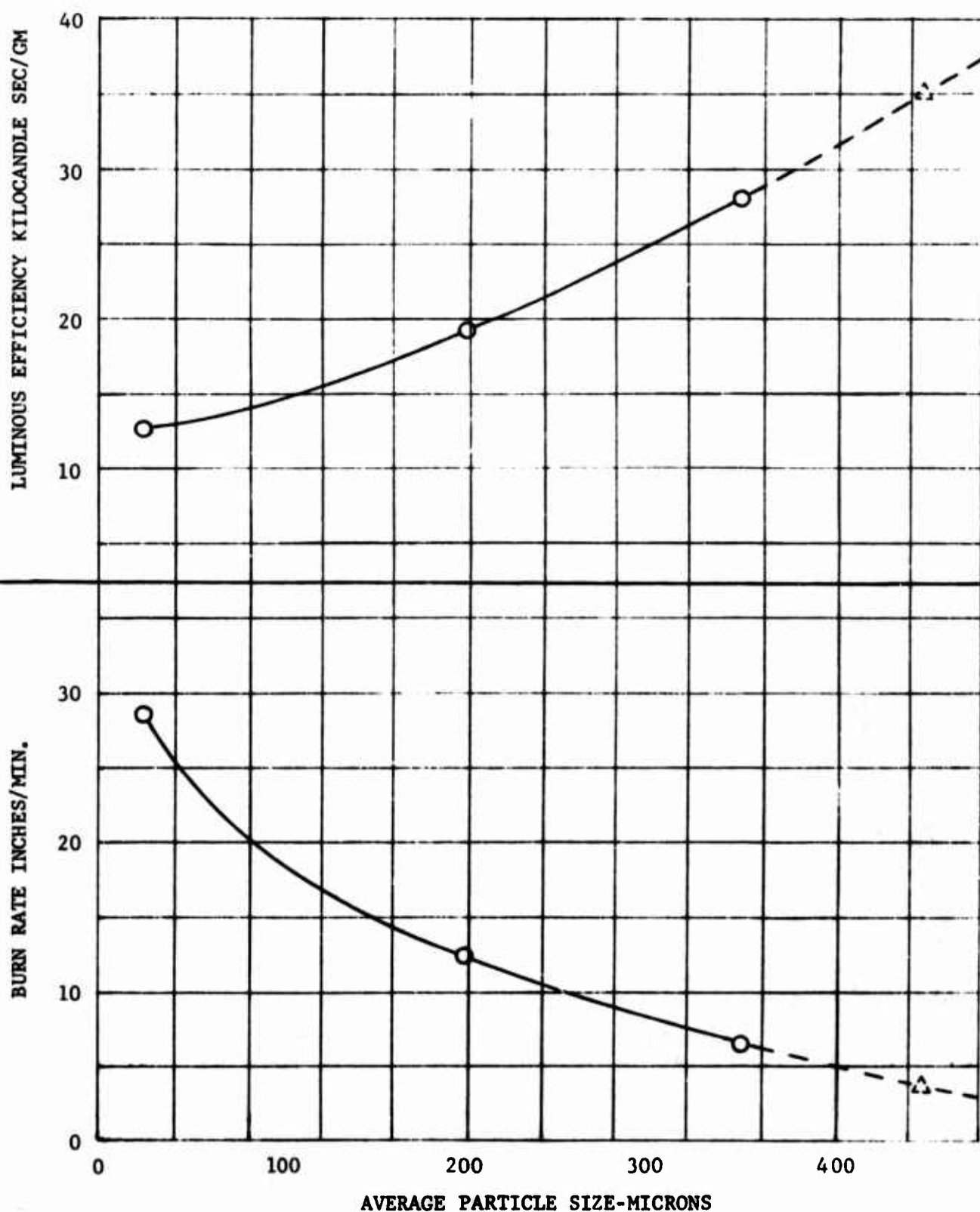


Figure 27 - Luminous efficiency and burn rate versus particle size for 46.5 magnesium/52.5 sodium nitrate/1.0 percent vinyl alcohol acetate resin flare system. Flare diameter 1.33 inches with .05 inch thick paper case. (Data from Reference 9).

sea level for magnesium content below 59 percent.

6. An analysis of the results indicates that data should be generated to determine the effects of variation in flare composition, including particle size, over a range of flare diameters.

LIST OF REFERENCES - SECTION III

1. A General Method for Automatic Computation of Equilibrium Compositions and Theoretical Rocket Performance of Propellants, NASA TN D-132, October 1959, by Sanford Gordon, Frank J. Zelesnik, and Vearl N. Huff
2. Processes Occurring in Pyrotechnic Flames, RDTR No. 35, April 1966, Contract N164-10520, AD637512, by R. M. Blunt, Denver Research Institute
3. Binder Study - Visual Cast Flares, RDTR 92, AD655821, March 1967, by H. R. Waite and Y. Arikawa, Ordnance Research Incorporated, Fort Walton Beach, Florida
4. 25 Million Candle Cast Flare, Diameter and Binder Study, RDTR No. 105, January 1968, Volumes I and II, by Bernard E. Douda, U. S. Naval Ammunition Depot, Crane, Indiana
5. Extending The High Temperature Capability of Aircraft Power Plant Fire Extinguishing Systems, by Matthew de Rouville, Jr., March 1968, Walter Kidde & Co., Inc., Belleville, New Jersey
6. A Method For Determining The Effective Emitting Temperature of a Radiating Body, RDTR 44, August 1964, AD604015, by George E. Laramore and Duane M. Johnson, NAD, Crane Indiana
7. New Flare Formulations For High Altitude Application, Technical Report 3360, AD641957, October 1966, by James A. Carrazza, Jr., Bossie Jackson, Jr., and Seymour M. Kaye, Picatinny Arsenal, Dover, New Jersey
8. The Effects of Processing on Pyrotechnic Compositions Part II: Statistical Analysis of Effects of Particle Size on Burning Rate and Illuminance for Consolidated Pyrotechnic Items, by D. E. Middlebrooks and S. M. Kaye, T. R. 3253, October 1965, Picatinny Arsenal, Dover, New Jersey
9. The Effects of Processing on Pyrotechnic Compositions Part III: Dimensional Effects of Paper Cases on Illuminance and Burning Rate of Flare Compositions, by D. E. Middlebrooks, S. M. Kaye, and G. Weingarten, T. R. 3275, January 1966, Picatinny Arsenal, Dover, New Jersey

SECTION IV

FLAME CHARACTERISTICS AND SPECTRAL ANALYSIS

INTRODUCTION

Exploratory studies of the combustion mechanisms in the flare plume have been conducted at the University of Minnesota. Because of the problems that were expected to be encountered with such phenomena as nonhomogeneous burning, turbulent mixing of flare gases with the surrounding gases, radiation to the surroundings, and self-absorption, several possible approaches were considered. These included still photography, fast-action movies, X-ray photographs, spectral analyses, particle studies, and visual studies. All of these were used with varying degrees of success; however, because of the clues to combustion behavior supplied by each of the experimental methods, it is difficult at this point to state which constitutes the most effective research method. The results of each approach are presented herein.

In order to establish a method of rating flares and thereby to evaluate the various aspects of plume behavior, a theoretical evaluation of rating methods was made.

Theoretical considerations are presented in the first section of the report and are followed in order by experimental approach, experimental results, discussion of results, concluding remarks, and summary of results.

THEORETICAL CONSIDERATIONS

A convenient way of considering flame characteristics in the flare plume is to establish a measure of "goodness" and to evaluate various mechanisms which contribute or detract from performance. A usual way of rating flare performance is to compare the light energy emitted in the visible to the heat of reaction. For example, Douda^{(1)*} measures the energy radiated at $4000 \text{ \AA} < \lambda < 7500 \text{ \AA}$ divides by the heat of reaction and refers to this quotient as flare efficiency. Flare efficiencies as high as 10% have been reported⁽¹⁾ on this basis. This performance is influenced by the flare composition and by the way the composition is employed. In this section, two measures of goodness are proposed.

The first measure of goodness, the flare ideal efficacy, borrows its name from the illumination industry literature⁽²⁾ and has the same sense: it is the amount of illumination produced by an element of flare product gas as it cools divided by the amount of illumination that would have been produced if all the energy had been emitted at the wave length at which the eye is most sensitive. Thus, the ideal efficacy is a measure of goodness of the flare constituents. A second measure, the flare efficiency, is the ratio of the actual efficacy to the ideal efficacy and measures the extent to which the burning process approaches the ideal process.

Ideal Efficacy of Gray Gas and D-line Emitters

Light sensitivity of the eye varies somewhat with the individual. Illuminating engineers have therefore agreed upon a visibility curve that, on the average, estimates the relative effectiveness of a watt of radiation at λ to a watt of radiation at 5540 \AA ⁽²⁾. A plot of such a visibility curve $S(\lambda)$ is shown in figure 28(a)⁽²⁾. A Planckian radiator emits radiation as shown in figure 28(b). A gray body emitter radiating at a constant temperature T emits radiant energy over a wide range of wave lengths. Some of this energy contributes to vision. The efficacy of any radiator at fixed T is defined by:

$$\frac{\int_0^{\infty} S(\lambda) I(\lambda) d\lambda}{\int_0^{\infty} I(\lambda) d\lambda}$$

shown in figure 28(c) for a Planckian Radiator.

*Numbers in parentheses refer to list of references, page 92

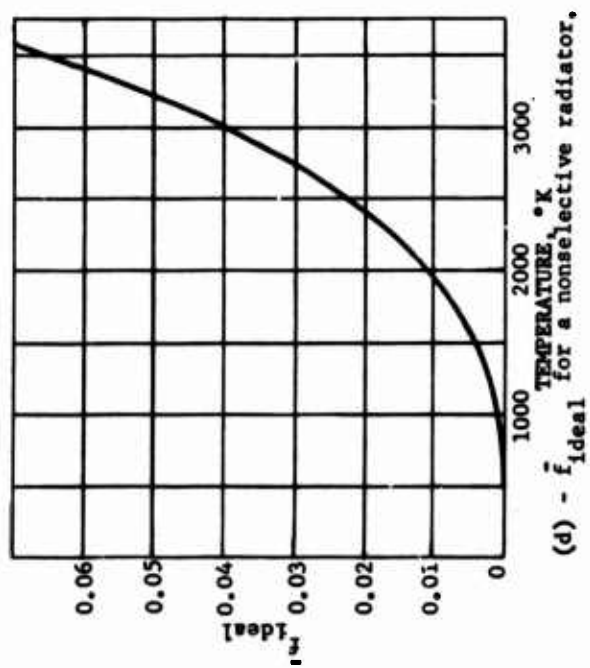
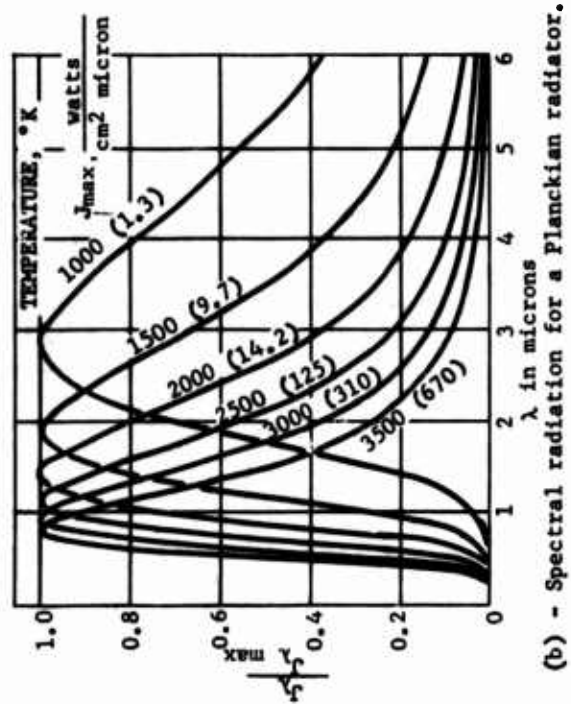
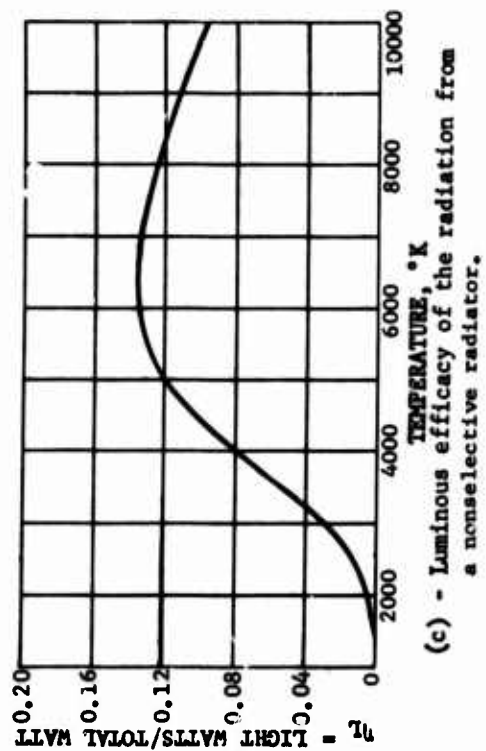
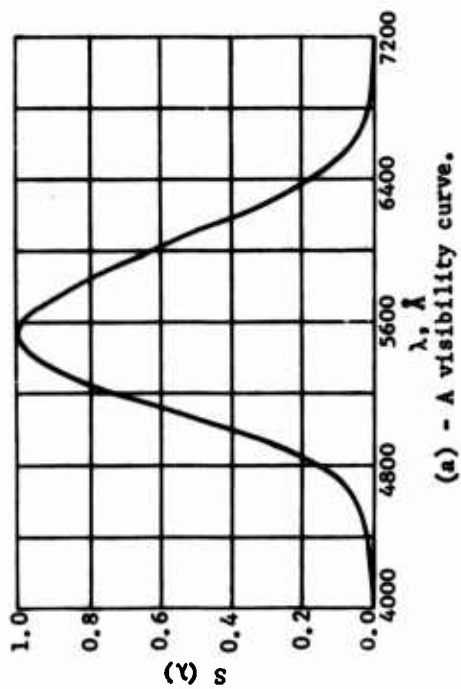


Figure 28 - Curves from reference 2.

The efficacy of a flowing gaseous light source may be defined as the efficacy of the light emitted as a particle of optically thin gas cools from a temperature T^* to $T-dT$ integrated from flame T to ambient T . For a gas of constant specific heat, this is:

$$\text{Ideal Efficacy} \equiv \bar{f}_{\text{ideal}} \equiv \frac{\int_{h_{\text{amb}}}^{h_i} \frac{\int_0^\infty S(\lambda) I(\lambda) d\lambda}{\int_0^\infty I(\lambda) d\lambda} dh}{\Delta h_{\text{reaction}}}$$

A plot of this quantity for a Planckian radiator is given in figure 28(d). If the gas (or particle suspension) departs from gray such that the visible is favored, these values will be higher. Sodium vapor, for example, radiating only at 5900 Å would have an efficacy of 0.77.

A similar idealization for the efficacy of optically thick gases can be made if it is supposed that conditions within the plume keep the temperature uniform throughout the plume. Thus, an optically thick gray gas again has an efficacy curve given in figure 28(c).

Optically thick (near the D-line) sodium vapor radiation has an efficacy given by⁽³⁾

$$\bar{f}_{\text{ideal}} = \frac{\int_0^\infty S(\lambda) \left[1 - \exp \left(-(0 \cdot D) W_0^2 / (W_0^2 + [\lambda - 5900]^2) \right) \right] d\lambda}{\int_0^\infty \left[1 - \exp \left(-(0 \cdot D) W_0^2 / (W_0^2 + [\lambda - 5900]^2) \right) \right] d\lambda}$$

where $W_0 = 0.049 \text{ Å}$ and $OD = \frac{N_{\text{Na}} L}{10^{11}}$. Because of the shape of the visible curve, this integral will again be:

$$\bar{f}_{\text{ideal}} \approx 0.77 \quad \text{for } OD \leq 10^6$$

for $OD > 10^6$, the value of \bar{f}_{ideal} will slowly fall with increase in OD .

Most particle plumes will have $OD \leq 10^6$ so that $\bar{f}_{\text{ideal}} = 0.77$ should suffice. If no interaction occurs, optically thin plumes of MgO solid and Na gas should have efficacies that lie somewhere between that of the indicated components and as calculated above.

*Symbols for this section are defined in Appendix X, page 182.

Efficacies of Mixtures of Na and MgO Particles in a Transparent Suspending Gas

As shown on page 43 the combustion products of the Mg- NaNO_3 flare contain on the order of 10% Na and 30% MgO(s) and the density of the hot gas is approximately 10^{-4} gms/cm³. Thus, an optical path length for sodium (at the D-lines) is 10^{-6} cm and of the MgO is 60 cm. Rossler (4) gives the emissivity of MgO by

$$\epsilon_{\text{MgO}} = 0.35 \tanh\left(\frac{L}{60}\right)$$

or for $L \ll 60$ cm. $\epsilon_{\text{MgO}} \approx 0.35 \times \frac{L}{60}$. Thus, for plane sheets of gas (and particles) of thickness L , negligible interactions between Na and MgO radiation may be expected so long as $L \ll 60$ cm. The energy emitted from a D-line at temperature T is then:

$$E_{\text{Na}} = J(5900, T) (0.049 \times 10^{-4}) \left(\frac{L}{10^{-6}}\right)^{1/2} \frac{\text{Watts}}{\text{cm}^2}$$

and from MgO(s).

$$E_{\text{MgO}} = E_{\text{BB}}(T) \times 0.35 \times \left(\frac{L}{60}\right), \quad L \ll 60$$

The efficacy of the mixture, then, at a fixed T is:

$$\frac{E_{\text{Na}}}{E_{\text{Na}} + E_{\text{MgO}}} \times 0.77 + \frac{E_{\text{MgO}}}{E_{\text{Na}} + E_{\text{MgO}}} \times (\text{efficacy for Planckian radiator})$$

Efficacies for layers 10^{-6} , 1 and 10 cm are shown in Table III at the temperature T . Table IV shows the integrated efficacy of the gas as it cools from T to ambient T (for $C_p = \text{const.}$). It can be seen that as the gas thickness increases and as temperature falls, the efficacy falls and becomes increasingly dominated by MgO(s) and its correspondingly low efficacy.

For $L \geq 60$ cm, the trend will continue; *i.e.*, the efficacy will continue to fall; however, the above approximations no longer apply. Thus, if the flare gas mixes internally but does not mix externally with its surrounding gas, its efficacy should fall with increasing size of flare, and approach the Planckian radiator. These calculations are obviously only approximations. It is felt, however, that the results give a reasonable qualitative picture of the way a mixture of gray and line emitters behave with thickness.

Douda (1) reports overall efficacies of 4% for a flare of plume thickness greater than 10 cm. It is clear then that the results of Table IV underestimate ideal efficacies. One possible explanation lies in the influence of the breadth of the D-line. Strong and Bundy (3) were followed in obtaining Tables III and IV. Experimentally observed D-line breadths are broader than predicted. It is believed that this broadening may be related to the continued active combustion of the Mg within the plume and the non-uniform temperature near these particles due to combustion.

TABLE III. RADIATION PROPERTIES OF A 30% MgO, 10% Na MIXTURE AT A FIXED TEMPERATURE

	TEMPERATURE, °K							Slab Thickness cm
	2000	2200	2400	2600	2800	3000	3500	
Efficacy, gray body	0.32	0.8	1.1	1.5	2.1	3.1	5.3	- -
Efficacy, Na(g)	77	77	77	77	77	77	77	- -
Fraction of radiation from MgO(s)	.032	.061	.009	.006	.004	.003	.002	10 ⁻⁶
Efficacy of mixture, %	74.5	75.6	76.3	76.5	76.6	76.7	76.8	10 ⁻⁶
Cooling rate, dT/dt °C/sec.	5.6·10 ⁵	1.7·10 ⁶	4.2·10 ⁶	8.4·10 ⁶	3.8·10 ⁷	3.1·10 ⁷	9.6·10 ⁷	10 ⁻⁶
Fraction of radiation from MgO	.97	.94	.90	.85	.80	.75	.63	1
Efficacy of mixture, %	2.61	5.37	8.61	12.83	17.08	21.58	31.84	1
Cooling rate, dT/dt °C/sec.	1.8·10 ⁴	2.8·10 ⁴	4.2·10 ⁴	6.2·10 ⁴	8.8·10 ⁴	1.2·10 ⁵	2.7·10 ⁵	1
Fraction of radiation from MgO	.99	.98	.968	.950	.930	.914	.855	10
Efficacy of mixture, %	1.09	2.10	3.52	5.28	7.34	9.44	15.64	10
Cooling rate, dT/dt °C/sec.	1.6·10 ⁴	2.7·10 ⁴	3.9·10 ⁴	5.5·10 ⁴	7.5·10 ⁴	1.0·10 ⁵	2.0·10 ⁵	10

TABLE IV. IDEAL EFFICACY FOR A FLUID ELEMENT CONTAINING 30% MgO and 10% Na FROM THE INITIAL TEMPERATURE SHOWN TO 300°K

Initial Temp.	Ideal Efficacy, %		
	10 ⁻⁶ cm slab	1 cm slab	10 cm slab
1500°K	0	0.0	0.0
2000	21	0.38	0.19
2500	33	1.87	0.93
3000	40	4.30	2.15
3500	47	7.8	3.90

Also shown in Table III is an estimation of the rate of cooling which a fluid element would experience due to radiation. Observing that relatively little illumination results from gas cooling below 2000°K, cooling time may be estimated from the time it takes the gas to cool the first 1000°K. Thus, for the 1 and 10 cm slabs, the cooling time is of order 2×10^{-2} seconds.

Of particular interest is the interaction between the two emitters. Perhaps the most important interaction is the influence of the continued magnesium combustion in the plume. This can result in temperatures higher than the adiabatic temperature near burning particles. Phase changes associated with the condensation and solidification of MgO strongly influence the enthalpy-temperature relationship. For example, the quantity of energy radiated for given enthalpy difference will be fixed. The rate of energy radiated will depend upon the distribution of $\left. \frac{\partial h}{\partial T} \right|_p$ with temperature. This value is higher at higher temperatures than at lower (as it is for MgO flames), the radiation is higher than if $\left. \frac{\partial h}{\partial T} \right|_p$ is constant. Thus, in the ideal model (where radiation is the only mode of heat loss) the efficacy of the Na contribution will be enhanced by the presence of MgO. In an actual flare where the rate of radiation competes with the rate of dilution, the presence of the MgO should be an even more important factor.

Flare Efficiency

All of the many factors that influence the performance of the actual flare and cause the light emitted to be less than that of the ideal flare can be ascribed to the inefficiency of the flare burning process. The efficiency of the process may be defined as:

$$\eta = \frac{\bar{f}}{\bar{f}_{\text{ideal}}}$$

in which \bar{f} is the measured efficacy and \bar{f}_{ideal} is the ideal efficacy. The flare studied here has an ideal efficacy (from the above) which is conservatively estimated as 4%. Douda's measurements(1) yield an actual efficacy (according to the definition stated herein) of approximately 2%. Thus, the flare burning process is approximately 50% efficient.

Clearly, any reduction in temperature in an element of gas that does not result from radiation to surroundings represents a degradation in the illuminating potential of the flare and results in the lowering of the flare efficiency. Two major sources of inefficiency seem obvious: convective mixing with cool ambient gas and self-absorption in the cooler plume gases. Self-absorption increases with flare size. Thus, once the cool outer envelope of the flare becomes optically thick ($L > 60$ cm) the flare should appear from without to be at a lower temperature than it is within. Thus, large flares must be more inefficient than smaller flares.

The mixing between flare gases and the surrounding air has not been solved for the inverted jet or distributed sources. An approximate value of mixing time may be obtained by considering the following model. The flare of diameter d_0

produces a volume of gas $\rho_o U_o \pi d_o^2 / 4$ which is brought to rest and reversed by the approaching flow, U_a , with density ρ_a . Then the plume flowing back around the flare will have a velocity,

$$U_p = U_a \sqrt{\left(\frac{\rho_a}{\rho_o}\right)}$$

and a diameter,

$$D = d_o \sqrt{\left\{ \frac{U_o}{U_a} \sqrt{\left(\frac{\rho_o}{\rho_a}\right)} + 1 \right\}}$$

Then the mixing length the plume produces should be proportional to L and the mixing time; therefore,

$$\tau_{\text{mixing}} \approx \frac{L}{U_p} = \frac{d_o \sqrt{\left\{ \left(\frac{\rho_o}{\rho_a}\right) \left[\frac{U_o}{U_a} \sqrt{\left(\frac{\rho_o}{\rho_a}\right)} + 1 \right] \right\}}}{U_a}$$

Mixing time is seen to vary directly with diameter, inversely as the rate of fall U_a , and as the burning rate to approximately the 1/2 power. Thus, a flare of 10^{-1} foot diameter falling at a rate of 10 feet per second would have a mixing time of order 10^{-2} seconds. When this τ_{mixing} is small compared to $\tau_{\text{radiation}}$ inefficiencies due to too rapid mixing will occur. As the flare gets larger, the cool outside of the flare gets progressively more opaque, and the flare becomes less efficient even though given more than adequate radiation time. The effect of gravity will be to reduce the mixing time by increasing U_p .

EXPERIMENTAL APPROACH

Test Apparatus

Spectroscopic Measurements

The optical equipment used for spectrometric measurements is shown schematically in Fig. 29. The lens L_1 , with a focal length of 31 cm, projects an image without enlargement of an area 1 mm high from the center of the flare on the entrance slit of the spectrometer. A Jarrel-Ash .5 m focal length scanning monochromator (82-020) was used. The light intensity was recorded by a photomultiplier (RCA 1P28 for the blue region, RCA 7102 for the red region of the spectrum), and displayed on the strip of a Bristol strip chart recorder. The experimental arrangement is shown photographically in Figure 30. A screw jack driven by an electric motor which was used to raise the flare during combustion can be seen in Figure 30(a). The burning surface of the flare can be kept at constant elevation by manually regulating the motor speed. The apparatus can accommodate a ten-inch long flare.

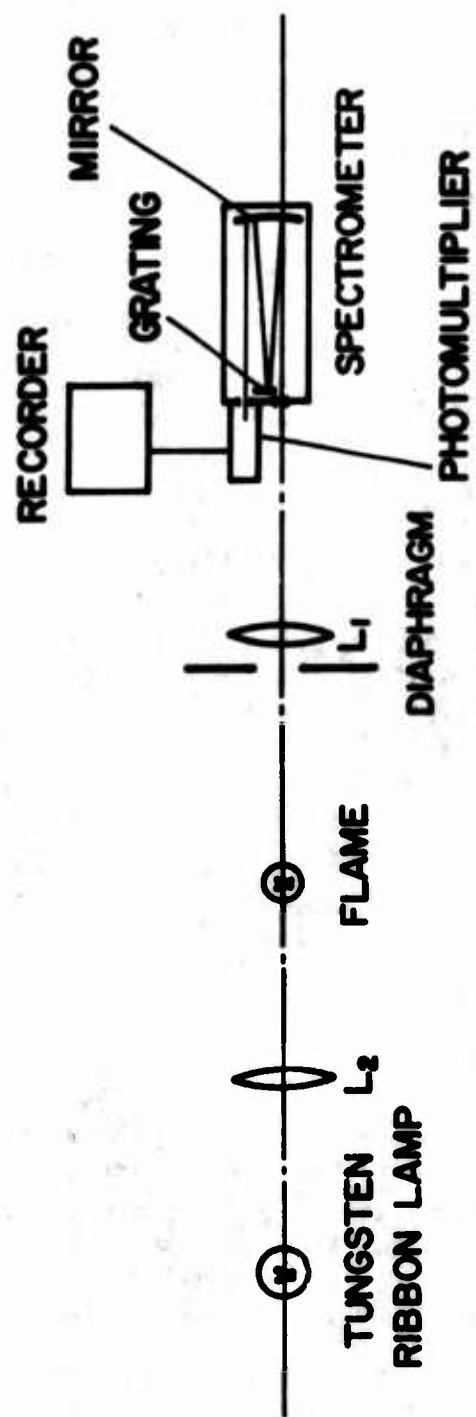


Figure 29 - Schematic of optical apparatus.



(a) Setup showing recorder.



(b) Setup showing lamp arrangement.



(c) Close-up of screw jack mechanism.

Figure 30 - Photographs of spectroscopic setup.

A 10 inch length of 1 inch diameter pipe standing concentrically with a similar length of 2 inch diameter pipe (shown in Figure 30(c)) served to guide the flare. Nitrogen flowing from the annular space between the two pipes provided a gaseous shield around the plume during all spectrometric studies. Input pressure of the N_2 flow was regulated to give a velocity of approximately 20 to 50 feet per second. When several 1 inch diameter by 2 inch long flares were stacked and burned consecutively, the inhibitor material was scraped off the bottom end of all but the bottom-most flare in the stack.

X-Ray

The arrangement of the X-ray apparatus is shown in Figure 31. A helium filled chamber containing the flare made up virtually the entire path-length between the X-ray source (X-Ray Corporation of America model 8-A) and the Polaroid film pack. A 0.001 inch thick aluminum foil masked the film pack from the intense light of the burning flare.

The chamber shown in Figure 31 was 10 inches in diameter and 14 inches in height, with two 4 inch ports on the sides and a 1 1/2 inch port at the top. The chamber was bolted to a matching base plate forming a loose seal.

A Polaroid 4 inch x 5 inch Land film holder was adapted to one of the side ports, while a 27 inch long, 4 inch diameter pipe spaced the X-ray tube away from the flare. Final dimensions were 34 1/2 inches from X-ray tube to flare, and 8 inches from flare to film plane. An optical wedge consisting of 6 stepped layers of aluminum foil was included at the camera port.

The top port was loosely capped during the 1 to 3 minute helium purge prior to flare ignition. The port was uncapped after ignition. After ensuring a steady state burning of the flare (usually 5 to 7 seconds after ignition) X-ray photographs were taken.

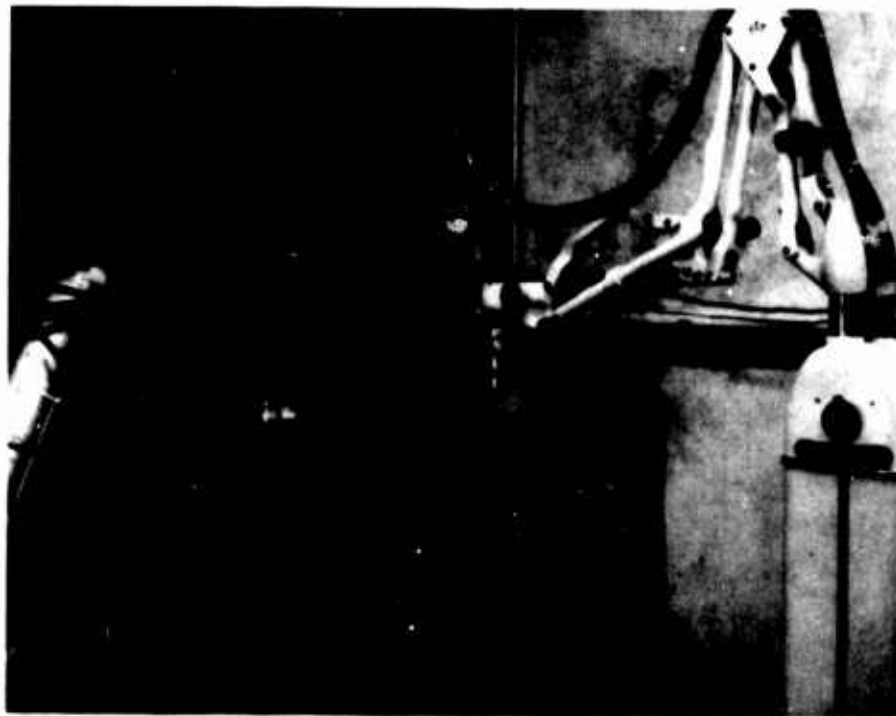
Flare Orientation

The orientation apparatus consisted of a horizontal shaft with an extended arm holding the flare perpendicular to the shaft axis as shown in Figure 32. A hole drilled in the base of each flare accepted a number 12 x 3/4 inch sheet metal screw in the support arm. The one inch square wire mesh located 3 inches in front of the flare as shown in Figure 32 provided a convenient scale for the photographs.

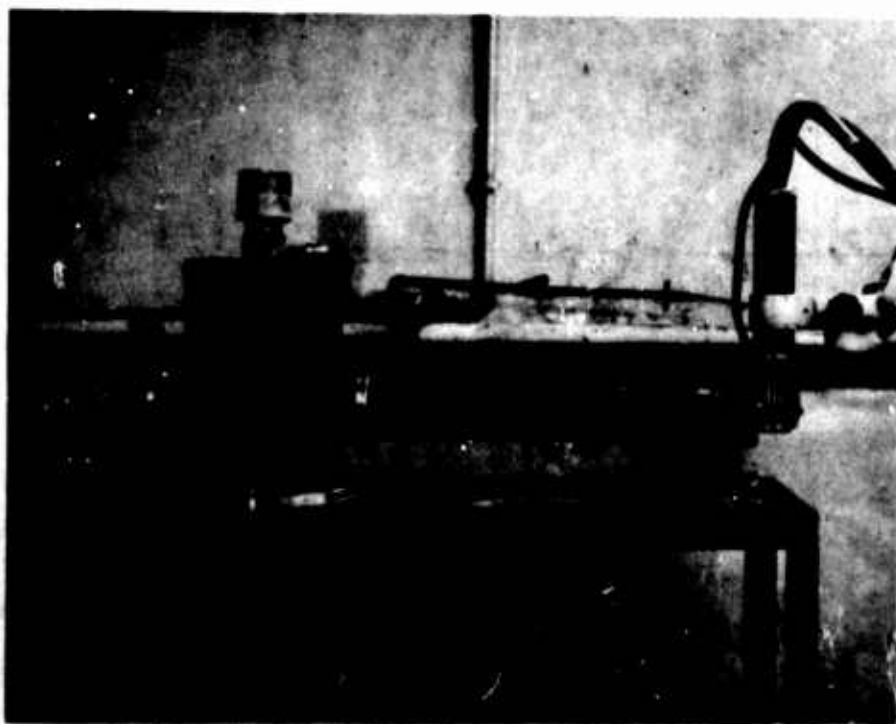
In all cases, the flare was ignited in the vertically up position, then manually rotated to the desired orientation using a 3 1/2 foot extension shaft.

Flare Ignition

Ignition was most conveniently accomplished with a combination of Atlas type M100 electric matches and intermediate initiator material consisting of a mixture of ground flare and gunpowder. The match was taped to the flare, with the head bent so as to lie across the top of the flare. Powder was poured over the match head inside a masking tape collar around the flare top and was then stabilized by a light spray of Krylon clear plastic coating. The firing circuit consisted of four number six dry cells, a switch, and wiring. For convenience, the ignition wires terminated in clips mounted in an asbestos block located near the flare. The match leads from the flare were connected to the clips.

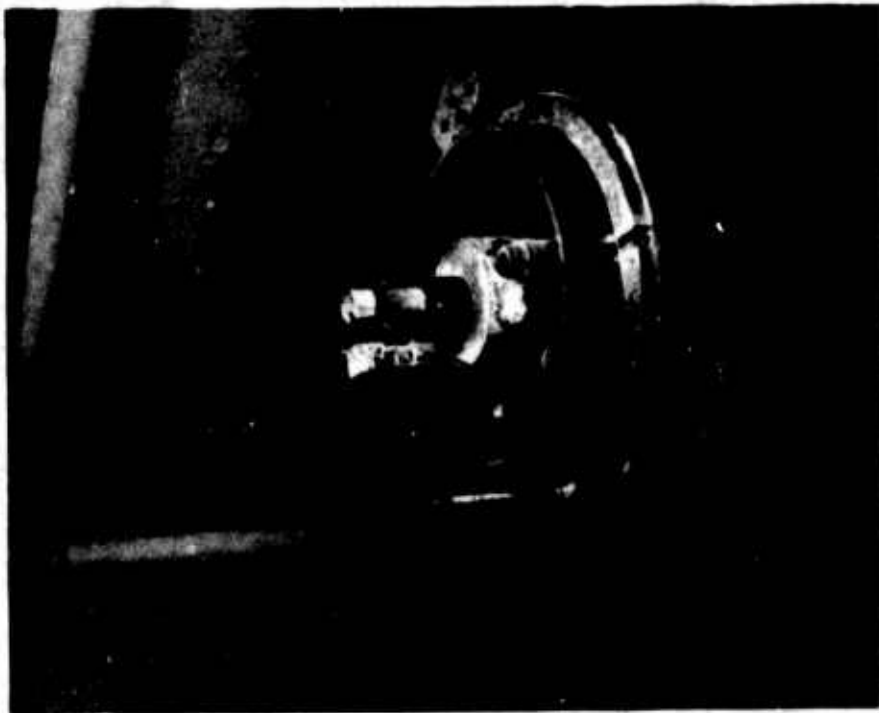


(a) Helium chamber and X-Ray machine.



(b) Helium chamber only.

Figure 31 - Photographs of X-Ray apparatus.



(c) Flare with the igniter attached and chamber ready to be lowered.

Figure 31 concluded - Photographs of X-Ray apparatus.

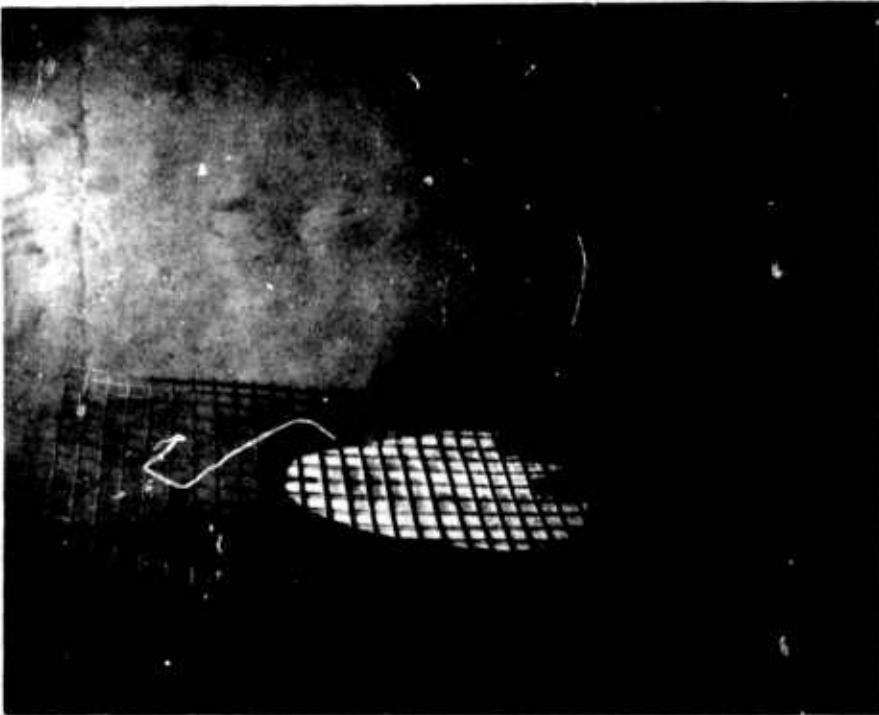


Figure 32 - Apparatus to study orientation effects on plume shape.

EXPERIMENTAL RESULTS

Spectroscopic Studies

A number of spectrometric measurements of the flare were performed in order to determine the wavelength dependence of the emitted radiation, to determine the flare temperature, and to obtain information about the optical depth in the flare at different wavelengths.

The resolution of detail in the emitted spectrum required low recording speeds. In order to keep the number of flares required for the desired wavelength scans within reasonable limits the highest possible scan speed of the spectrometer (500 Å/min) was chosen which allowed sufficient spectral resolution. The wavelength range covered during the burning time of a single flare was approximately 150 to 200 Å with a resolution of 1.6 Å. For a continuous scan over approximately 1,000 Å a stack of 5 two inch flares was utilized. The burning surface was held at a constant position by the feeding mechanism shown in Figure 30(c). With this arrangement the ignition of successive flares sometimes caused large-scale fluctuations of the emitted light intensity. Besides these disturbances, strong short-time as well as long-time fluctuations were observed which may have been caused by inhomogeneities of the solid flare material. These fluctuations caused uncertainties in the recorded light intensities. Figures 33, 34 and 35 show the relative intensity of the flare as a function of the wavelength observed in the center of the flare .75 and 6 inches above the burning surface. The recorded intensities are corrected for the spectral response of the photomultiplier tube. The dashed curve in Figure 33 represents recordings taken with the red sensitive photomultiplier tube.

For the wavelength range between 5400 Å and 6400 Å a longer flare consisting of one piece was utilized for the wavelength scan. The relative intensity of the emitted radiation was in this case, somewhat less than in the case of the short flares. In addition, the wide intensity valley between 5600 Å and 5800 Å was found in this run only.

The spectra reveal several molecular bands in the green region of the spectrum mainly originating from N₂ and CO molecules. In addition, three magnesium lines at 5154 Å, 5173 Å, and 5184 Å are clearly detectable. A considerable amount of radiation in the visible range of the spectrum was emitted by the broadened MgO lines at 4996 Å and 5007 Å. As shown in Figure 34, which refers to measurements taken 6 inches above the burning surface, the percentage of this contribution is much less than the percentage found 3/4 inch above the burning surface. Also, the self-absorption dip of the sodium D-lines is, at this distance, much narrower than close to the burning surface, indicating that the absorbing sodium atoms are at lower temperatures. The measurements taken at this height are more reproducible than the other measurements because there is less disturbance of the emitted radiation. Close to the burning surface larger particles leaving the surface may have caused severe fluctuations of the emitted radiation. Figure 35 shows the neighborhood of the sodium D-lines taken with a smaller scanning speed (125 Å/min).

According to Figures 33, 34 and 35 most of the radiation in the visible region falls in the wavelength range between 4900 Å and 6500 Å. The sodium resonance doublet appears strongly broadened with a deep center dip due to self absorption.

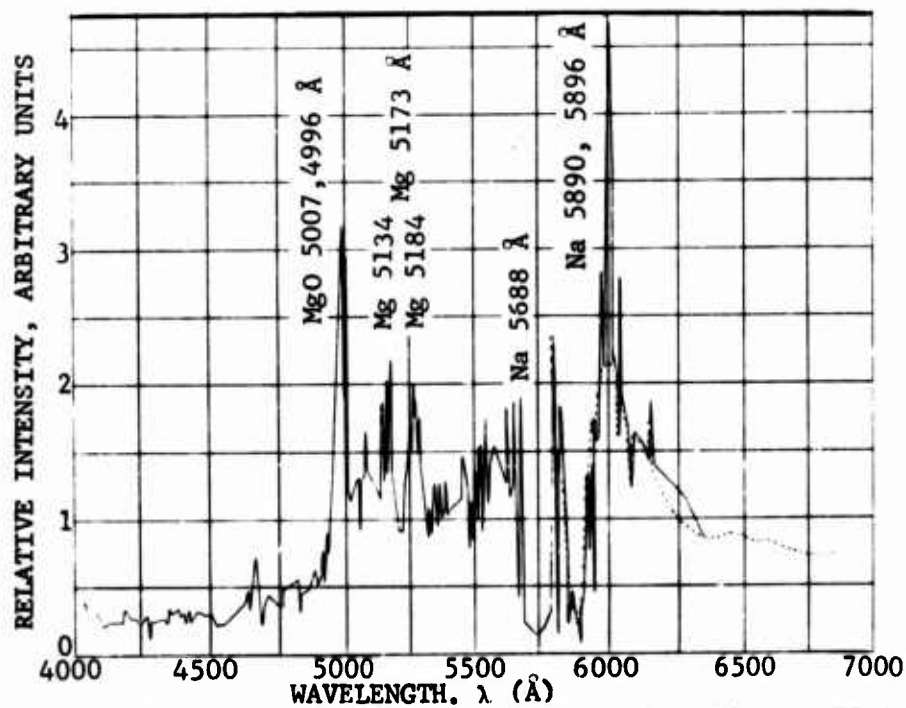


Figure 33 - Wavelength dependence of flare intensity, .75 inches above burning surface.

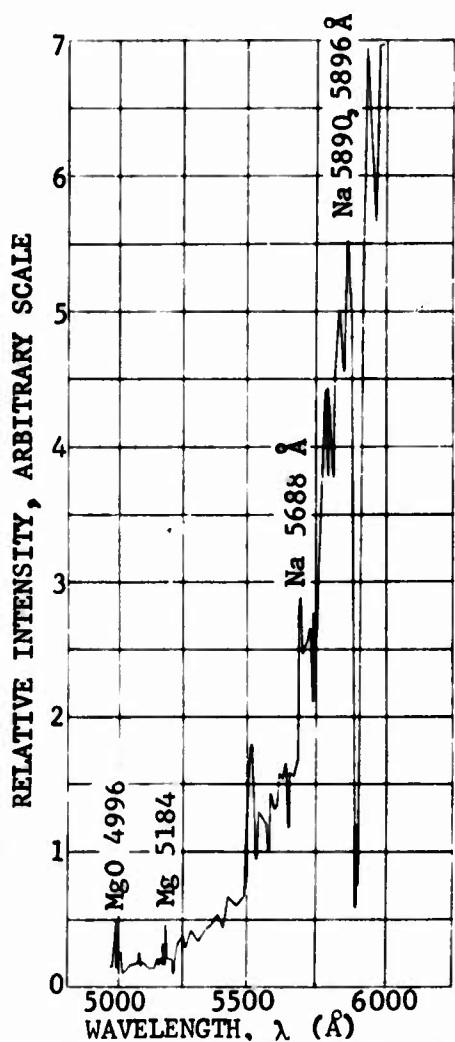


Figure 34 - Wavelength dependence of the flare intensity, 6 inches above burning surface.

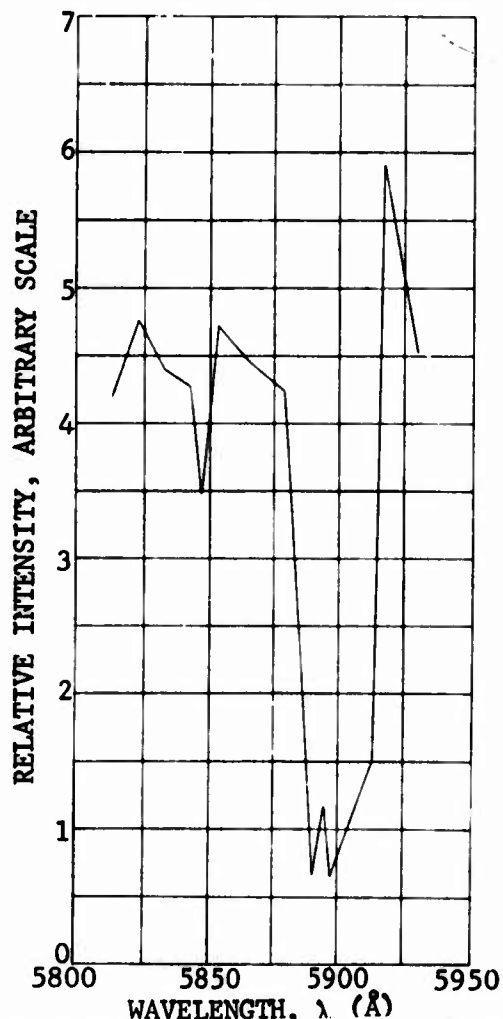


Figure 35 - Self absorption of the Na D-Douplet, 6 inches above the burning surface.

The mixing region near the flare surface should be thin (<1 mm). That the self-absorption observed has been broadened so much appears peculiar. It may be that the gas near the base contains a mixture of cold and hot sodium atoms and that absorption by the cold sodium occurs throughout the flare instead of simply in the external mixing region.

Optical Thickness in the Flare Plume

Attempts were made to obtain some preliminary information about the optical thickness (nontransparency) of the flare at different wavelengths. For this purpose two different experiments were conducted.

First the glowing tungsten ribbon of the lamp of Figure 29 was projected into the center of the flame by the lens L_2 and the change of the radiation intensity with and without the lamp was recorded. An intensity change was observed at 4000 Å as well as at 8000 Å, indicating that the flame was not optically thick at these wavelengths. The change in intensity, however, was too small compared with the intensity fluctuations to draw any quantitative conclusions. Close to the wavelength of the Na D-lines no difference in radiation intensity could be detected with and without the tungsten lamp, even when the point of observation was 6 inches above the burning surface of the flare.

Similar results were obtained from a second experiment in which a metal plate oriented perpendicular to the optical axis was moved through the flame in the direction of the optical axis. As the plate approached the middle of the flame, the recorded light intensity at 4000 Å and at 8000 Å was reduced to about half of its original value, whereas in the neighborhood of the sodium lines no change of the light intensity was detected until the plate covered the flame entirely. The results of these experiments indicate that the flare was approximately optically thin for 4000 and 8000 Å, whereas the opposite is true for wavelengths close to the Na D-lines. For more definitive quantitative measurements, a more elaborate device would have to be used which would allow an accurate indication of dependence of flare intensity on position of the metal plate. Also, in future experiments, a standard carbon arc should be used as a background source. The radiation intensity of the tungsten ribbon lamp is too small compared with that of the flare due to the low emissivity of tungsten (at $\lambda = 5800$ Å, $T = 3000^\circ\text{K}$, $\epsilon = .434$).

Flare Temperature in the Plume

For the determination of the temperature in the plume the absolute intensity of the radiation on both sides of the self-absorption dip of the sodium resonance doublet was measured. The spectrometer was calibrated at these wavelengths with the tungsten ribbon lamp. Since the brightness temperature of the tungsten ribbon lamp is given for a wavelength of 6500 Å, a correction was necessary for the wavelengths at 6000 Å and 5800 Å. The radiation losses due to reflection and absorption at lens L_2 were taken into account. Thus, a calibration factor, C , was obtained as

$$C = \frac{I_{Lm}}{B(\lambda, T_{BL})} \left(\frac{\text{Amps cm}^3}{\text{watt}} \right)$$

and the brightness temperature of the flare can be calculated from

$$\frac{1}{T_{BF}} = \frac{k\lambda}{hc} \ln \left(\frac{I_{Fm}}{C} \frac{\lambda^5}{hc^2} \right)$$

where I_{Lm} and I_{Fm} are the measured intensities of the lamp and the flare respectively, measured in units of the photomultiplier current (amps). $B(\lambda, T_{BL})$ is the emission of the lamp, k is Boltzmann's constant, h is Planck's constant, c is the velocity of light and T_{BF} is the brightness temperature of the flare. For the derivation of this equation, Wien's approximation of Planck's radiation law was used ($hc/\lambda kT \gg 1$). This brightness temperature of the flare is equal to the true flare temperature if the emissivity of the flare in this wavelength range is equal to one. Values of the temperatures are listed for two different heights in Table V. In this table it is also shown that changes in the radiation intensity of 20 percent to 25 percent will result in temperature changes of only 65 to 100°C. If the emissivity of the flare at these wavelengths is smaller than one, the flare temperature would be somewhat higher. T_R ($\epsilon=.8$) in Table V gives the flare temperature for an emissivity of .8, which is considered to be a lower limit. Considering the different uncertainties and errors, the total error of the determined flare temperatures is believed to be not larger than $\pm 100^\circ K$. More accurate temperature measurements may be possible if the light intensity fluctuations of the flare can be eliminated.

X-Ray Experiments

An X-ray photograph of a flare burning in a helium jet is given in figure 36. In theory the soft X-rays should have been absorbed at the jet center-line in an amount equal to the thinnest segment of the optical wedge shown on the left of the photograph. Such absorption seems to occur near the surface but clearly does not at 2 inches above the surface. This is thought to be related to the speed and angle of the ejected Mg particles. Also apparent in figure 36 is the irregular nature of the surface and a typical buildup of oxide deposits on the ignition wire.

The fact that a substantial fraction of the flare material is ejected as Mg was found to appreciably influence X-ray absorption by plume gases in the helium-filled chamber.

Plume Shape

Typical flare plumes are shown in figure 37 for flares with burning surface facing up, to the side, and down. The grid mesh size in figure 37(b) and 37(c) is one inch. The flares in figure 37 were inhibited on the sides and bottom with a cellulose acetate coating. Movie sequences of flares were also taken. For comparison purposes a flare plume is shown in figure 38 for a flare wrapped with four layers of masking tape in addition to the cellulose acetate coating. The additional inhibitor provided a jet effect which can be observed in figure 38.

TABLE V - PLUME BRIGHTNESS TEMPERATURES

height above burning surface	wavelength λ (Å)	correction factor $(10^{-19} \frac{\text{amp cm}^3}{\text{watt}})$	relative intensity I_{Fm} (10^{-7} Amps)	$T_{BF} (^{\circ}\text{K})$	Temperature $T_F (\epsilon=.8) (^{\circ}\text{K})$
.75	6000	70.5	110	2823	
.75	6000	70.5	90	2758	
.75	5850	83.7	110	2797	
.75	5850	83.7	90	2735	
6	6000	2.0	4.0	2908	2989
6	6000	2.0	3.0	2810	
6	5800	2.2	4.0	2915	2993
6	5800	2.2	3.0	2820	

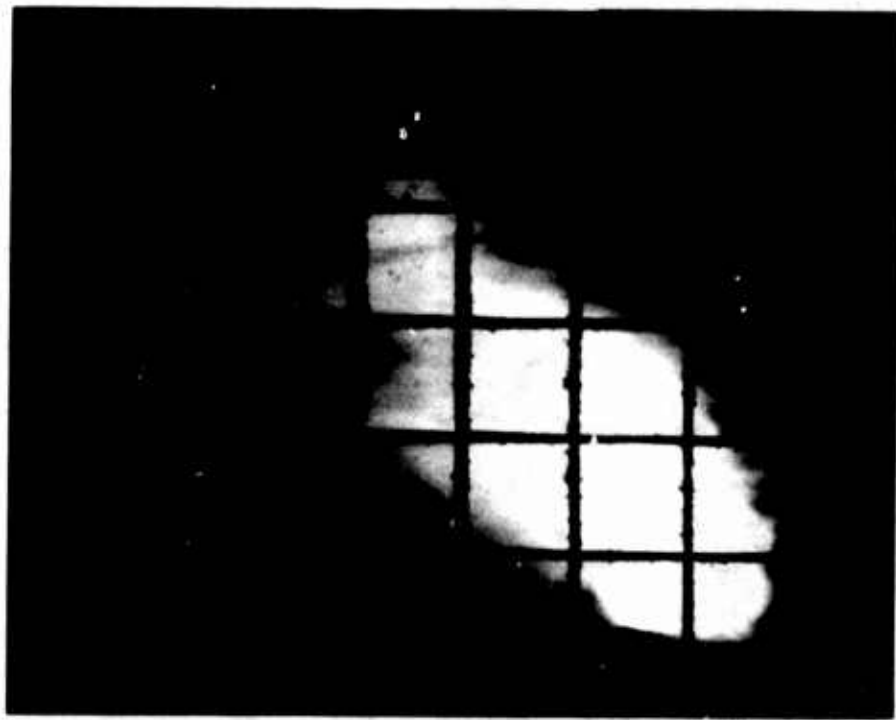


Figure 36 - X-Ray photograph of flare burning in helium chamber. (X-Ray power 15 KV, 20 Ma with 3 second exposure on Polaroid film type 51.)



(a) Flare with burning surface facing up; distance between flare and lens 45 inches; Polaroid film type 55; exposure 1/200 second, F45 with 1.2 neutral density filter.

Figure 37 - Flare plume.



(b) Flare with burning surface facing sideways; distance between flare and lens 20 inches; Polaroid film type 55; exposure 1/200 second, f32 with 1.5 neutral density filter; reference mesh size 1 inch.



(c) Flare with burning surface facing down; distance between flare and lens 20 inches; Polaroid film type 55; 2.1 neutral density filter; reference mesh size 1 inch.

Figure 37 concluded - Flare plume.



Figure 38 - Flare with burning surface facing sideways; distance between flare and lens 20 inches; Polaroid film type 55; exposure 1/200 second, f32 with 1.5 neutral density filter; reference mesh size 1 inch; flare wrapped with four layers of masking tape.

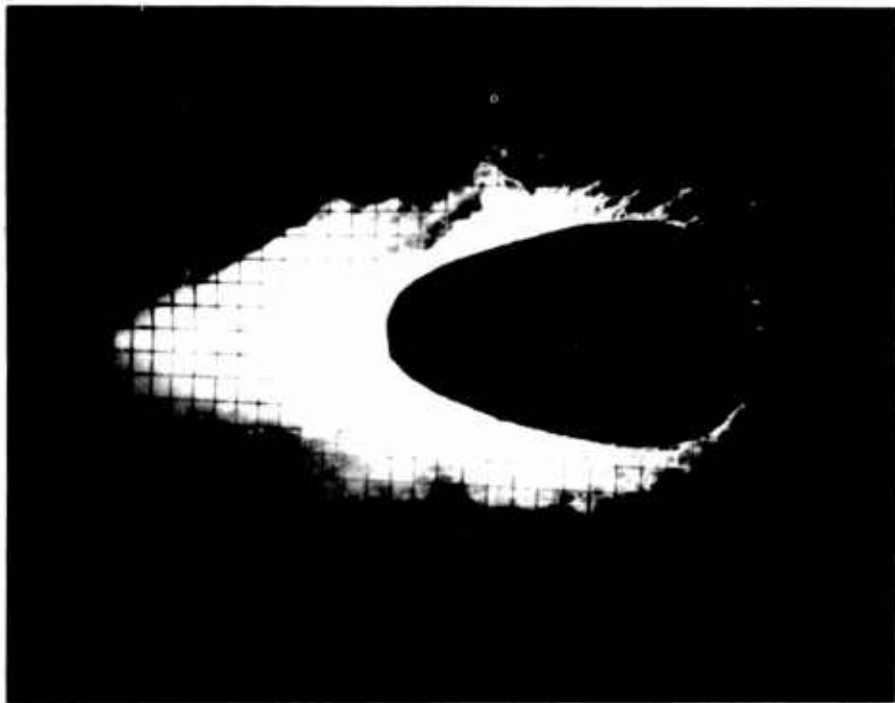


Figure 39 - Burning flare showing particle ejection from the plume. Burning surface facing up; bright part of the plume is masked; Polaroid film type 55; exposure 1/200 second; f22; no neutral density filters; reference mesh size 1 inch.

Particle Distribution

In figure 39 in which the bright part of the flare was masked, particles can be seen falling out of the plume. The bright particle trace represents the particle trajectory during the 1/200 second exposure indicating a fall velocity of approximately 2 feet per second. The thin trail of MgO left by the particle is typical of magnesium particles burning in air which occurs when unburned Mg leaves the plume. Particles collected 2 feet below the plume as well as those 2 inches above flare surface but within the plume were completely burned. Sample micrographs are shown in figure 40. In the case of both the cenosphere figure 40(a) and the particle aggregate figure 40(b), the large particles appear composed of clusters of particles of the order of 10 microns. Thus, all MgO particles observed appear to be 10 microns or greater in diameter.

Particles ejected from the plume were sampled over a fraction of the flare burning time. (Starting and burnout transients gave excessive particle ejection and so were not considered.) It was found that these particles contained enough magnesium to account for 25% of the initial weight of the flare burned during the sample time.

MgO distribution in the ascending part of the flare plume was estimated by observing, scraping, and weighing the deposits collected on the 1/2 inch wide, flat surface support arm (figure 32) following several flare burnings. The results are shown in figure 41. No attempt was made to correct for collection efficiency.

The profile is qualitatively that which would be expected for the velocity profile next to a hot cylinder. There was no evidence of Mg deposits except for a single Mg particle collected 6 inches from flare center line. Thus, nearly all particles were completely reacted by the time they reached the support rod. Deposits of magnesium oxide greater than .002 grams/cm² completely covered the support rod.

DISCUSSION

Plume Spectra

The objective of the spectral evaluations was to find the chief contributions to radiation in the visible region and a measure of optical mean path length in plume gases as a function of wave length in the visible range. The spectra shown in figures 33 and 34 are characteristically similar to those reported in reference 7, a gray body continuum with superposed broadened lines at 5000 Å and on either side of 5900 Å, with the exception that broadened absorption lines virtually obscure the radiation at 5900 Å. A segment of the spectrum near 5900 Å is shown in figure 42 which also shows the fluctuations in intensity (presumably due to flame temperature fluctuations which, in turn, probably relate to particle combustion and the broadening of the D-lines in emission (approximately 500 Å) and absorption (approximately 100 Å).

According to Strong and Bundy⁽³⁾, D-line broadening occurs due to absorption broadening. However, the amount of broadening observed here is much greater than expected from reference 3 as was pointed out in the section on theoretical considerations.



(a) Micrograph of the MgO cenosphere.



(b) Micrograph of MgO particle aggregate.

Figure 40 - Particle micrographs.

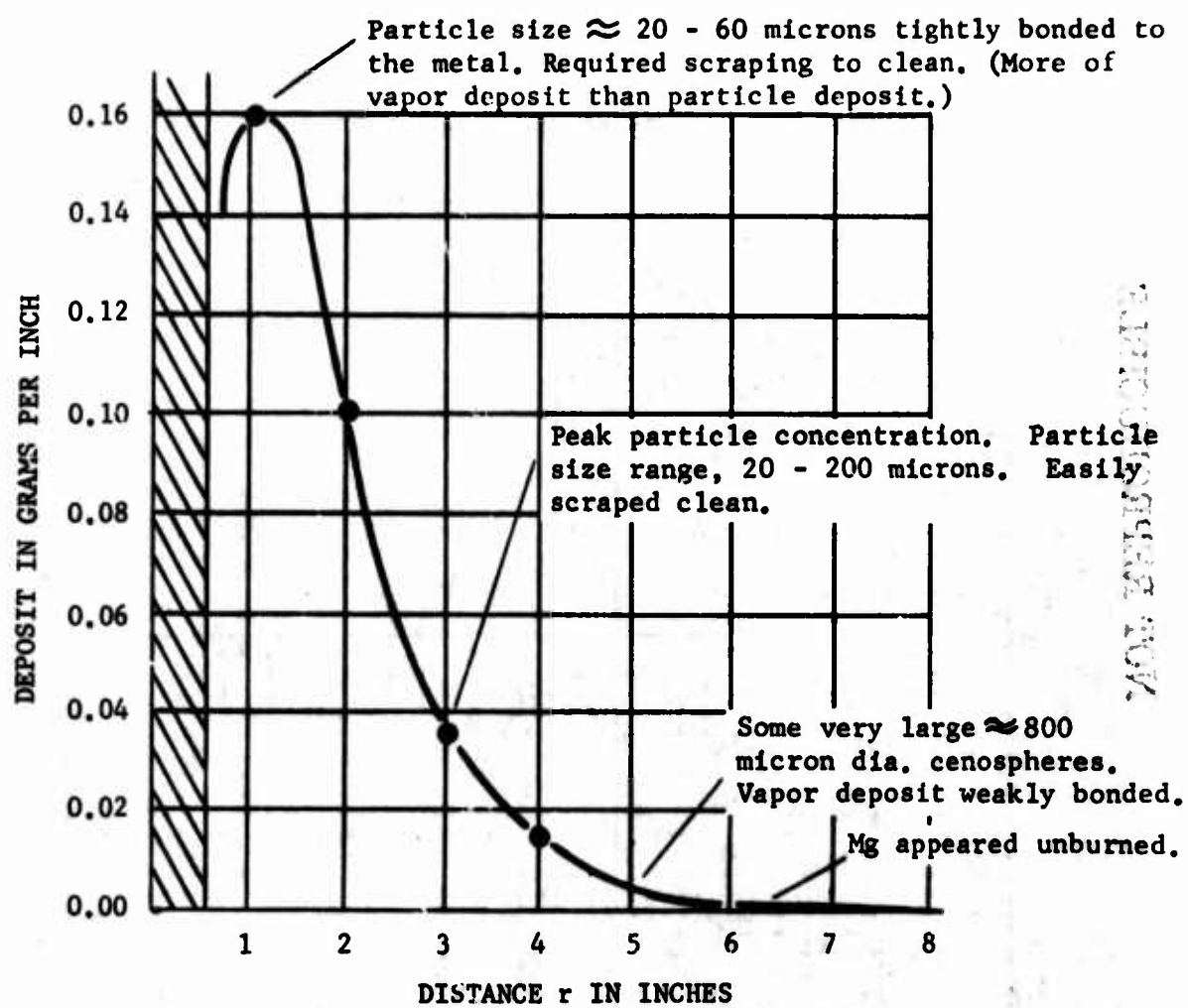


Figure 41 - Distribution of MgO deposit on the support surface after several runs.

NOT REPRODUCIBLE

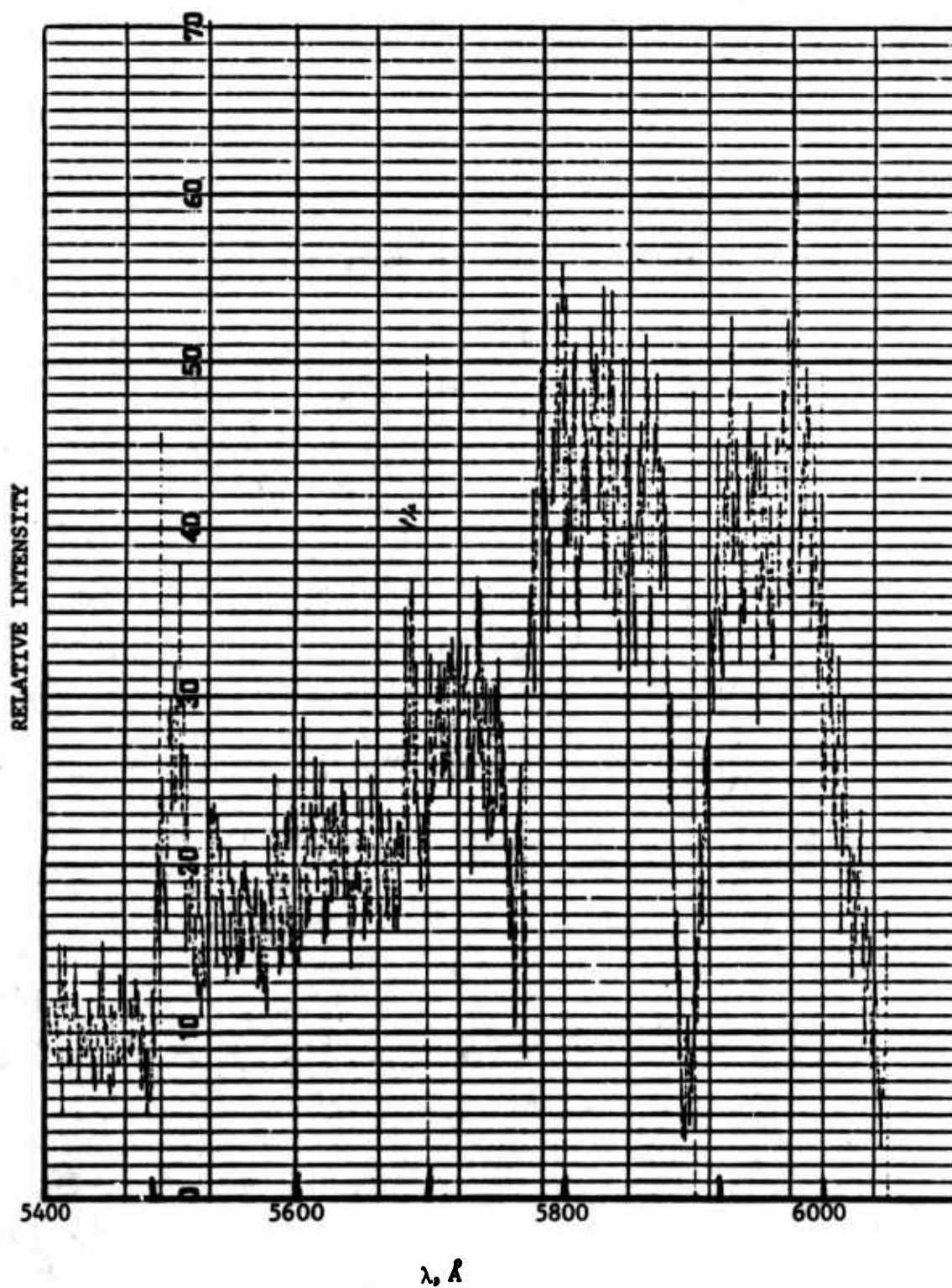


Figure 42 - A segment of the spectrum near D-line.

The results of the experiments to determine optical depth in the plume combined with the results of references 3, 4, 5, and 6 suggest the following model for illumination from a Mg - NaNO₃ flare. Radiation in the visible comes chiefly from the broadened D-lines and from MgO_s particles. A radiating slab of gas requires approximately 2×10^{-3} gms of MgO particles/cm² to be optically thick over the entire visible region, but only 10^{-4} gms/cm² of Na to be optically thick at the D-line. Thus, the plume is always black at a D-line. Near a D-line, the emissivity⁽³⁾ is given by $(1 - e^{-OD \cdot SF})$ where $OD = \frac{N_{Na}}{10^{11}} \times L$, $W_0 = 0.049$ ⁽³⁾ and $SF = \frac{W_0^2}{W_0^2 + (\Delta\lambda)^2}$ where $(\Delta\lambda)$ is distance in microns from line center. Therefore, for $OD \cdot SF > 1$, plume is nearly optically thick; for $OD \cdot SF < 1$, (i.e., far from D-lines) emission due to sodium radiation vanishes and emissivity due to MgO is (from Rossler⁽⁴⁾),

$$\epsilon = 0.35 \tanh \left(\frac{\rho_{MgO(S)} \cdot L}{0.002} \right)$$

(Note for $\left(\frac{\rho_{MgO(S)}}{0.002} \cdot L \right) \rightarrow \infty \quad \epsilon \rightarrow 0.35$)

Thus, even in the limit that both sodium and MgO particles are optically thick, a substantial fraction of the broadened D-line will have $\epsilon \approx 1$ and therefore will have approximately three times the intensity of the MgO particle continuum on either side. (A plume 2 feet thick contains enough MgO particles to be optically thick.) Plume size influences the sodium radiation in a different way--as plume thickness increases, the breadth of the D-line increases: the emissivity at wave lengths near the D-line approaches unity. These considerations are predicated on the assumption of a uniform gas temperature and composition between particles. Because active combustion of magnesium particles persists in the plume, temperature inhomogeneity may play a significant role in the breadth of the D-line observed.

Flare Temperature

It is clear that because of ejection of Mg, plume composition and temperature throughout the plume cannot be taken as that predicted from the initial composition. It appears that particles are sufficiently large for scattering to be neglected and sufficiently scarce for the plume not to be optically thick but to cause absorption on the order of 10 percent. Further, particle burning time should be sufficiently long so that thermodynamic equilibrium could not be approximated near the surface of the flare and the temperature and composition in the plume should be influenced by the existence of burning particles.

The nominal flare composition in the preceding experiments was 55 percent Mg. Observing that 25 percent of the Mg was ejected and that no solid Mg was collected in the plume, we may deduce that even for this fuel-rich flare, the actual plume gas composition lies somewhere less than 35 percent of Mg by weight: i.e., the flame temperature is more nearly 3000°K, the mole fraction of Na approximately 20 percent, the mole fraction MgO solid approximately 38 percent, and the mole fraction of MgO(g) approximately 0.8 percent.

X-Ray Experiments

X-ray plume density measurement was one of the parts of the research program that required the most elaborate preparation and equipment, but it yielded less useful information than relatively much simpler experiments such as the measurement of MgO fallout from the plume.

Only a superficial consideration has been given the interpretation of the X-ray results thus far; the data on hand warrant more extensive evaluation. Perhaps the most valuable lesson to be learned from the experimental techniques that were pursued is what kinds of data can be obtained at what price.

Plume Shape

It can be seen from figure 37 orientations that differ with respect to the gravitational field produce markedly different plumes for two reasons: (1) Buoyancy forces and inertial forces have different relationships in the different orientations and (2) the heat transfer to the burning surface produces different shapes of burning surfaces and markedly different plume momentum distribution. For example, if the plume shape of figure 37(b) is compared with the shape expected of a hot jet of jet velocity, U_0 , we find U_0 equals approximately 6 feet per second.⁽⁷⁾ On the other hand, the jet of figure 37(c) gives a penetration to be expected of a jet of velocity 30 feet per second.⁽⁸⁾ Plumes in figures 37(b) and 37(c) appear to be more strongly influenced by non-normal velocities at the burning plane than does the plume in figure 37(a).

A second factor dealing with the influence of the burning surface configuration is that it changes radically with time. These changes in turn produce modifications in plume shape. Such changes observed in high speed movie sequences show a transient accretion of MgO particles on parts of the burning surface and a related irregular character of the shape of the flare plume. In addition to the radical plume shape changes with time, burning magnesium being ejected from the plume could be observed in the high speed movies.

To see the importance of the shape of the burning surface on the plume configuration, figure 38, where the flare was wrapped with four layers of masking tape before igniting, may be compared with figure 37(b), where only the thin cellulose acetate inhibitor was employed. In figure 38 the plume is that which would be expected of a jet of U_0 approximately equal to 100 feet per second as determined from the burning rate.

Currently, it is not clear what controls the plume configuration in the absence of the confining collar which produces a jet. Section II results show that distributed sources across a plane will give a plume different from a jet in counter flow.⁽⁹⁾ In addition, the marked inhomogeneity of the unconfined plume suggests the occurrence of small jetlets which may entrain ambient air and decrease the length of jet penetration.

It thus appears that the plume can be treated like a buoyant jet if the burning surface is recessed behind a confining collar. Without the confining collar the plume is strongly influenced by subtle changes in burning surface configuration which, in turn, is influenced by heat transfer from the hot plume gas.

In the case of the jet-like behavior, adequate experimental and analytical information is available to estimate the plume composition and temperature distributions in the case of upward facing jet^(7,10) and the side facing jet.⁽⁷⁾ Inadequate information is available for obtaining distribution in the case of the downward facing plume.^(8,9) It is not clear how the mixing of the unconfined plume can be handled. Because in practice, irregularities occur and have a large effect on plume shape, a single idealized model of a flat surface with distributed sources may not be expected to serve as an adequate model for all of the shape determining factors.

Particle Distribution

Perhaps the most noticeable aspect of the burning plume is the large number of particles that are ejected, as is demonstrated in figures 37 and 39. The size of the particles is such as to suggest that scattering phenomena may be negligible in estimating the light emission from flare plumes; however, the removal of these particles, no doubt, greatly influences temperature composition and light emission.

As was noted in the experimental results, deposits of less than .002 grams per cm² did not cover the support arm. According to Sato⁽¹¹⁾ this value can be used to estimate the mass of comparable particles that produce an optically thick cloud. On this basis a plume of mean molecular weight M of approximately 40, temperature 3000°K, and concentration of 30% MgO particles would be optically thick when the path length is approximately 60 cm. The plumes pictured herein are at least 10 cm in depth. The fact that the flare can be observed through the plume (as well as photographed (figure 37(c)) substantiates that it is in fact not optically thick at all wavelengths in the visible range.

In the sampling experiments the homogeneous and shiny appearance of approximately 50% of the condensed MgO suggests that a substantial fraction of the MgO present in the plume is present in the form of MgO(g) or supercooled vapor. Because of the substantial departure from the ideal adiabatic state, it seems that the conditions as the plume gases mix with air may be only crudely estimated.

To a first approximation (in the hotter parts of the plume),

$$\frac{\rho_{mix}}{\rho_o} \approx \frac{T_o}{T_{mix}}$$

and mass fraction of a species i ,

$$\frac{M_{i mix}}{M_{i o}} \approx \frac{T_{mix}}{T_o}$$

so that $m_{i mix} \times \rho_{mix} \approx m_{i o} \times \rho_o \approx \text{constant}$. To a first approximation, the MgO(s) and the Na volume concentrations should be uniform in the plume as it becomes diluted. It seems proper to select a value of $m_{i o} \times \rho_o$ appropriate to conditions corrected for Mg depletion (due to particle ejection; i.e.,

$$\rho_{MgO, solid} \approx 0.3 \times 10^{-4} \text{ gms/cm}^3 \text{ and } \rho_{Na(g)} \approx 10^{-5} \text{ gms/cm}^3.$$

These values of partial density were used in estimating efficacies.

CONCLUDING REMARKS

It appears that the ideal flare should radiate its energy to the surroundings with negligible internal absorption and before convective mixing can lower the flare gas temperature. The successful process demands a plume that minimizes mixing with the surrounding air. This study shows that plume shape (and, hence, mixing time) is intimately related to the nature of the burning surface. When the casing wall is thick, the gases formed produce a jet, mixing is enhanced, and flare efficiency suffers. Mixing time for the inverted plume formed without the jet effect should be inversely proportional to fall rate--too fast a rate should impair performance.

The ideal efficacy developed in this paper presupposed a homogeneous plume of $MgO(s)$ and gaseous products. The observation that actual flares have actual efficacies that exceed the predicted ideal efficacies shows the model to be faulty. The relatively large size of the magnesium particles insures continued particle burning in a major part of the plume. A qualitative consideration suggests that the resulting inhomogeneous plume temperature distribution would result in an increased ideal efficacy. Such a model demands further consideration.

Although the large particles would appear to be beneficial if they remain in the plume, a substantial fraction are seen to fall out and burn in air. The light produced in the absence of the sodium vapor has a much lower efficacy than in its presence.

This study points to the need for basic work on the mixing of inverted plumes and on the nature of magnesium particle combustion in the presence of Na , O_2 and N_2 mixtures.

SUMMARY

This study of light production in a magnesium-sodium nitrate flare has yielded the following results.

1. Two measures of goodness of flare performance are proposed: The efficacy which rates the flare constituents, and the efficiency which rates the burning process. The efficacy is seen to depend upon plume composition, size and homogeneity. The efficiency is shown to depend upon the way the plume mixes with the surrounding air.

2. The visible radiation is due primarily to broadened sodium D-line and a gray continuum from $MgO(s)$. The flare plume is approximately 10% Na and 30% $MgO(s)$. This composition is influenced by large particles of magnesium solids being ejected from the plume. Plume inhomogeneities in composition and temperature occur in relation to the burning of large (300-600 μ) magnesium

particles. Observed efficacies are higher than efficacies computed for a homogenous ideal plume. Also, the breadth of the sodium D-line is almost 10 times that predicted from absorption broadening. It is suggested that the high efficacies are related to D-line breadth which is, in turn, related to hot spots caused by particle burning.

3. Plume shape is influenced by flare orientation in two ways: The relationship between gas momentum direction and gravity, and heat flux to the burning surface which influences surface shape. Flares aimed up retain a collar and are jet-like: those aimed to the side have an asymmetrical burning surface and those aimed down have no collar but more directed momentum than the side facing surface. These factors influence plume size and dilution rates.

4. Extinction lengths are estimated to be 10^{-6} cm at the Na D-line and 60 cm at wave lengths other than that of the D-line.

LIST OF REFERENCES - SECTION IV

- (1) Douda, G. E., U. S. Naval Ammunition Depot., Crane, Indiana, RDTN 135, July, 1961.
- (2) Moon, P., The Scientific Basis of Illuminating Engineering, Dover, 1961, p. 49, 120 and 135.
- (3) Strong, H. M. and Bundy, F. D., Appl. Phys., Vol. 25, No. 12, p. 1521, December, 1954.
- (4) Rossler, F., Supersonic Flow, Chemical Processes and Radiative Transfer, D. B. Olfe and V. Zakkay, editors. Pergamon (1964), p. 433.
- (5) Johnson, D. M., (Report available at D.D.C.A.D. 627649) Proposed Kinetics and Mechanics of Illuminant Flares: Maximizing Efficiency. U. S. Naval Ammunition Depot, Crane, Indiana.
- (6) Strong, H. M. and Bundy, F. D., p. 641, 3rd Symposium on Combustion. Williams and Wilkins (1949).
- (7) Abramovich, G. N., Theory of Turbulent Jets, M.I.T. Press, 1966.
- (8) Turner, J. S., Jets and Plumes with Negative or Reversing Buoyancy. Woods Hole, Mass. Ref. No. 67-8, March, 1968.
- (9) Arendt, J., Babco, H. A. and Schuster, J. C., Rouse H. Penetration of a Jet in Counterflow, J. Hydraulic Div., Proc. of ASCE Vol. 82, p. 1038-8
- (10) Ricou, F. T. and Spalding, D. B., J. Fl. Mech., Part I, Vol. II, p. 21, 1961.
- (11) Sato, T. and Kunitomo, T., Memoirs of the Faculty of Engineering, Kyoto University, Vol- XXVII, Part I, January, 1965.

SECTION V

LUMINOUS INTENSITY DISTRIBUTION

INTRODUCTION

Various techniques have been utilized in previous work by other investigators to develop apparatus that could measure intensity in plumes other than those for illuminating flares to provide isointensity contours. The earlier approaches relied almost exclusively on temperature measuring techniques. Temperatures were measured by devices such as high temperature thermocouples, melting wires and optical pyrometers. Although temperature profiles of varying but acceptable resolution were obtained, the data could not be readily or accurately translated into intensity because of the variation of emissivity throughout the plume.

Other investigators attempted to develop, for illuminating flares, a scanning photometer that optically traversed the flare plume along one axis by means of a nutating mirror. The orthogonal axis of the mirror was displaced by means of a stepping motor or rotating helical slits. The major problem with such techniques was that of identifying which portion of the plume was actually being viewed at a given time. Usually this was done by determining the angles of the nutating mirror in both the horizontal and vertical directions by the elapsed time of the nutating cycle. This produced a prolific amount of data that when coupled with the problem of resolution of the viewing area resulted in an unwieldy data reduction problem. The cost of constructing instrumentation of this variety was, and still is, prohibitive.

Another, and perhaps the most useful, of earlier techniques was quasi-quantitative in nature: this was the photographic method. One variety employed a motion picture camera fitted with either a rotating neutral density filter whose optical density varied with angle of rotation, or a number of separate filters that were sequentially placed in the optical path of the camera. These techniques resulted in pictures of a flare plume whose size was inversely proportional to the luminous flux density of the area being viewed. However, as previously mentioned, this method lacked the accuracy in intensity measurements required in a truly quantitative study of the luminous intensity distributions within a flare plume. The apparatus used in the study covered by this report to accomplish the measurement of luminous intensity distribution was conceived and designed to incorporate the following features, thereby overcoming the deficiencies of earlier attempts. These features are described in the following paragraphs.

An accurate and relatively simple technique of scanning with a well defined field of view was accomplished by utilizing a fixed field of view with the object of interest being imaged on a well defined plane within the instrument. The collecting optics are such that the image size is as large as possible with respect to the image plane without being larger than the plane in any one direction. The image plane is drilled with accurately measured apertures which are in a rectilinear pattern in the plane. Thus, with fixed optics, fixed apertures, and a fixed image plane, the field of view of each aperture, and the instrument as a whole, is rigidly defined. Since each aperture views a specific and constant portion of the overall field of view, a means of allowing only one aperture at a time to pass energy to the detector

is required. This is accomplished by sweeping an opaque, endless tape across the image plane. This tape has apertures oriented in such a manner that one aperture of the tape sweeps horizontally across the image plane, alternately coinciding with all of the image plane apertures in a horizontal row with the coincidence of tape and image apertures allowing energy to pass on to the detector of the system. After this particular aperture in the tape has fully traversed the image plane, it is followed by another aperture which is displaced in the vertical direction and sweeps the adjacent horizontal row of apertures in the image plane. By the repetitive cycling of the opaque tape, the image on the image plane is repeatedly sampled with the area of each sample being well defined.

An accurate and reliable means of measuring the luminous intensity of the area being viewed was accomplished by selecting and matching all components in such a manner as to provide the instrument with a relative spectral response essentially equivalent to that of the human eye. A vacuum photodiode is used in lieu of a photomultiplier or semiconductor to bypass the complexity and non-linearity of the former and the slow response time and poor sensitivity (within comparable cost figures) of the latter. With the use of the vacuum photodiode the instrument has a fast rise time, good linearity, and known spectral response. One other feature worthy of note was incorporated in the instrument. By the use of an integrating diffuse sphere it was possible to assure that the detector surface was always being uniformly illuminated. If the detector had viewed the image plane directly, each aperture would have been focused on a different portion of the detector surface and since such surfaces are notoriously non-uniform, the accuracy of the instrument would have been compromised. Utilization of the techniques described leaves the apparatus inherently free of complex optics and scanning schemes. The major cost factors were thus eliminated and the resulting instrument is simple, effective and reliable.

Using the above described apparatus the luminous intensity distributions of one inch diameter magnesium, sodium nitrate, Laminac flares burned in both nitrogen and air were obtained and the results are presented herein in terms of relative luminous intensity contours, relative intensity versus projected plume area, and percent of total luminous intensity as a function of percent plume area. Conclusions are presented regarding the results of the effort and recommendations are made for further investigations.

INSTRUMENTATION

Profile Radiometer (Scanner). The investigation of light intensity distribution within the flare plume was accomplished by a scanning radiometer. An exact reproduction of the plume was reduced in size and imaged onto a sampling grid through the use of an achromatic lens. The sampling grid is a multi-apertured device through which the light enters an integrating sphere to be detected by a vacuum photodiode. The combination of the photodiode and a suitable filter results in a standard eye response. The entrance of the light into the sphere is controlled by a perforated tape driven past the holes in the sampling grid by a synchronous motor. This perforated tape will open only one sampling aperture at a time; therefore, a definite portion of the plume is sampled at each coincidence of tape aperture and grid aperture located within the boundaries of the plume image. The detector is a linear device in that a calibrated increase of light impingement on the diode cathode will result in an increase in voltage output from the detector. The detector

output is fed into an operational amplifier with a closed loop voltage gain of 75 db. This operational amplifier has the high input impedance and low output impedance needed to match to the photodiode detector and recorder. Figure 43 represents typical data from the scanner.

EG&G Radiometer. An EG&G Inc. Model 580-11 Radiometer was used to obtain the total flare luminous intensity versus time. When the radiometer is used in conjunction with a suitable recorder it provides a strip chart readout of calibrated deflection with flare burn time. Figure 44 represents typical data from the EG&G radiometer.

Recorders. An oscillographic recorder with peak response of the order of 5 kc was used with the scanning radiometer. A five inch chart width allowed a maximum and minimum discernable signal ratio of 500 to 1. The low input impedance of the recorder amplifiers allowed a direct connection from the scanner radiometer to the recorder without going through a device to match impedance.

In conjunction with the EG&G radiometer a Texas Instruments Inc. Model P1CAH hot wire recorder was used. This recorder is a mechanical type with a low frequency response; however, due to the nature of the data to be recorded, the response was sufficient. The EG&G radiometer with the Texas Instruments recorder was calibrated against a secondary standard light source so that candlepower readings could be taken directly from the recorder chart.

EXPERIMENTAL PROCEDURE

Flare Holder. Each individual flare was epoxied to an aluminum bar which was rigidly mounted in a test stand movable in azimuth and elevation so that before each test the flare could be positioned according to test procedure. The flare was mounted in a plume-down position and held rigidly in place during the burning cycle. It was necessary to wrap the outer case of the flares with overlapping masking tape so that flash-by would not occur while burning in the plume-down position. The flares were prepared for burning by painting three coats of first-fire material to the end surface. The first two coats of first-fire were allowed to dry before applying the next coat. After the flares were wrapped in masking tape, a six-inch piece of viscose fuse was placed and taped onto the first-fire surface. The flare holder is depicted on the left side of Figure 45. The four plies of masking tape provided approximately 0.025 inches of total thickness.

Physical Arrangement. The flare holder was placed six feet from the radiometer in all cases. This distance was selected so that the flare plume image would fill the sampling grid borders on the radiometer. At this distance the radiometer detector and amplifier were operating in the medium power density curves thereby allowing more accurate measurements.

Rigid mounting of the flare presented a problem in that as the flare burned the plume changed position upward by the length of the flare. This was solved by relating the actual plume movement to the reduced image size on the radiometer sampling grid. Simply by plotting the plume movement versus time the position of the plume may be found at any particular sampling cycle. This data was then used as a function of sampling cycle and time. The complete mechanical and optical test apparatus is depicted in Figure 45. The flare



Figure 43 - Typical scanner radiometer display

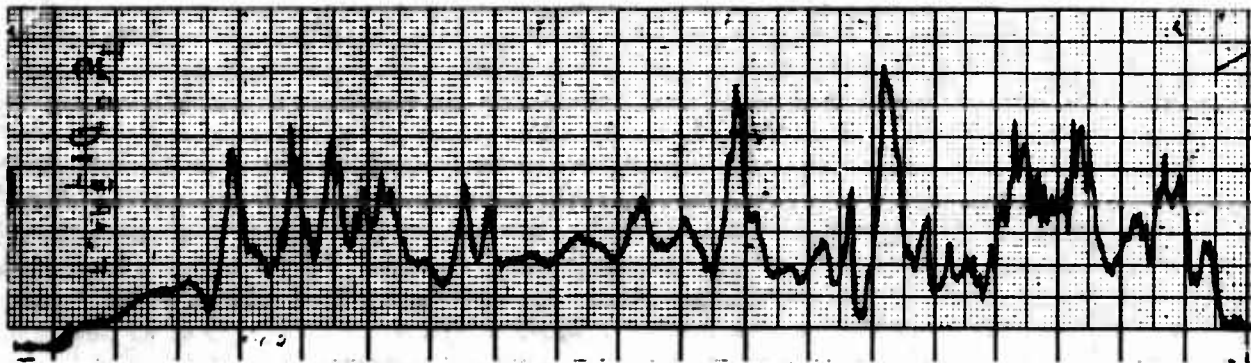


Figure 44 - Typical EG&G radiometer display

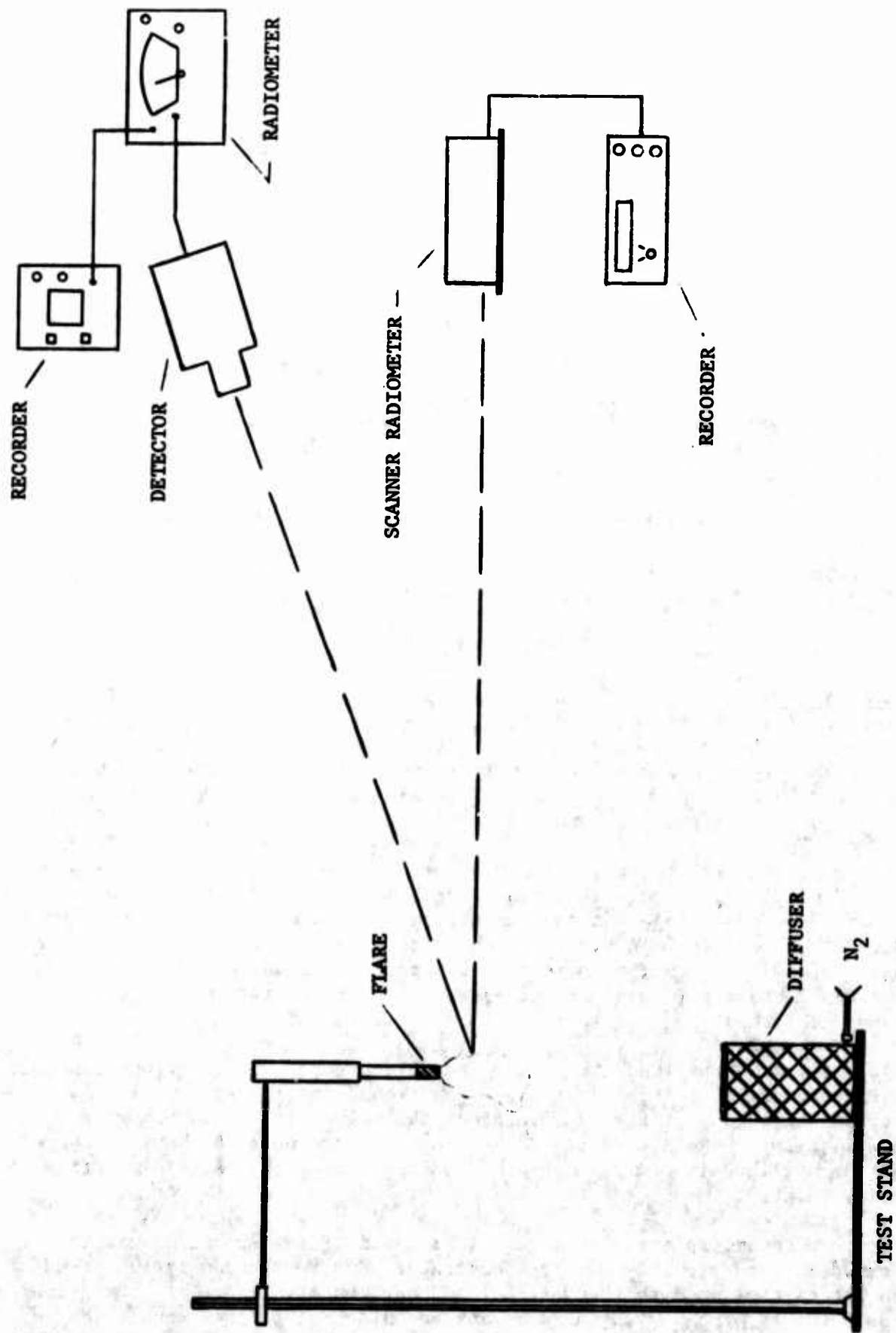


Figure 45 - Flare test stand and physical arrangement.

image was positioned precisely at the same point on the sampling grid for each individual experiment.

Environmental Conditions

Air. Half of the sample flares tested were run in normal atmosphere. It is apparent from the relative luminous intensity curves that cross winds of varying velocities were present when the data was taken. In no case were these cross winds above 7 feet per second. Within this limit the winds are referred to as "light" or "heavy" depending upon observed effects on the plume rather than on measured wind velocity. Efforts were made to place the radiometers upwind from the flare to lessen the attenuation due to smoke.

Nitrogen. Nitrogen was used as an inert atmosphere in which to test half of the flares. The flares were placed directly above a grid diffuser so that they might become totally surrounded by a continuous flow of nitrogen. The nitrogen was taken directly from a tank, regulated, and then fed through a solenoid-operated valve. From the solenoid valve the nitrogen was piped to a diffuser pot placed directly below the flare. The diffuser pot was constructed so as to provide a uniform flow of nitrogen forming a column eight inches in diameter. The nitrogen velocity was held at six to seven feet per second during all these tests. Not unlike the flares burned in atmosphere there are minor cross wind effects in these data. These winds did not appear to alter the operation of the flare other than for a slight deforming of the relative luminous intensity lines.

DATA REDUCTION

Scanning and Plotting. Each recorded pulse from the scanning radiometer is a result of a coincidence of particular apertures of the grid and rotating tape which are within the boundary of the flare image. The amplitude of the pulse is directly proportional to the luminous intensity in candlepower of the area of the flare plume being viewed at any particular time as a result of the alignment of grid aperture and tape aperture. (See Figure 43)

For a given flare the pulse heights for each area of the plume viewed by coincidence of aperture were averaged and then normalized to the most intense region, resulting in a two-dimensional matrix of relative intensities. In order to present the contours of each flare in a uniform manner, relative intensities of 90 percent, 50 percent, 10 percent, 2.5 percent, and 1.0 percent were selected, primarily on the basis of their separation when depicted in graphical form.

To obtain the physical location of these contours the following technique was utilized. Each position in the aforementioned matrix represents a particular portion of a given flare plume. Since the values in the matrix were seldom, if ever, the exact values to be plotted, interpolation between these values was utilized in order to obtain the location of the desired relative intensity point.

It soon became apparent that graphical means of interpolation was the most expedient and probably the most accurate. Due to the consistent trend of the intensities in both the vertical and horizontal directions, the graphical interpolation is probably as valid as any technique other than sophisticated statistical analysis such as is possible only with high-speed computers.

Accuracy of Results. Considering the optical parameters of the scanning radiometer and the physical arrangement of the experimental apparatus, the area being viewed at any given time was a circle 0.66 inch in diameter. The height of the data pulse is determined by emission from this total surface area; however, in presenting the data in the form discussed it had to be assumed that the intensity of any given area emitted from a point at the center of the circle.

This introduces an inherent inaccuracy into the data as presented. This inaccuracy in terms of location of a given relative intensity point could be not greater than the distance from the center of the circle to its periphery, which is, of course, the radius of that circle. Therefore, it must be kept in mind that due to this assumption alone there are possible errors of ± 0.33 inches included in the relative intensity contours. Also, there are obviously random errors involved due to rapid fluctuations within the flare plume and only large numbers of data points could reduce this error. Since the fluctuations such as those caused by wind effects obviously appear in their averaged form (as shown in the graphical presentation), it is felt that it is safe to assume that the relative intensity contours shown are reasonably within the ± 0.33 inch variation resulting from the geometry of the system as long as it is kept in mind that the contours presented are essentially time-averaged, but still transient, pictures of a continuously changing source.

EXPERIMENTAL RESULTS

The results are shown in terms of relative luminous intensity contours, relative intensity versus projected plume area (referred to hereafter only as plume area) and percent of total luminous intensity as a function of plume area. Table VI shows averaged data for all flares burned in both air and nitrogen.

TABLE VI - AVERAGED DATA FOR FLARES
BURNED IN NITROGEN AND AIR

FLARES BURNED IN AIR ENVIRONMENT:

AeReCo Series*	Intensity cp	Time Sec	Area sq. in.	<u>Efficiency</u> <u>candle-sec</u> gm
845	35,000	42.5	94	29,300
855	51,500	32.5	138	33,000
860	68,000	30.5	124	40,900
868	91,000	32.0	170	57,400

FLARES BURNED IN NITROGEN ENVIRONMENT:

AeReCo Series*	Intensity cp	Time Sec	Area sq. in.	<u>Efficiency</u> <u>candle-sec</u> gm
845	30,000	43.5	78	25,700
855	45,000	36.0	107	31,900
860	62,000	31.5	171	38,500
868	85,000	31.0	440	52,000

*The last two digits indicate the percent magnesium.

There was no attempt to correct the data for the random effects of wind velocity in the preceding table.

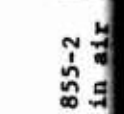
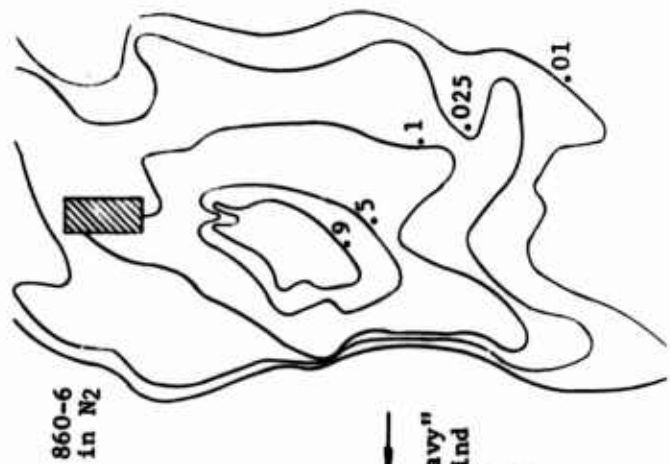
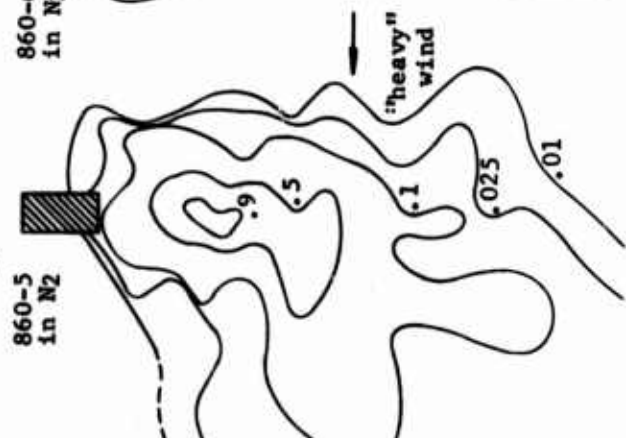
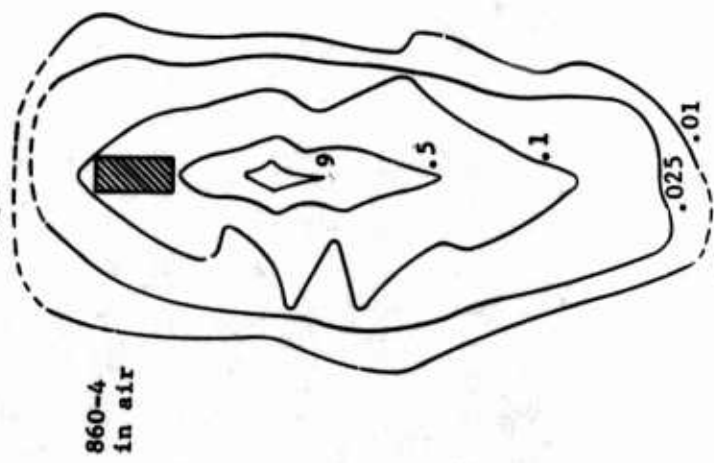
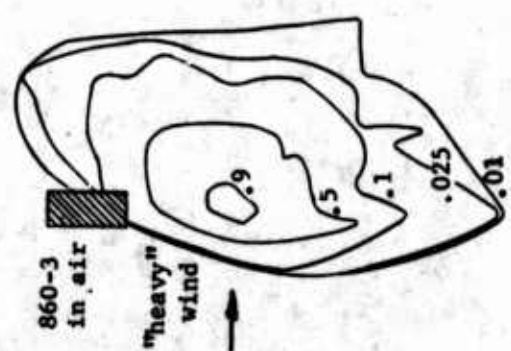
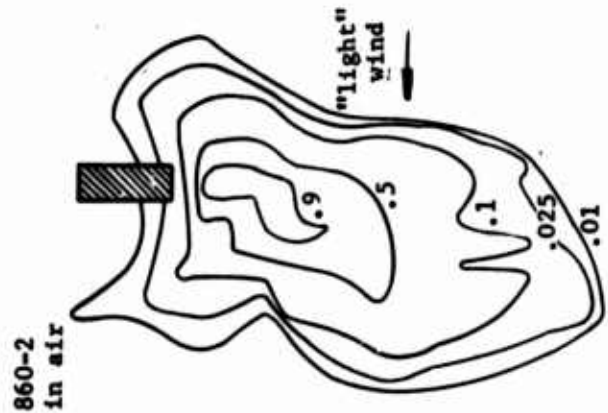
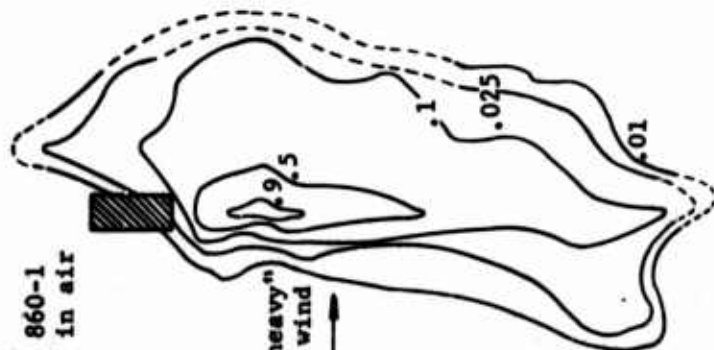
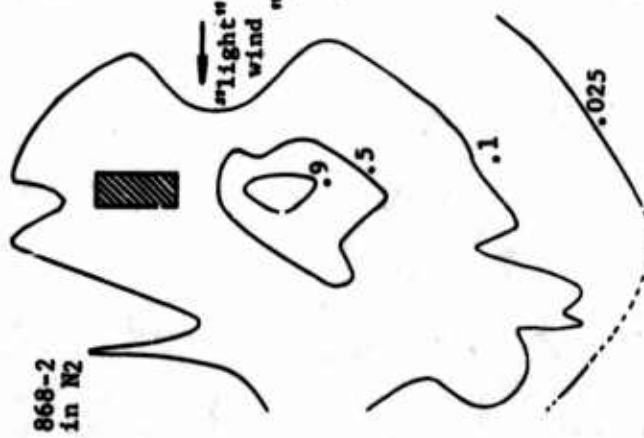
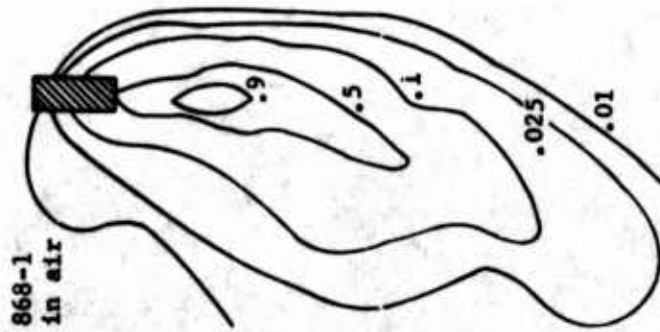
Relative Luminous Intensity Contours - Contours were plotted for a total of sixteen plumes. These are shown in Figure 46. The results for all sixteen plumes are shown in one figure in order to allow easy comparison for burning in both air and nitrogen and for varying percentages of magnesium. Radiation emitted outside the area bounded by the minimum relative contour of .01 was considered to be quite small. Therefore, the area of the plume is considered to be, for all practical purposes, that area inside the .01 relative intensity contour. This area was used in all intensity evaluations. For a few of the burnings, data were not obtained to complete all of the outside contours. Therefore, completion of these contours was estimated as shown by broken lines. The amount of luminous intensity involved in these estimates is not large, and having them drawn in eases the process of establishing the curves shown in the subsequent figures, which depend upon the areas bounded by the contours.

Inasmuch as the relative intensity contours represent only the relationship to the maximum intensity within the plume, it is necessary to consider the total luminous intensity in conjunction with the relative luminous intensity in order to show which areas are most significant from the standpoint of visible radiation.

Total Luminous Intensity - The total measured luminous intensity is shown in Table VI. It can be seen that for flares burned in air the intensity varies from 35,000 candlepower for 45 percent magnesium to 91,000 candlepower for 68 percent magnesium. For flares burned in nitrogen the intensity is five to six thousand candlepower lower.

By considering the product of the mean relative luminous intensity between contours and the area between contours, the relative luminous intensity can be related to total luminous intensity, and the percent of total luminous intensity as a function of area can be determined. The percent of total luminous intensity relates to the amount of visible radiation emitted from a given area within the plume and differs from relative intensity which relates the luminous intensity at a given point to the maximum. Inasmuch as the variation in relative luminous intensity is not linear with distance from one contour to the next, a plot of relative intensity versus plume area is used as a means of obtaining the product of relative luminous intensity and plume area. In Figure 47 the area under the curve between two contours divided by the area under the entire curve gives the percent of the total luminous intensity attributed to the area between contours. Using this relationship, curves showing percent of total luminous intensity versus percent of plume area were plotted and are shown in Figure 48. As with Figure 5, symbols identify the contours with the areas they bound. It can be seen from these curves that the maximum percent of total intensity lies generally between adjacent contours .10 and .50. For example, on the curve for flare AeReCo 868-1 the total luminous intensity between contours .10 and .50 is approximately 46 percent of the total for an area which is 26 percent of the total.

A



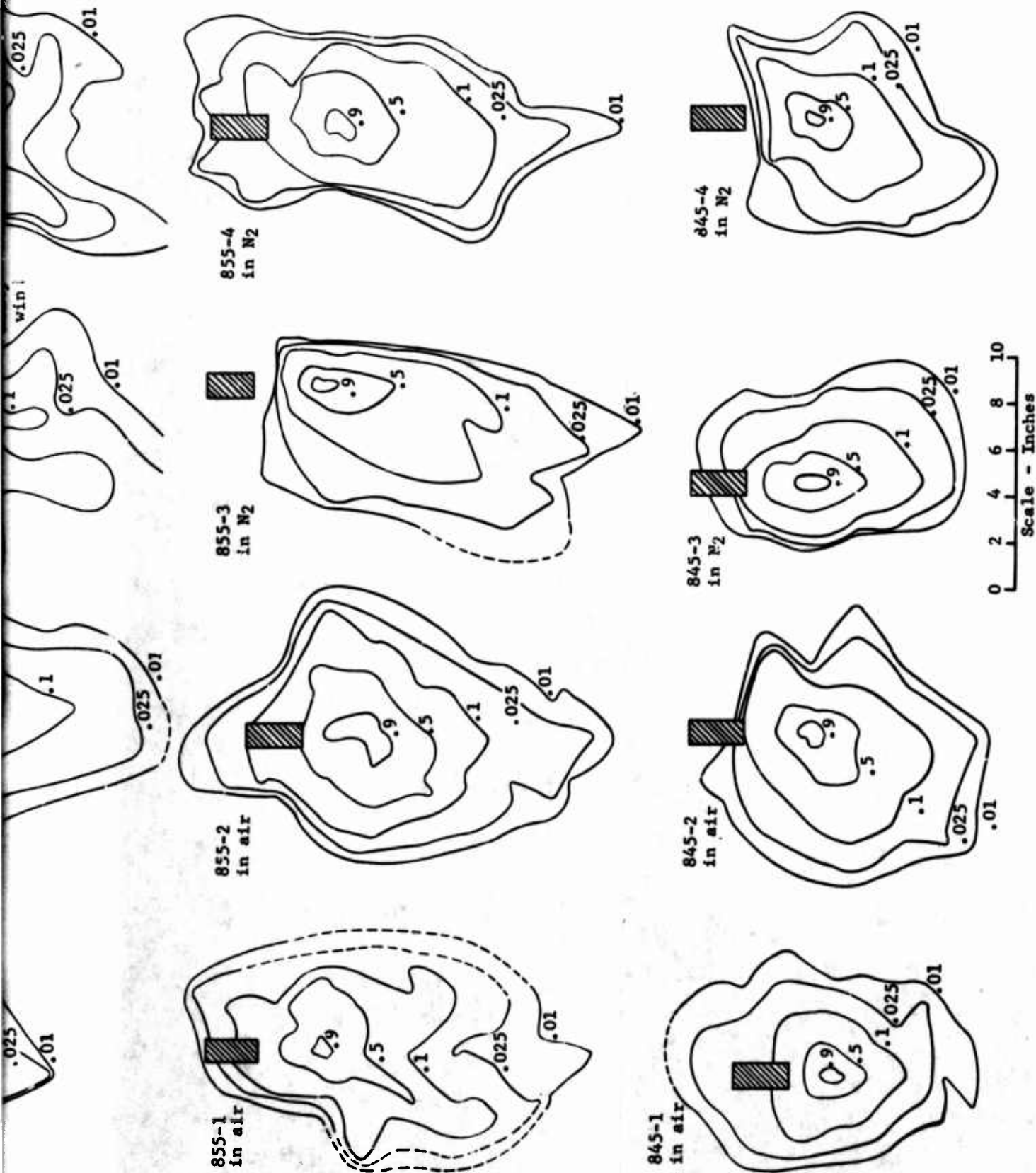


Figure 46 - Relative luminous intensity of AeReCo 800 type flares burning in air and nitrogen. Last two digits indicate percent magnesium. Nitrogen velocity was approximately 6 feet per second upward.

B

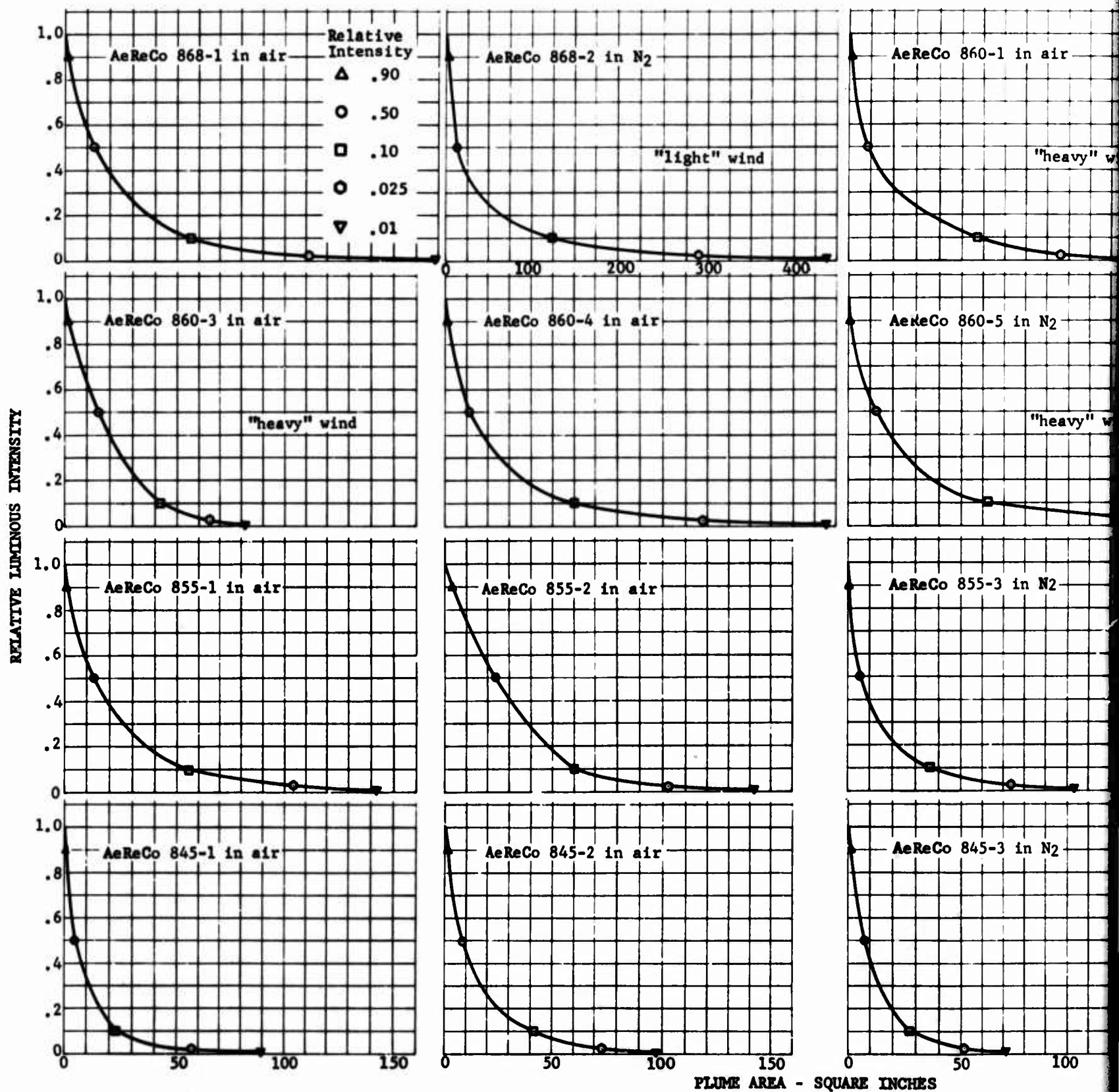
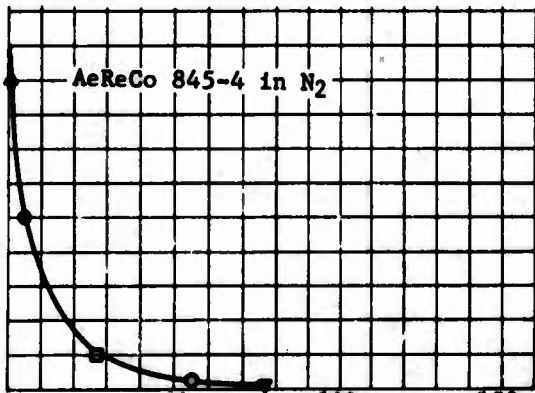
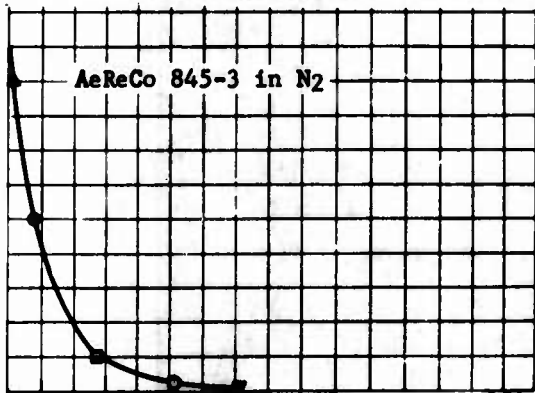
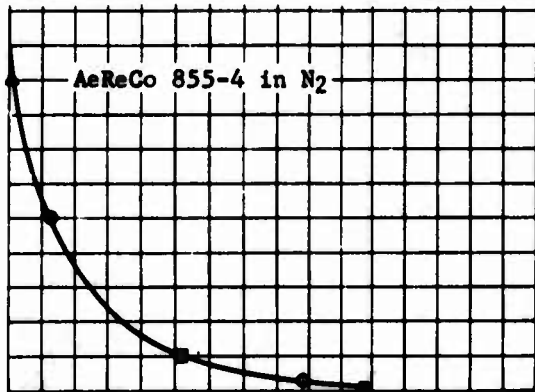
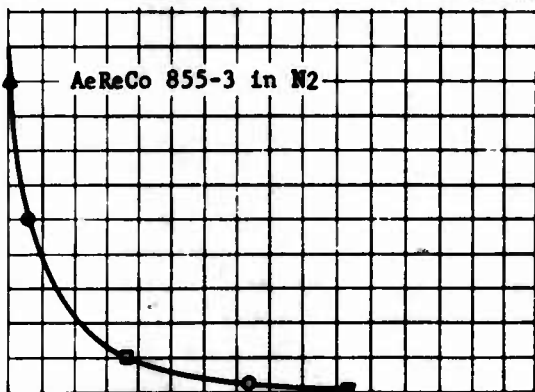
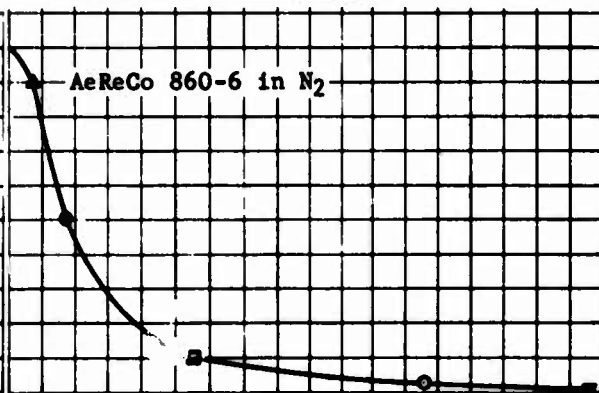
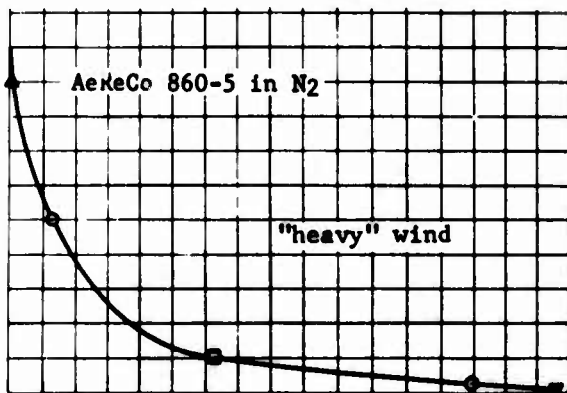
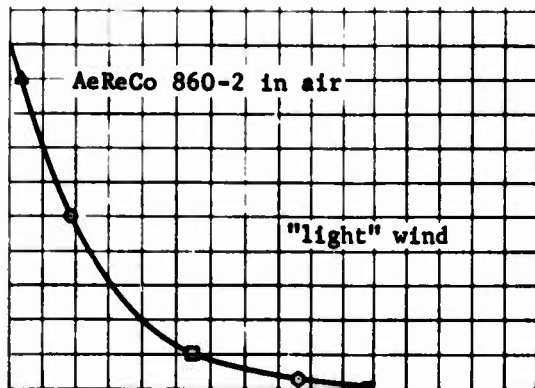
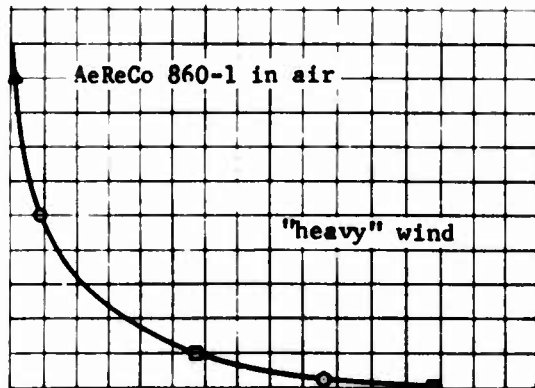


Figure 47 - Plots of relative luminous intensity versus plume area as determined from results of tests. The abscissa scale difference for AeReCo 868-2 flare. Relative luminous intensity



SQUARE INCHES

area as determined from results shown in figure 4. Note
Relative luminous intensity contour points are shown.

B

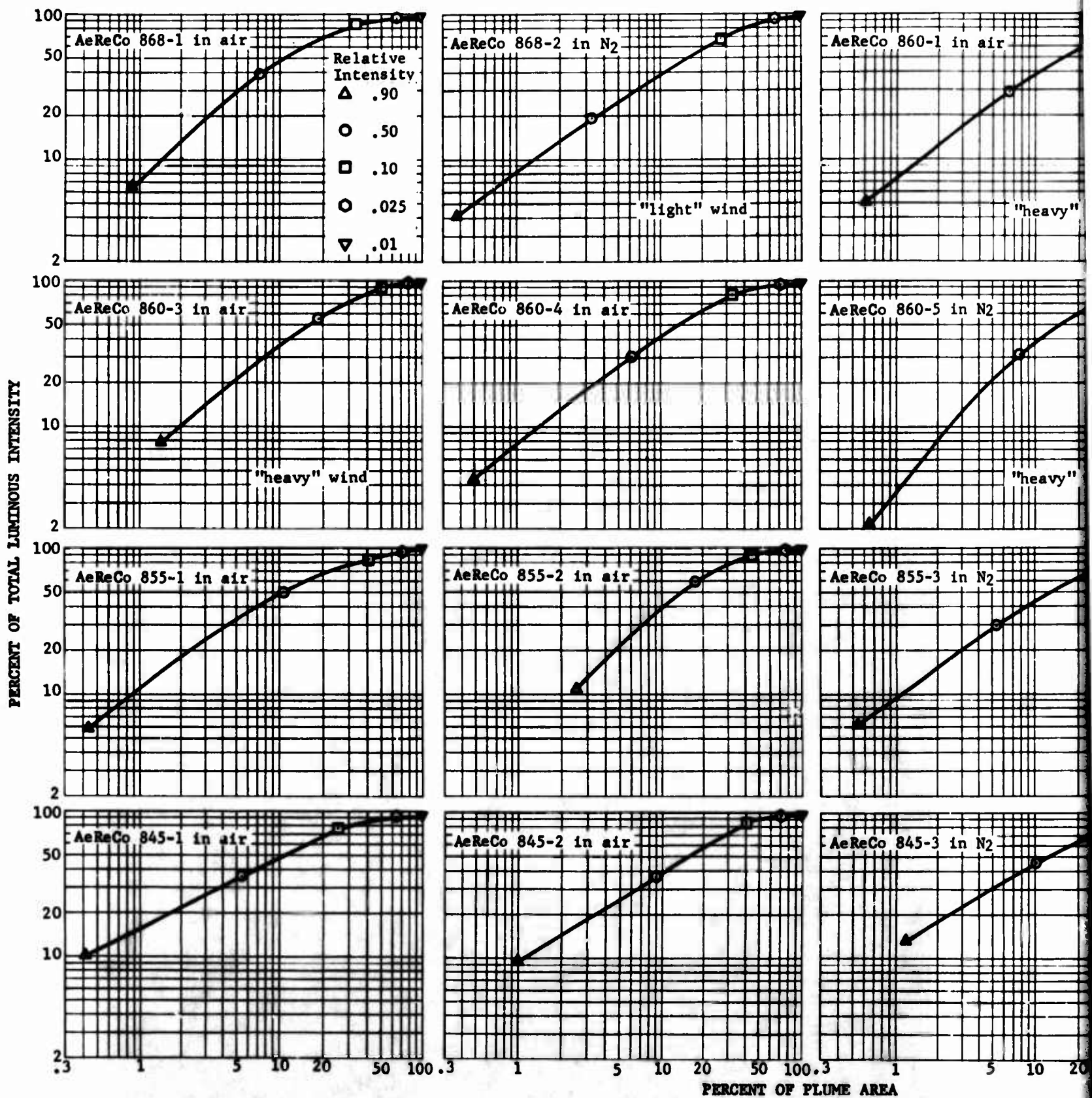
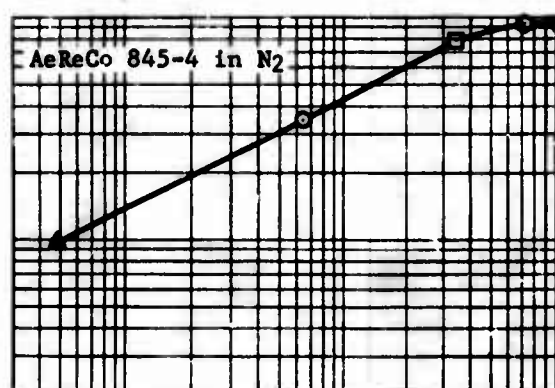
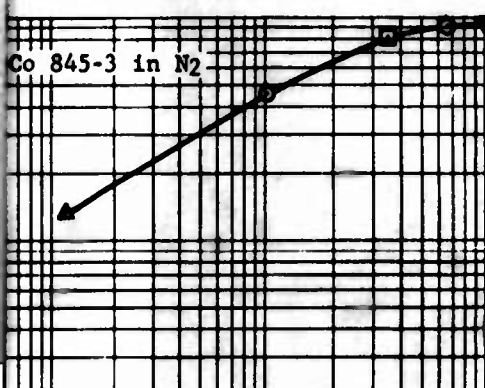
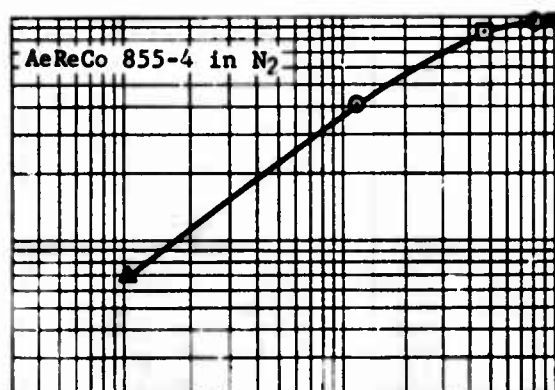
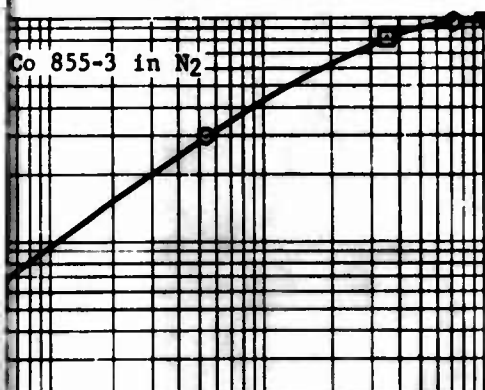
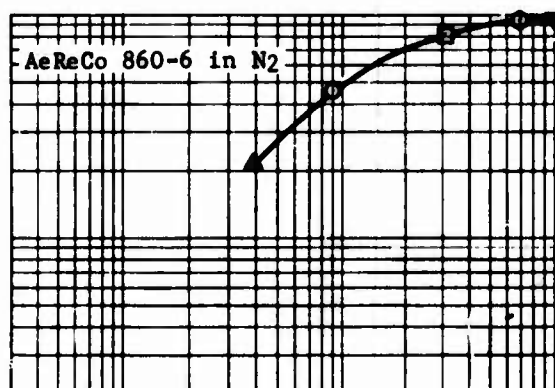
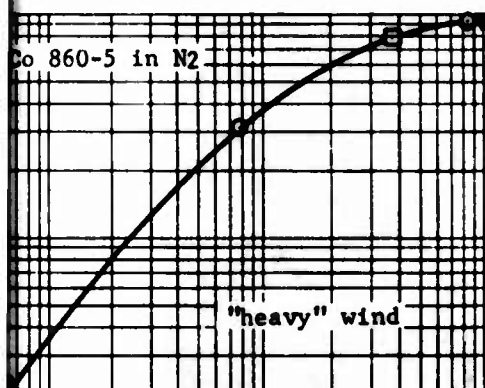
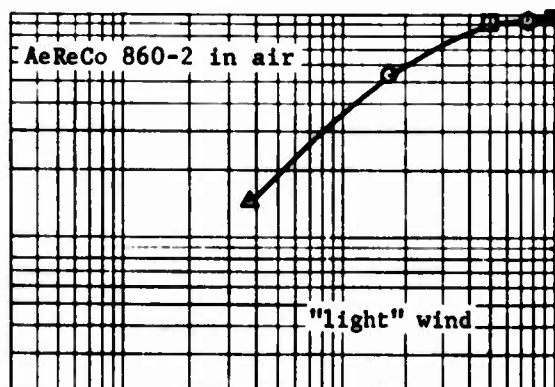
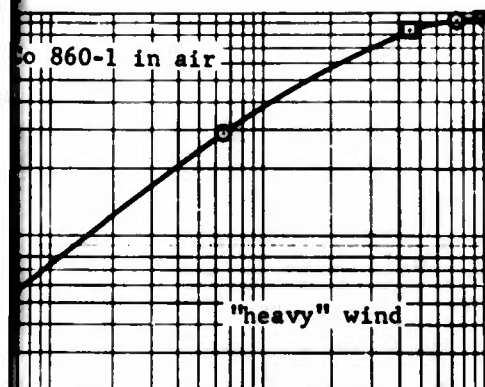


Figure 48 - Plots of percent of total luminous intensity versus percent of plume from figure 5. Relative luminous intensity contour points are shown.

A



AREA
versus percent of plume area as determined
four points are shown.

B

SUMMARY

It became apparent after observation of the luminous intensity profiles of the various flares studied that the flames resulting from these solid fuel and oxidizer mixtures are not too different in shape and form factor than a flame from a wax candle or a propane burner. It is true that the flare is far more erratic in its flame structure, but when viewed from a time and area average point of view which is accomplished by the scanning device previously discussed, and by appropriate data reduction techniques, it is found that these time and area profiles do indeed exhibit a similarity to ordinary flame profiles as well as show the effects of the prevailing ambient conditions during the course of the experiments.

This similarity in form can probably prove to be a useful tool in future analyses as long as it is kept in mind that only the integrated plume shares these similarities.

Certain conclusions can be drawn from the results of the measurement of these luminous intensity profiles. These can be based essentially on the effects created by three variables:

1. Percent Fuel (Magnesium)
2. Environment (Air or Nitrogen)
3. Wind Velocity

The effect of these variables are noted, or observed, through the resultant variation in at least four parameters.

1. Intensity (Candlepower)
2. Burn Time (Seconds)
3. Plume Area (Square Inches)
4. Plume Shape (Relative Intensity Contour Lines)

The following comments briefly, and in very general terms, consider each of the three variables and point out its effect on each of the aforementioned parameters where applicable.

Effect of Percent Fuel - The sample flares consisted of fuel percentages (magnesium) of 45, 55, 60, and 68. The following effects were observed.

1. Luminous Intensity. In all cases, the luminous intensity increased with increasing percent fuel.
2. Burn Time. Generally, the burn time decreased with increasing percent fuel. The one exception observed does not necessarily indicate a discontinuity in the trend. (Ref. Table I, Series 860, in Air)
3. Plume Area. Generally, the plume areas tended to increase with increasing percent fuel.
4. Plume Shape. While no definite trend was established it was observed that the larger plumes (higher percent fuels) were more subject to distortion from wind loading than smaller ones.

Effects of Environment - The sample flares were all burned in a plume downward position, under ambient atmospheric conditions at sea level. The differences in environment for each type of flare was the difference between burning under pure ambient conditions and when subjected to an upward and diffuse flow of nitrogen at approximately 6 feet per second to simulate the loss of ambient oxidizer to the system. While this technique did not fully isolate the flares from ambient oxidizer, its effect was observable.

1. Luminous Intensity. In all cases, the flares subjected to a flow of nitrogen were less intense than those burned in air alone.
2. Burn Time. In general, the flares subjected to the nitrogen flow burned at a slower rate. There was evidence that this difference in burn time diminishes under fuel rich conditions approaching 68 percent fuel.
3. Plume Area. For the lower percentages of fuel (45 percent and 55 percent) the flares burned in air alone had larger plumes. For the higher percentage fuels (60 percent and 68 percent) the flares subjected to a flow of nitrogen had the larger plumes. Some of this may be due to variations in wind load but definitely not all. It would be worthwhile to confirm this under more rigidly controlled conditions.
4. Plume Shape. No general conclusion can be made for the effects of the two environmental conditions as the flares burned under a flow of nitrogen probably had a greater tendency to distort.

Effects of Wind Velocity - While no attempt was made to control or measure the wind velocity, its effect was noticeable and was observed in a qualitative sense.

1. Luminous Intensity. In general the flares suffered a loss in intensity when subjected to moderate wind loads. However, some interesting effects are noted on the parameters to follow.
2. Burn Time. Under the previously described test conditions this was probably the least affected parameter. There were instances when heavy winds distorted the plumes to such an extent that the flames lapped upward, preheating and/or burning through. The data from these instances were not included in this study.
3. Plume Area and Shape. In terms of overall actual area it would be difficult to conclude either the absence or presence of a trend. Perhaps it is sufficient to conclude that these experiments are inconclusive in this regard. From Figure 46 it can be noted that the percentage plume area occupied by the higher intensity zones is less affected by wind conditions than the percentage area occupied by the less intense zones.

SECTION VI

DISCUSSION OF RESULTS

There are several areas which, after study of SECTIONS II through V may fruitfully be submitted to further analysis and evaluation. It is apparent from this study that the interdependence of parameters is so great that isolation of the variables is a very difficult task and is possibly the most severe of the problems encountered. It is likely as a result of the work reported herein and the work of others herein referred to that most, if not all, of the relevant variables have been identified. It is shown by the results that, although the assumption of a given set of equilibrium conditions in the flare plume allows fruitful treatment of many of the parameters, a state of overall equilibrium does not exist and that a group of superimposed submechanisms probably are responsible for a significant amount, if not most, of the light production.

It is the objective in the following pages to discuss the nature of the light producing mechanisms in view of the work done in this program and that in the references. These are, in order: (1) temperature measurements and correlation with luminous intensity, (2) analysis of particle behavior in the plume, (3) effects of magnesium particle size, (4) effect of velocities of particles in the plume, (5) effect of the surrounding gaseous medium, (6) effect of flare diameter variation, (7) binder formulations, and (8) case effects. It must be emphasized that the conclusions reached in these analyses are tentative. In many of the analyses the data are inadequate either to prove or disprove the conclusions reached, but an attempt has been made to provide a sound base for planning of further experimentation and study.

(1) Temperature Measurements and Correlation with Luminous Intensity - For most of the plumes shown in figure 46, page 101, the point of maximum luminous intensity is approximately 3 inches from the burning face of the flare along the flare centerline. The temperature as measured by thermocouple for all flares at this three inch point varied from approximately 2200 to 2700°F (figures 22, 23, and 24, pages 50, 51, 52.) Only for AeReCo 868 flares was this the point of maximum temperature. That the maximum luminous intensity point does not necessarily occur at the point of maximum average temperature may possibly be explained by the results reported in Table V, page 79, in which maximum temperatures of 2700 to 2900°K (4400 to 4760°F) at wavelengths of 5800 to 6000 Å were detected by spectrometer. The existence of these temperatures within the plume which are so high above the computed equilibrium temperature indicates continued sporadic combustion of magnesium throughout the plume. Inasmuch as the thermocouple temperature measurements were made within a chamber in which there was only nitrogen or argon, whereas the isolation from air was not so complete with the Ordnance Research and University of Minnesota experiments, comparisons of luminous intensity with temperature away from the maximum luminous intensity point are less meaningful than near it. The fact that at Ordnance Research the flares were burned in a downward facing position whereas the thermocouple measurements were made with flares burning in an upward facing position probably makes little difference near the maximum luminous intensity point in view of the apparent constancy of that position with varying flare compositions.

If for the upward facing flares, particles of magnesium were ejected as they were with the downward facing flares as described in SECTION IV, a large amount of sodium nitrate must have also been ejected at least for flares with 60 and 68 percent magnesium. This statement is based on the fact that the maximum temperatures as measured by thermocouple were in such close agreement with the computed equilibrium temperatures.

The sodium nitrate, with its low decomposition temperature (716°F), would rapidly decompose in the plume and react with the surrounding magnesium vapor which is greatly in excess. This could account for the high temperatures observed by spectrometer and may also explain the higher illumination intensity with the large magnesium excess. Further discussion of this effect is provided in the next subsection on analysis of particle behavior.

(2) Analysis of Particle Behavior in the Plume - As conjectured in the previous section, the ejection of particles of magnesium into the plume may be accompanied by substantial amounts of sodium nitrate. It can be logically supposed that the magnesium particle leaves the flare surface coated with molten sodium nitrate which upon evaporating and decomposing cools the magnesium particle and reacts more readily with the surrounding magnesium vapor than with the solid particle. The foregoing analysis is based upon the assumption that adequate melting of the sodium nitrate (melting point 584°F) and binder at the flare surface occurs to allow the particles of solid magnesium (melting point 1204°F) to float in the liquid sodium nitrate in the case of upward burning flares. In the case of downward burning flares, particles of magnesium probably would tend to fall but may be held to some extent by surface tension. Thus, the size and quantity of the magnesium particles as well as the orientation of the flares would have a significant effect upon flare performance. It is probable that some of the larger magnesium particles are forcefully unseated by the melting and decomposition of confined sodium nitrate and binder in which the particles are embedded.

If the foregoing analysis is correct the probability of the computed equilibrium temperature equalling that measured by thermocouple in the plume of a downward burning flare is lower than for an upward burning flare. This is an area which requires further investigation as it may hold the key to particle size selection as well as a clear understanding of the combustion mechanisms.

(3) Effects of Magnesium Particle Size - In view of the foregoing analysis and results discussed in SECTION III there is good indication that the burning mechanisms are such that not only the average size but the combination of magnesium particle sizes may be very important. Currently, production flares utilize granulations specified by MIL P-14067 and primarily Type I magnesium, 30/50 nominal mesh size. The particle size is nominally 350 ± 50 microns. If the light producing mechanism is enhanced by particles of magnesium being dispersed through the plume then the magnesium particles serve at least three functions: (1) initial combustion with oxidizer to form the basic plume, (2) formation of magnesium vapor which reacts with the oxidizer as it is dispersed throughout the plume, and (3) as carriers of the molten sodium nitrate during ejection through the plume. These three separate functions might most efficiently be carried out by providing three (or more) particle sizes, one which would control burning rate, another formation of magnesium vapor, and another particle dispersal. Thus, the 30/50 magnesium which contains a maximum of 5 percent of particles of a size less than 149 microns may be inefficient for some functions which it performs. For

example, if large particles are required for provision of highest illumination efficiency as is indicated by Table II page 57, and small particles are required for highest burn rate, then a mix of 350 micron and 22 micron particles might provide the desired burn rate and a higher luminous efficiency. Indeed, larger average particle size than 350 microns in combination with the 22 micron particles could prove even more effective. If the oxidizer melts on the burning surface of the flare, it can be assumed that oxidizer particle size would not greatly affect flare performance. This assumption is given some support by the results of tests reported in reference 1 of this part of the report. These results show that increasing sodium perchlorate particle size from 100/200 mesh to 325 mesh did not change flare burn rate or performance. The results are not conclusive, however, because of the partial solubility of the sodium perchlorate in the binder. With perchlorates, large particles of aluminum may prove effective.

A second factor to consider with regard to the results shown in reference 1 is that best luminous efficiencies were obtained with a one to one ratio of magnesium and oxidizer. This may have resulted from the magnesium particle size chosen, which was limited to a maximum of 200 microns. In Table II, page 57, particle size did not appear to be a factor between performances of .62 and 1.35 inch diameter flares for particle sizes at or below 200 microns. Further, it is noted that with a 350 micron average particle size in Table VI, page 99, the maximum luminous efficiency was 57,400 candleseconds per gram for a one inch pressed flare with 68 percent magnesium. This luminous efficiency was determined with the same EG&G 580 radiometer system that was used to measure the luminous efficiencies of the 3.2 and 4.0 inch diameter flares of reference 1 and for which the maximum luminous efficiencies were lower (51,000 candleseconds per gram.) On the basis of a 68 percent magnesium pressed flare and comparisons of data in figures 18 and 19, pages 43 and 45, at 4000°F the maximum luminous efficiency for the cast flare could occur with a 48 percent magnesium, 37 percent oxidizer, and 15 percent binder ratio if MIL P-14067, 30/50 magnesium particle size were used. This, of course, is based on the assumption that the particle ejection mechanism theory is correct. It should be noted that the burn rates of the cast flares are in the 4 to 5 inch per minute range which is approximately the same as that for the 68 percent pressed magnesium flares of 30/50 particle size. The amount of magnesium gas in the plume is only slightly less for the cast flare than for the pressed flare, but it has not been determined if the velocities in the two plumes are similar. Perhaps clues to the effects of particle sizes can be obtained by considering the velocities of particles within the plume.

(4) Effect of Velocities of Particles Within the Plume - It is indicated by the results of computations using the mathematical model in SECTION II that residence time (which is a measure of velocity) of a particle at least within a radius of one half of the flare diameter in the plume is not greatly affected by fall rate. Experimentally this appears to be true not only with differing counter flows but also for flares with the same magnesium particle size and varying percents of magnesium, an observation which is based on the constancy of the maximum luminous intensity position evident in figure 46, page 101 for all of the conditions shown. There is some indication that longer residence time, which is assumed to be in some degree synonymous with low burn rate, provides higher luminous efficiency. This is generally supported by the results shown in Table I, page 56, and Table II, page 57, but is not supported by the results shown in Table VI, page 99, in which the burn rate decreases with decreasing magnesium content below 60 percent along with a decrease in luminous efficiency. There is indication in Table II page 57, that higher velocities generated by thick walled casings

may have contributed to conditions in .62 inch casing diameters which resulted in the same low luminous efficiency with 30/50 magnesium as was obtained with 50/100 magnesium. As the casing diameter was increased to 1.33 inches, the 30/50 system was superior to the 50/100 system. It is assumed that the slower burn through of the thicker casing resulted in a rim which caused a jet effect in the .62 inch casing, and thus higher velocities occurred in the plume. The jet effect is not the only factor involved as will be discussed in a subsequent section but it is clear that particle size effects and study of these effects will require carefully controlled conditions including type and thickness of inhibitor as well as exact sizing of particles. Factors related to the problems that may be encountered in simulated fall rates as well as the surrounding medium are discussed in the following section.

(5) Effect of Surrounding Gaseous Medium - In SECTION II, it was indicated that the edge effect on the burning plume surface should be subjected to further study. This should be extended to include evaluation of a rim simulating the casing which produces the jet. It is indicated in the concluding remarks of SECTION IV, page 90, that producing the jet effect enhances plume mixing with air, causing lower flare efficiency.

If this thesis is correct then the lower luminous intensities obtained with nitrogen as shown in Table VI, page 99, are readily explained. The flares burned in air experienced no counter velocities (other than those due to convection) as the air was not being ejected upward as was the nitrogen. One consequence of increased mixing of the plume with surrounding air is provided by comparing the first four AeReCo 860 flares in figure 46, page 101. Three of the flares 860-1, 860-2, and 860-3 were subjected to cross winds and the resulting plumes were smaller than the plume for the flare 860-4 for which there was no cross wind. For the 868 and 860 flares burned in nitrogen, figure 46, page 101, it appears that mixing of air with the nitrogen in the edge of the plume resulted in scattered burning of magnesium (and perhaps sodium) in the lower velocity oxygen-lean mixture, with consequent broader plumes than those for still air. The plumes for the AeReCo 855 and 845 flares were smaller and apparently adequately enveloped by the nitrogen to prevent this broadening. Tests of flares in a still nitrogen atmosphere as well as in counterflow air and nitrogen atmospheres will have to be performed to check the validity of the foregoing tentative explanation. In the future the upward flowing columns of air and nitrogen should be large enough to preclude effects on the plume due to mixing or slowing down of gases in the column due to the surrounding air. The results of such tests may be necessary for optimizing flare fall rate. For example, the average luminous efficiency for all flares subjected to upward flowing nitrogen was 95 percent of those in still air. If a similar reduction should be experienced with upward flowing air, a close examination of fall rates is in order. Such an examination should include the effect of varying the flare diameter. A discussion of diameter effects is included in the following section.

(6) Effects of Flare Diameter Variation - It was indicated on page 31 that for a given value of time ratio at a given point in the flow field, the larger the flare radius and the lower the burning rate (equation 15 (c) page 28) the longer the time that the fluid particle has existed in the plume. It was concluded on page 31 that if a longer time in the plume results in lower particle temperature, it can be concluded that the luminosity per unit area of burning surface is higher for smaller diameter flares. In Table III page 67 it is shown that radiation

properties of a 30 percent MgO, 10 percent sodium mixture are such that the efficacy of the mixture drops rapidly as the body of gas thickens. It is also shown that the cooling rate of the mixture is more than 10 times as great at 3500°K (5840°F) as it is at 2000°K (3140°F.) Both of these factors support the thesis that a longer particle residence time in the plume reduces its luminous output, for although the plume constituents may block luminous radiation they do not necessarily block infrared radiation which plays a large part in particle cooling. Thus, by the time a particle has moved through the optically thick portion of the plume it may have cooled to a temperature at which it is a much less effective illuminant than it would have been in an optically thin plume. This analysis is based on the assumption that the hot particle is generated near the flare surface, and that the smallest diameter flare would provide the highest luminous efficiency. It has been demonstrated that this is not the case, which gives further support to the assumption that oxidizer is ejected into the plume where it burns with magnesium vapor. It should be emphasized that this in no way impairs the usefulness of the conclusions regarding particle residence time and the results of Table III, page 67. However, it does suggest that arrival at the optimum flare diameter will require inclusion of the path length of the ejected particles as a contributing function and that the originating point of the hot particle must be clearly defined. Some information relevant to this problem may be drawn from the results shown in Table II, page 57. For thin cased flares using 22 micron magnesium, the 1.33 inch diameter flares were slightly less efficient than the 0.62 inch diameter flares. The same is true for the flares in which 200 micron magnesium was used. However, for the flares using 350 micron magnesium there was a thirty percent increase in luminous efficiency in going to the larger diameter. The size of this change is such as to preclude the jet effect and mixing as the dominant factors and to suggest that an additional light-producing mechanism was introduced with the increased diameter. A plausible explanation is that the ejected particles of oxidizer left the plume of the 0.62 inch diameter flare before decomposing sufficiently to burn completely with the magnesium vapor whereas in the 1.33 inch diameter flare there was adequate time to complete the process. Further tests to determine the flare and plume diameter at which the maximum rate of drop in luminous efficiency occurs might supply some clue as to the nature of the change in mechanisms. Luminous efficiencies for varying diameters and magnesium percentages are indicated in Table VI, page 99, Table I, page 56, Table II, page 57, and figure 26, page 55. An attempt was made to integrate all of these results in order to provide greater comprehensiveness, but this was not possible due to differences in formulations, processing methods, particle sizes, inhibitors, and light measuring techniques. This is emphasized by the results of Table VI, page 99, in which the luminous efficiency (57,400 candleseconds per gram) for the 68 percent magnesium flare burned in air exceeds the maximum shown (46,000 candleseconds per gram) for the 4.25 inch diameter flare in figure 26, page 55. As the formulations and magnesium particle sizes are identical the major difference appears to be in the luminosity measuring system. This does not impair the usefulness of the data derived from a given system but emphasizes the precariousness of comparing data obtained in different experiments of this kind. With this in view an analysis of the results using the single system (from Doua et al ref. 4 SECTION III) shown in figure 26, page 55, was attempted. As shown in that figure, the efficiency of 30/50 magnesium sodium nitrate, Laminac flares increases with diameter up to approximately 4.25 inches. Above this diameter the luminous efficiency drops off rapidly. For other flare compositions (see figure 9 of Vol. I. of ref. 4, page 61) the efficiency continues dropping to between

5000 and 10,000 candleseconds per gram depending upon the binder system and remains constant for diameters above approximately 15 inches. It is indicated by these results that the mechanism involving particle ejection is more effective with increase in flare diameter to approximately four inches for the 30/50 magnesium, sodium nitrate, Laminac system. In plumes of flares of the same composition above that diameter the increasing optical thickness of the plume with diameter causes an observed fall off in luminous efficiency until finally most of the illumination is provided by gray body radiation from the luminous cloud of magnesium oxide particles. It is estimated by the theoretical results in Section IV that extinction lengths in MgO clouds are approximately 10^{-6} cm at the D-lines and 60 cm away from the D-lines. With flares from which a great deal of illumination is derived from D-line radiation, this would require that oxidation of the magnesium vapor and heating of the sodium vapor take place on the fringes of the plume. Thus it is indicated from figure 26, page 55, that the optimum path length of the sodium nitrate particles probably far exceeds two inches for the flares tested. The sizes of the plumes were not given for these tests, but based on the results of figure 46, page 101, a four-inch diameter pressed flare would exhibit a plume on the order of 40 inches in diameter, and 60 inches high, which places the optimum path length of the oxidizer particles at approximately twenty inches, a distance which would require approximately one second to traverse. Without experimental evidence to the contrary it is assumed at this point that unused sodium nitrate escaped from the plume for flare diameters below 4.25 inches and that the optical thickness of the plume caused blockage of a great deal of the radiation for the 7.35 inch diameter flares. For cast flares exceeding 15 inches in diameter the projected plume size would be on the order of 100 inches in diameter by 175 inches high based on the plume size shown in figure 49. The plume radius of 50 inches exceeds the 20 inch optimum by approximately 30 inches (76 cm.) This exceeds by 16 cm the optical path length of 60 cm as computed in Section IV. If the foregoing analysis is correct, it explains why the luminous efficiency levels out above 15 inches for cast flares. It also demonstrates that plume size rather than flare diameter determines the luminous efficiency. Therefore, the optimum flare diameter will vary with flare composition and processing methods. If the ejection theory is correct, a study of the rate of rise and decline in luminous efficiency with varying diameter for various magnesium ratios and for different particle size combinations may provide the basis for a more complete understanding of the light producing mechanisms. As ejection of particles can be greatly affected by the type and percentage of binder, the merits of different binder systems might also be more easily evaluated by such a study. Both the binder and the inhibitor (or casing) present problems that have been evaluated to some extent in the past. Some of the work is referred to in Section III. The problems involved are discussed briefly in the next two sections.

(7) Binder Formulations - With pressed flares the percent of binder required is approximately one-fourth of that required for casting because consolidation of ingredients depends upon both binder and pressure. However, production problems anticipated with large flares using available presses has led to experimentation with casting of flares. The binders used in both pressed and cast flares are usually relatively low viscosity liquids which polymerize upon adding chemicals that cross-link the binder molecules. It was pointed out herein that binders which contain fluorocarbons may be better because they are oxidizers. However, it is not known how they will behave with regard to ejection into the plume or as illuminants. Both magnesium and sodium fluorides are stable at high temper-



Figure 49- Plume of a Cast Flare 4.75 inches in diameter. Flare and Photograph Provided by Ordnance Research Incorporated. Scale 7/16 inch = 1 foot zero inches

atures and their behavior as illuminants is not well known. Binders that are oxygenated and also dissolve the oxidizers have been investigated (refs. 3 and 4, page 61), but primary emphasis was placed upon physical integrity rather than upon the effect upon burning mechanisms. The results in reference 3 show rapidly decreasing luminous efficiency with increase in binder content. The amount of decrease as indicated by the figure on page 6 in reference 3 is much in excess of what would be expected from the decrease in fuel and oxidizer due to displacement by the binder. This could be due to effects on the ejection mechanism. It has already been stated under the discussion of particle size that the luminous efficiency might be increased by introducing a larger average magnesium particle size. Just how the increased binder content might affect ejection and other mechanisms is not known. The effects of such factors as melting point of the binder versus that of the oxidizer, heat transfer coefficient of the binder, and oxidizer dilution may be significant and should be evaluated.

(8) Casing Effects - The rim effect and experimental results obtained with changing inhibitor thickness have already been mentioned. However, there are a few additional remarks regarding effects of the casing upon performance. If the formation of a rim is beneficial, for example, in inverted burning, then the inhibitor material should be so designed as to form the optimum rim height. It is conceivable, however, that if the rim were burned off so as to present a rounded edge, the ejection of particles with a large radial component outward could occur which could be highly beneficial. There are methods of designing such inhibitors such as by the use of metals, binders partially loaded with oxidizer, or combinations of the two. As previously indicated a theoretical evaluation of the flow around the rim should be incorporated into the study of the edge effect.

LIST OF REFERENCES - SECTION VI

1. Study of Visual Cast Flare Binder Material, RDTR No. 113, January 1968, Hal R. Waite, Yoshiyuki Arikawa, Ordnance Research Incorporated.

SECTION VII

SUMMARY OF RESULTS

A report has been compiled which includes four sub-reports (SECTIONS II through V), one from each of the principal investigating teams, and a discussion of the results. In SECTION VI (DISCUSSION OF RESULTS) the nature of the light producing mechanism based on work done in the program as well as that covered in the references is discussed. The results may be summarized as follows:

1. A mathematical flow model has been developed for plane two-dimensional illuminating flares dropping through the atmosphere and simulating face down burning. Numerical results are given in field plots showing streamlines, velocity potential lines, constant velocity lines, and constant time lines for two-dimensional, incompressible flow. These results show:
 - (a) The residence time of a particle in the plume is not significantly affected by the fall rate of the flare.
 - (b) There is a significant edge effect on flow at the corner of the flare which will require further refinements of the model.
2. Thermochemical calculations based on shifting equilibrium were made for combustion in the flare plume over a range of various mixture ratios. The results are provided in the form of curves and tables showing reaction products, equilibrium temperatures, and other thermodynamic data. Temperatures in plumes of one inch diameter flares were measured by thermocouple with the following results:
 - (a) The maximum temperatures in plumes of flares burning upward in a nitrogen atmosphere containing 60 and 68 percent magnesium were within 100°F of the computed equilibrium temperature.
 - (b) The temperatures measured in plumes of flares containing 55 percent magnesium were approximately 1100°F less than computed.
3. A theoretical evaluation of optical density in the plume and experiments to evaluate optical density were performed. The results are provided in tables, photographs of plumes, and traces obtained by spectrograph. The following results were obtained:
 - (a) Computations show that in the flare plume the optical path length for MgO at a temperature of 3000°K and concentration of 30 percent is 60 cm and for sodium at the D-lines is 10^{-6} cm.
 - (b) Temperatures determined from spectral data show maximum temperatures in the plume of 4400°F to 4670°F at wavelengths of 5800 Å to 6000 Å. (This was determined for flares in which the maximum temperature measured by the thermocouple was 3500°F.)

- (c) Particles ejected from the flare into the flare plume result in hot spots which contribute to the visible radiation.
4. Relative luminous intensity distributions in the plumes of downward burning flares were determined and the results are shown in terms of relative intensity contours, plots of relative intensity versus plume area, and plots of percent total intensity versus percent of plume area. The following results were observed:
- (a) The luminous intensity increased with increasing percent of magnesium from 45 to 68 percent.
 - (b) The plume volume increased with increasing percent of magnesium.
 - (c) The plume volume and luminous intensity decreased when subjected to cross winds or to nitrogen in counterflow.
5. An analysis of overall results was made utilizing information from the literature as well as that generated in the program with the following tentative conclusions:
- (a) Although the maximum measured temperatures as determined by thermocouple for flares burning in nitrogen atmospheres tend to agree with the computed equilibrium temperatures (for 60 percent magnesium and above) ejection of particles into the plume results in hot spots with temperatures approaching that for stoichiometric burning.
 - (b) The ejection mechanism is hypothesized to depend upon melting of sodium nitrate at the burning surface with ejection of magnesium particles coated with sodium nitrate into the plume where the sodium nitrate decomposes and reacts with the magnesium vapor in the plume, the magnesium particle size playing a dominant role.
 - (c) The residence time of the particle in the plume as shown by the constancy of the location of the maximum luminous intensity point in the plume with and without cross or counter flows tends to confirm the calculations.
 - (d) The evaporation and decomposition rate of the sodium nitrate (with subsequent reaction with the magnesium vapor) establishes the optimum size of the plume. Thus, the optimum flare diameter will vary with flare composition. The leveling out of luminous efficiency for cast flares above 15 inches (approximately 38 cm) diameter tends to confirm the computed optical path length of 60 cm for magnesium oxide.
 - (e) Counter or cross flows, whether air or nitrogen, result in lower luminous intensity.
 - (f) Binder formulations have a large effect upon the ejection mechanism, and therefore, luminous efficiency.
 - (g) The casing or inhibitor material and thickness can have a large effect on flare performance.

SECTION VIII

AREAS FOR FURTHER EXPLORATORY DEVELOPMENT

As previously stated, most, if not all, of the relevant variables have been identified in the first phase of the program. To provide more definitive information about these variables, the following recommendations are made:

1. The mathematical model should be modified to include more detailed information about the flow pattern at the edge or corner of the burning flare surface including the rim which is left by the flare casing or inhibitor.
2. The computations for the mathematical model should be expanded to include density variations, heat exchange in turbulent mixing of the plume gases with air cooling of the flare plume due to heat radiation, and enthalpy distribution.
3. Temperature measurements with thermocouples should be made in magnesium-sodium nitrate flares up to at least four inches in diameter. These flares should incorporate a range of magnesium particle sizes.
4. A study of particle history should be made from the time the particle begins to heat up on the flare surface until it leaves the plume. This would include movies of action on the flare surface, movies of the plume, and spectroscopic measurements for flares having both small particles alone and a mixture of small and large magnesium particle sizes. The spectroscopic measurements in this case should be primarily concerned with absorption broadening and techniques of derivation of temperature from sodium doublet broadening.
5. Luminosity distribution in plumes of one inch diameter flares in still air and nitrogen as well as in counter flow air and nitrogen should be obtained for flares containing both small and a mixture of small and large magnesium particle sizes. Luminous distribution should also be obtained in plumes of flares up to at least four inches in diameter in still air.
6. Spectral distribution in the plume should be determined by means of a scanning spectrometer. This would provide identification of the chemical species and possibly their temperature in direct association with their luminous intensity.

APPENDIX I

LIST OF ABBREVIATIONS AND SYMBOLS FOR SECTION II

A	complex constant, Eq. (3a)
A_1	real constant, Eq. (6e)
A_2	constant, Eq. (7a)
A, B, C, D, E F, G, GG, H, I	$\left\{ \begin{array}{l} \text{parameters, Eq. (10g)} \end{array} \right.$
a, b, c, \dots	locations in ascending order on ξ -axis of t -plane, corresponding to vertices of polygon in z -plane, Fig. 8
B	complex constant, Eq. (3a)
B_ϕ	constant, Eq. (6f)
B_ψ	constant, Eq. (6f)
i	imaginary, $\sqrt{-1}$
K	drop rate parameter, Eq. (12ü)
$m_t(\xi)$	local strength of point source distribution along burning face of flare in t -plane, Eq. (6b)
$m_z(x)$	local strength of point source distribution along burning face of flare in z -plane, Eq. (6c)
P	static pressure parameter (dimensionless), Eq. (13c)
p	local static pressure (dimensional)
p_a	atmospheric static pressure (dimensional)
p_t	total pressure (dimensional)
q or Q	dimensionless velocity relative to flare, expressed in units of v_B^* , Eq. (2a) and Fig. 3
q^*	velocity relative to flare (dimensional)
R	radius parameter, Eq. (5c)

r^*	radius, or half-width, of flare (dimensional)
s	distance along streamline from burning face of flare (dimensionless), expressed in units of r^*
s^*	distance along streamline (dimensional)
t	location in transformed t -plane, Eq. (4) and Fig. 4
t	time
u	dimensionless velocity component in direction of abscissa (x-direction), expressed in units of v_B^* , Fig. 3
v	dimensionless velocity component in direction of ordinate (y-direction), expressed in units of v_B^* , Fig. 3
v_B^*	velocity component normal to burning face of flare (dimensional)
v_D^*	drop rate of flare (dimensional)
v_D^{**}	"effective" drop rate of flare (dimensional), Eq. (12a)
v_{FL}^*	burning rate of solid flare material (dimensional), Eq. (12c)
w	complex potential, Eq. (1)
x	dimensionless abscissa in physical z -plane, expressed in units of r^* , Fig. 2
y	dimensionless ordinate in physical z -plane, expressed in units of r^* , Fig. 2
y_0	location of stagnation point (of plume) on y -axis, Eq. (14b)
z	dimensionless location in physical z -plane, expressed in units of r^* , Eq. (4) and Fig. 2

Greek symbols:

α	flow direction measured counterclockwise from positive x -axis in physical z -plane, Eq. (2b) and Fig. 3
$\alpha, \beta, \gamma, \dots$	deflection angles of polygon in z -plane, Fig. 8
β	angle parameter, Eq. (6j)
$\Delta\psi$	change in ψ
η	ordinate in t -plane, Fig. 4
θ	angle parameter, Eq. (5d)
ξ	abscissa in t -plane, Fig. 4

ρ_{air}	weight density (constant) of air, Eq. (12a)
ρ_{FL}	weight density of solid flare material, Eq. (12c)
ρ_{gas}	weight density (constant) of plume, Eq. (12a)
τ	dimensionless time parameter, Eq. (15c)
ϕ	velocity potential function (equals Φ)
ψ	stream function

Subscripts:

\circ	stagnation point
1	continuous distribution of point sources along burning face of flare
2	"approach" flow in t-plane, corresponding to drop rate of flare in physical z-plane, Eq. (7a)

Superscripts:

$()^*$	dimensional quantity, when applied to velocities and to linear distances
---------	--

APPENDIX II

SOLUTION OF INTEGRAL EQUATION (6e)

To solve integral equation (6e) for w_1 , first differentiate under the integral sign with respect to t . Thus,

$$\frac{dw_1}{dt} = A_1 \int_{-1}^{+1} \frac{\sqrt{1-\xi^2}}{t-\xi} d\xi \quad (\text{II-1})$$

Equation (II-1) then integrates to give

$$\frac{dw_1}{dt} = A_1 (t - \sqrt{t^2 - 1}) \quad (\text{II-2})$$

And, from equation (II-2),

$$w_1 = A_1 \int (t - \sqrt{t^2 - 1}) dt + \text{constant}$$

or

$$w_1 = \frac{A}{2} \left[t^2 - t\sqrt{t^2 - 1} + \ln (t + \sqrt{t^2 - 1}) \right] + (B_\phi + i B_\psi) \quad (6f)$$

where $(B_\phi + i B_\psi)$ is a complex constant of integration, to be determined later.

APPENDIX III

COMPUTER PROGRAM FOR TWO-DIMENSIONAL-FLARE-PLUME FLOW MODEL

by Edward J. Davis

This program was written in the FORTRAN IV E level language for the IBM System 360 Model 50 digital computer. To insure compatibility with all FORTRAN compilers, no special features of higher level compilers (logical IF statements, etc.) were used. The program occupies approximately 9000 bytes of core storage, and utilizes the standard set of FORTRAN supplied mathematical subprograms.

Execution time varies directly with number of input variables. On the IBM System 360 Model 50, a typical case requires fifteen minutes. The program is designed to operate in a "load and go" mode. No special operating procedures are necessary; the input data cards are simply appended to the FORTRAN source deck.

INPUT FORMAT

Card Columns

Card	1 - 5	6 - 10	11 - 15
I	Number of Xi's	Number of Eta's	Number of K's
	No decimal point - right justified		
	1 - 10	11 - 20	21 - 30
	31 - 40	41 - 50	51 - 60
	61 - 70	71 - 80	
II - III K values	The number of K's, Eta's and Xi's must equal that input on Card I (Use CARD III only when necessary.)		
IV-VI Xi values	These variables must occupy consecutive fields but not all the fields or columns have to be used. Each variable must contain a decimal point.		
VII - IX Eta values			

A typical set of card input is shown on the following pages.

	1.2	1.4	1.6	1.9	2.0	2.2	2.4	2.6	VIII
	1.2	1.4	1.6	1.9	2.0	2.2	2.4	2.6	VII

CARD VIII

[illegible]

CARD IX

[illegible]

```

C      NUMK = NUMBER OF $K(L)
C      M = NUMBER OF XI(J)
C      N = NUMBER OF ETA(K)
S.0001      DIMENSION XI(500),ETA(500),$K(10)
S.0002      READ(5,1001)M,N,NUMK
S.0003      100  FORMAT(3I5)
S.0004      READ(5,1003)($K(L),L=1,NUMK)
S.0005      1003  FORMAT(8F10.4)
S.0006      READ(5,1011)(XI(J),J=1,M)
S.0007      101  FORMAT(8F10.4)
S.0008      READ(5,1021)(ETA(K),K=1,N)
S.0009      102  FORMAT(8F10.4)
S.0010      DO 1004 L = 1, NUMK
S.0011      WRITE(6,823)
S.0012      823  FORMAT('1',T6,'PLANE, TWO-DIMENSIONAL, ISOTHERMAL
FLARES WITH',1T53,'CONSTANT DROP RATES')
S.0013      WRITE(6,824)$K(L)
S.0014      824  FORMAT('0',T6,'K = ',T10,F10.3)
S.0015      WRITE(6,825)
S.0016      825  FORMAT('0',T6,'XI',T16,'ETA',T26,'X',T36,'Y',T46,'PHI',
T56,'PSI',1T66,'U',T76,'V',T86,'Q',T96,'ALPHA',T106,'P')
S.0017      DO 1000 J = 1,M
S.0018      DO 1001 K = 1,N
S.0019      CA=2*(XI(J))*(ETA(K))
S.0020      CB=1-(XI(J)**2)+(ETA(K)**2)
S.0021      CI=(XI(J)**2)-(ETA(K)**2)
C      CALCULATE R
S.0022      R=SQRT((CB**2)+(CA**2))
C      CALCULATE THETA
S.0023      IF(ETA(K))107,108,109
S.0024      107  IF(XI(J))109,112,109
S.0025      109  ZZ7=(-CA)/CB
S.0026      THETA=ATAN(ZZ7)
S.0027      IF(THETA)116,116,117
S.0028      117  THETA=THETA-3.1416
S.0029      GO TO 116
S.0030      108  IF(XI(J))111,112,111
S.0031      112  THETA=0.0
S.0032      GO TO 116
S.0033      111  DD=XI(J)-1.
S.0034      IF(DD)114,114,115
S.0035      114  THETA=0.0
S.0036      GO TO 116
S.0037      115  THETA=-3.1416
S.0038      116  ZP=THETA/2.
S.0039      CC=(XI(J))*(COS(ZP))
S.0040      CD=(ETA(K))*(SIN(ZP))
S.0041      CE=(SQRT(R))*(SIN(ZP))
S.0042      CF=(SQRT(R))*(COS(ZP))
S.0043      CG=(ETA(K))*(COS(ZP))
S.0044      CH=(XI(J))*(SIN(ZP))
C      CALCULATE X
S.0045      XC=((XI(J))+CE)/((-ETA(K))+CF)

```

```

S.0046      XA=ATAN(XC)
S.0047      IF(XA)118,119,119
S.0048      118  XA=XA+3.1416
S.0049      119  XB=(SQRT(R))*(CC-CD)
S.0050      X=(.6366)*(XB+XA)
              C
S.0051      YA=(((-ETA(K))+CF)**2)+(((XI(J))+CE)**2)
S.0052      YB=(1./2.)*(ALOG(YA))
S.0053      YC=SQRT(R)*(CG+CH)
S.0054      Y=(.6366)*(YC-YB)
              C
S.0055      IF(ETA(K))120,121,120
S.0056      120  IF(XI(J))123,124,123
S.0057      123  FB=((XI(J)**2)-(ETA(K)**2)-1.)
S.0058      ZA=CA/FB
S.0059      BETA=ATAN(ZA)
S.0060      IF(BETA)129,128,128
S.0061      129  BETA=BETA+3.1416
S.0062      GO TO 128
S.0063      121  IF(XI(J))125,124,125
S.0064      124  BETA=3.1416
S.0065      GO TO 128
S.0066      125  FA=XI(J)-1.
S.0067      IF(FA)126,126,127
S.0068      126  BETA=3.1416
S.0069      GO TO 128
S.0070      127  BETA=0.0
S.0071      128  ZK=BETA/2.
S.0072      CJ=(XI(J))*(COS(ZK))
S.0073      CK=(ETA(K))*(SIN(ZK))
S.0074      CL=(SQRT(R))*(COS(ZK))
S.0075      CM=(SQRT(R))*(SIN(ZK))
S.0076      CN=(ETA(K))*(COS(ZK))
S.0077      CD=(XI(J))*(SIN(ZK))
              C
S.0078      CHIA=(SQRT(R))*(CJ-CK)
S.0079      CHIB=SQRT(((XI(J)+CL)**2)+((ETA(K)+CM)**2))
S.0080      CHIC=ALOG(CHIB)
S.0081      CHI=((.6366)*(CI-CHIA+CHIC))+($K(L)*.6366*CI)
              C
S.0082      ZB=(ETA(K)+CM)/(XI(J)+CL)
S.0083      PSIA=ATAN(ZB)
S.0084      PSIB=(SQRT(R))*((CN+CD)
S.0085      PSI=((.6366)*(CA-PSIB+PSIA))+($K(L)*.6366*CA)
S.0086      A=(CB**2)+(CA**2)
              C
S.0087      B=D(R)/D(XI)
S.0088      BA=2.*XI(J)*((XI(J)**2)-1.)
S.0089      BB=2.*XI(J)*(ETA(K)**2)
              C
S.0090      C=D(R)/D(ETA)
S.0091      CAA=2.*ETA(K)*(1.+(ETA(K)**2))
S.0092      CAB=2.*(XI(J)**2)*ETA(K)
              C
S.0093      DA=1.+(XI(J)**2)+(ETA(K)**2)

```

```

S.0094      D=(1./A)*((-2.)*(ETA(K))*DA)
C          CALCULATE D(THETA)/D(ETA)
S.0095      EA=1.-(XI(J)**2)-(ETA(K)**2)
S.0096      E=(1./A)*((-2.)*(XI(J))*EA)
S.0097      F=(((-ETA(K))+CF)**2)+(((XI(J))+CE)**2)
S.0098      G=CF+((1./F)*((-ETA(K))+CF))
S.0099      GG=CE-((1./F)*((XI(J))+CE))
S.0100      H=(CC-CD)-((1./F)*(CC+CD))
S.0101      $I=(CG+CH)-((1./F)*((-CG)+CH+(SQRT(R))))
C          CALCULATE D(Y)/D(ETA)
S.0102      $LA=(SQRT(R)/2.)*H*E
S.0103      $LB=($I*C)/(2.*SQRT(R))
S.0104      $L=(.6366)*(G+$LA+$LB)
C          CALCULATE D(Y)/D(XI)
S.0105      $MA=(SQRT(R)/2.)*H*D
S.0106      $MB=($I*B)/(2.*SQRT(R))
S.0107      $M=(.6366)*(GG+$MA+$MB)
C          CALCULATE D(X)/D(ETA)
S.0108      $NA=(SQRT(R)/2.)*(-$I)*(E)
S.0109      $NB=(H*C)/(2.*SQRT(R))
S.0110      $N=(.6366)*(-GG+$NA+$NB)
C          CALCULATE D(X)/D(XI)
S.0111      SA=(SQRT(R)/2.)*(-$I)*(D)
S.0112      SB=(H*B)/(2.*SQRT(R))
S.0113      S=(.6366)*(G+SA+SB)
C          CALCULATE (U1 + U2)
S.0114      T=(1.2732)*(((1.+$K(L))*(XI(J)))-CL)
C          CALCULATE (V1 + V2)
S.0115      W=(1.2732)*(-((1.+$K(L))*(ETA(K)))+CM)
S.0116      V=((T*$N)-((W*$S)))/((S*$N)-($L*$S))
S.0117      U=((T*$L)-((W*$M)))/((S*$L)-($N*$M))
S.0118      Q=SQRT((U**2)+(V**2))
C          CALCULATE ALPHA
S.0119      ZC=V/U
S.0120      ALPHAZ=ATAN(ZC)
S.0121      ALPHA=ALPHAZ*57.2958
S.0122      P=($K(L)**2)-(Q**2)
S.0123      WRITE(6,826) XI(J),ETA(K),X,Y,CHI,PSI,U,V,Q,ALPHA,P
S.0124      826  FORMAT('0',11F10.4)
S.0125      1001 CONTINUE
S.0126      1000 CONTINUE
S.0127      1004 CONTINUE
S.0128      1002 STOP 99999
S.0129      END

```


STORAGE MAP VARIABLES (TAGS: C=COMMON, E=EQUIVALENCE)

NAME	TAG	REL ADR	NAME	TAG	REL ADR	NAME	TAG	REL ADR	NAME	TAG	REL ADR
M		000080	N		000084	L		000088	J		00008C
K		000090	R		000094	X		000098	Y		00009C
A		0000A0	B		0000A4	C		0000A8	D		0000AC
E		0000B0	F		0000B4	G		0000B8	H		0000BC
S		0000C0	T		0000C4	W		0000C8	V		0000CC
U		0000D0	Q		0000D4	P		0000D8	XI		0000DC

NAME	TAG	REL ADR	NAME	TAG	REL ADR	NAME	TAG	REL ADR	NAME	TAG	REL ADR
SK		0008AC	CA		0008D4	CB		0008D8	CI		0008DC
DD		0008E0	ZP		0008E4	CC		0008E8	CD		0008EC
CE		0008F0	CF		0008F4	CG		0008F8	CH		0008FC
XC		000900	XA		000904	XB		000908	YA		00090C
YB		000910	YC		000914	FB		000918	ZA		00091C
FA		000920	ZK		000924	CJ		000928	CK		00092C
CL		000930	CM		000934	CN		000938	CO		00093C
ZB		000940	BA		000944	BB		000948	DA		00094C
EA		000950	GG		000954	SI		000958	SL		00095C
SM		000960	SN		000964	SA		000968	SR		00096C
ZC		000970	ETA		000974	ZZZ		001144	CHI		001148
PSI		00114C	CAA		001150	CAB		001154	SLA		001158
SLB		00115C	\$MA		001160	\$MB		001164	\$NA		001168
SNB		00116C	NUMK		001170	BETA		001174	CHIA		001178
CHIB		00117C	CHIC		001180	PSIA		001184	PSIR		001188
THETA		00118C	ALPHA		001190	ALPHAZ		001194			

EXTERNAL REFERENCES

NAME	REL ADR	NAME	REL ADR	NAME	REL ADR
COS	001198	SIN	00119C	SORT	0011A0
ALOG	0011A8				0011A4

CONSTANTS

NAME	REL ADR	NAME	REL ADR	NAME	REL ADR
00000002	00120C	00000001	001210	413243FE	001214
41100000	00121C	41200000	001220	40A2F837	001224
42394889	00122C				41145F06

IMPLIED EXTERNAL REFERENCES

NAME	REL ADR	NAME	REL ADR	NAME	REL ADR
IBCOM#	001484	FRXPI#	0014C8		

STATEMENT NUMBER	REL ADR	STATEMENT NUMBER	REL ADR	STATEMENT NUMBER	REL ADR
00100	001230	01003	001238	00101	001240
00823	001250	00824	0012A0	00825	0012R4
00109	001756	00117	001782	00108	001794
00111	001786	00114	0017D6	00115	0017E4
00118	0018E8	00119	0018F4	00120	0019CC
00129	001A58	00121	001A6A	00124	001A7E
00126	001AAC	00127	001ABA	00128	001AC2
01001	002238	01000	00224C	01004	002260
				00102	001248
				00107	001742
				00112	0017A8
				00116	0017FE
				00123	0019E0
				00125	001A8C
				00826	0012FC
				01002	002274

SIZE OF COMMON 000000 PROGRAM 008856

END OF COMPILATION MAIN

APPENDIX IV

LIST OF ABBREVIATIONS AND SYMBOLS FOR SECTION III

AE/AT	ratio of area at nozzle exit to nozzle throat area
CF,IDEAL	ideal thrust coefficient
CF,VAC	thrust coefficient in vacuum
CP, CAL/(G) (K)	specific heat, calories per gram per degree Kelvin
CSTAR	characteristic exhaust velocity, feet per second
DFPM	tetrafluoroethylene
GAMMA	isentropic exponent, $(\partial \ln P / \partial \ln RHO)_s$
ISP,IDEAL	ideal specific impulse, (lb force) (sec)(lb mass)
ISP*RHO/B	product of ISP,IDEAL and RHO/B
ISP,VAC	specific impulse in vacuum
MACH NUMBER	ratio of velocity to speed of sound
MOL WT	molecular weight of products
O/F	oxidizer to fuel ratio
PRESS.,ATM	atmospheric pressure
PRESS.,PSIA	pressure, pounds per square inch, absolute
RHO/B	bulk density of combustion products
S, CAL/(G) (K)	entropy, calories per gram per degree Kelvin
T, DEG F	temperature, degrees fahrenheit
T, DEG K	temperature, degrees Kelvin

APPENDIX V

THERMOCHEMICAL COMPUTATIONS FOR MAGNESIUM- LAMINAC-SODIUM NITRATE FLARE COMPOSITIONS

	% BY WT.	ENTHALPY KCAL/MOL	STATE	TEMP DEG K	DENSITY G/CC
NANO3	75.00	-111.540	S	298.15	2.261000
MG	20.00	0.0	S	298.15	1.740000
LAMINAC	5.00	-76.200	S	298.15	1.190000

EMPIRICAL FORMULA					
FUEL	NA	1.00000	N	1.00000	O 3.00000
FUEL	MG	1.00000			
FUEL	O	1.77324	C	5.46749	H 5.91080
					O/F= 0.0
					DENSITY= 2.0464

PARAMETERS	CHAMBER	THROAT	EXIT
PRESS., PSIA	14.70	8.49	14.30
PRESS., ATM	1.00	0.58	0.97
T, DEG K	1934	1818	1928
T, DEG F	3022	2813	3011
S, CAL/(G)(K)	1.5953	1.5953	1.5953

MOL WT	48.671	48.819	48.676
CP, CAL/(G)(K)	0.4004	0.4767	0.4029
GAMMA	1.1401	1.1287	1.1397
MACH NUMBER	0.0	1.000	0.217
CSTAR		2974	2974

CF, IDEAL	0.652	0.147
CF, VAC	1.230	2.882
AE/AT	1.00	2.81
ISP, IDEAL	60.3	13.5
ISP*RHOB	123.4	27.7

MOLE FRACTIONS OF PRODUCTS

ClO1(G)	0.00015	0.00007	0.00014
ClO2(G)	0.09487	0.09516	0.09489
H1NA1O1(G)	0.10271	0.10294	0.10271
H1O1(G)	0.00001	0.00000	0.00001
N1O1(G)	0.00257	0.00179	0.00252
N2(G)	0.15206	0.15279	0.15210
NA1(G)	0.15383	0.15361	0.15385
NA1O1(G)	0.04533	0.04250	0.04520
NA1O2(G)	0.00429	0.00789	0.00443
NA2(G)	0.00027	0.00021	0.00027
O1(G)	0.00013	0.00006	0.00013
O2(G)	0.15792	0.15651	0.15789
MG1O1(S)	0.28585	0.28646	0.28586

	% BY WT.	ENTHALPY KCAL/MOL	STATE	TEMP DEG K	DENSITY G/CC
NANO3	70.00	-111.540	S	298.15	2.261000
MG	25.00	0.0	S	298.15	1.740000
LAMINAC	5.00	-76.200	S	298.15	1.190000

EMPIRICAL FORMULA					
FUEL	NA	1.00000	N	1.00000	O 3.00000 O/F= 0.0
FUEL	MG	1.00000			
FUEL	O	1.77324	C	5.46749	H 5.91080 DENSITY= 2.0190

PARAMETERS	CHAMBER	THROAT	EXIT
PRESS., PSIA	14.70	8.56	14.30
PRESS., ATM	1.00	0.58	0.97
T, DEG K	2726	2611	2721
T, DEG F	4448	4240	4437
S, CAL/(G)(K)	1.6342	1.6343	1.6342

MOL WT	51.864	52.216	51.881
CP, CAL/(G)(K)	0.8075	0.7504	0.8047
GAMMA	1.1020	1.1031	1.1020
MACH NUMBER	0.0	1.000	0.219
CSTAR		3460	3460

CF, IDEAL	0.642	0.144
CF, VAC	1.224	2.863
AE/AT	1.00	2.79
ISP, IDEAL	69.0	15.5
ISP*RHOB	139.4	31.3

MOLE FRACTIONS OF PRODUCTS

CI01(G)	0.01933	0.01556	0.01914
CI02(G)	0.07329	0.07740	0.07349
HI(G)	0.00082	0.00060	0.00081
H1NA1(G)	0.00004	0.00002	0.00004
H1NA101(G)	0.07984	0.08199	0.07993
H101(G)	0.00562	0.00462	0.00557
H2(G)	0.00026	0.00020	0.00026
H201(G)	0.00664	0.00643	0.00663
MG1(G)	0.00072	0.00039	0.00070
MG101(G)	0.00074	0.00041	0.00072
N101(G)	0.01037	0.00879	0.01029
N102(G)	0.00001	0.00000	0.00001
N2(G)	0.13431	0.13563	0.13437
NA1(G)	0.18146	0.18284	0.18156
NA101(G)	0.01743	0.01504	0.01730
NA102(G)	0.00003	0.00003	0.00003
NA2(G)	0.00009	0.00006	0.00009
O1(G)	0.01077	0.00859	0.01066
O2(G)	0.11144	0.11262	0.11150
MG101(S)	0.34679	0.34876	0.34689

	% BY WT.	ENTHALPY KCAL/MOL	STATE	TEMP DEG K	DENSITY G/CC
NANO3	65.00	-111.540	S	298.15	2.261000
MG	30.00	0.0	S	298.15	1.740000
LAMINAC	5.00	-76.200	S	298.15	1.190000

EMPIRICAL FORMULA						
FUEL	NA	1.00000	N	1.00000	O 3.00000	O/F= 0.0
FUEL	MG	1.00000				
FUEL	O	1.77324	C	5.46749	H 5.91080	DENSITY= 1.9924

PARAMETERS	CHAMBER	THROAT	EXIT
PRESS.,PSIA	14.70	8.61	14.30
PRESS.,ATM	1.00	0.59	0.97
T, DEG K	3012	2914	3007
T, DEG F	4962	4786	4953
S, CAL/(G)(K)	1.6434	1.6435	1.6435

MOL WT	52.331	52.863	52.356
CP, CAL/(G)(K)	2.1898	2.0511	2.1842
GAMMA	1.0887	1.0876	1.0887
MACH NUMBER	0.0	1.000	0.216
CSTAR		3637	3637

CF,IDEAL	0.637	0.141
CF,VAC	1.222	2.904
AE/AT	1.00	2.84
ISP,IDEAL	72.0	15.9
ISP*RHOB	143.4	31.7

MOLE FRACTIONS OF PRODUCTS

C1O1(G)	0.04511	0.04281	0.04500
C1O2(G)	0.04401	0.04646	0.04412
H1(G)	0.00574	0.00550	0.00573
H1MG1(G)	0.00002	0.00001	0.00002
H1MG1O1(G)	0.00003	0.00002	0.00003
H1NA1(G)	0.00012	0.00009	0.00012
H1NA1O1(G)	0.04441	0.04302	0.04432
H1O1(G)	0.01409	0.01351	0.01407
H2(G)	0.00198	0.00199	0.00198
H2O1(G)	0.01398	0.01520	0.01405
MG1(G)	0.01689	0.01423	0.01677
MG1O1(G)	0.00802	0.00624	0.00793
N1O1(G)	0.01122	0.01001	0.01116
N2(G)	0.11902	0.11985	0.11906
NA1(G)	0.19275	0.19646	0.19295
NA1O1(G)	0.01184	0.01003	0.01174
NA1O2(G)	0.00001	0.00001	0.00001
NA2(G)	0.00008	0.00005	0.00008
O1(G)	0.02425	0.02244	0.02417
O2(G)	0.06931	0.06979	0.06934
MG1O1(S)	0.37712	0.38230	0.37736

	% BY WT.	ENTHALPY KCAL/MOL	STATE	TEMP DEG K	DENSITY G/CC
NANO3	60.00	-111.540	S	298.15	2.261000
MG	35.00	0.0	S	298.15	1.740000
LAMINAC	5.00	-76.200	S	298.15	1.190000

EMPIRICAL FORMULA							
FUEL	NA	1.00000	N	1.00000	O	3.00000	O/F= 0.0
FUEL	MG	1.00000					
FUEL	O	1.77324	C	5.46749	H	5.91080	DENSITY= 1.9664

PARAMETERS	CHAMBER	THROAT	EXIT
PRESS.,PSIA	14.70	8.62	14.30
PRESS.,ATM	1.00	0.59	0.97
T, DEG K	3117	3024	3112
T, DEG F	5152	4983	5143
S, CAL/(G)(K)	1.6432	1.6434	1.6433

MOL WT	51.763	52.383	51.793
CP, CAL/(G)(K)	4.5451	4.4473	4.5413
GAMMA	1.0875	1.0857	1.0874
MACH NUMBER	0.0	1.000	0.221
CSTAR		3719	3719

CF, IDEAL	0.637	0.144
CF, VAC	1.224	2.845
AE/AT	1.00	2.78
ISP, IDEAL	73.6	16.6
ISP*RHOB	144.8	32.7

MOLE FRACTIONS OF PRODUCTS

C101(G)	0.05734	0.05614	0.05728
C102(G)	0.02978	0.03106	0.02985
H1(G)	0.01092	0.01095	0.01092
H1MG1(G)	0.00010	0.00007	0.00010
H1MG101(G)	0.00009	0.00007	0.00009
H1NA1(G)	0.00016	0.00013	0.00016
H1NA101(G)	0.02916	0.02721	0.02906
H101(G)	0.01585	0.01543	0.01583
H2(G)	0.00390	0.00403	0.00391
H201(G)	0.01505	0.01618	0.01510
MG1(G)	0.05682	0.05319	0.05664
MG101(G)	0.01730	0.01463	0.01715
N1(G)	0.00001	0.00001	0.00001
N101(G)	0.00921	0.00829	0.00916
N2(G)	0.10787	0.10843	0.10789
NA1(G)	0.18731	0.19086	0.18749
NA101(G)	0.00819	0.00687	0.00812
NA2(G)	0.00007	0.00004	0.00006
O1(G)	0.02605	0.02488	0.02600
O2(G)	0.04049	0.04043	0.04049
MG101(S)	0.38433	0.39107	0.38467

	% BY WT.	ENTHALPY KCAL/MOL	STATE	TEMP DEG K	DENSITY G/CC
NANO3	57.50	-111.540	S	298.15	2.261000
MG	37.50	0.0	S	298.15	1.740000
LAMINAC	5.00	-76.200	S	298.15	1.190000

EMPIRICAL FORMULA					
FUEL	NA	1.00000	N	1.00000	O/F= 0.0
FUEL	MG	1.00000			
FUEL	O	1.77324	C	5.46749	DENSITY= 1.9537

PARAMETERS	CHAMBER	THR/AT	EXIT
PRESS., PSIA	14.70	3.63	14.30
PRESS., ATM	1.00	0.59	0.97
T, DEG K	3142	3049	3137
T, DEG F	5195	5028	5186
S, CAL/(G)(K)	1.6412	1.6413	1.6413

MOL WT	51.284	51.929	51.311
CP, CAL/(G)(K)	5.5129	5.4590	5.5124
GAMMA	1.0880	1.0861	1.0879
MACH NUMBER	0.0	1.000	0.217
CSTAR		3749	3749

CF, IDEAL	0.637	0.141
CF, VAC	1.224	2.901
AE/AT	1.00	2.84
ISP, IDEAL	74.2	16.4
ISP*RM708	145.0	32.1

MOLE FRACTIONS OF PRODUCTS

ClO1(G)	0.06126	0.06035	0.06121
ClO2(G)	0.02509	0.02608	0.02514
H1(G)	0.01313	0.01325	0.01314
H1MG1(G)	0.00017	0.00012	0.00017
H1MG1O1(G)	0.00012	0.00009	0.00012
H1NA1(G)	0.00018	0.00014	0.00018
H1NA1O1(G)	0.02451	0.02263	0.02441
H1O1(G)	0.01537	0.01495	0.01536
H2(G)	0.00491	0.00508	0.00492
H2O1(G)	0.01503	0.01605	0.01508
MG1(G)	0.08217	0.07843	0.08200
MG1O1(G)	0.02055	0.01763	0.02040
N1(G)	0.00001	0.00001	0.00001
N1O1(G)	0.00791	0.00711	0.00787
N2(G)	0.10288	0.10337	0.10291
NA1(G)	0.18217	0.18542	0.18234
NA1O1(G)	0.00670	0.00559	0.00664
NA2(G)	0.00006	0.00004	0.00006
O1(G)	0.02407	0.02305	0.02403
O2(G)	0.02964	0.02941	0.02964
MG1O1(S)	0.38406	0.39120	0.38438

	% BY WT.	ENTHALPY KCAL/MOL	STATE	TEMP DEG K	DENSITY G/CC
MG	45.00	0.0	S	298.15	1.740000
NANO3	50.00	-111.540	S	298.15	2.261000
LAMINAC	5.00	-76.200	S	298.15	1.190000

EMPIRICAL FORMULA						
FUEL	MG	1.00000				O/F= 0.0
FUEL	NA	1.00000	N	1.00000	O	3.00000
FUEL	O	1.77324	C	5.46749	H	5.91080
						DENSITY= 1.9165

PARAMETERS	CHAMBER	THROAT	EXIT
PRESS., PSIA	14.70	8.61	14.30
PRESS., ATM	1.00	0.59	0.97
T, DEG K	3147	3053	3142
T, DEG F	5205	5035	5196
S, CAL/(G)(K)	1.6294	1.6295	1.6295
MOL WT	49.342	50.024	49.374
CP, CAL/(G)(K)	4.5349	4.4041	4.5302
GAMMA	1.0912	1.0893	1.0911
MACH NUMBER	0.0	1.000	0.219
CSTAR		3823	3823
CF, IDEAL		0.638	0.143
CF, VAC		1.224	2.872
AE/AT		1.00	2.80
ISP, IDEAL		75.8	17.0
ISP*RHOB		145.3	32.5

MOLE FRACTIONS OF PRODUCTS

ClO1(G)	0.06988	0.06965	0.06987
ClO2(G)	0.01429	0.01462	0.01431
H1(G)	0.01831	0.01851	0.01832
H1MG1(G)	0.00048	0.00036	0.00047
H1MG1O1(G)	0.00017	0.00013	0.00017
H1NA1(G)	0.00022	0.00017	0.00022
H1NA1O1(G)	0.01477	0.01329	0.01470
H1O1(G)	0.01076	0.01019	0.01073
H2(G)	0.00915	0.00956	0.00917
H2O1(G)	0.01400	0.01467	0.01403
MG1(G)	0.17150	0.16759	0.17131
MG1O1(G)	0.02161	0.01842	0.02144
N1(G)	0.00001	0.00001	0.00001
N1O1(G)	0.00378	0.00329	0.00375
N2(G)	0.08867	0.08901	0.08869
NA1(G)	0.16300	0.16534	0.16312
NA1O1(G)	0.00304	0.00245	0.00300
NA2(G)	0.00005	0.00003	0.00005
O1(G)	0.01260	0.01166	0.01255
O2(G)	0.00775	0.00723	0.00773
MG1O1(S)	0.37598	0.38384	0.37636

	% BY WT.	ENTHALPY KCAL/MOL	STATE	TEMP DEG K	DENSITY G/CC
MG	50.00	0.0	S	298.15	1.740000
NANO3	45.00	-111.540	S	298.15	2.261000
LAMINAC	5.00	-76.200	S	298.15	1.190000

EMPIRICAL FORMULA

FUEL	MG	1.00000					O/F= 0.0
FUEL	NA	1.00000	N	1.00000	O	3.00000	
FUEL	O	1.77324	C	5.46749	H	5.91080	DENSITY= 1.8925

PARAMETERS	CHAMBER	THROAT	EXIT
PRESS., PSIA	14.70	8.59	14.30
PRESS., ATM	1.00	0.58	0.97
T, DEG K	3080	2979	3075
T, DEG F	5085	4902	5075
S, CAL/(G)(K)	1.6167	1.6168	1.6167

MOL WT	47.589	48.227	47.619
CP, CAL/(G)(K)	2.1481	1.9338	2.1387
GAMMA	1.0963	1.0952	1.0963
MACH NUMBER	0.0	1.000	0.218
CSTAR		3844	3844

CF, IDEAL	0.640	0.143
CF, VAC	1.224	2.879
AE/AT	1.00	2.81
ISP, IDEAL	76.5	17.1
ISP*RHOB	144.8	32.3

MOLE FRACTIONS OF PRODUCTS

ClO1(G)	0.07472	0.07509	0.07473
ClO2(G)	0.00773	0.00743	0.00772
H1(G)	0.01964	0.01954	0.01964
H1MG1(G)	0.00083	0.00064	0.00082
H1MG1O1(G)	0.00015	0.00010	0.00014
H1NA1(G)	0.00025	0.00020	0.00025
H1NA1O1(G)	0.00931	0.00800	0.00924
H1O1(G)	0.00548	0.00470	0.00544
H2(G)	0.01518	0.01638	0.01523
H2O1(G)	0.01156	0.01164	0.01157
MG1(G)	0.23927	0.23525	0.23908
MG1O1(G)	0.01361	0.01066	0.01346
N1(G)	0.00001	0.00000	0.00001
N1O1(G)	0.00135	0.00104	0.00133
N2(G)	0.07916	0.07939	0.07917
NA1(G)	0.14886	0.15072	0.14895
NA1O1(G)	0.00117	0.00085	0.00116
NA2(G)	0.00004	0.00003	0.00004
O1(G)	0.00418	0.00334	0.00414
O2(G)	0.00128	0.00096	0.00127
MG1O1(S)	0.36622	0.37402	0.36660

	% BY WT.	ENTHALPY KCAL/MOL	STATE	TEMP DEG K	DENSITY G/CC
MG	55.00	0.0	S	298.15	1.740000
NANO3	40.00	-111.540	S	298.15	2.261000
LAMINAC	5.00	-76.200	S	298.15	1.190000

EMPIRICAL FORMULA						
FUEL	MG	1.00000				O/F= 0.0
FUEL	NA	1.00000	N	1.00000	O	3.00000
FUEL	O	1.77324	C	5.46749	H	5.91080
						DENSITY= 1.8691

PARAMETERS	CHAMBER	THROAT	EXIT
PRESS., PSIA	14.70	8.50	14.30
PRESS., ATM	1.00	0.58	0.97
T, DEG K	2849	2704	2842
T, DEG F	4668	4407	4655
S, CAL/(G)(K)	1.5975	1.5975	1.5975

MOL WT	45.079	45.463	45.099
CP, CAL/(G)(K)	0.6763	0.5586	0.6702
GAMMA	1.1217	1.1281	1.1219
MACH NUMBER	0.0	1.000	0.219
CSTAR		3757	3757

CF, IDEAL	0.652	0.146
CF, VAC	1.230	2.874
AE/AT	1.00	2.80
ISP, IDEAL	76.1	17.1
ISP*RHOB	142.3	32.0

MOLE FRACTIONS OF PRODUCTS

ClO1(G)	0.07870	0.07932	0.07873
ClO2(G)	0.00158	0.00102	0.00155
H1(G)	0.01348	0.01111	0.01338
H1MG1(G)	0.00141	0.00108	0.00139
H1MG1O1(G)	0.00004	0.00002	0.00004
H1NA1(G)	0.00030	0.00023	0.00030
H1NA1O1(G)	0.00291	0.00179	0.00285
H1O1(G)	0.00057	0.00025	0.00055
H2(G)	0.02989	0.03337	0.03005
H2O1(G)	0.00416	0.00282	0.00409
MG1(G)	0.31195	0.30893	0.31179
MG1O1(G)	0.00222	0.00102	0.00215
N1O1(G)	0.00008	0.00003	0.00008
N2(G)	0.06906	0.06913	0.06907
NA1(G)	0.13481	0.13617	0.13488
NA1O1(G)	0.00010	0.00004	0.00010
NA2(G)	0.00004	0.00003	0.00004
O1(G)	0.00016	0.00005	0.00015
O2(G)	0.00001	0.00000	0.00001
MG1O1(S)	0.34853	0.35358	0.34880

	X BY WT.	ENTHALPY KCAL/MOL	STATE	TEMP DEG K	DENSITY G/CC
MG	59.00	0.0	S	298.15	1.740000
NANO3	36.00	-111.540	S	298.15	2.261000
LAMINAC	5.00	-76.200	S	298.15	1.190000

EMPIRICAL FORMULA

FUEL	MG	1.00000			
FUEL	NA	1.00000	N	1.00000	O 3.00000
FUEL	O	1.77324	C	5.46749	H 5.91080

O/F= 0.0

DENSITY= 1.8508

PARAMETERS

	CHAMBER	THROAT	EXIT
PRESS., PSIA	14.70	8.30	14.30
PRESS., ATM	1.00	0.57	0.97
T, DEG K	2284	2082	2275
T, DEG F	3652	3289	3635
S, CAL/(G)(K)	1.5692	1.5692	1.5692
MOL WT	41.739	41.756	41.740
CP, CAL/(G)(K)	0.3028	0.2936	0.3021
GAMMA	1.1916	1.1967	1.1919
MACH NUMBER	0.0	1.000	0.211
CSTAR		3418	3418
CF, IDEAL		0.676	0.149
CF, VAC		1.241	2.949
AE/AT		1.00	2.88
ISP, IDEAL		71.8	15.8
ISP*RHOB		133.0	29.3

MOLE FRACTIONS OF PRODUCTS

CIHIN1(G)	0.00001	0.00005	0.00002
CI01(G)	0.07850	0.07848	0.07850
CI02(G)	0.00001	0.00000	0.00001
H1(G)	0.00149	0.00063	0.00143
H1MG1(G)	0.00159	0.00109	0.00157
H1NA1(G)	0.00026	0.00018	0.00025
H1NA101(G)	0.00005	0.00001	0.00005
H2(G)	0.04070	0.04147	0.04075
H201(G)	0.00004	0.00001	0.00003
MG1(G)	0.38343	0.38386	0.38345
MG101(G)	0.00001	0.00000	0.00000
N2(G)	0.06082	0.06081	0.06082
NA1(G)	0.12119	0.12135	0.12120
NA2(G)	0.00008	0.00007	0.00008
MG101(S)	0.31182	0.31200	0.31183

	% BY WT.	ENTHALPY KCAL/MOL	STATE	TEMP DEG K	DENSITY G/CC
MG	60.00	0.0	S	298.15	1.740000
NaNO3	35.00	-111.540	S	298.15	2.261000
LANINAC	5.00	-76.200	S	298.15	1.190000

EMPIRICAL FORMULA

FUEL	MG	1.00000			
FUEL	NA	1.00000	N	1.00000	O 3.00000
FUEL	O	1.77324	C	5.46749	H 5.91080

O/F= 0.0 DENSITY= 1.8462

PARAMETERS

	CHAMBER	THROAT	EXIT
PRESS., PSIA	14.70	8.69	14.30
PRESS., ATM	1.00	0.59	0.97
T, DEG K	2087	1914	2077
T, DEG F	3296	2986	3279
S, CAL/(G)(K)	1.5577	1.5577	1.5577
MOL WT	40.789	40.845	40.789
CP, CAL/(G)(K)	0.2956	0.3298	0.2960
GAMMA	1.2028	1.1942	1.2028
MACH NUMBER	0.0	0.959	0.212
CSTAR		3305	3305
CF, IDEAL		0.649	0.150
CF, VAC		1.241	2.926
AE/AT		1.00	2.85
ISP, IDEAL		66.7	15.4
ISP*RMOB		123.2	28.5

MOLE FRACTIONS OF PRODUCTS

CH4N1(G)	0.00016	0.00067	0.00017
ClO1(G)	0.07788	0.07737	0.07787
C2H2(G)	0.00000	0.00002	0.00000
H1(G)	0.00048	0.00019	0.00046
H1MG1(G)	0.00150	0.00104	0.00148
H1NA1(G)	0.00023	0.00016	0.00022
H1NA1O1(G)	0.00001	0.00000	0.00001
H2(G)	0.04099	0.04115	0.04101
MG1(G)	0.40275	0.40282	0.40277
N2(G)	0.05870	0.05847	0.05869
NA1(G)	0.11710	0.11724	0.11711
NA2(G)	0.00011	0.00010	0.00011
MG1O1(S)	0.30008	0.30076	0.30009

	% BY WT.	ENTHALPY KCAL/MOL	STATE	TEMP DEG K	DENSITY G/CC
MG	63.00	0.0	S	298.15	1.740000
NANO3	32.00	-111.540	S	298.15	2.261000
LAMINAC	5.00	-76.200	S	298.15	1.190000

EMPIRICAL FORMULA

FUEL	MG	1.00000			
FUEL	NA	1.00000	N	1.00000	O 3.00000
FUEL	O	1.77324	C	5.46749	H 5.91080

O/F= 0.0

DENSITY= 1.8328

PARAMETERS

	CHAMBER	THROAT	EXIT
PRESS., PSIA	14.70	8.60	14.30
PRESS., ATM	1.00	0.59	0.97
T, DEG K	1948	1889	1945
T, DEG F	3046	2940	3041
S, CAL/(G)(K)	1.5141	1.5141	1.5141
MOL WT	41.023	41.772	41.062
CP, CAL/(G)(K)	6.3885	5.9598	6.3622
GAMMA	1.1018	1.0992	1.1017
MACH NUMBER	0.0	1.000	0.224
CSTAR		3278	3278
CF, IDEAL		0.643	0.148
CF, VAC		1.229	2.819
AE/AT		1.00	2.75
ISP, IDEAL		65.6	15.0
ISP*RMOR		120.1	27.6

MOLE FRACTIONS OF PRODUCTS

CHIN1(G)	0.00077	0.00060	0.00076
CI01(G)	0.04984	0.04358	0.04951
C2H2(G)	0.00002	0.00002	0.00002
H1(G)	0.00019	0.00016	0.00018
H1MG1(G)	0.00149	0.00109	0.00146
H1NA1(G)	0.00019	0.00014	0.00019
H2(G)	0.04005	0.04036	0.04006
MG1(G)	0.43275	0.42672	0.43243
N2(G)	0.05234	0.05240	0.05234
NA1(G)	0.10500	0.10508	0.10501
NA2(G)	0.00013	0.00009	0.00012
MG101(S)	0.29133	0.29745	0.29165
CI(S)	0.02591	0.03232	0.02625

	% BY WT.	ENTHALPY KCAL/MOL	STATE	TEMP DEG K	DENSITY G/CC
MG	64.00	0.0	S	298.15	1.740000
NANO3	31.00	-111.540	S	298.15	2.261000
LAMINAC	5.00	-76.200	S	298.15	1.190000

EMPIRICAL FORMULA					
FUEL	MG	1.00000			
FUEL	NA	1.00000	N	1.00000	O 3.00000
FUEL	O	1.77324	C	5.46749	H 5.91080

O/F= 0.0

DENSITY= 1.8284

PARAMETERS

	CHAMBER	THROAT	EXIT
PRESS., PSIA	14.70	8.59	14.30
PRESS., ATM	1.00	0.58	0.97
T, DEG K	1937	1877	1934
T, DEG F	3027	2919	3022
S, CAL/(G)(K)	1.4991	1.4991	1.4991
MOL WT	41.331	42.068	41.348
CP, CAL/(G)(K)	4.9324	4.3912	4.9060
GAMMA	1.1024	1.1001	1.1023
MACH NUMBER	0.0	1.000	0.228
CSTAR		3259	3259
CF, IDEAL		0.643	0.147
CF, VAC		1.228	2.832
AE/AT		1.00	2.76
ISP, IDEAL		65.1	14.9
ISP*RMQB		119.1	27.2

MOLE FRACTIONS OF PRODUCTS

CH4N1(G)	0.00072	0.00056	0.00071
ClO1(G)	0.03882	0.03279	0.03851
C2H2(G)	0.00002	0.00001	0.00002
H1(G)	0.00017	0.00014	0.00017
H1MG1(G)	0.00151	0.00111	0.00148
H1NA1(G)	0.00018	0.00014	0.00018
H2(G)	0.03980	0.04011	0.03982
MG1(G)	0.44044	0.43464	0.44014
N2(G)	0.05038	0.05044	0.05038
NA1(G)	0.10106	0.10113	0.10106
NA2(G)	0.00012	0.00009	0.00012
MG1O1(S)	0.29029	0.29619	0.29059
Cl(S)	0.03648	0.04266	0.03680

	% BY WT.	ENTHALPY KCAL/MOL	STATE	TEMP DEG K	DENSITY G/CC
MG	65.00	0.0	S	298.15	1.740000
NAND3	30.00	-111.540	S	298.15	2.261000
LAMINAC	5.00	-76.200	S	298.15	1.190000

EMPIRICAL FORMULA

FUEL	MG	1.00000			
FUEL	NA	1.00000	N	1.00000	O 3.00000
FUEL	O	1.77324	C	5.46749	H 5.91080

O/F= C.0

DENSITY= 1.8239

PARAMETERS

	CHAMBER	THROAT	EXIT
PRESS., PSIA	14.70	8.59	14.30
PRESS., ATM	1.00	0.58	0.97
T, DEG K	1923	1861	1920
T, DEG F	3002	2890	2996
S, CAL/(G)(K)	1.4838	1.4838	1.4838
MOL WT	41.619	42.337	41.655
CP, CAL/(G)(K)	3.5903	3.0433	3.5632
GAMMA	1.1036	1.1019	1.1035
MACH NUMBER	0.0	1.000	0.222
CSTAR		3234	3234
CF, IDEAL		0.644	0.147
CF, VAC		1.228	2.834
AE/AT		1.00	2.76
ISP, IDEAL		64.7	14.8
ISP*RHOB		118.0	26.9

MOLE FRACTIONS OF PRODUCTS

CH4N1(G)	0.00066	0.00051	0.00066
CO1(G)	0.02814	0.02238	0.02784
C2H2(G)	0.00002	0.00001	0.00002
H1(G)	0.00015	0.00012	0.00015
H1MG1(G)	0.00153	0.00112	0.00150
H1NA1(G)	0.00017	0.00013	0.00017
H2(G)	0.03957	0.03988	0.03959
MG1(G)	0.44824	0.44271	0.44795
N2(G)	0.04845	0.04851	0.04845
NA1(G)	0.09716	0.09723	0.09716
NA2(G)	0.00012	0.00008	0.00012
MG1O1(S)	0.28907	0.29470	0.28936
Cl(S)	0.04672	0.05262	0.04703

	% BY WT.	ENTHALPY KCAL/MOL	STATE	TEMP DEG K	DENSITY G/CC
MG	68.00	0.0	S	298.15	1.740000
NANO3	27.00	-111.540	S	298.15	2.261000
LAMINAC	5.00	-76.200	S	298.15	1.190000

EMPIRICAL FORMULA

FUEL	MG	1.00000			
FUEL	NA	1.00000	N	1.00000	O 3.00000
FUEL	O	1.77324	C	5.46749	H 5.91080

O/F= 0.0 DENSITY= 1.8108

PARAMETERS

	CHAMBER	THROAT	EXIT
PRESS., PSIA	14.70	8.29	14.30
PRESS., ATM	1.00	0.56	0.97
T, DEG K	1537	1409	1531
T, DEG F	2306	2077	2296
S, CAL/(G)(K)	1.4112	1.4112	1.4112
MOL WT	41.931	42.063	41.943
CP, CAL/(G)(K)	0.3983	0.2930	0.3898
GAMMA	1.1697	1.1995	1.1713
MACH NUMBER	0.0	1.000	0.217
CSTAR		2803	2803
CF, IDEAL		0.677	0.152
CF, VAC		1.241	2.894
AE/AT		1.00	2.82
ISP, IDEAL		58.9	13.2
ISP*RHOB		106.7	23.9

MOLE FRACTIONS OF PRODUCTS

CIH1N1(G)	0.01714	0.01564	0.01708
CIH4(G)	0.00003	0.00006	0.00003
CI01(G)	0.00122	0.00012	0.00112
C2H2(G)	0.03060	0.03194	0.03068
C2H4(G)	0.00003	0.00006	0.00003
C2N2(G)	0.00011	0.00007	0.00011
H1MG1(G)	0.00038	0.00022	0.00037
H1NA1(G)	0.00004	0.00002	0.00004
H2(G)	0.00367	0.00310	0.00363
MG1(G)	0.51350	0.51309	0.51345
N2(G)	0.03773	0.03856	0.03776
NA1(G)	0.09205	0.09216	0.09206
NA2(G)	0.00037	0.00037	0.00036
MG101(S)	0.30314	0.30457	0.30327

	Z BY WT.	ENTHALPY KCAL/MOL	STATE	TEMP DEG K	DENSITY G/CC
MG	20.00	0.0	S	298.15	1.740000
LAMINAC	5.00	-76.200	S	298.15	1.190000
NANO3	75.00	-111.540	S	298.15	2.261000

EMPIRICAL FORMULA

FUEL	MG	1.00000			
FUEL	C	5.46749	H	5.91080	O 1.77324
FUEL	O	3.00000	NA	1.00000	N 1.00000

O/F= 0.0 DENSITY= 2.0464

PARAMETERS

	CHAMBER	THRJET	EXIT
PRESS., PSIA	0.39	0.22	0.20
PRESS., ATM	0.03	0.02	0.01
T, DEG K	1859	1728	1703
T, DEG F	2886	2650	2605
S, CAL/(G)(K)	1.7461	1.7462	1.7462
MOL WT	47.217	47.279	47.293
CP, CAL/(G)(K)	0.3446	0.3380	0.3412
GAMMA	1.1520	1.1549	1.1543
MACH NUMBER	0.0	1.000	1.101
CSTAR		2938	2938
CF, IDEAL		0.662	0.722
CF, VAC		1.234	1.230
AE/AT		1.00	1.01
ISP, IDEAL		60.4	66.0
ISP, NON		123.6	135.0

MOLE FRACTIONS OF PRODUCTS

C101(G)	0.00042	0.00014	0.00011
C102(G)	0.09255	0.09292	0.09298
H1NA101(G)	0.09999	0.10048	0.10054
H101(G)	0.00010	0.00003	0.00002
H201(G)	0.00021	0.00006	0.00004
N101(G)	0.00213	0.00137	0.00125
N2(G)	0.14898	0.14951	0.14960
NA1(G)	0.19885	0.18835	0.19820
NA101(G)	0.01091	0.01073	0.01072
NA102(G)	0.00032	0.00080	0.00098
NA2(G)	0.00001	0.00001	0.00001
O1(G)	0.00045	0.00017	0.00014
O2(G)	0.17537	0.17547	0.17539
MG101(S)	0.27969	0.27996	0.28002

	% BY WT.	ENTHALPY KCAL/MOL	STATE	TEMP DEG K	DENSITY G/CC
MG	25.00	0.0	S	298.15	1.740000
LAMINAC	5.00	-76.200	S	298.15	1.190000
NAND3	70.00	-111.540	S	298.15	2.261000

EMPIRICAL FORMULA						
FUEL	MG	1.00000				O/F= 0.0
FUEL	C	5.46749	H	5.91080	O	1.77324
FUEL	O	3.00000	NA	1.00000	N	1.00000
						DENSITY= 2.0190

PARAMETERS	CHAMBER	THROAT	EXIT
PRESS., PSIA	0.39	0.23	0.20
PRESS., ATM	0.03	0.02	0.01
T, DEG K	2408	2323	2302
T, DEG F	3874	3721	3684
S, CAL/(G)(K)	1.7781	1.7782	1.7781

MOL WT	48.581	49.055	49.171
CP, CAL/(G)(K)	1.2826	1.1535	1.1250
GAMMA	1.0926	1.0939	1.0943
MACH NUMBER	0.0	1.001	1.121
CSTAR		3364	3364

CF, IDEAL	0.641	0.713
CF, VAC	1.225	1.232
AE/AT	1.00	1.01
ISP, IDEAL	67.0	74.6
ISP*RHOR	135.3	150.6
ISP, VAC	128.1	128.9

MOLE FRACTIONS OF PRODUCTS

C1O1(G)	0.02122	0.01766	0.01679
C1O2(G)	0.06766	0.07167	0.07266
H1(G)	0.00272	0.00215	0.00202
H1NA1(G)	0.00001	0.00001	0.00001
H1NA1O1(G)	0.04128	0.04255	0.04299
H1O1(G)	0.00969	0.00838	0.00805
H2(G)	0.00108	0.00092	0.00088
H2O1(G)	0.02011	0.02082	0.02094
MG1(G)	0.00246	0.00145	0.00126
MG1O1(G)	0.00093	0.00054	0.00047
VO1(G)	0.00635	0.00541	0.00520
N2(G)	0.13070	0.13184	0.13213
NA1(G)	0.22146	0.22229	0.22237
NA1O1(G)	0.00496	0.00423	0.00407
NA2(G)	0.00001	0.00000	0.00000
NI(G)	0.01574	0.01288	0.01221
O2(G)	0.12291	0.12327	0.12336
MG1O1(S)	0.33040	0.33390	0.33460

	% BY WT.	ENTHALPY KCAL/MOL	STATE	TEMP DEG K	DENSITY G/CC
MG	30.00	0.0	S	298.15	1.740000
LAMINAC	5.00	-76.200	S	298.15	1.190000
NANO3	65.00	-111.540	S	298.15	2.261000

EMPIRICAL FORMULA						
FUEL	MG	1.00000				O/F= 0.0
FUEL	C	5.46749	H	5.91080	O	1.77324
FUEL	O	3.00000	NA	1.00000	N	1.00000
						DENSITY= 1.9924

PARAMETERS	CHAMPER	THROAT	EXIT
PRESS., PSIA	0.39	0.23	0.20
PRESS., ATM	0.03	0.02	0.01
T, DEG K	2577	2509	2492
T, DEG F	4179	4057	4025
S, CAL/(G)(K)	1.7870	1.7871	1.7870

MOL WT.	48.467	49.071	49.230
CP, CAL/(G)(K)	4.0053	3.7455	3.6756
GAMMA	1.0806	1.0793	1.0790
MACH NUMER	0.0	1.000	1.127
CSTAR		3498	3498

CF, IDEAL	0.635	0.712
CF, VAC	1.224	1.232
AF/AT	1.00	1.01
ISP, IDEAL	69.1	77.4
ISP, PROP	137.4	154.2

MOLE FRACTIONS OF PRODUCTS

C1O1(G)	0.04135	0.03964	0.03917
C1O2(G)	0.04461	0.04658	0.04711
H1(G)	0.00969	0.00940	0.00932
H1MG1(G)	0.00001	0.00000	0.00000
H1MG1O1(G)	0.00001	0.00001	0.00001
H1NA1(G)	0.00002	0.00002	0.00002
H1NA1O1(G)	0.01874	0.01750	0.01719
H1O1(G)	0.01533	0.01461	0.01442
H2(G)	0.00316	0.00316	0.00315
H2O1(G)	0.02141	0.02268	0.02301
MG1(G)	0.03038	0.02670	0.02575
MG1O1(G)	0.00622	0.00498	0.00468
N1O1(G)	0.00664	0.00592	0.00575
N2(G)	0.11691	0.11762	0.11781
NA1(G)	0.21826	0.22080	0.22144
NA1O1(G)	0.00341	0.00284	0.00271
O1(G)	0.02955	0.02763	0.02712
O2(G)	0.08305	0.08258	0.08244
MG1O1(S)	0.35125	0.35733	0.35889

	BY WT.	ENTHALPY KCAL/MOL	STATE	TEMP DEG K	DENSITY G/CC
MG	35.00	0.0	S	298.15	1.740000
LAMINAC	5.00	-76.200	S	298.15	1.190000
NANO3	60.00	-111.540	S	298.15	2.261000

EMPIRICAL FORMULA						O/F= 0.0
FUEL	MG	1.00000				
FUEL	C	5.46749	H	5.91080	O	1.77324
FUEL	O	3.00000	NA	1.00000	N	1.00000

DENSITY= 1.9664

PARAMETERS	CHAMBER	THROAT	EXIT
PRESS., PSIA	0.39	0.23	0.20
PRESS., ATM	0.03	0.02	0.01
T, DEG K	2636	2570	2554
T, DEG F	4285	4167	4137
S, CAL/(G)(K)	1.7887	1.7887	1.7887
MOL WT	47.846	48.501	48.669
CP, CAL/(G)(K)	8.0337	7.8593	7.8132
GAMMA	1.0800	1.0784	1.0780
MACH NUMBER	0.0	1.001	1.126
CSTAR		3560	3560
CF, IDEAL		0.636	0.712
CF, VAC		1.224	1.232
AE/AT		1.00	1.02
ISP, IDEAL		70.4	78.7
ISP, RHOA		138.4	154.8

MOLE FRACTIONS OF PRODUCTS

C101(G)	0.05080	0.04983	0.04957
C102(G)	0.03341	0.03481	0.03512
H1(G)	0.01485	0.01486	0.01485
H1MG1(G)	0.00002	0.00002	0.00001
H1MG101(G)	0.00002	0.00001	0.00001
H1NA1(G)	0.00003	0.00002	0.00002
H1NA101(G)	0.01203	0.01089	0.01061
H101(G)	0.01570	0.01507	0.01491
H2(G)	0.00462	0.00470	0.00472
H201(G)	0.01969	0.02061	0.02084
MG1(G)	0.07834	0.07416	0.07309
MG101(G)	0.01140	0.00965	0.00925
N101(G)	0.00566	0.00507	0.00493
N2(G)	0.10616	0.10673	0.10688
NA1(G)	0.20346	0.20559	0.20611
NA101(G)	0.00245	0.00202	0.00192
O1(G)	0.03138	0.02992	0.02955
O2(G)	0.05516	0.05433	0.05411
MG101(S)	0.35462	0.36169	0.36347

	% BY WT.	ENTHALPY KCAL/MOL	STATE	TEMP DEG K	DENSITY G/CC
MG	40.00	0.0	S	298.15	1.740000
LAMINAC	5.00	-76.200	S	298.15	1.190000
NAND3	55.00	-111.540	S	298.15	2.261000

EMPIRICAL FORMULA

FUEL	MG	1.00000					O/F= 0.0
FUEL	C	5.46749	H	5.91080	N	1.77324	
FUEL	O	3.00000	NA	1.00000	N	1.00000	DENSITY= 1.9412

PARAMETERS	CHAMBER	THROAT	EXIT
PRESS., PSIA	0.39	0.23	0.20
PRESS., ATM	0.03	0.02	0.01
T, DEG K	2659	2594	2577
T, DEG F	4327	4209	4179
S, CAL/(G)(K)	1.7864	1.7864	1.7864

MOL WT	47.013	47.685	47.860
CP, CAL/(G)(K)	10.5922	10.4788	10.4483
GAMMA	1.0808	1.0791	1.0787
MACH NUMBER	0.0	1.001	1.126
CSTAR		3604	3604

CF, IDEAL	0.636	0.712
CF, VAC	1.275	1.233
AE/AT	1.00	1.02
ISP, IDEAL	71.3	79.8
ISPRHON	138.4	154.0

MOLE FRACTIONS OF PRODUCTS

ClO1(G)	0.05690	0.05630	0.05615
ClO2(G)	0.02635	0.02716	0.02737
H1(G)	0.01864	0.01878	0.01881
H1MG1(G)	0.00004	0.00003	0.00003
H1MG1O1(G)	0.00003	0.00002	0.00002
H1NA1(G)	0.00003	0.00002	0.00002
H1NA1O1(G)	0.00856	0.00765	0.00743
H1O1(G)	0.01425	0.01362	0.01346
H2(G)	0.00605	0.00618	0.00621
H2O1(G)	0.01818	0.01887	0.01905
MG1(G)	0.13411	0.12991	0.12883
MG1O1(G)	0.01444	0.01240	0.01191
N1O1(G)	0.00437	0.00390	0.00378
N2(G)	0.09634	0.09683	0.09695
NA1(G)	0.18674	0.18846	0.18889
NA1O1(G)	0.00172	0.00141	0.00133
O1(G)	0.02724	0.02592	0.02559
O2(G)	0.03376	0.03276	0.03250
MG1O1(S)	0.35225	0.35978	0.36168

	% BY WT.	ENTHALPY KCAL/MOL	STATE	TEMP DEG K	DENSITY G/CC
MG	45.00	0.0	S	298.15	1.740000
NAO3	50.00	-111.540	S	298.15	2.261000
LAMINAC	5.00	-76.200	S	298.15	1.190000

EMPIRICAL FORMULA						
FUEL	MG	1.00000				O/F= 0.0
FUEL	NA	1.00000	N	1.00000	O	3.00000
FUEL	O	1.77324	C	5.46749	H	5.91080
						DENSITY= 1.9165

PARAMETERS	CHAMBER	THROAT	EXIT
PRESS., PSIA	0.39	0.23	0.20
PRESS., ATM	0.03	0.02	0.01
T, DEG K	2661	2595	2578
T, DEG F	4331	4211	4181
S, CAL/(G)(K)	1.7811	1.7812	1.7811

MOL WT	46.047	46.723	46.899
CP, CAL/(G)(K)	9.2101	8.9600	8.8892
GAMMA	1.0821	1.0804	1.0800
MACH NUMBER	0.0	1.000	1.126
CSTAR		3646	3646

CF, IDEAL	0.636	0.712
CF, VAC	1.224	1.232
AE/AT	1.00	1.01
ISP, IDEAL	72.1	80.7
ISP*RHOB	138.1	154.6

MOLE FRACTIONS OF PRODUCTS

ClO1(G)	0.06195	0.06170	0.06164
ClO2(G)	0.02024	0.02070	0.02082
HI(G)	0.02154	0.02173	0.02177
HIMG1(G)	0.00007	0.00005	0.00005
HIMG1O1(G)	0.00003	0.00002	0.00002
HINA1(G)	0.00003	0.00002	0.00002
HINA1O1(G)	0.00622	0.00550	0.00532
H1O1(G)	0.01164	0.01098	0.01080
H2(G)	0.00790	0.00812	0.00818
H2O1(G)	0.01676	0.01727	0.01739
MG1(G)	0.19427	0.19007	0.18897
MG1O1(G)	0.01482	0.01265	0.01214
N1O1(G)	0.00298	0.00260	0.00251
N2(G)	0.08694	0.08735	0.08745
NA1(G)	0.16949	0.17088	0.17123
NA1O1(G)	0.00111	0.00089	0.00084
O1(G)	0.01969	0.01838	0.01804
O2(G)	0.01722	0.01617	0.01588
MG1O1(S)	0.34709	0.35491	0.35690

	Z BY WT.	ENTHALPY KCAL/MOL	STATE	TEMP DEG K	DENSITY G/CC
MG	55.00	0.0	S	298.15	1.740000
NANO3	40.00	-111.540	S	298.15	2.261000
LANTHAC	5.00	-76.200	S	298.15	1.190000

EMPIRICAL FORMULA						O/F= 0.0
FUEL	MG	1.00000				
FUEL	NA	1.00000	N	1.00000	O	3.00000
FUEL	O	1.77324	C	5.46749	H	5.91080
						DENSITY= 1.8691

PARAMETERS	CHAMBER	THROAT	EXIT
PRESS.,PSIA	0.39	0.23	0.20
PRESS.,ATH	0.03	0.02	0.01
T, DEG K	2543	2455	2433
T, DEG F	4118	3959	3919
S, CAL/(G)(K)	1.7604	1.7604	1.7604

MOL WT	43.490	44.042	44.173
CP, CAL/(G)(K)	1.5371	1.2421	1.1775
GAMMA	1.0970	1.0996	1.1004
MACH NUMBER	0.0	1.000	1.119
CSTAR		3640	3640

CF, IDEAL	0.643	0.716
CF, VAC	1.228	1.235
AE/AT	1.00	1.01
ISP, IDEAL	72.8	81.0
ISP*RHOB	136.1	151.4

MOLE FRACTIONS OF PRODUCTS

ClO1(G)	0.07381	0.07502	0.07534
ClO2(G)	0.00583	0.00476	0.00448
HT(G)	0.02150	0.02018	0.01977
HING1(G)	0.00017	0.00014	0.00013
HING1O1(G)	0.00002	0.00001	0.00001
HINA1(G)	0.00004	0.00003	0.00003
HINA1O1(G)	0.00220	0.00165	0.00153
H1O1(G)	0.00237	0.00155	0.00137
H2(G)	0.02007	0.02273	0.02348
H2O1(G)	0.00983	0.00861	0.00825
MG1(G)	0.32412	0.31974	0.31869
MG1O1(G)	0.00445	0.00277	0.00243
N1O1(G)	0.00030	0.00017	0.00014
N2(G)	0.06840	0.06859	0.06863
NA1(G)	0.13472	0.13558	0.13578
NA1O1(G)	0.00013	0.00007	0.00006
O1(G)	0.00160	0.00088	0.00074
O2(G)	0.00033	0.00014	0.00011
MG1O1(S)	0.33011	0.33736	0.33904

	% BY WT.	ENTHALPY KCAL/MOL	STATE	TEMP DEG K	DENSITY G/CC
MG	59.00	0.0	S	298.15	1.740000
NANO3	36.00	-111.540	S	298.15	2.261000
LAMINAC	5.00	-76.200	S	298.15	1.190000

EMPIRICAL FORMULA

FUEL	MG	1.00000			
FUEL	NA	1.00000	N	1.00000	O 3.00000
FUEL	O	1.77324	C	3.46749	H 5.91080

O/F= 0.0

DENSITY= 1.8508

PARAMETERS

	CHAMBER	THROAT	EXIT
PRESS., PSIA	0.39	0.22	0.20
PRESS., ATM	0.03	0.01	0.01
T, DEG K	2233	2064	2036
T, DEG F	3559	3256	3205
S, CAL/(G)(K)	1.7429	1.7429	1.7430
MOL WT	41.455	41.614	41.630
CP, CAL/(G)(K)	0.4074	0.3376	0.3299
GAMMA	1.1609	1.1794	1.1821
MACH NUMBER	0.0	1.000	1.082
CSTAR		3416	3416
CF, IDEAL		0.670	0.720
CF, VAC		1.238	1.241
AE/AT		1.00	1.01
ISP, IDEAL		71.1	76.5
ISP+RHO		131.6	141.6

MOLE FRACTIONS OF PRODUCTS

ClO1(G)	0.07797	0.07831	0.07835
ClO2(G)	0.00029	0.00007	0.00005
H1(G)	0.00672	0.00338	0.00296
H1MG1(G)	0.00024	0.00017	0.00016
H1NA1(G)	0.00004	0.00003	0.00003
H1NA1O1(G)	0.00020	0.00005	0.00004
H1O1(G)	0.00002	0.00000	0.00000
H2(G)	0.03794	0.04037	0.04065
H2O1(G)	0.00074	0.00017	0.00013
MG1(G)	0.38462	0.38433	0.38434
MG1O1(G)	0.00010	0.00001	0.00001
N2(G)	0.06062	0.06071	0.06073
NA1(G)	0.12100	0.12135	0.12139
MG1O1(S)	0.30950	0.31103	0.31117

	% BY WT.	ENTHALPY KCAL/MOL	STATE	TEMP DEG K	DENSITY G/CC
MG	68.00	0.0	S	298.15	1.740000
NANO3	27.00	-111.540	S	298.15	2.261000
LAMINAC	5.00	-76.200	S	298.15	1.190000

EMPIRICAL FORMULA

FUEL	MG	1.00000			
FUEL	NA	1.00000	N	1.00000	O 3.00000
FUEL	O	1.77324	C	5.46749	H 5.91080

O/F= 0.0

DENSITY= 1.8108

PARAMETERS

	CHAMBER	THROAT	EXIT
PRESS., PSIA	0.39	0.23	0.20
PRESS., ATM	0.03	0.02	0.01
T, DEG K	1590	1538	1525
T, DEG F	2402	2308	2286
S, CAL/(G)(K)	1.6103	1.6103	1.6103
MOL WT	40.548	41.146	41.274
CP, CAL/(G)(K)	2.2777	1.5210	1.3539
GAMMA	1.0960	1.1006	1.1027
MACH NUMBER	0.0	1.000	1.110
CSTAR		2984	2984
CF, IDEAL		0.643	0.711
CF, VAC		1.227	1.233
AE/AT		1.00	1.01
ISP, IDEAL		59.6	65.9
ISP*RM08		108.0	119.3

MOLE FRACTIONS OF PRODUCTS

CIHINI(G)	0.00012	0.00008	0.00008
CI01(G)	0.01190	0.00703	0.00601
HI(G)	0.00005	0.00004	0.00003
HIMG1(G)	0.00020	0.00015	0.00014
H1NA1(G)	0.00002	0.00001	0.00001
H2(G)	0.03982	0.03987	0.03988
MG1(G)	0.42678	0.48194	0.48092
N2(G)	0.04295	0.04296	0.04297
NA1(G)	0.08598	0.08599	0.08599
NA2(G)	0.00001	0.00001	0.00000
MG101(S)	0.27016	0.27501	0.27603
CI(S)	0.06201	0.06690	0.06793

	% BY WT.	ENTHALPY KCAL/MOL	STATE	TEMP DEG K	DENSITY G/CC
MG	58.00	0.0	S	298.15	1.740000
NANO3	37.50	-111.540	S	298.15	2.261000
LAMINAC	4.50	-76.200	S	298.15	1.190000

EMPIRICAL FORMULA

FUEL	MG	1.00000				O/F= 0.0
FUEL	NA	1.00000	N	1.00000	O	3.00000
FUEL	C	1.77324	C	5.46749	H	5.91080
						DENSITY= 1.8622

PARAMETERS	CHAMBER	THRJET	EXIT
PRESS., PSIA	14.70	8.39	14.30
PRESS., ATM	1.00	0.57	0.97
T, DEG K	2620	2430	2611
T, DEG F	4256	3915	4240
S, CAL/(G)(K)	1.5722	1.5722	1.5722

MOL WT	43.833	43.973	43.842
CP, CAL/(G)(K)	0.3889	0.3391	0.3858
GAMMA	1.1566	1.1681	1.1572
MACH NUMBER	0.0	1.000	0.218
CSTAR		3608	3608

CF, IDEAL		0.666	0.150
CF, VAC		1.237	2.873
AE/AT		1.00	2.80
ISP, IDEAL		74.7	16.9
ISP*RM(B)		139.1	31.4

MOLE FRACTIONS OF PRODUCTS

ClO1(G)	C.07144	0.07166	0.07146
ClO2(G)	C.00025	0.00009	0.00024
H1(G)	C.00621	0.00373	0.00608
H1MG1(G)	C.00158	0.00115	0.00156
H1MG1O1(G)	C.00001	0.00000	0.00001
H1NA1(G)	C.00028	0.00021	0.00028
H1NA1O1(G)	C.00066	0.00024	0.00063
H1O1(G)	C.00003	0.00001	0.00003
H2(G)	C.03361	0.03585	0.03374
H2O1(G)	C.00075	0.00026	0.00072
MG1(G)	C.35743	0.35742	0.35779
MG1O1(G)	C.00026	0.00006	0.00025
N2(G)	C.06427	0.06433	0.06428
NA1(G)	C.12750	0.12813	0.12754
NA1O1(G)	C.00001	0.00000	0.00001
NA2(G)	C.00005	0.00004	0.00005
MG1O1(S)	C.33523	0.33683	0.33534

	% BY WT.	ENTHALPY KCAL/MOL	STATE	TEMP DEG K	DENSITY G/CC
MG	58.00	0.0	S	298.15	1.740000
NANO3	37.50	-111.540	S	298.15	2.261000
LAMINAC	4.50	-76.200	S	298.15	1.190000

EMPIRICAL FORMULA

FUEL	MG	1.00000				O/F= 0.0
FUEL	NA	1.00000	N	1.00000	O	3.00000
FUEL	O	1.77324	C	5.46749	H	5.91080

DENSITY= 1.8622

PARAMETERS	CHAMBER	THROAT	EXIT
PRESS., PSIA	0.39	0.22	0.20
PRESS., ATM	0.03	0.02	0.01
T, DEG K	2442	2323	2297
T, DEG F	3936	3722	3676
S, CAL/(G)(K)	1.7388	1.7388	1.7388

MOL WT	42.935	43.343	43.417
CP, CAL/(G)(K)	0.7717	0.5989	0.5687
GAMMA	1.1172	1.1274	1.1299
MACH NUMBER	0.0	0.999	1.099
CSTAR		3567	3567

CF, IDEAL	0.651	0.713
CF, VAC	1.230	1.235
AE/AT	1.00	1.01
ISP, IDEAL	72.2	79.0
ISP*RHOB	134.5	147.2

MOLE FRACTIONS OF PRODUCTS

C101(G)	0.06920	0.07022	0.07040
C102(G)	0.00207	0.00118	0.00102
H1(G)	0.01557	0.01231	0.01156
H1MG1(G)	0.00021	0.00016	0.00015
H1MG101(G)	0.00001	0.00000	0.00000
H1NA1(G)	0.00004	0.00003	0.00003
H1NA101(G)	0.00101	0.00056	0.00049
H101(G)	0.00055	0.00020	0.00015
H2(G)	0.02534	0.02922	0.03002
H201(G)	0.00449	0.00274	0.00240
MG1(G)	0.36383	0.36080	0.36031
MG101(G)	0.00143	0.00056	0.00044
N101(G)	0.00005	0.00002	0.00001
N2(G)	0.06388	0.06400	0.06403
NA1(G)	0.12672	0.12742	0.12755
NA101(G)	0.00003	0.00001	0.00001
O1(G)	0.00022	0.00005	0.00004
O2(G)	0.00002	0.00000	0.00000
MG101(S)	0.32534	0.33091	0.33139

APPENDIX VI
THERMOCHEMICAL COMPUTATIONS FOR
MAGNESIUM-GLYCIDYL METHACRYLATE-SODIUM
PERCHLORATE FLARE COMPOSITIONS
AND
COMPUTATIONS FOR ONE MAGNESIUM-
GLYCIDYL METHACRYLATE-SODIUM
NITRATE FLARE COMPOSITION

	BY WT.	ENTHALPY	STATE	TEMP	DENSITY
		KCAL/MOL		DEG K	G/CC
GLYMET	15.00	-104.000	L	298.15	1.000000
MG	22.00	0.0	S	298.15	1.740000
NACLO4	63.00	-92.180	S	298.15	2.379999

EMPIRICAL FORMULA					
FUEL	C 7	H 10	O 3		O/F= 0.0
FUEL	MG 1				
FUEL	O 4	NA 1	CL 1		DENSITY= 1.8479

PARAMETERS	CHAMBER	THROAT	EXIT
PRESS., PSIA	14.70	8.56	14.30
PRESS., ATM	1.00	0.58	0.97
T, DEG K	3083	2988	3078
T, DEG F	5089	4919	5080
S, CAL/(G)(K)	1.8948	1.8951	1.8949

MOL WT	41.193	41.832	41.223
CP, CAL/(G)(K)	5.1048	4.9898	5.1014
GAMMA	1.0959	1.0937	1.0958
MACH NUMBER	0.0	0.999	0.213
CSTAR		4155	4155

CF, IDEAL		0.636	0.139
CF, VAC		1.218	2.923
AE/AT		1.00	2.86
ISP, IDEAL		82.1	18.0
ISP, RHO		151.8	33.2

MOLE FRACTIONS OF PRODUCTS			
CL01(G)	0.16463	0.16288	0.16454
CL02(G)	0.07698	0.07976	0.07711
CL1(G)	0.02366	0.02366	0.02367
CL1H1(G)	0.03097	0.03141	0.03099
CL1MG1(G)	0.00134	0.00104	0.00132
CL1NA1(G)	0.10519	0.10652	0.10525
CL1O1(G)	0.00004	0.00003	0.00004
CL2(G)	0.00001	0.00000	0.00001
CL2MG1(G)	0.00353	0.00316	0.00351
CL2NA2(G)	0.00001	0.00001	0.00001
H1(G)	0.02907	0.02862	0.02905
H1MG1(G)	0.00028	0.00019	0.00027
H1MG1O1(G)	0.00022	0.00015	0.00021
H1NA1(G)	0.00009	0.00007	0.00009
H1NA1O1(G)	0.01525	0.01385	0.01517
H1O1(G)	0.03672	0.03441	0.03661
H2(G)	0.02616	0.02630	0.02616
H2O1(G)	0.09012	0.09266	0.09024
MG1(G)	0.06724	0.06340	0.06708
MG1O1(G)	0.01736	0.01447	0.01721
NA1(G)	0.04609	0.04718	0.04615
NA1O1(G)	0.00165	0.00136	0.00164
O1(G)	0.02404	0.02229	0.02396
O2(G)	0.03341	0.03182	0.03334
MG1O1(S)	0.20594	0.21473	0.20635

	g BY WT.	ENTHALPY, STATE KCAL/MOL	TEMP DEG K	DENSITY G/CC
GLYMET	19.00	-104.000	L 298.15	1.000000
NG	32.00	0.0	S 298.15	1.740000
NACLO4	39.00	-92.100	S 298.15	2.379999

EMPIRICAL FORMULA				
FUEL	C 7	H 10	O 3	O/F= 0.0
FUEL	MG 1			DENSITY= 1.7966
FUEL	O 4	NA 1	CL 1	

PARAMETERS	CHAMBER	THROAT	EXIT
PRESS., PSIA	14.70	8.57	14.30
PRESS., ATM	1.00	0.58	0.97
T, DEG K	3082	2985	3077
T, DEG F	5087	4913	5078
S, CAL/(G)(K)	1.8822	1.8824	1.8823

MOL WT	39.982	40.616	40.011
CP, CAL/(G)(K)	4.4479	4.2483	4.4407
GAMMA	1.0982	1.0963	1.0981
MACH NUMBER	0.0	1.000	0.219
CSTAR		4199	4199

CF, IDEAL	0.640	0.141
CF, VAC	1.223	2.909
AE/AT	1.00	2.85
ISP, IDEAL	83.9	18.4
ISP*RHOB	150.0	33.1
MOLE FRACTIONS OF PRODUCTS		

CH101(G)	0.00001	0.00000	0.00001
ClO1(G)	0.18975	0.19023	0.18975
ClO2(G)	0.03788	0.03801	0.03788
CL1(G)	0.01653	0.01634	0.01653
CL1H1(G)	0.02923	0.02996	0.02927
CL1MG1(G)	0.00218	0.00175	0.00216
CL1NA1(G)	0.07703	0.07790	0.07707
CL1O1(G)	0.00001	0.00001	0.00001
CL2MG1(G)	0.00419	0.00389	0.00417
CL2NA2(G)	0.00001	0.00001	0.00001
H1(G)	0.03788	0.03745	0.03786
H1MG1(G)	0.00084	0.00062	0.00083
H1MG1O1(G)	0.00028	0.00020	0.00028
H1NA1(G)	0.00012	0.00010	0.00012
H1NA1O1(G)	0.00887	0.00779	0.00882
H1O1(G)	0.02040	0.01830	0.02030
H2(G)	0.04606	0.04754	0.04611
H2O1(G)	0.06770	0.06828	0.06774
MG1(G)	0.15197	0.14727	0.15176
MG1O1(G)	0.01671	0.01362	0.01655
NA1(G)	0.04861	0.04739	0.04866
NA1O1(G)	0.00071	0.00055	0.00070
O1(G)	0.00988	0.00858	0.00983
O2(G)	0.00586	0.00499	0.00582
MG1O1(S)	0.22929	0.23923	0.22976

	% BY WT.	ENTHALPY KCAL/MOL	STATE	TEMP DEG K	DENSITY G/CC
GLYMET	15.00	-104.000	L	298.15	1.000000
MG	42.50	0.0	S	298.15	1.740000
NACLO4	42.50	-92.180	S	298.15	2.379999

EMPIRICAL FORMULA					
FUEL	C	7	H	10	O 3
FUEL	MG	1			
FUEL	O	4	NA	1	CL 1
O/F= 0.0					
DENSITY= 1.7457					

PARAMETERS	CHAMBER	THROAT	EXIT
PRESS., PSIA	14.70	8.53	14.30
PRESS., ATM	1.00	0.58	0.97
T, DEG K	2878	2764	2873
T, DEG F	4721	4515	4711
S, CAL/(G)(K)	1.8519	1.8520	1.8520

MOL WT	37.913	38.450	37.937
CP, CAL/(G)(K)	1.5278	1.3863	1.5218
GAMMA	1.1122	1.1120	1.1122
MACH NUMBER	0.0	1.001	0.212
CSTAR		4143	4143

CF, IDEAL	0.646	0.141
CF, VAC	1.226	2.948
AE/AT	1.00	2.89
ISP, IDEAL	83.2	18.1
ISP*RHOB	145.2	31.6

MOLE FRACTIONS OF PRODUCTS

CIH1O1(G)	0.00001	0.00000	0.00001
CI01(G)	0.20591	0.20770	0.20598
CI02(G)	0.00725	0.00592	0.00719
CL1(G)	0.00474	0.00404	0.00471
CL1H1(G)	0.02291	0.02278	0.02291
CL1MG1(G)	0.00225	0.00178	0.00223
CL1NA1(G)	0.05907	0.06050	0.05913
CL2MG1(G)	0.00559	0.00564	0.00559
CL2NA2(G)	0.00001	0.00001	0.00001
H1(G)	0.02923	0.02650	0.02912
H1MG1(G)	0.00194	0.00145	0.00191
H1MG1O1(G)	0.00010	0.00006	0.00010
H1NA1(G)	0.00014	0.00011	0.00014
H1NA1O1(G)	0.00236	0.00171	0.00233
H1O1(G)	0.00224	0.00143	0.00220
H2(G)	0.09858	0.10536	0.09887
H2O1(G)	0.02421	0.02021	0.02405
MG1(G)	0.25229	0.24665	0.25204
MG1O1(G)	0.00334	0.00208	0.00327
NA1(G)	0.03851	0.03803	0.03850
NA1O1(G)	0.00006	0.00003	0.00006
O1(G)	0.00040	0.00022	0.00039
O2(G)	0.00004	0.00002	0.00004
MG1O1(S)	0.23841	0.24779	0.23923

	g BY WT.	ENTHALPY KCAL/MOL	STATE	TEMP DEG K	DENSITY G/CC
GLYMET	45.00	-104.000	L	298.15	1.000000
MG	52.00	0.0	S	298.15	1.740000
NaClO4	33.00	-92.100	S	298.15	2.379999

EMPIRICAL FORMULA					
FUEL	C 7	H 10	O 3	O/F= 0.0	
FUEL	MG 1				
FUEL	O 4	NA 1	CL 1	DENSITY= 1.7021	

PARAMETERS	CHAMBER	THROAT	EXIT
PRESS., PSIA	14.70	52	14.30
PRESS., ATM	1.00	0.58	0.97
T, DEG K	1869	1794	1865
T, DEG F	2904	2769	2897
S, CAL/(G)(K)	1.7669	1.7670	1.7671
MOL WT	34.325	35.008	34.355
CP, CAL/(G)(K)	2.1446	3.2470	2.1942
GAMMA	1.1311	1.1210	1.1305
MACH NUMBER	0.0	1.000	0.212
CSTAR		3490	3490
CF, IDEAL		0.650	0.142
CF, VAC		1.229	2.942
AE/AT		1.00	2.88
ISP, IDEAL		70.5	19.5
ISP*RHOB		119.9	26.3

MOLE FRACTIONS OF PRODUCTS

CH3(G)	0.00001	0.00001	0.00001
CH4(G)	0.00017	0.00021	0.00017
CHO(G)	0.19028	0.18377	0.18999
C2H2(G)	0.00679	0.01082	0.00697
C2H4(G)	0.00002	0.00003	0.00002
CLH1(G)	0.00048	0.00037	0.00047
CLMG1(G)	0.00019	0.00013	0.00018
CL1NA1(G)	0.05088	0.05174	0.05092
CL2MG1(G)	0.01109	0.01103	0.01109
CL2NA2(G)	0.00036	0.00037	0.00036
H1(G)	0.00021	0.00019	0.00020
H1MG1(G)	0.00212	0.00150	0.00208
H1NA1(G)	0.00007	0.00005	0.00007
H2(G)	0.13716	0.13458	0.13705
HGI(G)	0.38235	0.37817	0.38217
NA1(G)	0.02277	0.02252	0.02276
NA2(G)	0.00001	0.00000	0.00001
MG1O1(S)	0.19504	0.20456	0.19546

	% BY WT.	ENTHALPY KCAL/MOL	STATE	TEMP DEG K	DENSITY G/CC
GLYMET	15.00	-104.000	L	298.15	1.000000
MG	42.50	0.0	S	298.15	1.740000
NANO3	42.50	-111.540	S	298.15	2.261000

EMPIRICAL FORMULA

FUEL	C	7	H	10	O	3
FUEL	MG	1				
FUEL	O	3	NA	1	N	1

O/F= 0.0 DENSITY= 1.7176

PARAMETERS

	CHAMBER	THROAT	EXIT
PRESS.,PSIA	14.70	8.39	14.30
PRESS.,ATM	1.00	0.57	0.97
T, DEG K	2488	2318	2481
T, DEG F	4019	3713	4005
S, CAL/(G)(K)	1.8507	1.9507	1.8508
MOL WT	36.930	37.101	36.939
CP, CAL/(G)(K)	0.5218	0.4258	0.5168
GAMMA	1.1481	1.1640	1.1487
MACH NUMBER	0.0	1.000	0.211
CSTAR		3839	3839
CF,IDEAL		0.665	0.144
CF,VAC		1.235	2.967
AE/AT		1.00	2.90
ISP,IDEAL		79.3	17.2
ISP*RHOB		136.2	29.6

MOLE FRACTIONS OF PRODUCTS

CIHINI(G)	0.00000	0.00001	0.00000
CI01(G)	0.19534	0.19581	0.19536
CI02(G)	0.00050	0.00018	0.00048
HI(G)	0.00735	0.00437	0.00720
HIMG1(G)	0.00144	0.00102	0.00142
HINA1(G)	0.00053	0.00038	0.00052
HINA101(G)	0.00114	0.00041	0.00109
HI01(G)	0.00002	0.00000	0.00002
H2(G)	0.13260	0.13621	0.13279
H201(G)	0.00205	0.00070	0.00197
MG1(G)	0.17980	0.17796	0.17968
MG101(G)	0.00007	0.00001	0.00006
N2(G)	0.06628	0.06634	0.06628
NA1(G)	0.13079	0.13180	0.13085
NA2(G)	0.00006	0.00005	0.00006
MG101(S)	0.28203	0.28474	0.28219

APPENDIX VII
THERMOCHEMICAL CALCULATIONS FOR
MAGNESIUM, VITON A, TETRAFLUOROETHYLENE,
AND SODIUM NITRATE

	% BY WT.	ENTHALPY KCAL/MOL	STATE	TEMP DEG K	DENSITY G/CC
VITON A	11.00	-177.900	L	298.15	1.820000
DFPM	11.00	-97.000	S	298.15	1.820000
MG	54.00	0.0	S	298.15	1.740000
NANO3	24.00	-111.540	S	298.15	2.261000

EMPIRICAL FORMULA					
FUEL	C	2.67200	H	1.80000	F 3.47890 O/F= 0.0
FUEL	C	1.00000	F	2.00000	
FUEL	MG	1.00000			DENSITY= 1.8609
FUEL	NA	1.00000	N	1.00000	O 3.00000

PARAMETERS	CHAMBER	THROAT	EXIT
PRESS., PSIA	14.70	8.61	14.30
PRESS., ATM	1.00	0.59	0.97
T, DEG K	1987	1929	1984
T, DEG F	3117	3013	3112
S, CAL/(G)(K)	1.5673	1.5674	1.5674

MOL WT	42.875	43.655	42.913
CP, CAL/(G)(K)	19.0548	18.8095	19.0463
GAMMA	1.0991	1.0963	1.0990
MACH NUMBER	0.0	1.000	0.221
CSTAR		3245	3245

CF, IDEAL	0.641	0.145
CF, VAC	1.227	2.851
AE/AT	1.00	2.78
ISP, IDEAL	64.7	14.7
ISP*RHOB	120.4	27.3

MOLE FRACTIONS OF PRODUCTS

CH4N1(G)	0.00069	0.00055	0.00068
CI01(G)	0.12000	0.11318	0.11965
C2H2(G)	0.00002	0.00002	0.00002
FIH1(G)	0.00152	0.00150	0.00152
F1MG1(G)	0.00001	0.00000	0.00001
F1NA1(G)	0.00456	0.00429	0.00455
F2MG1(G)	0.01731	0.01803	0.01735
H1(G)	0.00021	0.00018	0.00021
H1MG1(G)	0.00121	0.00089	0.00119
H1NA1(G)	0.00012	0.00009	0.00012
H2(G)	0.02851	0.02878	0.02853
MG1(G)	0.41740	0.41067	0.41706
N2(G)	0.04303	0.04309	0.04303
NA1(G)	0.08193	0.08224	0.08195
NA2(G)	0.00007	0.00005	0.00006
MG1O1(S)	0.14025	0.14698	0.14059
F2MG1(L)	0.10601	0.10539	0.10597
CI(S)	0.03714	0.04406	0.03749

	% BY WT.	ENTHALPY KCAL/MOL	STATE	TEMP DEG K	DENSITY G/CC
VITON A	11.00	-177.900	L	298.15	1.820000
DFPM	11.00	-97.000	S	298.15	1.820000
MG	50.00	0.0	S	298.15	1.740000
NANO3	28.00	-111.540	S	298.15	2.261000

EMPIRICAL FORMULA						
FUEL	C	2.67200	H	1.80000	F	3.47890
FUEL	C	1.00000	F	2.00000	O/F= 0.0	
FUEL	MG	1.00000				
FUEL	NA	1.00000	N	1.00000	O	3.00000
						DENSITY= 1.8794

PARAMETERS	CHAMBER	THROAT	EXIT
PRESS., PSIA	14.70	8.49	14.30
PRESS., ATM	1.00	0.58	0.97
T, DEG K	2060	1954	2055
T, DEG F	3249	3058	3239
S, CAL/(G)(K)	1.6234	1.6234	1.6234
MOL WT	41.691	42.265	41.719
CP, CAL/(G)(K)	0.9078	0.8249	0.9040
GAMMA	1.1390	1.1362	1.1388
MACH NUMBER	0.0	1.000	0.217
CSTAR		3306	3306
CF, IDEAL		0.656	0.147
CF, VAC		1.233	2.886
AE/AT		1.00	2.81
ISP, IDEAL		67.4	15.1
ISP*RHOB		126.7	26.4

MOLE FRACTIONS OF PRODUCTS

CIH1N1(G)	0.00029	0.00046	0.00030
CI01(G)	0.16203	0.16195	0.16203
C2H2(G)	0.00000	0.00001	0.00000
FIH1(G)	0.00322	0.00219	0.00317
F1MG1(G)	0.00001	0.00001	0.00001
F1NA1(G)	0.00849	0.00642	0.00838
F2MG1(G)	0.03199	0.02402	0.03159
H1(G)	0.00036	0.00023	0.00035
H1MG1(G)	0.00111	0.00080	0.00109
H1NA1(G)	0.00015	0.00011	0.00014
H2(G)	0.02870	0.02939	0.02874
MG1(G)	0.37416	0.37294	0.37410
N2(G)	0.05189	0.05183	0.05189
NA1(G)	0.09529	0.09748	0.09540
NA2(G)	0.00007	0.00006	0.00007
MG101(S)	0.15016	0.15043	0.15017
F2MG1(L)	0.09207	0.10168	0.09256

	% BY WT.	ENTHALPY KCAL/MOL	STATE	TEMP DEG K	DENSITY G/CC
VITON A	11.00	-177.900	L	298.15	1.820000
DFPM	11.00	-97.000	S	298.15	1.820000
MG	46.00	0.0	S	298.15	1.740000
NANO3	32.00	-111.540	S	298.15	2.261000

EMPIRICAL FORMULA					
FUEL	C	2.67200	H	1.80000	F 3.47890
FUEL	C	1.00000	F	2.00000	O/F= 0.0
FUEL	MG	1.00000			
FUEL	NA	1.00000	N	1.00000	O 3.00000
					DENSITY= 1.8983

PARAMETERS	CHAMBER	THRUT	EXIT
PRESS., PSIA	14.70	8.49	14.30
PRESS., ATM	1.00	0.58	0.97
T, DEG K	2236	2136	2231
T, DEG F	3565	3385	3555
S, CAL/(G)(K)	1.6692	1.6693	1.6693

MOL WT	40.762	41.545	40.796
CP, CAL/(G)(K)	2.0693	2.0427	2.0699
GAMMA	1.1371	1.1307	1.1367
MACH NUMBER	0.0	1.000	0.209
CSTAR		3491	3491

CF, IDEAL	0.654	0.141
CF, VAC	1.231	2.989
AE/AT	1.00	2.93
ISP, IDEAL	70.9	15.3
ISP*RHOB	134.6	29.0

MOLE FRACTIONS OF PRODUCTS

CH4N1(G)	0.00002	0.00003	0.00002
ClO1(G)	0.16628	0.16647	0.16629
ClO2(G)	0.00002	0.00001	0.00002
F1H1(G)	0.01339	0.01125	0.01328
F1MG1(G)	0.00006	0.00003	0.00006
F1NA1(G)	0.02286	0.01979	0.02271
F2MG1(G)	0.10828	0.09714	0.10780
H1(G)	0.00095	0.00072	0.00094
H1MG1(G)	0.00087	0.00065	0.00086
H1NA1(G)	0.00015	0.00012	0.00015
H1NA1O1(G)	0.00003	0.00002	0.00003
H2(G)	0.02432	0.02568	0.02439
H2O1(G)	0.00002	0.00001	0.00002
MG1(G)	0.29715	0.29503	0.29706
N2(G)	0.06092	0.06098	0.06092
NA1(G)	0.09873	0.10199	0.09889
NA2(G)	0.00005	0.00004	0.00005
MG1O1(S)	0.15920	0.19945	0.19921
F2MG1(L)	0.00669	0.02059	0.00730

	% BY WT.	ENTHALPY KCAL/MOL	STATE	TEMP DEG K	DENSITY G/CC
VITON A	11.00	-177.900	L	298.15	1.820000
DPPM	11.00	-97.000	S	298.15	1.820000
MG	42.00	0.0	S	298.15	1.740000
NANO3	36.00	-111.540	S	298.15	2.261000

EMPIRICAL FORMULA						
FUEL	C	2.67200	H	1.80000	F	3.47890
FUEL	C	1.00000	F	2.00000		O/F= 0.0
FUEL	MG	1.00000				
FUEL	NA	1.00000	N	1.00000	O	3.00000
						DENSITY= 1.9176

PARAMETERS	CHAMBER	THROAT	EXIT
PRESS., PSIA	14.70	8.40	14.30
PRESS., ATM	1.00	0.57	0.97
T, DEG K	2772	2597	2764
T, DEG F	4530	4214	4516
S, CAL/(G)(K)	1.6991	1.6993	1.6992

MOL WT	43.299	43.594	43.313
CP, CAL/(G)(K)	0.5084	0.4364	0.5042
GAMMA	1.1439	1.1538	1.1444
MACH NUMBER	0.0	1.000	0.208
CSTAR		3764	3764
CF, IDEAL		0.659	0.141
CF, VAC		1.230	2.993
AE/AT		1.00	2.93
ISP, IDEAL		77.0	16.5
ISP*RHOB		147.7	31.7

MOLE FRACTIONS OF PRODUCTS

C101(G)	0.16557	0.16743	0.16566
C102(G)	0.00315	0.00154	0.00307
F1(G)	0.00014	0.00005	0.00013
F1H1(G)	0.04169	0.03998	0.04167
F1MG1(G)	0.00038	0.00021	0.00037
F1NA1(G)	0.04003	0.03697	0.03990
F2MG1(G)	0.09393	0.09664	0.09402
H1(G)	0.00544	0.00421	0.00539
H1MG1(G)	0.00046	0.00037	0.00045
H1MG101(G)	0.00001	0.00000	0.00001
H1NA1(G)	0.00010	0.00008	0.00010
H1NA101(G)	0.00099	0.00054	0.00096
H101(G)	0.00020	0.00006	0.00019
H2(G)	0.00714	0.00939	0.00722
H201(G)	0.00092	0.00055	0.00090
MG1(G)	0.22927	0.22455	0.22907
MG101(G)	0.00131	0.00041	0.00126
N101(G)	0.00005	0.00001	0.00005
N2(G)	0.06951	0.06963	0.06951
NA1(G)	0.09786	0.10163	0.09802
NA101(G)	0.00006	0.00001	0.00005
NA2(G)	0.00002	0.00002	0.00002
O1(G)	0.00009	0.00002	0.00009
MG101(S)	0.24169	0.24570	0.24190

	% BY WT.	ENTHALPY KCAL/MOL	STATE	TEMP DEG K	DENSITY G/CC
VITON A	11.00	-177.900	L	298.15	1.320000
DFPM	11.00	-97.000	S	298.15	1.820000
MG	38.00	0.0	S	298.15	1.740000
NANO3	40.00	-111.540	S	298.15	2.261000
EMPIRICAL FORMULA					
FUEL	C 2.67200	H 1.80000	F 3.47890		
FUEL	C 1.00000	F 2.00000			O/F= 0.0
FUEL	MG 1.00000				
FUEL	NA 1.00000	N 1.00000	O 3.00000		DENSITY= 1.9373

PARAMETERS	CHAMBER	THROAT	EXIT
PRESS., PSIA	14.70	8.54	14.31
PRESS., ATM	1.00	0.58	0.97
T, DEG K	3015	2905	3010
T, DEG F	4967	4769	4958
S, CAL/(G)(K)	1.7139	1.7140	1.7141
MOL WT	45.304	45.909	45.328
CP, CAL/(G)(K)	1.6362	1.3604	1.6262
GAMMA	1.1028	1.1034	1.1028
MACH NUMBER	0.0	1.002	0.204
CSTAR		3892	3892

CF, IDEAL	0.643	0.134
CF, VAC	1.225	3.060
AE/AT	1.00	3.01
ISP, IDEAL	77.8	16.2
ISP*RHOB	150.8	31.4

MOLE FRACTIONS OF PRODUCTS

ClO1(G)	0.15429	0.15612	0.15433
ClO2(G)	0.01829	0.01667	0.01825
F1(G)	0.00094	0.00073	0.00093
F1H1(G)	0.04621	0.04827	0.04631
F1MG1(G)	0.00063	0.00046	0.00062
F1NA1(G)	0.05436	0.05277	0.05428
F2MG1(G)	0.08707	0.08719	0.08707
H1(G)	0.00677	0.00629	0.00675
H1MG1(G)	0.00021	0.00015	0.00020
H1MG1O1(G)	0.00004	0.00002	0.00004
H1NA1(G)	0.00006	0.00005	0.00006
H1NA1O1(G)	0.00274	0.00220	0.00272
H1O1(G)	0.00203	0.00150	0.00200
H2(G)	0.00227	0.00231	0.00227
H2O1(G)	0.00195	0.00173	0.00194
MG1(G)	0.16836	0.16309	0.16817
MG1O1(G)	0.00977	0.00691	0.00964
NI01(G)	0.00122	0.00083	0.00121
N2(G)	0.07841	0.07870	0.07842
NA1(G)	0.10010	0.10270	0.10023
NA1O1(G)	0.00075	0.00050	0.00074
NA2(G)	0.00002	0.00001	0.00002
O1(G)	0.00358	0.00246	0.00354
O2(G)	0.00125	0.00075	0.00123
MG1O1(S)	0.25869	0.26758	0.25905

S BY WT.				ENTHALPY	STATE	TEMP	DENSITY
				KCAL/MOL		DEG K	G/CC
VITON A		11.00		-177.900	L	298.15	1.820000
DPPH		11.00		-97.000	S	298.15	1.820000
MG		34.00		0.0	S	298.15	1.740000
NANO3		44.00		-41.540	S	298.15	2.261000
EMPIRICAL FORMULA							
FUEL	C	2.67200	H	1.80000	F	3.47890	O/F= 0.0
FUEL	C	1.00000	F	2.00000			
FUEL	MG	1.00000					DENSITY= 1.9574
FUEL	NA	1.00000	N	1.00000	O	3.00000	
PARAMETERS				CHAMBER	THROAT	EXIT	
PRESS.,PSIA				14.70	8.58	14.31	
PRESS.,ATM				1.00	0.58	0.97	
T, DEG K				3072	2975	3067	
T, DEG F				5070	4896	5061	
S, CAL/(G)(K)				1.7231	1.7233	1.7233	
MOL WT				46.515	47.188	46.541	
CP, CAL/(G)(K)				3.2204	3.0029	3.2139	
GAMMA				1.0958	1.0939	1.0957	
MACH NUMBER				0.0	1.000	0.209	
CSTAR					3889	3889	
CF, IDEAL				0.639	0.136		
CF, VAC				1.223	2.997		
AE/AT				1.00	2.94		
ISP, IDEAL				77.3	16.5		
ISP, RMOB				151.2	32.3		
MOLE FRACTIONS OF PRODUCTS							
ClO1(G)		0.14173		0.14178	0.14171		
ClO2(G)		0.03389		0.03420	0.03392		
F1(G)		0.00161		0.00143	0.00161		
F1H1(G)		0.04629		0.04848	0.04639		
F1MG1(G)		0.00058		0.00044	0.00057		
F1NA1(G)		0.06810		0.06705	0.06804		
F2MG1(G)		0.08226		0.08215	0.08226		
H1(G)		0.00605		0.00570	0.00603		
H1MG1(G)		0.00011		0.00008	0.00011		
H1MG1O1(G)		0.00004		0.00003	0.00004		
H1NA1(G)		0.00005		0.00004	0.00005		
H1NA1O1(G)		0.00408		0.00347	0.00405		
H1O1(G)		0.00387		0.00333	0.00384		
H2(G)		0.00130		0.00123	0.00130		
H2O1(G)		0.00229		0.00212	0.00228		
MG1(G)		0.11469		0.10975	0.11450		
MG1O1(G)		0.01487		0.01204	0.01473		
N1(G)		0.00001		0.00000	0.00001		
N1O1(G)		0.00338		0.00281	0.00336		
N2(G)		0.08676		0.08723	0.08678		
NA1(G)		0.10283		0.10526	0.10295		
NA1O1(G)		0.00183		0.00144	0.00181		
NA2(G)		0.00002		0.00001	0.00002		
O1(G)		0.01060		0.00922	0.01054		
O2(G)		0.00752		0.00646	0.00748		
MG1O1(S)		0.26525		0.27428	0.26562		

APPENDIX VIII
THERMOCHEMICAL COMPUTATIONS FOR
SILICON, VITON A, TETRAFLUOROETHYLENE,
AND SODIUM NITRATE

	% BY WT.	ENTHALPY KCAL/MOL	STATE	TEMP DEG K	DENSITY G/CC
SILICON	38.00	0.0	S	298.15	2.330000
TEFLON	11.00	-96.520	S	298.15	2.200000
VITON A	11.00	-177.900	L	298.15	1.820000
NANOS	40.00	-111.540	S	298.15	2.261000

EMPIRICAL FORMULA

FUEL	SI	1.00000					O/F= 0.0
FUEL	C	1.00000	F	2.00000			
FUEL	C	2.67200	F	3.47890	H	1.80000	DENSITY= 2.2200
FUEL	NA	1.00000	N	1.00000	O	3.00000	

PARAMETERS	CHAMBER	THROAT	EXIT
PRESS., PSIA	14.70	8.60	14.30
PRESS., ATM	1.00	0.59	0.97
T, DEG K	1932	1873	1929
T, DEG F	3018	2911	3013
S, CAL/(G)(K)	1.5255	1.5256	1.5255

MOL WT	50.240	51.044	50.276
CP, CAL/(G)(K)	3.7656	3.6375	3.7611
GAMMA	1.0980	1.0955	1.0979
MACH NUMBER	0.0	1.000	0.218
CSTAR		2960	2960

CF, IDEAL	0.641	0.143
CF, VAC	1.226	2.888
AE/AT	1.00	2.82
ISP, IDEAL	59.0	13.1
ISP, RHO8	130.9	29.2

MOLE FRACTIONS OF PRODUCTS

CIH1N1(G)	0.00024	0.00023	0.00024
CI01(G)	0.19206	0.19207	0.19206
CI02(G)	0.00001	0.00000	0.00001
FIH1(G)	0.00156	0.00136	0.00155
FIH1(G)	0.01006	0.00858	0.00998
F2O1S11(G)	0.00009	0.00007	0.00009
F2S11(G)	0.04095	0.04051	0.04091
F3S11(G)	0.06723	0.06792	0.06727
F4S11(G)	0.00312	0.00324	0.00312
H1(G)	0.00016	0.00014	0.00016
H1H1(G)	0.00027	0.00020	0.00026
H1H1O1(G)	0.00003	0.00002	0.00003
H2(G)	0.03591	0.03607	0.03592
H2O1(G)	0.00001	0.00000	0.00001
H2(G)	0.08794	0.08795	0.08794
NA1(G)	0.16517	0.16690	0.16527
NA2(G)	0.00030	0.00021	0.00029
O1S11(G)	0.13984	0.12768	0.13927
S11(G)	0.00002	0.00002	0.00002
S11(L)	0.15691	0.16258	0.15715
O2S11(S)	0.09816	0.10425	0.09845

	% BY WT.	ENTHALPY KCAL/MOL	STATE	TEMP DEG K	DENSITY G/CC
SILICON	38.00	0.0	S	298.15	2.330000
TEFLON	21.00	-96.520	S	298.15	2.200000
VITON A	11.00	-177.900	L	298.15	1.920000
WAND3	30.00	-111.540	S	298.15	2.261000

EMPIRICAL FORMULA

FUEL	SI	1.00000				O/F= 0.0
FUEL	C	1.00000	F	2.00000		
FUEL	C	2.67200	F	3.47890	H	1.80000
FUEL	NA	1.00000	N	1.00000	O	3.00000

DENSITY= 2.2140

PARAMETERS	CHAMBER	THROAT	EXIT
PRESS., PSIA	14.70	8.66	14.30
PRESS., ATM	1.00	0.59	0.97
T, DEG K	1850	1806	1848
T, DEG F	2871	2791	2866
S, CAL/(G)(K)	1.4998	1.4998	1.4999

MOL WT	53.402	54.169	53.436
CP, CAL/(G)(K)	15.3114	15.2674	15.3147
GAMMA	1.0790	1.0773	1.0789
MACH NUMBER	0.0	0.999	0.211
CSTAR		2827	2827

CF, IDEAL	0.634	0.137
CF, VAC	1.223	2.972
AE/AT	1.00	2.91
ISP, IDEAL	95.7	12.0
ISP, RHOB	123.3	26.6

MOLE FRACTIONS OF PRODUCTS

CH4N(G)	0.00053	0.00044	0.00053
ClO1(G)	0.24647	0.23450	0.24591
C2H2(G)	0.00001	0.00001	0.00001
FIH1(G)	0.00131	0.00119	0.00131
FINA1(G)	0.00890	0.00759	0.00882
F2O1S11(G)	0.00006	0.00005	0.00006
F2S11(G)	0.04229	0.04308	0.04233
F3S11(G)	0.10892	0.10898	0.10892
F4S11(G)	0.00800	0.00790	0.00799
H1(G)	0.00008	0.00008	0.00008
H1NA1(G)	0.00019	0.00015	0.00019
H1NA1O1(G)	0.00001	0.00001	0.00001
H2(G)	0.03565	0.03579	0.03566
N2(G)	0.06523	0.06527	0.06523
NA1(G)	0.12145	0.12242	0.12153
NA2(G)	0.00022	0.00015	0.00021
O1S11(G)	0.03561	0.03592	0.03569
S11(G)	0.00001	0.00001	0.00001
S11(L)	0.24178	0.23434	0.24141
O2S11(S)	0.04539	0.05071	0.04563
Cl(S)	0.01787	0.02492	0.01845

	% BY WT.	ENTHALPY KCAL/MOL	STATE	TEMP DEG K	DENSITY G/CC
SILICON	48.00	0.0	S	298.15	2.330000
TEFLON	11.00	-96.520	S	298.15	2.200000
VITON A	11.00	-177.900	L	298.15	1.820000
WANDS	30.00	-111.540	S	298.15	2.261000

EMPIRICAL FORMULA

FUEL	SI	1.00000					O/F= 0.0
FUEL	C	1.00000	F	2.00000			
FUEL	C	2.67200	F	3.47890	H	1.80000	DENSITY= 2.2265
FUEL	NA	1.00000	N	1.00000	O	3.00000	
PARAMETERS		CHAMBER		THROAT		EXIT	
PRESS. PSIA		1.00		0.59		0.97	
PRESS. ATM		0.07		0.04		0.07	
T, DEG K		1678		1637		1676	
T, DEG F		2561		2487		2557	
S, CAL/(G)(K)		1.4175		1.4175		1.4175	

MOL WT		58.843	59.651	58.882
CP, CAL/(G)(K)		3.9274	3.7529	3.9201
GAMMA		1.0794	1.0777	1.0793
MACH NUMBER		0.0	0.998	0.214
CSTAR			2567	2567

CF, IDEAL		0.633	0.138
CF, VAC		1.222	2.941
AE/AT		1.00	2.88
TSP, IDEAL		50.5	11.0
TSP, RHOB		112.4	24.5

MOLE FRACTIONS OF PRODUCTS

CH4N1(G)	0.00014	0.00012	0.00014
ClO1(G)	0.18005	0.18007	0.18005
FIH1(G)	0.00076	0.00070	0.00076
F1NA1(G)	0.00318	0.00278	0.00316
F2O1S11(G)	0.00002	0.00002	0.00002
F2S11(G)	0.03699	0.03596	0.03694
F3S11(G)	0.06562	0.06622	0.06565
F4S11(G)	0.00339	0.00358	0.00340
H1(G)	0.00007	0.00006	0.00006
H1NA1(G)	0.00005	0.00004	0.00005
H2(G)	0.03420	0.03426	0.03421
N2(G)	0.06182	0.06183	0.06182
NA1(G)	0.12048	0.12091	0.12050
NA2(G)	0.00003	0.00002	0.00003
O1S11(G)	0.08912	0.08130	0.08874
S11(G)	0.00001	0.00001	0.00001
S11(S)	0.35302	0.35718	0.35323
O2S11(S)	0.05105	0.05495	0.05123

183
0.0 15000.0 0.0

1011150
1011150
1011150

	% BY WT.	ENTHALPY KCAL/MOL	STATE	TEMP DEG C	DENSITY G/CC
SILICON	13.00	0.0	S	298.15	2.330000
TEFLON	36.00	-96.520	S	298.15	2.200000
VITON A	11.00	-177.900	L	298.15	1.920000
NAND3	40.00	-111.540	S	298.15	2.261000

EMPIRICAL FORMULA

FUEL	SI	1.00000				O/F= 0.0
FUEL	C	1.00000	F	2.00000		
FUEL	C	2.67200	F	3.47890	H	1.80000
FUEL	NA	1.00000	N	1.00000	O	3.00000
PARAMETERS	CHAMBER	THROAT	EXIT			DENSITY= 2.1892
PRESS., PSIA	14.70	8.53	14.30			
PRESS., ATM	1.00	0.58	0.97			
T, DEG K	2588	2457	2578			
T, DEG F	4198	3963	4181			
S, CAL/(G)(K)	1.8332	1.8334	1.8333			

MOL WT	42.067	42.451	42.072
CP, CAL/(G)(K)	0.3544	0.9969	0.3530
GAMMA	1.1738	1.1079	1.1743
MACH NUMBER	0.0	0.999	0.207
CSTAR		3728	3728

CF, IDEAL	0.642	0.141
CF, VAC	1.223	2.946
AE/AT	1.00	2.88
ISP, IDEAL	74.4	16.3
ISP, RHO	162.9	35.7

MOLE FRACTIONS OF PRODUCTS

C1O1(G)	0.31786	0.32416	0.31783
C1O2(G)	0.10860	0.10267	0.10869
F1(G)	0.00042	0.00021	0.00040
F1H1(G)	0.07828	0.07849	0.07823
F1NA1(G)	0.15878	0.15706	0.15857
F2O1S11(G)	0.02579	0.02209	0.02577
F2S11(G)	0.00310	0.00248	0.00307
F3S11(G)	0.08131	0.07631	0.08104
F4S11(G)	0.05685	0.06335	0.05717
H1(G)	0.00069	0.00056	0.00068
H1NA1(G)	0.00001	0.00001	0.00001
H1NA1O1(G)	0.00167	0.00163	0.00170
H1O1(G)	0.00035	0.00021	0.00034
H2(G)	0.00036	0.00043	0.00037
H2O1(G)	0.00078	0.00081	0.00080
N1O1(G)	0.00042	0.00021	0.00040
N2(G)	0.09877	0.09896	0.09880
NA1(G)	0.03731	0.03932	0.03752
NA1O1(G)	0.00019	0.00011	0.00019
O1(G)	0.00042	0.00018	0.00040
O1S11(G)	0.02677	0.02186	0.02681
O2(G)	0.00038	0.00014	0.00035
O2S11(G)	0.00087	0.00056	0.00086
O2S11(L)	0.0	0.00821	0.0

	% BY WT.	ENTHALPY KCAL/MOL	STATE	TEMP DEG K	DENSITY G/CC
SILICON	26.00	0.0	S	298.15	2.330000
TEFLON	23.00	-96.520	S	298.15	2.200000
VITON A	11.00	-177.900	L	298.15	1.920000
NANOS	40.00	-111.540	S	298.15	2.261000

EMPIRICAL FORMULA

FUEL	SI	1.00000					O/F= 0.0
FUEL	C	1.00000	F	2.00000			
FUEL	C	2.67200	F	3.47890	H	1.80000	DENSITY= 2.2051
FUEL	NA	1.00000	N	1.00000	O	3.00000	
PARAMETERS		CHAMBER	THROAT	EXIT			
PRESS., PSIA		14.70	8.47	14.30			
PRESS., ATM		1.00	0.58	0.97			
T, DEG K		2128	2019	2123			
T, DEG F		3371	3174	3362			
S, CAL/(G)(K)		1.7190	1.7191	1.7191			
MOL WT		42.363	42.760	42.382			
CP, CAL/(G)(K)		0.6631	0.6142	0.6610			
GAMMA		1.1273	1.1288	1.1273			
MACH NUMBER		0.0	1.004	0.216			
CSTAR			3346	3346			
CF, IDEAL			0.655	0.145			
CF, VAC			1.231	2.900			
AE/AT			1.00	2.83			
ISP, IDEAL			68.1	15.1			
ISPRHOB			150.2	33.3			

MOLE FRACTIONS OF PRODUCTS

CHINI(G)	0.00001	0.00002	0.00001
CI01(G)	0.30131	0.30207	0.30134
CI02(G)	0.00020	0.00008	0.00019
FIH1(G)	0.01268	0.00837	0.01247
FINA1(G)	0.03601	0.02656	0.03555
F2O1S11(G)	0.00093	0.00052	0.00091
F2S11(G)	0.03209	0.03567	0.03223
F3S11(G)	0.11910	0.12256	0.11928
F4S11(G)	0.01223	0.01178	0.01222
H1(G)	0.00065	0.00044	0.00064
H1NA1(G)	0.00023	0.00018	0.00023
H1NA101(G)	0.00026	0.00012	0.00026
H2(G)	0.03257	0.03507	0.03270
H2O1(G)	0.00011	0.00004	0.00010
H2(G)	0.09411	0.09431	0.09412
NA1(G)	0.15149	0.16198	0.15198
NA2(G)	0.00012	0.00010	0.00012
O1S11(G)	0.15009	0.13798	0.14953
S11(G)	0.00001	0.00001	0.00001
O2S11(L)	0.05580	0.06252	0.05612

APPENDIX IX

FLARES AND FLAME COMPONENTS BURNING IN AIR

[illegible]

	W BY WT.	ENTHALPY KCAL/MOL	STATE	TEMP DEG K	DENSITY G/CC
NG	98.00	0.0	S	298.15	1.740000
NaNO3	37.50	-111.540	S	298.15	2.261000
LANTHAC	4.50	-78.280	S	298.15	1.190000
AIR AMB	100.00	0.0	G	298.15	0.001200

EMPIRICAL FORMULA

O/F= 1.243999

FUEL	NG	1.00000				
FUEL	NA	1.00000	N	1.00000	O	3.00000
FUEL	O	1.77324	C	9.48749	H	9.91080
OXID	N	1.57600	O	0.42400		

DENSITY= 0.0022

PARAMETERS	CHAMBER	THROAT	EXIT
PRESS., PSIA	14.70	8.60	14.30
PRESS., ATM	1.00	0.59	0.97
T, DEG K	3081	2986	3076
T, DEG F	5086	4915	5077
S, CAL/(G)(K)	1.8898	1.8898	1.8897

MOL WT	40.572	41.220	40.603
CP, CAL/(G)(K)	4.3691	4.1757	4.3613
GAMMA	1.0978	1.0955	1.0976
MACH NUMBER	0.0	1.000	0.218
CSTAR		4199	4199

CF, IDEAL	0.641	0.143
CF, VAC	1.226	2.885
AE/AT	1.00	2.82
ISP, IDEAL	82.8	18.5
ISPRHOB	0.2	0.0

MOLE FRACTIONS OF PRODUCTS

ClO1(G)	0.02248	0.02206	0.02246
ClO2(G)	0.01099	0.01193	0.01102
H1(G)	0.00703	0.00695	0.00703
H1NG1(G)	0.00006	0.00004	0.00006
H1NG1O1(G)	0.00005	0.00004	0.00005
H1NA1(G)	0.00003	0.00002	0.00003
H1NA1O1(G)	0.00473	0.00442	0.00472
H1O1(G)	0.00927	0.00890	0.00929
H2(G)	0.00163	0.00167	0.00163
H2O1(G)	0.00587	0.00629	0.00589
NG1(G)	0.06032	0.05513	0.06008
NG1O1(G)	0.01624	0.01336	0.01609
N1(G)	0.00001	0.00001	0.00001
N1O1(G)	0.01721	0.01528	0.01710
N2(G)	0.48339	0.48606	0.48351
NA1(G)	0.05325	0.05412	0.05330
NA1O1(G)	0.00199	0.00165	0.00197
O1(G)	0.02354	0.02201	0.02347
O2(G)	0.03420	0.03351	0.03417
NG1O1(S)	0.24771	0.25894	0.24816

	S BY WT.	ENTHALPY KCAL/MOL	STATE	TEMP DEG K	DENSITY G/CC
MG	100.00	0.0	3	298.15	1.740000
AIR AND	100.00	0.0	6	298.15	0.001200

EMPIRICAL FORMULA

FUEL	MG	1.00000		
OXID	N	1.57600	O	0.42400

O/F= 2.798699 DENSITY= 0.0016

PARAMETERS

	CHAMBER	THROAT	EXIT
PRESS., PSTA	14.70	8.80	14.30
PRESS., ATH	1.00	0.58	0.97
T, DEG K	3115	3020	3110
T, DEG F	5147	4977	5138
S, CAL/(G)(K)	1.8981	1.8981	1.8981
MOL WT	38.357	39.023	38.391
CP, CAL/(G)(K)	5.7465	5.5683	5.7385
GAMMA	1.0999	1.0973	1.0997
MACH NUMBER	0.0	1.000	0.222
CSTAR		4297	4297
CF, IDEAL		0.642	0.146
CF, VAC		1.226	2.839
AE/AT		1.00	2.77
ISP, IDEAL		85.7	19.5
ISP+RHOB		0.1	0.0

MOLE FRACTIONS OF PRODUCTS

MG1(G)	0.09781	0.09213	0.09753
MG101(G)	0.02184	0.01831	0.02165
N1(G)	0.00002	0.00001	0.00002
N101(G)	0.01797	0.01587	0.01786
N2(G)	0.60147	0.60489	0.60164
O1(G)	0.02427	0.02269	0.02419
O2(G)	0.02777	0.02678	0.02773
MG101(S)	0.20883	0.21932	0.20937

	% BY WT.	ENTHALPY KCAL/MOL	STATE	TEMP DEG K	DENSITY G/CC
MG	68.00	0.0	S	298.15	1.740000
NANO3	27.00	-111.540	S	298.15	2.261000
LANTHAC	5.00	-78.200	S	298.15	1.190000
AIR AMB	100.00	0.0	G	298.15	0.001200

EMPIRICAL FORMULA

FUEL	MG	1.00000				O/F= 1.775000
FUEL	NA	1.00000	N	1.00000	O	3.00000
FUEL	O	1.77324	C	9.48749	H	9.91080
OXID	N	1.57600	O	0.42400		DENSITY= 0.0019

PARAMETERS	CHAMBER	THROAT	EXIT
PRESS., PSIA	14.70	8.61	14.30
PRESS., ATM	1.00	0.59	0.97
T, DEG K	3076	2981	3071
T, DEG F	5077	4906	5068
S, CAL/(G)(K)	1.9067	1.9067	1.9067

MOL WT	39.088	39.732	41.122
CP, CAL/(G)(K)	4.4277	4.2244	4.4173
GAMMA	1.0990	1.0967	1.0989
MACH NUMBER	0.0	1.000	0.225
CSTAR		4229	4229

CF, IDEAL	0.642	0.148
CF, VAC	1.228	2.811
AE/AT	1.00	2.74
ISP, IDEAL	84.4	19.4
TSPURHOB	0.2	0.0

MOLE FRACTIONS OF PRODUCTS

ClO1(G)	0.02041	0.02007	0.02039
ClO2(G)	0.00944	0.00989	0.00948
H1(G)	0.00695	0.00686	0.00695
H1MG1(G)	0.00007	0.00005	0.00006
H1MG1O1(G)	0.00005	0.00004	0.00005
H1NA1(G)	0.00002	0.00001	0.00002
H1NA1O1(G)	0.00255	0.00237	0.00254
H1O1(G)	0.00863	0.00824	0.00861
H2(G)	0.00159	0.00163	0.00159
H2O1(G)	0.00541	0.00578	0.00543
MG1(G)	0.06400	0.05850	0.06371
MG1O1(G)	0.01616	0.01325	0.01600
N1(G)	0.00001	0.00001	0.00001
N1O1(G)	0.01705	0.01506	0.01694
N2(G)	0.53787	0.54097	0.53804
NA1(G)	0.03103	0.03153	0.03106
NA1O1(G)	0.00108	0.00089	0.00107
O1(G)	0.02222	0.02064	0.02214
O2(G)	0.03050	0.02960	0.03045
MG1O1(S)	0.22497	0.23459	0.22548

	% BY WT.	ENTHALPY KCAL/MOL	STATE	TEMP DEG K	DENSITY G/CC
NA	100.00	0.0	S	298.15	0.970000
AIR AMB	100.00	0.0	G	298.15	0.001200

EMPIRICAL FORMULA

FUEL	NA 1.00000		
OXID	N 1.57600	O 0.42400	

O/F= 1.480300 DENSITY= 0.0020

PARAMETERS

	CHAMBER	THROAT	EXIT
PRESS., PSIA	14.70	8.56	14.30
PRESS., ATM	1.00	0.58	0.97
T, DEG K	1884	1807	1880
T, DEG F	2932	2793	2925
S, CAL/(G)(K)	1.7054	1.7054	1.7054
MOL WT	47.413	48.006	47.443
CP, CAL/(G)(K)	2.6621	2.7180	2.6652
GAMMA	1.1135	1.1099	1.1133
MACH NUMBER	0.0	1.000	0.223
CSTAR		2995	2995
CF, IDEAL		0.645	0.148
CF, VAC		1.227	2.820
AE/AT		1.00	2.75
ISP, IDEAL		60.1	13.8
ISP*RHOB		0.1	0.0

MOLE FRACTIONS OF PRODUCTS

N101(G)	0.00177	0.00137	0.00175
N2(G)	0.58447	0.58770	0.58464
NA1(G)	0.12761	0.12239	0.12734
NA101(G)	0.01630	0.01370	0.01616
NA102(G)	0.00090	0.00111	0.00091
NA2(G)	0.00020	0.00013	0.00019
O1(G)	0.00004	0.00002	0.00004
O2(G)	0.02634	0.02571	0.02631
NA201(L)	0.24236	0.24786	0.24265

APPENDIX X

LIST OF ABBREVIATIONS AND SYMBOLS FOR SECTION IV

<u>Symbol</u>	<u>Definition</u>
\AA	Angstrom units
B	Emission function
C	Calibration factor
c	Velocity of light
D	Plume diameter
d_o	Flare diameter
ϵ	Emissivity
E_{BB}	Energy emitted by a blackbody
E_{MgO}	Energy emitted by magnesium oxide
E_{Na}	Energy emitted by sodium
\bar{f}_{ideal}	Ideal efficacy
h	Enthalpy of combustion product, also Planck's constant
h_{amb}	Enthalpy of the products having been cooled to ambient temperature
h_i	Initial enthalpy of reactants (equals enthalpy of reactants following adiabatic combustion)
$I(\lambda), J(\lambda)$	Blackbody radiation intensity
I_{LM}	Measured intensity of the lamp
I_{FM}	Measured intensity of the flare
k	Boltzmann constant
L	A characteristic length
m_i	Mass fraction of species i
N_{Na}	Concentration of sodium atoms per cm^3

<u>Symbol</u>	<u>Definition</u>
O·D	Optical depth
S _F	equal to $\frac{W_0^2}{W_0^2 + (\Delta\lambda)^2}$
S (λ)	Spectral sensitivity of eye
T _{BF}	Brightness temperature of the flare
T _{BL}	Brightness temperature of the lamp
T _{mix}	Temperature of plume gases mixed with air
T _o	Temperature of flare gases
U _a	Velocity of approach flow
U _o	Average velocity of gas leaving flare surface
U _p	Plume velocity around the inverted flare
W _o	Spectral width
Δh _{reaction}	Enthalpy of the combustion reaction = h _i - h _{amb}
Δλ	Distance in microns from line center
η	Flare efficiency (actual efficacy/ideal efficacy)
λ	Wavelength
ρ _a	Density of ambient air
ρ _{mix}	Density of plume gases mixed with air
ρ _o	Density of the flare gases
τ _{mixing}	Mixing time

UNCLASSIFIED

Security Classification

DOCUMENT CONTROL DATA - R & D		
(Security classification of title, body of abstract and indexing annotation must be entered when the overall report is classified)		
1. ORIGINATING ACTIVITY (Corporate author) Aerospace Research Corporation 5454 JAE Valley Road, S.E. Roanoke, Virginia 24014		2a. REPORT SECURITY CLASSIFICATION Unclassified
		2b. GROUP
3. REPORT TITLE EXPLORATORY DEVELOPMENT OF ILLUMINATING FLARES		
4. DESCRIPTIVE NOTES (Type of report and inclusive dates) Final Report - July 1967 to July 1968		
5. AUTHOR(S) (First name, middle initial, last name) Hamrick, Joseph T., Blackshear, Perry L. Jr., Stanitz, John D., and Waite, Hal R.		
6. REPORT DATE August 1968	7a. TOTAL NO. OF PAGES 193	7b. NO. OF REFS 21
8a. CONTRACT OR GRANT NO. F08635-67-C-0161	9a. ORIGINATOR'S REPORT NUMBER(S) ET-402	
b. PROJECT NO.	9b. OTHER REPORT NO(S) (Any other numbers that may be assigned this report) AFATL-TR-68-91	
c.		
d.		
10. DISTRIBUTION STATEMENT This document is subject to special export controls and each transmittal to foreign governments or foreign nationals may be made only with prior approval of the Air Force Armament Laboratory (ATTI), Eglin AFB, Florida 32542.		
11. SUPPLEMENTARY NOTES Available in DDC		12. SPONSORING MILITARY ACTIVITY Air Force Armament Laboratory Air Force Systems Command Eglin Air Force Base, Florida
13. ABSTRACT A mathematical flow model has been developed for plane two-dimensional illuminating flares dropping through the atmosphere and simulating face down burning. Numerical results are given infield plots showing streamlines, velocity potential lines, constant velocity lines, and constant time lines for two-dimensional, incompressible flow. Thermochemical calculations based on shifting equilibrium were made for combustion in the flare plume over a range of various mixture ratios. The results are provided in the form of curves and tables showing reaction products, equilibrium temperature, and other thermodynamic data. Temperatures in plumes of one inch diameter flares were measured by thermocouple. A theoretical evaluation of optical density in the plume and experiments to evaluate optical density were performed. The results are provided in tables, photographs of plumes, and traces obtained by spectrograph. Relative luminous intensity distribution in the plumes of downward burning flares was determined and the results are shown in terms of relative intensity contours, plots of relative intensity versus plume area, and plots of percent total intensity versus percent of plume area. An analysis of overall results was made utilizing information from the literature as well as that obtained in the program.		

DD FORM 1 NOV 65 1473

UNCLASSIFIED

Security Classification

UNCLASSIFIED

Security Classification

14. KEY WORDS	LINK A		LINK B		LINK C	
	ROLE	WT	ROLE	WT	ROLE	WT
Two-dimensional illuminating flares Streamlines Velocity potential lines Constant velocity lines Constant time lines						

UNCLASSIFIED

Security Classification